FP7 2013 Cooperation Work Programme
Theme 6: Environment (Including Climate Change)

Novel indicators for identifying critical *INFRA*structure at *RISK* from Natural Hazards

Deliverable D3.2 – Fragility Functions Matrix

Primary Author	Dina D'Ayala, Pierre Gehl, et al./ University College London (UCL)
WP	3
Submission Date	10/12/2015
Primary Reviewer	Maria Teresa Salceda, Miguel Jose Segarra/Dragados (DSA)
Dissemination Level	Public

This project has received funding from the European Union's Seventh Programme for research, technological development and demonstration under grant agreement No 603960.

Project Information

Project Duration: 1/10/2013 - 30/09/2016

Project Coordinator:
Professor Eugene O' Brien
Roughan & O' Donovan Limited
eugene.obrien@rod.ie

Work Programme: 2013 Cooperation Theme 6:
Environment (Including Climate Change).

Call Topic: Env.2013.6.4-4 Towards Stress Testing of Critical Infrastructure Against Natural Hazards-FP7-ENV-2013-two stage.

Project Website: www.infrarisk-fp7.eu

Partners:

Roughan & O' Donovan Limited, Ireland

Eidgenössische Technische Hochschule Zürich, Switzerland.

Dragados SA, Spain.

Gavin and Doherty Geosolutions Ltd., Ireland.

Probabilistic Solutions Consult and Training BV, Netherlands.

Agencia Estatal Consejo Superior de Investigaciones Científicas, Spain.

University College London, United Kingdom.

PSJ, Netherlands.

Stiftelsen SINTEF, Norway.

Ritchey Consulting AB, Sweden.

University of Southampton (IT Innovation Centre), United Kingdom.

Document Information

Version	Date	Description	Primary Author
Rev01	30/09/2015	Deliverable D3.2 on fragility curves for critical infrastructure components for review	D. D'Ayala, P. Gehl, K. Martinovic, K. Gavin, J. Clarke, M. Tucker, R. Corbally, Y.V. Avdeeva, P. van Gelder, M. T. Salceda Page, M. J. Segarra Martinez
Rev02	10/12/2015	Final version for submission	D. D'Ayala, P. Gehl, K. Martinovic, K. Gavin, J. Clarke, M. Tucker, R. Corbally, Y.V. Avdeeva, P. van Gelder, M. T. Salceda Page, M. J. Segarra Martinez

Abbreviations

BN	Bayesian Network
CI	Critical Infrastructure
Co	Repair Cost
CPT	Conditional Probability Table
DS	Damage State
Du	Repair Duration
EDP	Engineering Demand Parameter
FL	Functional Loss
FLI	Functional Loss during Intervention
IM	Intensity Measure
PGA	Peak Ground Acceleration
PGD	Permanent Ground Deformation
PGV	Peak Ground Velocity
SA	Spectral Acceleration (Displacement)

Executive Summary

This report reviews or develops, where necessary fragility functions for transport infrastructure elements at risk (i.e. bridges, tunnels and road segments) due to one or more of (or a combination of) the three hazards being considered in the INFRARISK project (i.e. earthquakes, landslides and floods).

To do so, infrastructure network elements are decomposed into their structural components, which may be susceptible to hazard-specific damage mechanisms. The possible failure modes are then identified and corresponding fragility models can subsequently be derived or selected from existing literature references. Specific developments are carried out for the seismic fragility of bridge components and for the fragility of road sections due to rainfall-triggered landslides.

The harmonization of the damage states across the different hazard types is ensured at the level of functional consequences, i.e. metrics such as loss of functionality or the duration of repair are estimated for each infrastructure component at each damage state based on expert opinion within the - INFRARISK project team. System failure modes are then defined so that they are consistent in terms of functional losses. This approach is demonstrated through the derivation of a harmonized multi-risk fragility model for a bridge system, using a Bayesian Network to assemble the component fragility curves.

Finally, fragility functions of interest are summarized in a Fragility Functions Matrix. To do so, the fragility functions are grouped by element type, hazard type and system failure mode. While the various failure modes are well documented, some fragility functions are currently not available.

Table of Contents

1.0 INTRODUCTION

The vulnerability or the susceptibility of transport infrastructure elements to extreme loading scenarios, such as natural hazard events, can be quantified through fragility curves, which have become a popular tool, particularly in seismic risk analyses. The Performance-Based Earthquake Engineering (PBEE) framework has formalized the use of fragility curves, which enables the evaluation of the risk λ_{EDP} (i.e. probability of exceedance of a given EDP value) by convoluting the fragility curve (i.e. probability of exceeding the EDP value given an IM value) with the hazard rate λ_{IM} (Deierlein et al., 2003):

$$\lambda_{\mathrm{EDP}}(edp) = \int P(\mathrm{EDP} \geq edp | \mathrm{IM} = im) \cdot \mathrm{d}\,\lambda_{\mathrm{IM}}(im) \quad (1)$$

These probabilistic tools may be applied to other hazard types such as ground failures or floods. To do so, the corresponding engineering demand parameters, intensity measures and associated damage mechanisms must be defined. Since a given infrastructure element is usually comprised of a wide range of structural or non-structural components, the same damage mechanism or engineering demand parameter cannot usually be applied to all components. The same rationale can also be developed for the hazard types, which generate various types of loadings on each component. A summary of the damage mechanisms and the associated fragility functions for various hazards and network components may be presented according to Figure 1, where the need to develop hazard-specific fragility curves at the component level is highlighted.

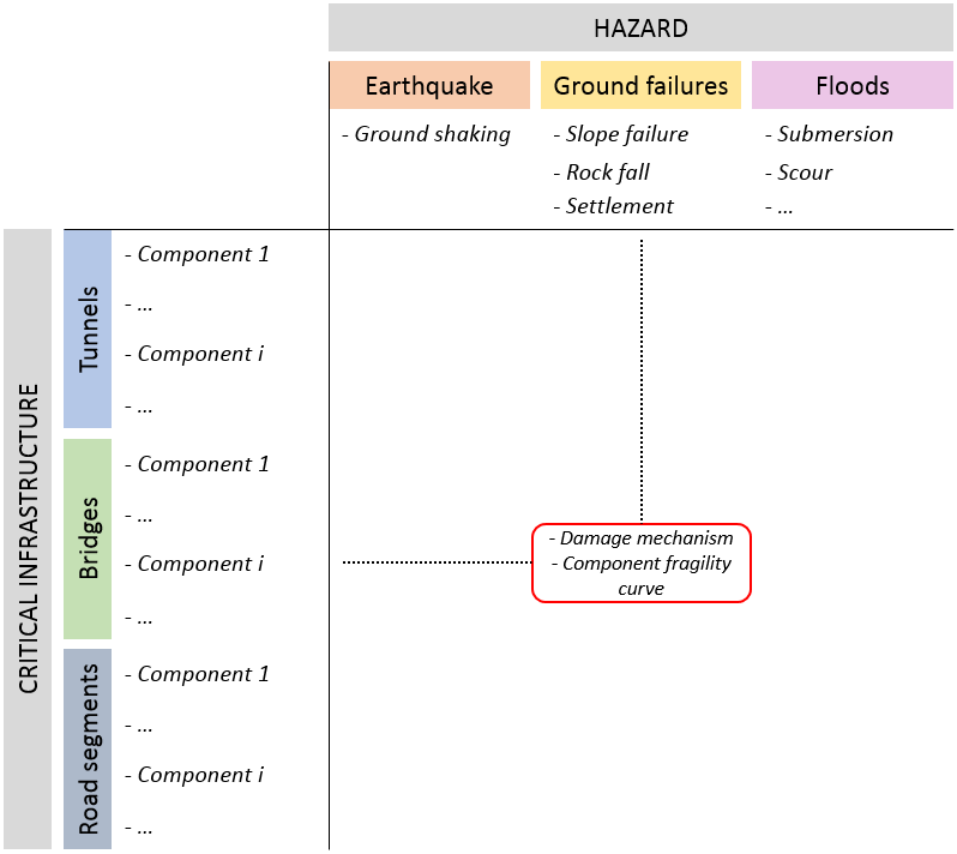

Figure 1: Decomposition of transport infrastructure network into element types (and associated components) and related hazards

Another specificity of the study of infrastructure systems lies in the dependency between its elements, which is crucial when assessing the global performance of a system (Modaressi et al., 2014). The physical damage of the infrastructure elements due to a hazard event, along with the associated repair costs (i.e. the direct losses), only constitutes a portion of the consequences and there may also be indirect losses associated with the failure of the infrastructure network, which can have more severe and long-term impacts (e.g. increased travel times, economic losses). It is therefore important to estimate the loss of functionality that corresponds to each damage state: this analysis should be done at the level of each component for each damage mechanism in order to benefit from a better resolution of the functionality models. An advantage of this approach is that it facilitates the harmonization of the damage states for the various infrastructure components for different hazard types since the network elements may be grouped according to the level of functionality loss (i.e. creation of system failure modes comprised of consistent damage mechanisms). Fragility functions for theses system failure modes may then subsequently be aggregated by using system reliability methods or Bayesian approaches.

In this report, a brief literature review is initially presented, which summarises various methods for the derivation of analytical fragility curves and for the reliability assessment of systems (Section 2): these theoretical tools are be applied to example scenarios throughout the report. Then, the structure of the proposed Fragility Functions Matrix is introduced in Section 3, where the integration with the hazard assessment models from INFRARISK deliverable D3.1 (D'Ayala et al., 2014) is discussed.

Sections 4 to 6 specifically outline fragility functions for bridges, tunnels and road segments respectively. Within each section, a description of the typology for the infrastructure element is provided, along with a summary of the common components. The associated damage mechanisms for each infrastructure component for the various hazards considered are also identified. In each case, fragility functions are either selected from literature references or are analytically derived. In addition, the associated functional consequences (e.g. loss of function, repair duration, etc.) are identified in each case according to a tentative functionality matrix that is being developed by the INFRARISK project team. Finally, Section 7 presents the Fragility Functions Matrix, which summarizes the developments that have been carried out for the individual infrastructure elements for the various hazards considered. System failure modes are proposed for each element in order to harmonize the performance assessment of the infrastructure across all hazard types.

2.0 THEORETICAL BACKGROUND

This section details the theoretical tools and assumptions that underlie the derivation of fragility functions for structural elements. It is mainly focused on the fragility curves in the context of earthquake engineering, since a lot of effort has been devoted to fragility analyses for seismic risk. However, most of the concepts detailed are fully applicable to other hazard types, such as ground failures or floods.

2.1 General principles

Over the past number of decades, fragility functions have become widely employed as a probabilistic tool for the vulnerability assessment of a given structural system (Calvi et al., 2006; D'Ayala et al., 2014). Most theoretical developments have been proposed for buildings first, however they can also be applied to infrastructure elements. Fragility functions are based on a set of prerequisites, which include the following (Negulescu and Gehl, 2013):

- An Intensity Measure (IM) that represents the seismic loading applied to the structure. It is usually a ground-motion parameter such a Peak Ground Acceleration (PGA) or Spectral Acceleration (SA) at a period of interest.
- A damage scale that is comprised of a set of discrete Damage States (DS). The damage states are bounded by limit states or damage levels, which usually correspond to a given threshold in the potential values of a given engineering demand parameter (EDP).
- A functional form linking the probability of reaching or exceeding a damage state as a function of the selected IM. For instance, if a cumulative lognormal distribution is adopted, then the distribution parameters (i.e. mean and standard deviation) represent the fragility parameters (see Figure 2). The mean represents the IM value that corresponds to 50% damage exceedance and the standard deviation represents the spread of the curve between the 16th and 84th percentile values.

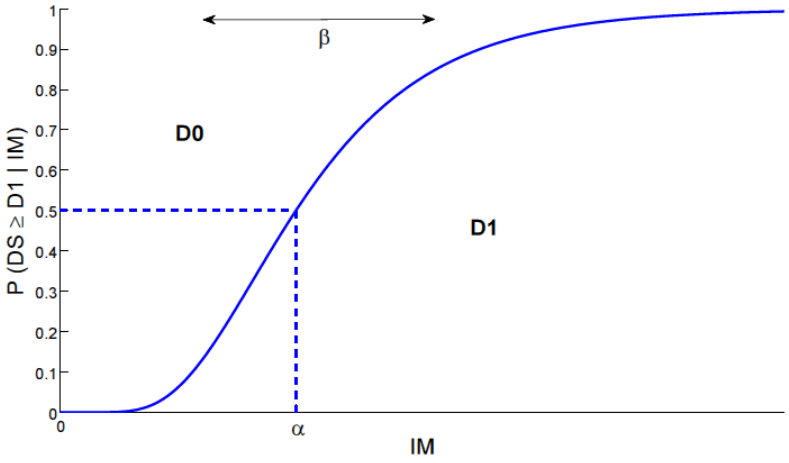

Figure 2: Fragility curves for damage level 1, representing the probability of reaching or exceeding damage state D1

The mathematical expression of a fragility curve with mean α and standard deviation β can then be written as a conditional probability, assuming a standard normal cumulative distribution function ϕ:

$$P(ds \geq DS \mid IM) = \phi\left(\frac{\log IM - \log \alpha}{\beta}\right) \quad (2)$$

Fragility curves are a key element of the Performance-Based Earthquake Engineering (PBEE) framework (Krawinkler, 1999) and are used to account for the various uncertainties associated with the seismic hazard and the structural response estimation. These uncertainties are usually classified as either aleatory or epistemic (Kennedy et al., 1980). It is also possible to decompose the total standard deviation (β) into the various sources of uncertainty, such as the loading demand or the structural capacity (Bradley, 2010; D'Ayala et al. 2014; Wen et al., 2003), as follows:

- β_c is the standard deviation due to the uncertainties in the capacity of the studied structure (e.g. modelling uncertainties, variability in the mechanical or geometrical properties).
- β_d is the standard deviation due to the uncertainty in the seismic demand, e.g. the record-to-record variability.
- β_{DS} is the standard deviation that is linked to the probabilistic EDP threshold identifying the damage level. For instance, β_{DS} = 0.4 is recommended by HAZUS (NIBS, 2004) for buildings. In the case of bridges, the damage states can also be estimated by compiling field data or conducting surveys with engineers or inspectors in order to obtain a distribution of the EDP thresholds for a given damage state (Nielson, 2005).

The standard deviations described can subsequently be combined in order to obtain the total dispersion of the fragility model, as follows (D'Ayala et al., 2014):

$$\beta = \sqrt{\beta_c^2 + \beta_d^2 + \beta_{DS}^2} \quad (3)$$

Fragility curves are derived through regression models for data points that may be obtained from a variety of sources. Empirical fragility curves may be derived based on post-earthquake field observations, whereby the observed damage may be related to the ground motion levels that have been recorded in the vicinity of the structure (Elnashai et al., 2004; Basoz et al., 1999; Shinozuka et al., 2000). While the empirical approach results from direct observations, this method still presents some shortcomings, such as the difficulty in obtaining accurate measurements of ground motion intensity at the site of interest or the presence of gaps in the data obtained, particularly at high seismic intensity levels.

In the case of scarce data, expert judgement may be employed to derive fragility functions. This requires the gathering of data from a panel of experts in the relevant technical field to derive the mean and standard deviation values for the fragility functions. Each expert judgement can be weighted depending on the level of expertise of the contributor or their confidence level as regards their estimation (Porter et al., 2007; Jaiswal et al., 2013).

Finally, fragility functions may be derived based on analytical methods, for example by employing numerical methods to simulate the structure under examination and analysing the structural response for a range of ground motion intensities. For instance, Mander (1999) has derived fragility functions for bridges using a static capacity spectrum approach and considered the uncertainties associated with the mechanical properties of the models and the seismic demand. Recently, non-linear dynamic analyses for a large set of ground motion records have also become popular due to

the increase in computing capacity and the development of more robust finite element codes (Tsionis and Fardis, 2014). These analyses may be conducted according to a Monte Carlo simulation approach (Nielson and DesRoches, 2007; Shinozuka et al., 2000) or using Incremental Dynamic Analysis (Vamvatsikos and Cornell, 2002). Although analytical approaches enable sensitivity analyses to be performed to evaluate the influence of various input parameters, the use of numerical methods may introduce additional modelling uncertainties into the analysis.

Hybrid fragility curves (Kappos et al., 2006) can also be derived in order to calibrate analytical results with posterior post-earthquake observations (Singhal and Kiremidjian, 1998) or using in-situ measurements (Michel et al., 2010), according to a Bayesian updating process. Jaiswal et al. (2011) employed Bayesian updating based on post-earthquake field observations to update fragility functions that had previously been derived based on expert judgement or estimated according to the vulnerability classes outlined in the European Macroseismic Scale (EMS) (Grunthal, 1998).

2.2 Fitting fragility functions to data

Fragility functions may be fitted to empirical, judgemental or analytical data by performing a regression analysis. Two distinct approaches are outlined in the literature and are commonly employed in practice. The first consists of the so-called `regression on a cloud' method, as described by Baker (2007) and Cornell et al. (2002), where a least-squares regression is performed on the [IM-EDP] points, according to the following model:

$$\log EDP = a \cdot \log IM + b \tag{4}$$

The response residuals of the regression are then computed, and β_ε denotes the standard deviation of the residuals. After selecting a given damage threshold EDP_{th}, the fragility parameters (mean α and standard deviation β) can then be expressed as:

$$\begin{cases} \alpha = \exp\left(\dfrac{\log EDP_{th} - b}{a} \right) \\ \beta = \dfrac{\beta_\varepsilon}{a} \end{cases} \tag{5}$$

This approach is based on the actual EDP values in the dataset and it has proven to be rather stable, even with a low number of data points (Gehl et al., 2015). However, it appears that, in the case of a structure with multiple damage states, the estimated standard deviation stays the same for all damage levels. While this constraint may be desirable in order to avoid the overlapping of successive fragility curves, it constitutes also an oversimplification of the problem, since it assumes that the dispersion in the results does not change with the degree of non-linearity (see D'Ayala, 2005).

The second method is the maximum likelihood approach, as proposed by Shinozuka et al. (2000). Using this approach, the EDPs are directly translated into the corresponding damage states. For a fragility curve with a given damage level, binary values are subsequently assigned to the vector of damage states (1 if damaged, 0 if not). The fragility parameters are then estimated by maximising the following likelihood function:

$$L(\alpha,\beta) = \prod_{i=1}^{n} \left[\mathrm{P}_i(\alpha,\beta) \right]^{x_i} \cdot \left[1 - \mathrm{P}_i(\alpha,\beta) \right]^{1-x_i} \tag{6}$$

where $P_i(\alpha,\beta)$ is the probability of reaching damage, n is the number of data points and x_i is a binary variable (1 if damage is reached, 0 if not).

This approach is suitable for the derivation of empirical fragility functions due to the use of discrete damage states. It may also be used to derive fragility functions from analytical methods however due to the fact that the maximum likelihood model only requires a clear distinction between `damage' and `no damage' regardless of the actual EDP values (e.g. Baker, 2015; Gehl et al., 2013; Zentner, 2007). Consequently, the maximum likelihood approach may be applied in cases where the numerical model fails to accurately describe the response after the damage has occurred (e.g. derivation of collapse fragility curves). As a result, only a linear elastic model is required in order to estimate the fragility function associated with the yielding limit of a given structural component. However, it should be noted that the application of the maximum likelihood approach to a lognormal distribution is only one specific case amongst the more generic concept of Generalized Linear Model (GLM) regression, which has been applied to seismic fragility models (Ioannou et al., 2012).

2.3 Fragility functions for components and systems

For complex structural systems such as bridges or tunnels, the presence of a wide range of components and damage mechanisms often prevents the identification of a single engineering demand parameter for the structural system in order to derive fragility functions. In this case, the reliability of the overall system is initially assessed by defining system failure modes (i.e. global damage states), which correspond to specific configurations of component damages (e.g. components in series or in parallel, or both). The component fragility curves are then assembled in order to obtain the damage probabilities at the system level, as summarized in Figure 3. To subsequently derive system fragility functions from the individual component fragility functions, two methods are available; a matrix-based system reliability method and an approach based on Bayesian Networks, as will be subsequently described.

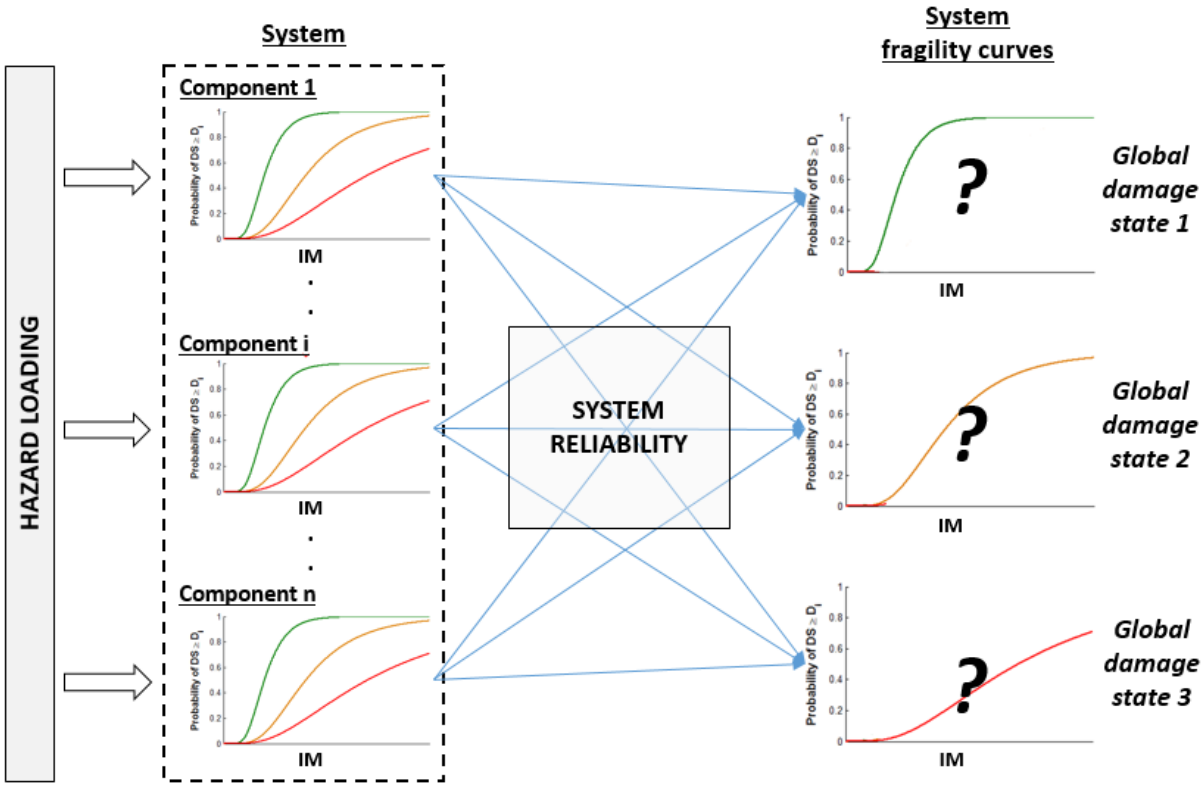

Figure 3: General principles of system reliability methods

2.3.1 Matrix-based system reliability method (MSR)

A matrix-based system reliability method was proposed by Song and Kang (2007) and Kang et al. (2008) to quantify the vulnerability of complex systems based on the associated component fragilities. For a system with n components (each component *i* having k_i states), the sample space is composed of $m = \prod_{i=1}^{n} k_i$ events.

These basic events are mutually exclusive and collectively exhaustive (MECE) and they can be denoted as e_j =1…*m*. A vector **c** is then assigned to a given system event, where the j^{th} element of **c** is a binary variable, indicating whether the basic MECE event e_j is included or not at system level. The probability of a system event E_{sys} can then be expressed as a vector product according to the following equation where p_j as the probability of occurrence of e_j:

$$P(E_{sys}) = \sum_{j:e_j \subseteq E_{sys}} p_j = \mathbf{c}^T \cdot \mathbf{p} \quad (7)$$

The main advantage of this approach is the computational simplicity since the probabilities can be estimated using matrix-based operations. Additionally, Kang et al. (2008) and Song and Kang (2009) outline guidelines for an efficient assembly of vectors **c** and **p**.

In the case of large or complex systems, the size of the matrices can also be reduced by considering sub-systems and by adopting a multi-scale approach (Der Kiureghian and Song, 2008). However, when the components are statistically dependent, the vector **p** cannot be built with a straightforward product of the component failure probabilities. It is possible, however, to assume conditional independence between component damages given a set of random variables, which

represent `environmental dependence' or `common source effects' (Kang et al., 2008). A vector **x** of common source random variables (CSRV) may subsequently be introduced, with a joint probability distribution function f(**x**). This enables the system failure probability to be expressed as:

$$\mathrm{P}\left(\mathrm{E}_{sys}\right)=\int_{\mathbf{x}}\mathrm{P}\left(\mathrm{E}_{sys}\mid\mathbf{x}\right)\cdot\mathrm{f}\left(\mathbf{x}\right)\cdot d\mathbf{x}=\int_{\mathbf{x}}\mathbf{c}^{T}\cdot\mathbf{p}\left(\mathbf{x}\right)\cdot\mathrm{f}\left(\mathbf{x}\right)\cdot d\mathbf{x} \quad \textbf{(8)}$$

The CSRV vector **x** can be estimated by constructing a Dunnett-Sobel variable class (Dunnett and Sobel, 1955). For component *i*, the safety factor F_i is initially defined as the logarithm of the ratio of the structural demand over the structural capacity. Using the mean α_i and the standard-deviation β_i of the corresponding fragility curve, the safety factor can then be standardized into $\mathrm{Z}_i=\left(\mathrm{F}_i-\alpha_i\right)/\beta_i$, which can be approximated as follows:

$$\mathrm{Z}_i=\sqrt{1-r_i^2}\cdot V_i+r_i\cdot U \quad \textbf{(9)}$$

where V_i and U are independent standard normal random variables in the Dunnett-Sobel class. Therefore, for a given outcome of U, the Z_i variables become conditionally independent. The coefficients r_i have to be estimated so that the correlation coefficient between Z_j and Z_k, i.e. $\rho_{j,k}$, is accurately approximated by the product $r_j.r_k$, for all components. An optimization process over the correlation matrix of the component responses can then be used to evaluate the r_i coefficients. The Dunnett-Sobel class can finally be used to numerically compute the system fragility curve through an integration over U.

This method has been implemented into the FERUM toolbox (Der Kiureghian et al., 1999), which provides the probability of failure of a given system, given the failure probabilities of its components and the correlation between component failures.

2.3.2 Bayesian Networks for system fragility curves

As an alternative to the MSR method, the INFRARISK project has developed a formulation of the problem using Bayesian Networks (BNs), which has been verified in terms of its computational efficiency and flexibility. The BN theory has already been thoroughly detailed by Bensi et al. (2011) in the context of the seismic risk analysis of infrastructure systems, where BNs are used to model spatially distributed seismic demand, as well as component and system performance. The focus of the application of BNs within INFRARISK is on the construction of Bayesian Networks to assess the fragility of structural systems (e.g. bridges), as outlined in Gehl and D'Ayala (2015a,b). Such a BN starts from the node(s) that represents the hazard loading and ends with the node that represents the system event. The upstream part of the BN is composed of the following nodes, as outlined in Figure 4:

- Root node **IM** representing the hazard loading applied to the *n* components.
- Root node **U** representing the standard normal variable that is common to all components.
- Root nodes $\mathbf{V_1}$…$\mathbf{V_n}$ representing the standard normal variables that are specific to each component.
- Nodes $\mathbf{C_1}$...$\mathbf{C_n}$ representing the component damage events.

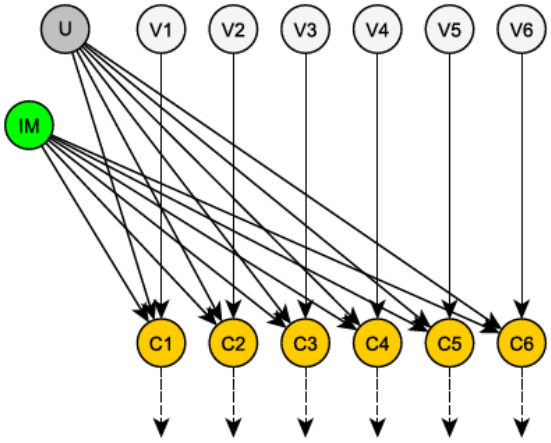

Figure 4: Bayesian Network accounting for statistical dependence between component failures for a system with six in-series components

As proposed by Bensi et al. (2011), the Dunnett-Sobel classes can be modelled in BNs by creating root nodes (i.e. **U** and $\mathbf{V}_i$) with a conditional probability table (CPT) that contains the discretised standard normal distribution. A component-event node $\mathbf{C}_i$ therefore has three parent nodes, namely **IM**, **U** and $\mathbf{V}_i$. For each combination of sampled values [*im*; *u*; v_i], the failure event of component *i* is expressed as the following condition:

$$z_i = \sqrt{1-r_i^2}\cdot v_i + r_i \cdot u \geq -\frac{\log im - \log \alpha_i}{\beta_i} \quad \textbf{(10)}$$

where α_i and β_i are the fragility parameters of component *i*, i.e. mean and standard deviation respectively. Using the corresponding probability density of values v_i and *u*, the final failure probability of component *i* can be estimated through Bayesian inference for any values of *im*.

The downstream part of the BN deals with the estimation of the system failure event, starting from the component events. Due to memory limitations in the size of the CPTs, a single system-level node **SYS** being the child of all component nodes (i.e. converging structure) is not recommended and is not computationally realistic. For example, a system with *n* components would result in a CPT of 2^{n+1} elements, assuming only binary states for the failure events. It is, therefore, proposed to introduce a set of intermediate nodes in order to gradually reduce the number of parent nodes and the size of the CPTs, via a chain structure. As shown in Figure **5** 5, the first two component event nodes create an intermediate node $\mathbf{In}_1$, which is, in turn, linked to the next component event node in order to define another intermediate node $\mathbf{In}_2$, and so on, until there are no component-event nodes left. The last intermediate node then becomes the **SYS** node. This layout corresponds to a chain-like BN topology, which has been acknowledged as more being computationally efficient than a converging structure (Bensi et al., 2013).

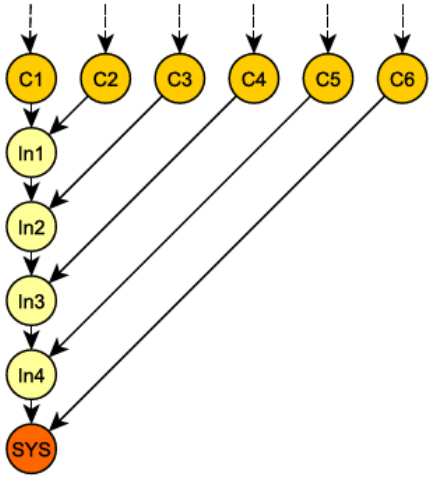

Figure 5: Layout considered for intermediate nodes, for a system with six in-series components. Each of the intermediate nodes represents an intermediate state of the partial combination of the components, in order to limit the computational load.

In the case of structural systems, most of the components are assembled in series, so that the failure of one the components results in the failure of the overall system. In this context, the CPTs of the intermediate nodes $\mathbf{In}_i$ are built as a Boolean table, as shown in Table 1.

Binary states			**Probabilities**	
C_{i+1}	In_{i-1}	In_i	**Series system**	**Parallel system**
0	0	0	1	1
1	0	0	0	1
0	1	0	0	1
1	1	0	0	0
0	0	1	0	0
1	0	1	1	0
0	1	1	1	0
1	1	1	1	1

Table 1: CPTs for intermediate nodes in the case of series or parallel systems. The convention used is 0 for survival (i.e. damage state 0) and 1 for failure (i.e. damage state 1).

While the aforementioned examples have been based on binary component events (i.e. either survival or failure) and on straightforward system failure events (i.e. in-series system with all components involved), most real structural systems may require more complex configurations, such as the use of multiple damage states for the components or the existence of multiple system failure modes. In the case of multiple damage states for the structural components, the insertion of intermediate component-event nodes with a binary output is proposed, by decomposing the states of the initial component-event nodes in a series of survival checks. An example is shown in Figure 6a, where three states are assumed for each of the six components (i.e. 'intact', 'DS1' and 'DS2'): each $\mathbf{C}_i$ node generates two child nodes $\mathbf{C}_{i1}$ (i.e. with states 'intact' and 'D1/D2') and $\mathbf{C}_{i2}$ (i.e. with states

'intact/'D1' and 'D2'), which are used separately to predict a system failure mode with two distinct severity levels (i.e. **SYS_1** and **SYS_2**).

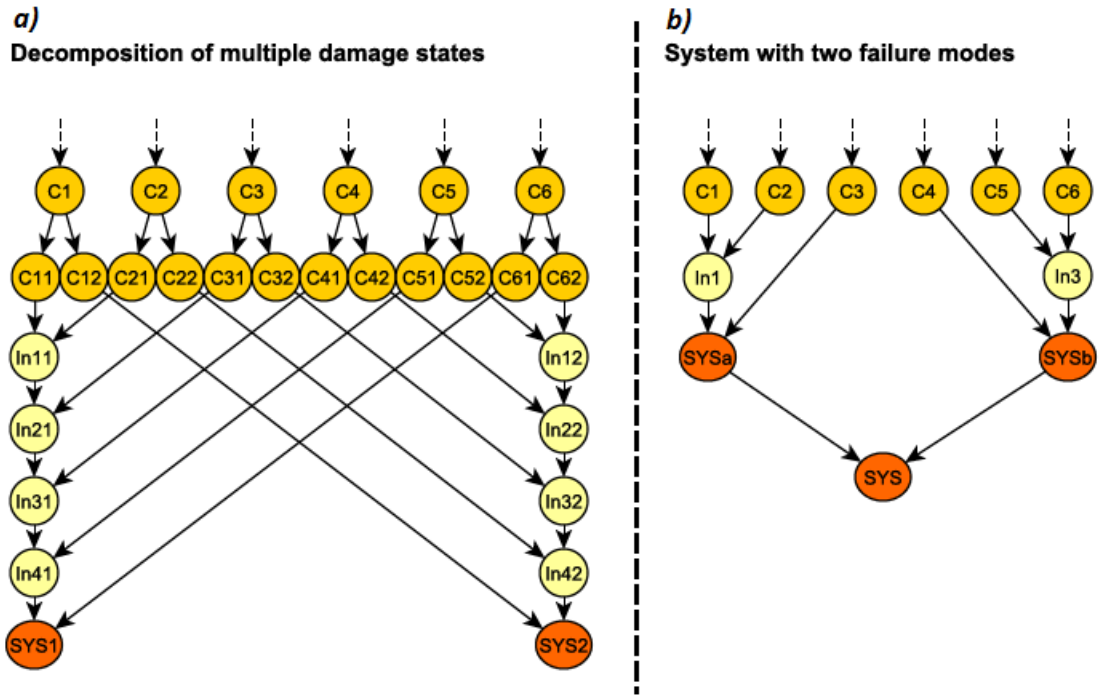

Figure 6: BN structure for components with multiple damage states (left), and BN structure for a system with two failure modes (right).

The BN on Figure 6b exemplifies another possibility, i.e. the case of a system with two failure modes, one being based on the state of the first three components, the other being based on the state of the remaining components: conversely to the example on the left, these two failure modes **SYS_a** and **SYS_b** may jointly occur for the same IM level and loading conditions, depending on the correlation between the component events. Therefore they have to be linked by a final SYS node, in order to facilitate the computation of the joint probability of the two failure modes during the Bayesian inference.

All the examples and BN layouts discussed above have been implemented into a Matlab code, which enables BNs to be automatically generated for a wide range of structural systems and configurations, which can then be solved by using the Matlab-based Bayes Net toolbox (Murphy, 2007). Gehl and D'Ayala (2015b) have conducted benchmarking in order to compare the performances of the BN and the MSR methods, in terms of accuracy and computation time. The following findings have been concluded:

- For a small number of structural components (i.e. below 20), the MSR method is less time-consuming since it is based on the direct numerical integration of the damage probabilities and the distribution of the common source variables.

- For a larger amount of components (i.e. greater than 20), the computation time of the BN method remains reasonable, whereas the MSR method starts to fail beyond 25 components due to memory errors (i.e. assembly of the vector **c** of component events).

- The discretisation of the continuous variables in the BN method does not generate any bias and the differences between the system fragility curves derived with the BN and the MSR methods were not significant.

Finally, the BN method is adopted to generate system fragility curves for infrastructure elements such as bridges, since it provides several important advantages:

- the capacity to deal with a large number of components, especially through the use of intermediate nodes;
- the flexibility in the BN construction, which allows multiple damage states and multiple system failure modes to be accounted for;
- the simultaneous computation of the joint probability of all failure modes, which can represent a significant gain in computation time.

3.0 STRUCTURE OF FRAGILITY FUNCTIONS MATRIX

In the INFRARISK Deliverable D3.1 (D'Ayala et al., 2014), a Hazard Distribution matrix has been defined in order to harmonize the hazard assessment steps that are specific to each hazard type (i.e. earthquakes, ground failures and floods). Each hazard type was defined in terms of the following: source event, propagation and site variables (i.e. following the source/pathway/receptor approach), recommended method of derivation, type of IM considered and potential uncertainty sources. When convoluted with the different input variables describing a given problem, this hazard distribution matrix provides all the necessary tools to quantify the distributed IMs at the susceptible sites of the infrastructure system.

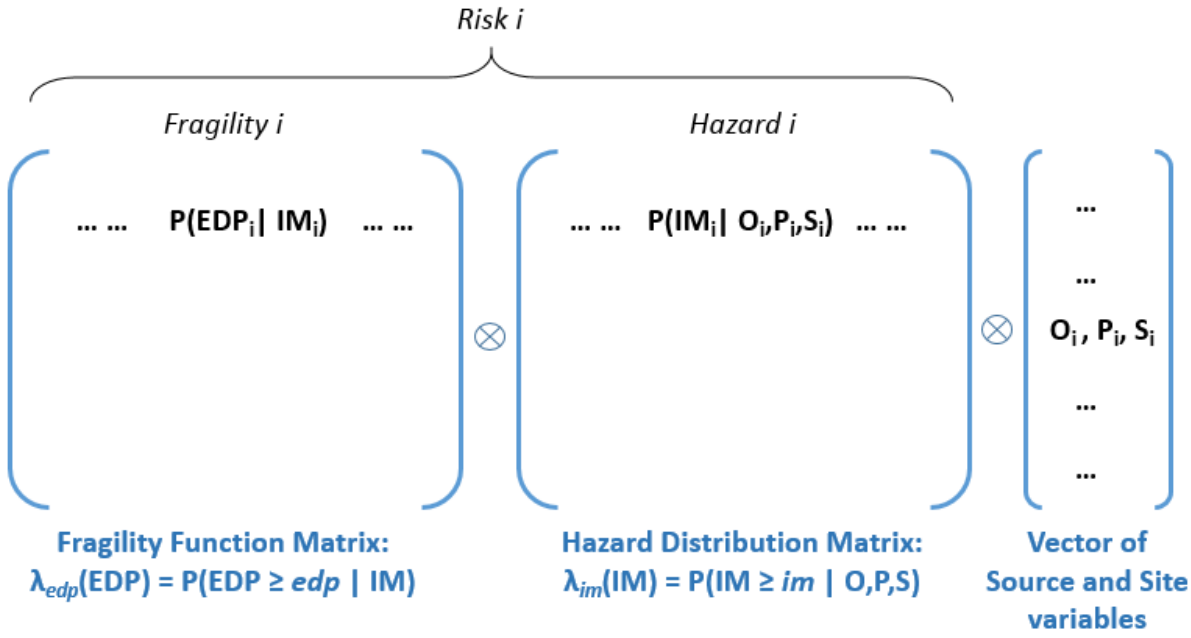

Figure 7: Proposed framework for the single risk analysis

The objective of this report is to build a Fragility Functions Matrix that can be convoluted with the hazard matrix and generate single risk estimates for each hazard type and each infrastructure element (see Figure 7). This risk convolution has to be useful for the subsequent steps of the infrastructure risk analysis, namely the estimation of the system performance depending on the failure/disruption of the individual elements. To this end, the failure modes of the elements have to be combined or aggregated from physical damage mechanisms to specific structural components (e.g. physical damage to piers or bearings in the case of a bridge system) in order to generate global failure modes that are consistent in terms of functional losses or repair duration. It is therefore proposed to organize the Fragility Functions Matrix by element type (i.e. bridge, tunnel, road segment) and by global failure mode, for which local failure modes and corresponding fragility models are identified. Finally, the proposed rows for this matrix are the following:

- **Type of infrastructure element:** bridges, tunnels or road segments;
- **Definition of a global failure mode**: a failure mode of the infrastructure element that can be directly associated with some functional losses (e.g. deck unseating or collapse of substructure components in the case of a bridge);

- **EDP:** which EDP is considered to monitor the physical damage of the structural components;
- **Physical damage states:** definition of the damage states for the structural components;
- **Recommend method in INFRARISK:** which fragility derivation method is advocated in each situation;
- **Fragility functions:** proposition of some relevant fragility models, which are either selected from previous literature references or derived in the present report;
- **Functional damage states:** level of functional losses (e.g. full closure of the element or extent of partial closure) or duration of the corresponding repair operations.

This conceptual matrix-based framework is only valid when independent hazards and risks are considered. If some multi-risk interactions are taken into account, whether at the hazard level or the fragility level, specific developments have to be carried out in order to model cascading hazards or cascading damage events. These cases are more specifically discussed in INFRARISK Deliverable D3.3 (D'Ayala and Gehl, 2015).

The following sections are devoted to the definition of all possible failure modes and the review/development of appropriate fragility models, which ultimately leads to the specification of the Fragility Functions Matrix, as presented in Section 7.

4.0 FRAGILITY FUNCTIONS FOR BRIDGES

This section provides a general description of bridge systems, in terms of typological features and component types. A literature review is subsequently conducted to identify the most common bridge failure modes and to collate available fragility functions. New developments are then proposed in order to enhance the practical use of the fragility models in the context of infrastructure risk assessment, which include the following: (i) derivation of probabilistic functionality models based on the physical failure modes of the bridge components, (ii) use of statistical methods to assign given bridge types to available fragility functions and (iii) development of component-based fragility models in order to refine the estimation of the functional losses and to build a modular multi-risk fragility framework.

4.1 General description of bridge elements

One of the key outcomes of the FP7 SYNER-G project is the collection and review of seismic fragility functions for critical infrastructure components. Specifically, fragility functions for road and railway bridges have been critically appraised and stored in a Fragility Function Manager Tool (Silva et al., 2014).

The SYNER-G Fragility Function Manager Tool proposes a taxonomy for the different bridge typologies based on over a dozen parameters. The taxonomy is inspired by the classifications that have been previsouly defined (e.g. Basoz and Kiremidjian, 1996; NIBS, 2004; Nielson, 2005). The SYNER-G taxonomy comprises the following parameters:

- **Material 1 (MM1):** Concrete (C), Masonry (M), Steel (S), Iron (I), Wood (W), Mixed (MX);
- **Material 2 (MM2)**: Reinforced concrete (RC), Post-tensioned or Pre-stressed reinforced concrete (PC), Unreinforced masonry (URM), Reinforced masonry (RM);
- **Type of superstructure (TD1):** Girder bridge (Gb), Arch bridge (Ab), Suspension bridge (Spb), Slab Bridge (Sb);
- **Type of deck (TD2):** Solid slab (Ss), Slab with voids (Sv), Box girder (B), Modern arch bridge (MA), Ancient arch bridge (AA);
- **Deck characteristics (DC):** width of the deck;
- **Deck structural system (DSS):** Simply Supported (SSu), Continuous (Co);
- **Pier to deck connection (PDC):** Not Isolated – monolithic (NIs), Isolated – through bearings (Is);
- **Type of pier to superstructure connection (TC1):** Single-column Pier (ScP), Multi-column Pier (McP);
- **Number of piers for column (NP);**
- **Type of section of the pier (TS1):** Cylindrical (Cy), Rectangular (R), Oblong (Ob), Wall-type (W);

- **Type of section of the pier (TS2):** Solid (So), Hollow (Ho);
- **Height of the pier (HP);**
- **Spans (Sp):** Single span (Ssp), Multi spans (Ms);
- **Spans characteristics (SC):** Number of Spans (NS), Span Length (SL);
- **Type of connection to the abutments (TCa):** Free (F), Monolithic (M), Isolated – through bearings or isolators (Isl);
- **Bridge configuration (BC):** Regular (R), Semi-regular (SR), Irregular (IR);
- **Level of seismicity (LS):** No seismic design – design for gravity loads only (NSD), Seismic design (SD);

The taxonomy outlined above has been specifically designed for seismic hazards so that bridges may be classified according to these parameters and potentially associated with a given typology with a known response behaviour represented by existing fragility functions. In the case of other hazard types (e.g. floods, landslides), fragility developments are usually case-specific due to the numerous parameters that have to be accounted for. For instance, the fragility of bridges due to fluvial floods and induced scour is heavily influenced by the shape of the channel, the material in the stream bed, the position of the piers, the foundations, etc. (see HEC-18; Richardson and Davis, 1995). A refined topography model and knowledge of the surrounding soil and its interaction with the bridge foundations are also required to assess the susceptibility of the bridge system to ground failure.

The bridge typology strongly influences the type of components that comprise the bridge system. The focus of the INFRARISK project is on multi-span RC girder bridges, with either simply-supported or continuous decks, which represent the most widely used typology for highway bridges in Europe. These bridge types are generally comprised of the following components:

- **RC piers:** single-/multi-column bents, rectangular or cylindrical columns;
- **Deck:** continuous or simply supported, slab, steel girder, concrete girder, concrete box girder;
- **Abutments:** seat-type abutment supported by a single / double row of RC piles or by a wall;
- **Bearings:** fixed / expansion bearings, bolted / unbolted neoprene pads, elastomeric pad and dowel bearings, steel pendulum bearings, sliding/roller bearings;
- **Shear Keys;**
- **Expansion joint;**
- **Energy dissipating systems, in retrofitted cases (e.g. viscous dampers or isolators).**

The same typologies and components may be applied to railway bridges. The main difference with road bridges resides in the limit states, which are usually more restrictive for railway bridges (i.e. smaller deformations are allowed for railway tracks).

a. Piers

The flexural behaviour of pier columns under seismic loading is usually assessed through the Moment-Curvature curve of the column section, allowing the yield and ultimate deformation limits of the column to be identified (see Figure 8). Nielson (2005) defines yield curvature as the curvature corresponding to the first reinforcement bar yielding. This is a purely numerical definition which would not have any correspondence to visible damage in practice in a real pier.

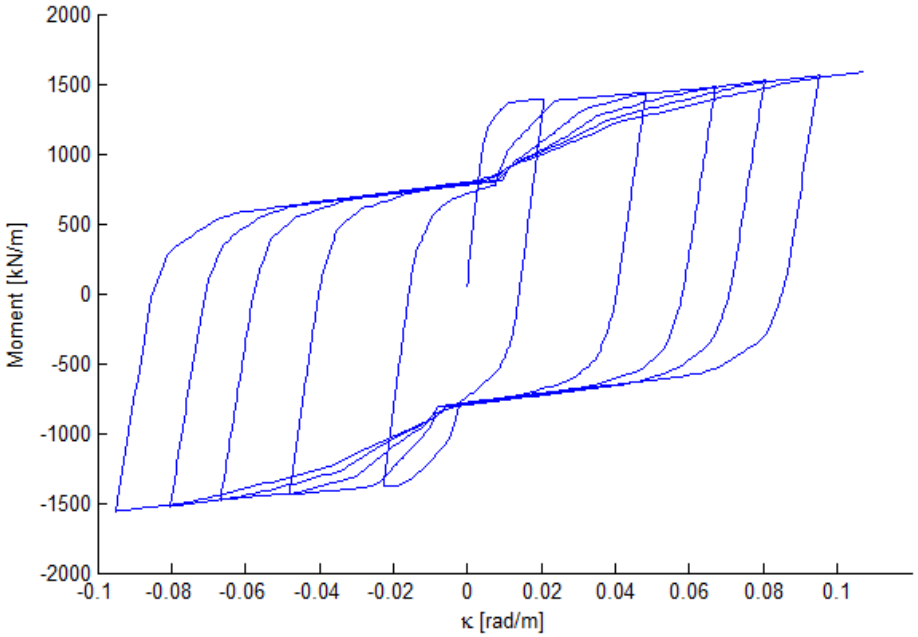

Figure 8: Example of a moment-curvature curve for a single RC pier column with free rotations at the top

Shear failure of the pier is estimated by comparing the shear capacity with the yield capacity associated with flexural behaviour. The occurrence of one of the two mechanisms depends strongly on the nature of the connection of the pier system to the deck, particularly in the case of transverse loading, where the value and location of the maximum bending moment can significantly vary depending on the pier-deck configuration, as shown in Figure 9 (Cardone, 2014). Smaller flexural moments due to the connection of the pier cap to the deck might then favour the shear failure as the main damage mechanism.

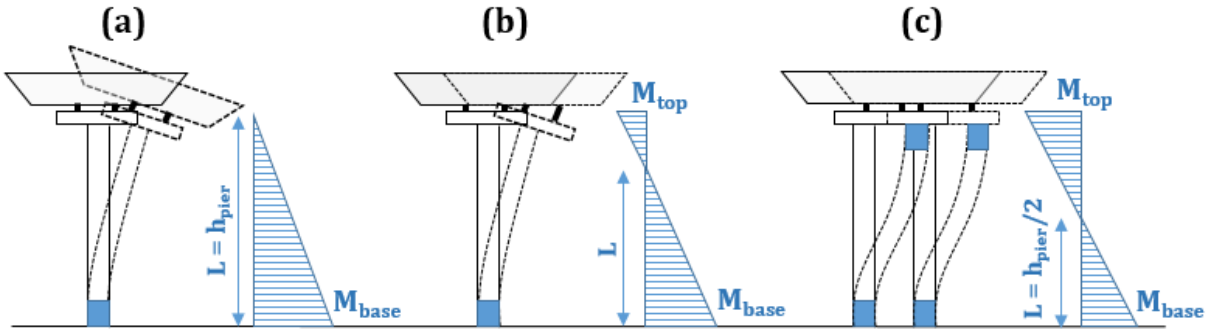

Figure 9: Typical flexural length *L* for (a) Cantilever pier with torsionally free deck; (b) Cantilever pier with torsionally constrained deck; (c) Double bending piers (adapted from Cardone, 2014)

b. Abutments

Seat-type abutments are specifically presented here, because they represent the most widely used abutment type in Italian highway bridges, according to Cardone (2014). Nielson (2005) presents four types of seat-type abutments, depending on the configuration of the supporting piles and walls (see Figure 10).

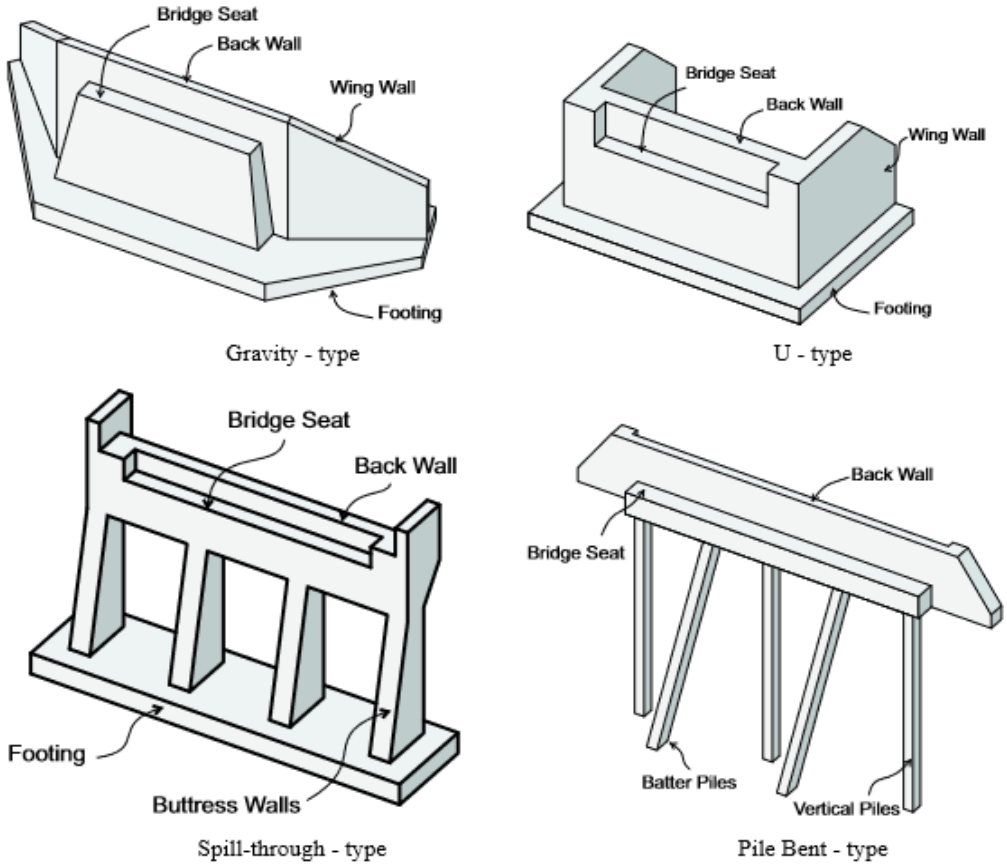

Figure 10: Possible configuration of seat-type abutments (Nielson, 2005; Tonias, 1995)

Whilst the main purpose of abutments is to ensure the support of vertical loads, their purpose is also to withstand horizontal loading, whether it results from traffic loads or from seismic actions.

In the case of longitudinal loading, two types of behaviour can be identified. The first consists of where the bridge deck is pulling away from the abutment (i.e. extension) and the resistance is only provided by the RC piles or walls (i.e. **active** resistance if the deck is connected rather than just seated on the abutment). The second behaviour type consists of where the bridge deck is pushing towards the abutment and the deck-abutment gap is closed (i.e. in compression) and the backfill soil starts to provide some resistance along with the RC pile/walls (i.e. **passive** resistance). The force-displacement relationship of an abutment system, therefore, usually consists of an asymmetrical curve, where both passive and active mechanisms are described, depending on whether the system is in compression or extension (see Figure 11). Dissipating devices, such as dampers, may also be placed at the interface between deck and abutment in order to control this movement and is an important mitigation measure in the case of seismic loading.

In the case of transverse loading, the lateral walls are usually not sufficiently large so as to provide horizontal resistance in terms of the backfill soil. It can therefore be assumed that the pile bent provides most of the resistance (i.e. active behaviour). Shear keys can also be added between the abutment and the deck in order to restrain some of the lateral movements.

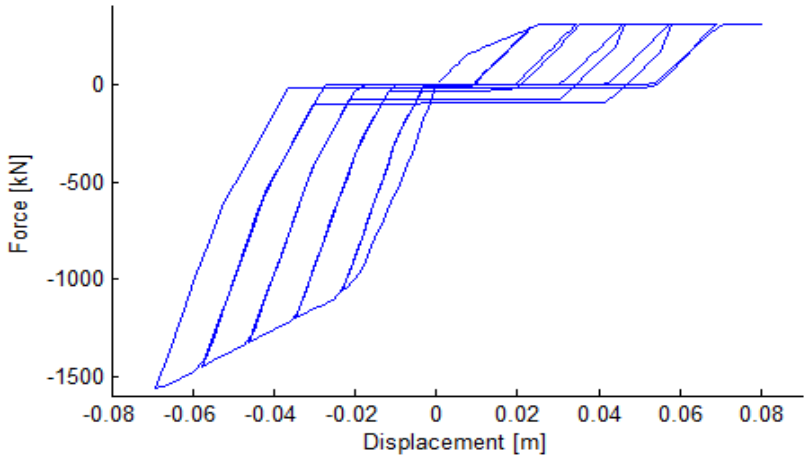

Figure 11: Example of a model representing the behaviour of a seat-type abutment with pile bents. Due to the contribution of the backfill soil, the passive resistance in compression is greater than the active one.

c. Shear keys

Shear keys are RC blocks that are usually present at bridge abutments in order to prevent excessive lateral displacement of the deck. They are generally used as restraints under non-seismic conditions or moderate earthquakes. However, in the case of large earthquakes, they may act as sacrificial elements in order to prevent the damage of more critical components such as abutment walls. According to Caltrans (1993), shear keys can be classified according to their aspect ratio $\alpha = h / d$ (see Figure 12):

- $\alpha < 0.5$: sliding shear friction model;
- $0.5 < \alpha < 1.0$: strut-and-tie model;
- $\alpha > 1.0$: flexural / moment resistance model.

An additional distinction can also be on the location of the shear keys, i.e. whether they are located on the extremity or on the inside of the transversal deck section (exterior and interior shear keys, respectively).

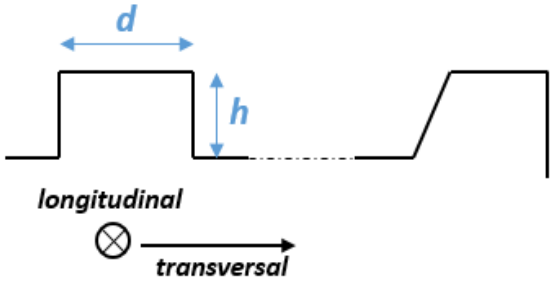

Figure 12: Schematic view of interior (left) and exterior (right) shear keys

d. Bearings

Bridge bearings can be classified depending on the type of movement they allow (Nielson, 2005), i.e. fixed or expansion bearings. Fixed bearings allow rotations only, while expansion bearings permit (to a certain extent) both rotations and translations.

Steel bearings can cover many shapes and designs. Some of the more common bearing types are as follows:

- **Pinned bearings** only allow rotations and they are usually composed of a cylindrical steel pin between the pier cap and the deck superstructure allowing free rotations (see Figure 13).

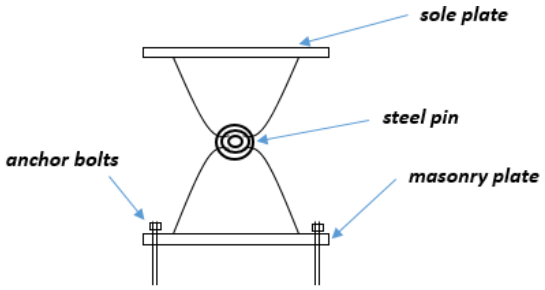

Figure 13: Schematic view of a pinned bearing

- **Rocker bearings**, which are sometimes referred to as steel pendulum bearings, allow only rotations if they are pinned and one-dimensional translations otherwise (see Figure 14). They are also referred to as high-type bearings, as opposed to sliding bearings (low-types).

Figure 14: Schematic view of an expansion rocker bearing (left) and a pinned rocker bearing (right)

- **Roller bearings** allow one-dimensional translations, but no rotational movements. They are composed of one or more steel cylinders than can roll when the bearing takes up forces from the superstructure (see Figure 15).

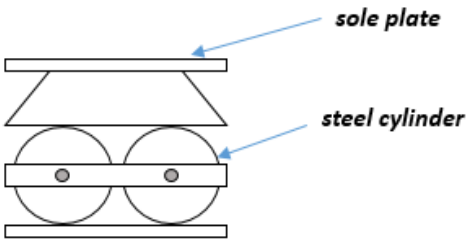

Figure 15: Schematic view of a roller bearing

- **Sliding bearings**, or expansion sliding bearings, allow one dimensional translations but no rotational movements. Meanwhile, the fixed version allows for rotation while restricting translations. They are the simplest form of bearing, since they are mainly comprised of the

sole plate and the masonry plate. The sliding plate is usually made of another material, such as stainless steel or bronze to ease up the sliding. Expansion bearings are usually found with a guide plate that is bolted to the masonry plate in order to limit the translation to one direction (see Figure 16).

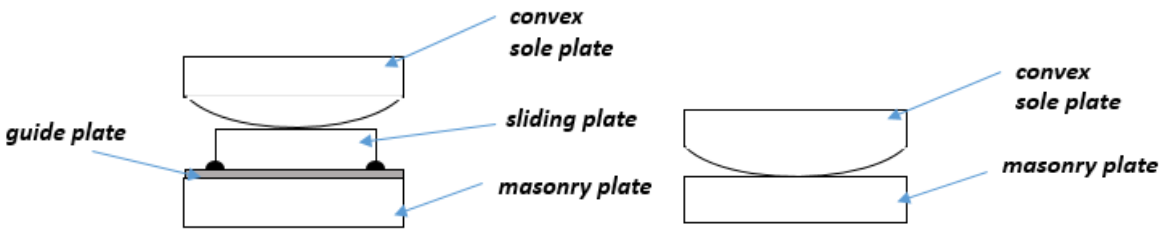

Figure 16: Schematic view of an expansion sliding bearing (left) and a fixed sliding bearing (right)

Apart from steel bearings, elastomeric pad bearings are also a common alternative, and expansion bearings of this type can allow bi-dimensional translations (in both the longitudinal and transversal directions), as well as rotational movements. Elastomeric pads can be either bolted or unbolted to the sole plate, meaning that their respective damage mechanisms differ, as illustrated in Figure 17.

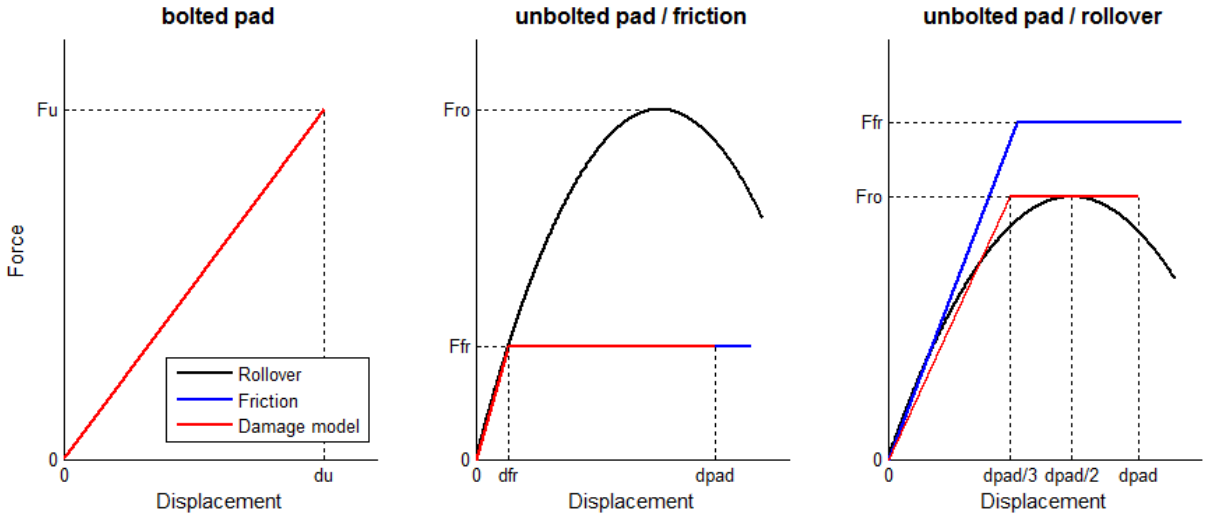

Figure 17: Possible failure mechanisms for neoprene pads: (a) bolted – rubber shear failure (b) unbolted – slipping, if low axial load and thin pad (c) unbolted – rollover, if high axial load and thick pad (adapted from Cardone, 2014)

e. Deck

The deck superstructure can either be made of reinforced concrete or steel, or composite materials. Deck spans are usually supported by steel girders or a box-girder system. For shorter span lengths, slab decks can also be found. These are assembled from precast prestressed concrete sections. Furthermore, a major typological feature that determines the global behaviour of the bridge is whether the deck is simply supported or continuous (i.e. no free rotations of the pier-deck connections).

4.2 Failure modes

The various bridge components have a very specific susceptibility to the different hazard types, as will be outlined in the subsequent. The selected failure modes are summarised in **Table 47** (see Appendix A).

4.2.1 Possible failure modes and corresponding limit states for seismic hazards

In this section, a review is provided of recent studies that describe damage states and limit values for various bridge components exposed to seismic hazards.

a. HAZUS technical manual for earthquakes (NIBS, 2004)

In the HAZUS (NIBS, 2004) framework, the following damage states are identified for bridges:

- **DS2 (Slight/minor damage):** Minor cracking and spalling to the abutment, cracks in shear keys at abutments, minor spalling and cracks at hinges, minor spalling at the column (damage requires no more than cosmetic repair) or minor cracking to the deck.
- **DS3 (Moderate damage):** Any column experiencing moderate (shear cracks) cracking and spalling (column structurally still sound), moderate movement of the abutment (< 2 inches), extensive cracking and spalling of shear keys, any connection having cracked shear keys or bent bolts, keeper bar failure without unseating, rocker bearing failure or moderate settlement of the approach.
- **DS4 (Extensive damage):** Any column degrading without collapse – shear failure - (column structurally unsafe), significant residual movement at connections, or major settlement of the approach, vertical offset of the abutment, differential settlement at connections, shear key failure at abutments.
- **DS5 (Complete damage):** Any column collapsing and connection losing all bearing support, which may lead to imminent deck collapse, tilting of substructure due to foundation failure.

The HAZUS damage scale contains five damage states, with DS1 representing the Intact/No damage State.

b. Nielson (2005)

Nielson (2005) proposes a set of prescriptive limit states for various bridge components (see Table 2). The limit states were defined that at a level that would be evident during physical inspection of a bridge. Specification of each damage state at the component-level by Nielson (2005) is summarized in Table 3.

Component	Damage state			
	Slight	Moderate	Extensive	Complete
Concrete column (curvature ductility)	1.0	1.58	3.22	6.84
High - steel fixed bearing – long. (mm)	6	20	40	255
High - steel fixed bearing – trans. (mm)	6	20	40	255
High - steel rocker bearing – long. (mm)	50	100	150	255
High - steel rocker bearing – trans. (mm)	6	20	40	255
Low - steel fixed bearing – long. (mm)	6	20	40	255
Low - steel fixed bearing – trans. (mm)	6	20	40	255
Low - steel sliding bearing – long. (mm)	50	100	150	255
Low - steel sliding bearing – trans. (mm)	6	20	40	255
Elastomeric fixed bearing – long. (mm)	30	100	150	255
Elastomeric fixed bearing – trans. (mm)	30	100	150	255
Elastomeric expansion bearing – long. (mm)	30	100	150	255
Elastomeric expansion bearing – trans. (mm)	30	100	150	255
Abutment – active (mm)	4	8	25	50
Abutment – trans. (mm)	4	8	25	50

Table 2: Quantitative limit states for bridge components (Nielson,2005).

Component	Damage description			
	Slight	Moderate	Extensive	Complete
Steel bearings	Generation of cracks in the concrete pier	Severe deformation in the anchor bolts	Complete fracture of the bolts (toppling or sliding of the bearings)	Unseating
Elastomeric bearings	Noticeable deformation	Deck may have to be realigned and possible dowel fracture	Necessary girder retention and deck realignment	Unseating
Columns (piers)	Yielding	Cracking	Spalling	Reinforcement buckling
Abutments	Half of first yielding point	First yielding point	Ultimate deformation	Twice the ultimate deformation

Table 3: Description of proposed limit states for bridge piers (Nielson, 2005).

c. SYNER-G project (Crowley et al., 2011; Tsionis and Fardis, 2014)

The FP7 SYNER-G project (2009-2013) has outlined a review of existing fragility curves for roadway and railway bridges. The available fragility functions are harmonized into two damage states, i.e. yielding and near collapse. Damage measures have been defined for piers and elastomeric bearings only. Damage to piers is assessed based on the value of peak chord rotation demand at the member end (at the yield and near collapse damage states), and the member peak shear force demand (at the near collapse damage state only).

For railway bridges, the horizontal deformations, in terms of maximum angle of rotation of the deck ends and maximum curvature across the deck, were also considered in the SYNER-G project as damage measures for the yielding limit state. Values from the Annex A2 to EN 1990 (CEN, 2005) code were adopted (see Table 4).

Speed range V (km/h)	Rotation (rad)	Curvature (1/m)
V ≤ 120	0.0035	1,700
120 < V ≤ 200	0.0020	6,000
V > 200	0.0016	14,000

Table 4: Maximum horizontal rotation and maximum horizontal curvature as a function of traffic speed (CEN, 2005).

For bridge bearings, the SYNER-G project has adopted shear strain deformation and unseating as criteria for the near collapse damage state. Experimental data provided by Bousias et al. (2007) suggest an ultimate shear deformation of γ = 156%. Meanwhile, unseating occurs when the displacement of the deck relative to the pier (in any direction) exceeds half of the bearing length.

The review of available fragility functions in the literature has enabled the different existing limit states for piers and elastomeric bearings to be compared (see Table 5 and Table 6 respectively). There is a large variability between the different limit states proposed. In some cases, absolute drift values are proposed, whilst in other cases, relative measures are proposed in relation to yield curvature or rotation. These values depend greatly on the pier type and the defined damage states, therefore generating epistemic uncertainties in relation to the estimation of the limit state value, as discussed in INFRARISK Deliverable D3.3 (D'Ayala and Gehl, 2015).

Damage measure	Reference	Damage state			
		Slight	Moderate	Extensive	Complete
Drift ratio δ/h	Banerjee & Shinozuka (2008)	1.0%	2.5%	5.0%	7.5%
	Kim & Shinozuka (2004)	0.7%	1.5%	2.5%	5.0%
	Li et al. (2012)	1.5%	2.6%	4.3%	6.9%
	Yi et al. (2007)	0.7%	1.5%	2.5%	5.0%
Curvature ϕ	Avsar et al. (2011)	ϕ_y			ϕ_u
	Cardone et al. (2011)	ϕ_y	0.5 ϕ_u		ϕ_u
	Choi et al. (2004)	ϕ_y	2.0 ϕ_y	4.0 ϕ_y	7.0 ϕ_y
	Jeong & Elnashai (2007)	ϕ_y			
	Nielson & DesRoches (2007)	1.3 ϕ_y	2.1 ϕ_y	3.5 ϕ_y	5.2 ϕ_y
	Padgett & DesRoches (2009)	9.4 ϕ_y	17.7 ϕ_y	26.1 ϕ_y	30.2 ϕ_y
	Zhang et al. (2008)	ϕ_y	2.0 ϕ_y	4.0 ϕ_y	7.0 ϕ_y
Rotation Θ	Qi'ang et al. (2012)	Θ_y	2.0 Θ_y	6.0 Θ_y	11.0 Θ_y
	Saxena et al. (2000)	Θ_y	2.0 Θ_y	6.0 Θ_y	11.0 Θ_y
	Shinozuka et al. (2000)	Θ_y		2.0 Θ_y	
	Yi et al. (2007)	Θ_y	1.3 Θ_y	2.6 Θ_y	
Displacement δ	Monti & Nistico (2002)	0.5 δ_u		0.7 δ_u	δ_u

Table 5: Review of proposed limit states for bridge piers (Tsionis and Fardis, 2014).

Damage measure	Reference	Damage state			
		Slight	Moderate	Extensive	Complete
Shear deformation of elastomeric bearings, γ	Moschonas et al. (2009)	20%	150%	200%	500%
	Zhang et al. (2008)	100%	150%	200%	250%
Displacement in longitudinal direction, δ (mm)	Choi et al. (2004)	1 / -	6 / 50	20 / 100	40 /150
	Ghosh & Padgett (2010)	6 / 37	20 / 104	40 / 136	187 / 187

Table 6: Review of proposed limit states for bridge bearings (Tsionis and Fardis, 2014). (Note: Where two values are present, the left one corresponds to fixed bearings, and the right one to expansion bearings.)

d. Cardone (2014)

In the direct displacement-based seismic assessment of Italian bridges outlined by Cardone (2014), the following performance levels (PL) have been proposed:

- **PL1:** Vey limited structural damage has occurred. The structure retains nearly all of its pre-earthquake strength and stiffness, and although some minor structural repairs may be appropriate, these generally do not require any traffic interruption.
- **PL2:** Significant damage to some structural elements has occurred but a large margin against partial or global collapse still remains. Although the damaged structure is not at imminent collapse risk, it would be prudent to implement structural repairs. This may require traffic interruptions or the installation of temporary bracing systems. The overall risk of life-threatening injury as a result of structural damage is expected to be low.
- **PL3:** Severe damage to some structural elements has occurred but some margin against either partial or global collapse still remains. The structure may be technically repairable but costs would be very high and the closure of the bridge for a long time is inevitable. Injuries may occur during the earthquake; however, the overall risk of life-threatening injury as a result of structural damage is expected to be low.
- **PL4:** The structure continues to support gravity loads but retains no margin against collapse. Extensive structural damage has occurred that potentially implies significant degradation in the stiffness and strength of the lateral-force resisting system and large permanent lateral deformations. Aftershock could induce structural collapse. Significant risk of injury exists and the structure may not be technically repairable.

According to Cardone (2014), the deformation limit states for each of the bridge components (see Table 7) are consistent with each other. Therefore, it is assumed that one component reaching a given damage state corresponds to the equivalent performance level of the bridge system.

+ Piers:

Damage states for piers depend on whether the expected collapse mechanism consists of ductile collapse due to the formation of plastic hinges or brittle shear failure. In the case of flexural failure, the yield and ultimate displacements at the top of the pier, d_y and d_u respectively, can be estimated by assuming an elastic perfectly plastic moment-curvature relationship. In the case of shear failure, the displacement, d_{sh}, is set to correspond to the intersection between the flexural behaviour of the pier and its shear strength (see Figure 18).

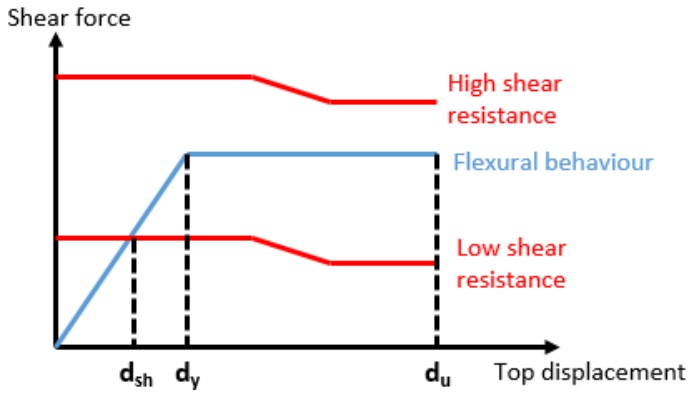

Figure 18: Possible failure modes for piers and corresponding limit values (Cardone, 2014)

+ Abutments:

The focus in this section is on the longitudinal response of seat-type abutments on piles, which represent a typical abutment type in Italian bridges. The behaviour of the abutment depends on the gap between the deck extremity and the abutment back-wall. Until the gap is closed, the deck's inertia forces are mainly soliciting the bearings. After gap closure, the deck is in direct contact with the abutment back-wall and can mobilize the passive backfill pressure. Therefore, the following damage states can be defined:

- **DS1:** deck displacement is equal to d_{gap} (gap width, usually ranging from 20 to 50mm in Italian highway bridges), which corresponds to joint closure.
- **DS2:** deck displacement is equal to $d_{y,ab}$, which corresponds to the attainment of the passive resistance of the backfill soil. Typical values of $d_{y,ab}$ are ranging from 80 to 120mm.
- **DS3:** deck displacement is equal to $d_{y,ab}+2/3(d_{u,ab}-d_{y,ab})$, where $d_{u,ab}$ corresponds to the ultimate displacement of the abutment-backfill system. Experimental studies by Stewart et al. (2007) propose $d_{u,ab} = d_{gap} + 0.10h_w$, where h_w is the back-wall height.
- **DS4:** deck displacement is equal to $d_{u,ab}$.

+ Shear keys:

Shear keys located at the abutments of bridges are generally designed to provide transverse restraint to the deck during service load and moderate earthquakes. In the case of strong earthquakes, shear keys are designed as sacrificial elements to protect abutment walls and piles from damage. This implies that the shear keys should break off before damage occurs in piles and abutment walls. Two damage states are proposed:

- **DS1:** deck displacement in the transverse direction is equal to $d_{gap,t}$, corresponding to joint closure.

- **DS3:** deck displacement in the transverse direction is equal to $d_{u,sk}$, corresponding to shear key failure, either by sliding shear mechanism or by strut and tie mechanism.

+ Fixed bearings:

Fixed bearings that are based on steel hinges or dowel steel bars experience an elastic behaviour until collapse, which is characterized by either attainment of shear strength or premature failure of anchor bolts:

- **DS2:** displacement is equal to d_{fix}, corresponding to the collapse of the device or of the anchor bolts (ratio between shear strength and elastic stiffness).

- **DS3:** displacement is equal to d_{fix}+2/3(d_{uns}-d_{fix}), where d_{uns} is the displacement corresponding to deck unseating from pier cap or lintels.

- **DS4:** displacement is equal to d_{uns}.

+ Pendulum, sliding or roller bearings:

The cyclic behaviour of these bearings is governed by the frictional resistance between sliding/rolling surfaces. These types of bearings are not designed to absorb seismic displacements and their displacement capacity is generally quite low. Sometimes, sliding and roller bearings present a stopper, after reaching their displacement capacity, to prevent deck unseating. On the other hand, pendulum bearings may be subjected to vertical instability. The following damage states are then proposed for sliding and roller bearings:

- **DS1:** displacement is equal to d_{max}, corresponding to the displacement capacity of the bearing under non-seismic conditions (traffic loads, temperature changes, shrinkage, creep, impact forces, etc.).

- **DS2:** displacement is equal to d_{max}+1/3(d_{uns}-d_{max}), where d_{uns} is the displacement corresponding to deck unseating from pier cap or lintels.

- **DS3:** displacement is equal to d_{max}+2/3(d_{uns}-d_{max}), where d_{uns} is the displacement corresponding to deck unseating from pier cap or lintels.

- **DS4:** displacement is equal to d_{uns}.

For pendulum bearings, the proposed damage states are:

- **DS1:** displacement is equal to d_{max}, corresponding to the displacement capacity of the bearing under non-seismic conditions (traffic loads, temperature changes, shrinkage, creep, impact forces, etc.).

- **DS2:** displacement is equal to d_{lim}, where d_{lim} is the horizontal displacement corresponding to vertical instability (e.g. 50-60% of the effective height of the pendulum.

- **DS3:** displacement is equal to d_{lim}+1/3(d_{uns}-d_{lim}), where d_{uns} is the displacement corresponding to deck unseating from pier cap or lintels.
- **DS4:** displacement is equal to d_{uns}.

+ Neoprene pads:

Neoprene bearings exhibit a visco-elastic behaviour and can experience different failure mechanisms. These include the following: rubber shear failure for bolted neoprene pads; slipping between neoprene and concrete surfaces, and roll-over mechanism for unbolted neoprene pads.

Bolted neoprene pads usually exhibit a linear visco-elastic behaviour up to shear strains of the order of 200-300%. Therefore, the proposed limit states are expressed as a function of the shear strain amplitude of rubber. Unbolted neoprene pads with small rubber thickness and/or low load pressure usually experience a slipping failure mechanism. Beside large residual displacements, slipping can also produce damage to bearings, through tearing of rubber, distortion of steel reinforcement and heating generated by sliding. A linear visco-elastic behaviour followed by pure friction behaviour is expected for such a mechanism. Therefore the proposed limit states are the following:

- **DS1:** displacement is equal to d_{fr}, corresponding to the attainment of the friction resistance.
- **DS2:** displacement is equal to d_{fr}+1/3(d_{pad}-d_{fr}) where d_{pad} is the pad dimension in the motion direction.
- **DS3:** displacement is equal to d_{pad}.
- **DS4:** displacement is equal to d_{uns}.

The roll-over mechanism may occur with unbolted neoprene pads with large rubber thickness and/or high load pressure. The free edges of the bearing rotate and the originally vertical surfaces of each side come in contact with horizontal surfaces at both top and bottom. Horizontal displacement beyond this point can only be achieved by slipping. It is assumed that the peak horizontal force associated with a roll-over mechanism is attained for a displacement of the order of $d_{pad}/2$. Therefore the proposed limit states are as follows:

- **DS1:** displacement is equal to $d_{pad}/3$.
- **DS2:** displacement is equal to $d_{pad}/2$.
- **DS3:** displacement is equal to d_{pad}.
- **DS4:** displacement is equal to d_{uns}.

Element	Failure mode	PL1	PL2	PL3	PL4
		Slight Damage	Moderate Damage	Severe Damage	Collapse Prevention
Piers	Flexural	d_y	$d_y+1/2(d_u-d_y)$	$d_y+2/3(d_u-d_y)$	d_u
	Shear	-	-	d_{sh}	$1.1d_{sh}$
Abutment		$d_{gap,l}$	$d_{y,ab}$	$d_{y,ab}+2/3(d_{u,ab}-d_{y,ab})$	$d_{u,abs}$
Shear keys		$d_{gap,t}$	-	$d_{u,sk}$	-
Fixed bearings		-	d_{fix}	$d_{fix}+2/3(d_{uns}-d_{fix})$	d_{uns}
Steel pendulum		d_{max}	d_{lim}	$d_{lim}+1/3(d_{uns}-d_{lim})$	d_{uns}
Sliding/roller bearings		d_{max}	$d_{max}+1/3(d_{uns}-d_{max})$	$d_{max}+2/3(d_{uns}-d_{max})$	d_{uns}
Neoprene pads (unbolted)	Friction / slipping	d_{fr}	$d_{fr}+1/3(d_{pad}-d_{fr})$	d_{pad}	d_{uns}
	Rollover	$d_{pad}/3$	$d_{pad}/2$	d_{pad}	d_{uns}
Neoprene pads (bolted)		$d_{\gamma=150\%}$	$d_{\gamma=200\%}$	$d_{\gamma=300\%}$	d_{uns}

Table 7: Proposed limit states for bridge components, from Cardone (2014).

e. Summary of possible failure modes

A summary of the literature in relation to fragility functions for bridge components has demonstrated that the damage states, in general, have been selected to ensure consistency of the performance of both component- and system-level. In other words, if any component has reached a given local damage state, it is assumed that the whole bridge system is in a similar global damage state.

Each of the studies examined have proposed the same number of damage states, with roughly equivalent descriptions in terms of failure types. Therefore, it is possible to identify four distinct damage states (i.e. Slight / Moderate / Extensive / Complete) that could include most of the damage definitions found in the literature, as outlined in Figure 19.

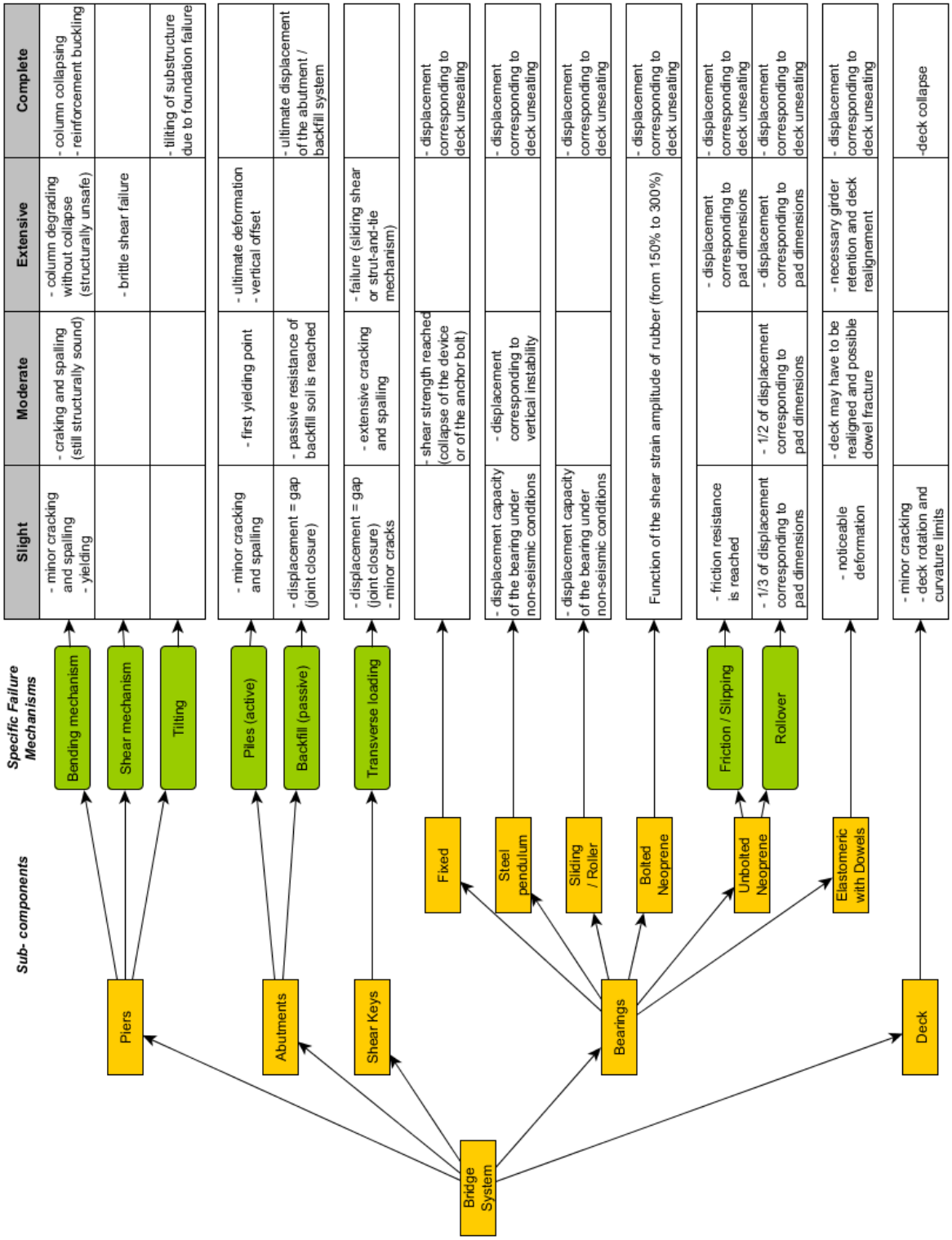

Figure 19: Summary of possible failure modes for common bridge components due to ground shaking.

4.2.2 Possible failure modes and corresponding limit states for ground failure hazard

There is little available information in the literature in relation to bridge failures due to ground failures, which may be due to the fact that bridge piers are commonly designed with deep footings and foundations, thus preventing the immediate failure of piers due to ground displacement.

In the case of deep landslides or slope failures that generate ground displacement below the depth of the pier footing however, it is possible to witness significant differential displacements at the bridge deck level. For example, the Peace River suspension bridge in Canada collapsed in 1957 due a deep landslide that occurred beneath the bridge abutment at the level of the shale bedrock.

A more common failure associated with the bridge abutment is where the backfill soil behind the abutment has not been well compacted during the construction phase: earthquake shaking can induce substantial differential settlements and pavement damage on the approach to the abutment (i.e. earthquake-induced ground failure). This type of failure is commonly known as the highway "bump" (Puppala et al., 1999; Helwany et al., 2007) and is mainly due to the difference in foundation quality between the abutment and the approach slab, with the bridge system usually experiencing considerably less vertical settlement than the adjacent pavement. This failure type does not result in very extensive damage and Werner et al. (2006) propose a damage scale based on the extent of approach-fill settlement in inches:

- **No damage:** settlement < 1 in, no repairs needed.
- **Slight damage:** settlement between 1 and 6 in, repair consists of mud jacking (coring holes and pumping in grout) and then ramping up with A/C.
- **Moderate damage:** settlement > 6 in, temporary repairs involve building up an A/C ramp, and permanent repairs can be done during off hours (assuming only small-moderate settlement and no fault rupture).

The different damage modes identified are summarized in Figure 20.

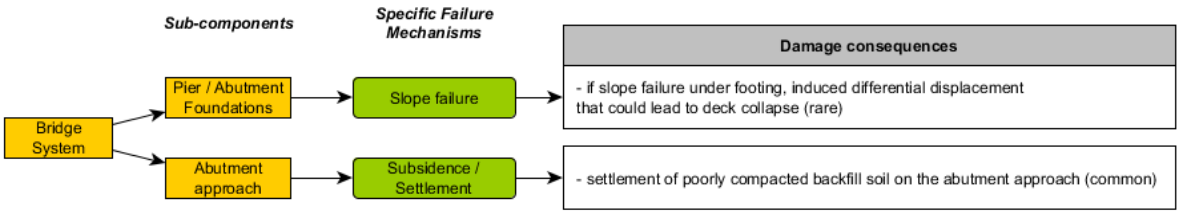

Figure 20: Summary of possible failure modes for common bridge components due to soil failure.

Another common damage mode is the impact of debris that may have been generated by an upstream landslide, with the potential to damage the piers and the deck or to obstruct the water channel.

Other examples of bridge damage due to earthquake-induced liquefaction have been described by Dickenson et al. (2002) and Bartlett (2014), which occurred during the following earthquakes: Alaska, 1964; Niigata, 1964; Loma Prieta, 1989; Costa Rica, 1991; Kobe earthquakes, 1995. Most of

the identified failure modes consist of the deformation of bridge embankments or the settlement or tilting of pile foundations, potentially leading to deck unseating in bridges with shallow foundations. Bird and Bommer (2004) have reviewed the effect of earthquake-induced ground failures and have described two main damage mechanisms: 1) lateral spreading of the ground resulting in the failure of slopes or free face (e.g. at bridge abutments) and 2) the vertical settlement of the approach embankments. These two failure modes correspond to the failures previously described in

Figure **20**. Dickenson et al. (2002) come up with the same conclusions (i.e. lateral spread on slopes and ground settlement at bridge approaches), even though some pile failure modes are also mentioned (e.g. buckling, plastic hinge or excessive rotation).

4.2.3 Possible failure modes and corresponding limit states for flood hazard

This section reviews some of the recent studies that describe damage states and limit values for various bridge components exposed to flood hazards.

a. HAZUS technical manual for floods (NIBS, 2005)

According to the HAZUS Flood Model (NIBS, 2005), bridges are not considered as highly vulnerable to inundation mechanisms. However, the foundations of bridge piers can be strongly affected by erosion or scour and the bridge deck is also susceptible to dislodgement by the hydraulic pressure. Therefore the following failure modes can be considered for bridges due to flood hazards:

- Scour at the pier / abutment foundations: the impact on the overall bridge stability may be different whether the deck simply supported or continuous. Most bridge failures occur with simple spans, therefore HAZUS (NIBS, 2005) recommend that the expected damage for continuous span bridges should be taken to be 25% of that for simple span bridges.
- Overtopping and hydraulic pressure applied on deck.

Scour vulnerability grades are defined for bridges that range from excellent to critical conditions, which depend on the current state of the foundations, the scour level or the existence of scour countermeasures. Damage tables linking scour vulnerability grades and scour depth (expressed as a dimensionless ratio) were proposed by Pearson et al. (2002) in the HYRISK methodology (see Table 8**Error! Reference source not found.** and Figure 21).

Scour Vulnerability Grade	Dimensionless Depth Ratio				
	0 – 0.25	**0.25 – 0.50**	**0.50 – 0.75**	**0.75 – 1.00**	**> 1.00**
0 (Bridge failure)	1.000	1.000	1.000	1.000	1.000
1 (Bridge closed)	1.000	1.000	1.000	1.000	1.000
2 (Extremely vulnerable)	0.250	0.400	0.550	0.700	0.880
3 (Unstable foundations)	0.140	0.200	0.300	0.450	0.650
4 (Stable, action required)	0.060	0.100	0.150	0.260	0.410
5 (Stable, limited life)	0.002	0.002	0.002	0.030	0.100
6, U (Unassessed / Unknown)	0.100	0.150	0.225	0.355	0.530
7 (Countermeasure installed)	0.100	0.150	0.225	0.355	0.530
8 (Very good conditions)	0.002	0.002	0.002	0.010	0.050
9 (Excellent conditions)	0.002	0.002	0.002	0.002	0.010

Table 8: Scour failure probability as a function of scour vulnerability grade and the dimensionless depth ratio (Pearson et al., 2002).

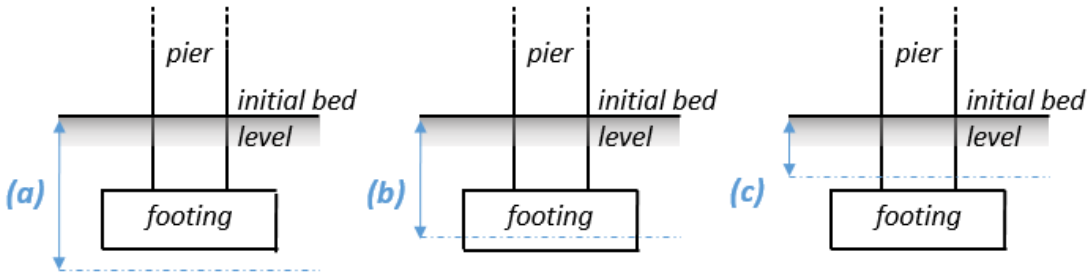

Figure 21: Scour levels with respect to bridge footing: (a) below footing (grades 2 and 3); (b) within limits of footing (grades 4 and 5); (c) above top of footing (grades 8 and 9).

b. American Lifeline Alliance report (ALA, 2005)

The American Lifeline Alliance report (ALA, 2005) on local road systems is based on the analysis of several case studies. This led to the identification of some of the most common failures modes for roadway bridges due to flood hazards, which include the following:

- Local scour at piers and abutments with and without permanent structural damage;
- Downcutting of streambeds, which may affect bridge abutments/piers and undercut culvert inlets and outlets;
- Washout of gravel low-water crossings;
- Deposition of bed load that restricts the hydraulic capacity of crossings;
- Debris accumulation that may contribute to backup of water and damage to adjacent properties;
- Shifting of bridge decks due to pressure of rising floodwaters;
- Shifting or migration of waterway channel alignment.

However, some of these damage mechanisms are mostly applicable to minor roads with low clearance crossings, and therefore, are not applicable to highway bridges, which are the main focus in the INFRARISK project.

c. Lin (2012)

Lin (2012) has identified four main types of bridge failure modes due to scour:

- Vertical failure - this is mainly due to inadequate vertical bearing capacity of the soil and it can manifest through four different failure modes:
    - Undermining of footing base;
    - Penetration of friction pile;
    - Undermining of pile tip;

- Buckling of pile.

- Lateral failure - this is due to the reduction of the lateral restraints of pier foundations, which may lead to three different failure modes:
  - Pushover failures of piers: significant scour depths reduce the lateral resistance capacity of the soil and the pier, which alters the pushover capacity of the bridge, while lateral loads due to water flow and accumulation of debris tend to increase;
  - Structural hinging of piles: it occurs when the transverse loads applied to the piers trigger excessive bending moments at the base of the piers;
  - Kick-out failures of foundations: if the scour excavates most of the depth of the pier foundations, the lateral loads may dislodge the foundations from the remaining soil cover. This failure mode is especially frequent in the case of shallow foundations.

- Torsional failure - this may occur when skewed flows (i.e. flows with an angle of attack) produce eccentric loads and lead to torsional deformation of piers and piles;

- Bridge deck failure – this may occur when the flow height reaches the deck level and washes out the deck (i.e. overtopping), especially in the case of simply-supported deck spans. It could be argued that this failure mode is more generic to fluvial flood and not limited to scour failure.

A summary of the different failure modes observed over 36 case-study bridges in New Zealand, United States and Canada is detailed in Table 9 (Lin, 2012).

Failure modes	Number	Percentage
Vertical failure	**11**	**30%**
Buckling	2	5%
Other	9	25%
Lateral failure	**14**	**39%**
Structural hinge	5	14%
Pushover failure	4	11%
Other	5	14%
Torsional failure	**1**	**3%**
Bridge deck failure	**1**	**3%**
Others	**5**	**14%**
Not identified	**4**	**11%**
Total	*36*	*100%*

Table 9: Review of **f**ailure modes of 36 scour failures (Lin, 2012).

d. Railway bridge failure during flood in the UK and Ireland (Benn, 2012)

Benn (2012) has compiled historical events of railway bridge failures due to scour. In total, 69 events were recorded between 1845 and 2012 and they are summarized in Table 10.

Dominant cause of failure	Number of events	Percentage
Pier scour	23	34%
Abutment scour	14	20%
Floating debris	10	14%
Other debris	10	14%
Embankment scour	8	12%
Channel modification (e.g. dredging)	4	6%

Table 10: Failure classification of 69 water-related failures to railway structures (Benn, 2012).

e. Summary of possible failure modes

It has been shown that the most common bridge components to be affected by flood hazards are the pier/abutment foundations (due to scour) and the bridge deck in specific situations (i.e. overtopping). Floods can also result in more spatially distributed disruptions, such as the modification of the waterway channel, which may affect larger areas around the bridge.

Unfortunately, available studies and reports are usually limited to a qualitative description of the various failure modes, without any indication on the severity of the induced damage. Only for local scour is it possible to introduce some progressive limit states, though the use of the scour vulnerability grades and of the scour depth with respect to the position of the footings. The most common failures modes are presented in Figure 22.

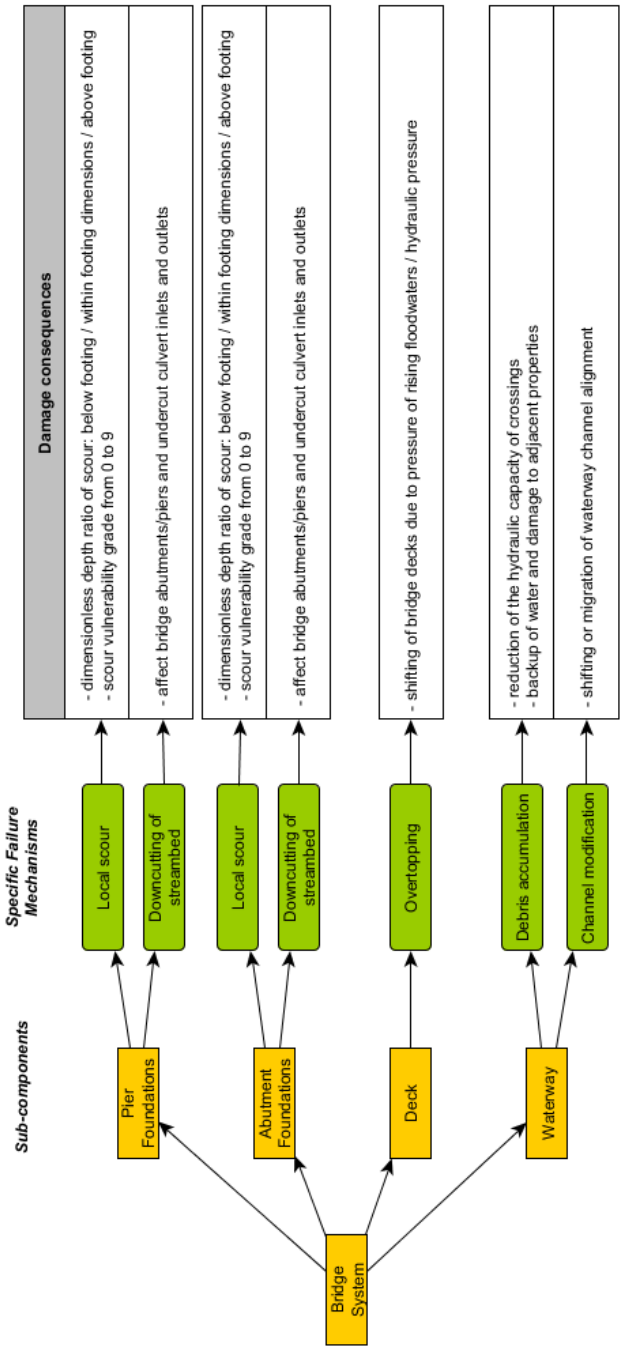

Figure 22: Summary of possible failure modes for common bridge components due to flooding.

4.3 Available fragility functions

This section describes the available bridge fragility functions in relation to seismic, ground failure and flood hazards.

4.3.1 Fragility functions for seismic hazard

The SYNER-G database of bridge fragility functions (Silva et al., 2014) contains 373 curves for various typologies, extracted from approximately 30 literature references. The distribution of the fragility derivation methods is detailed in Figure 23, where the majority of fragility curves were derived from

dynamic non-linear analyses and PGA is the most common IM of choice. The reason for the low proportion of empirical fragility curves for bridges may lie in the lack of focus on infrastructure components during post-earthquake surveys (at least until recently), as well as the limited number of bridges damaged by an earthquake in any given event, when compared to buildings.

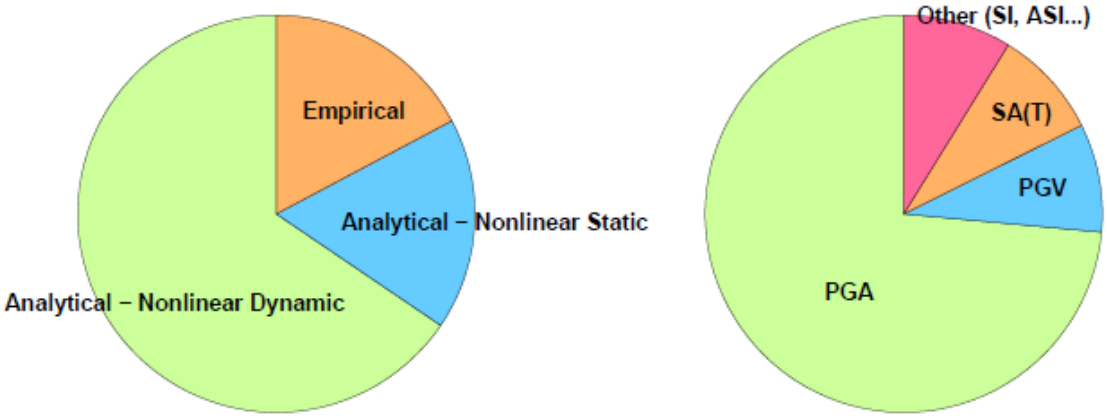

Figure 23: Proportion of derivation methods (left) and selected IMs (right) among the references considered in the SYNER-G database.

According to Crowley et al. (2011), RC bridges represent the vast majority of the studied typologies, 76% of them consisting of bearing-isolated pier-deck connections, the rest of them forming a monolithic pier-deck block. In the case of bridge decks that are supported by bearings, a further distinction has to be made between independent deck spans (i.e. bearings allowing translational movement between two deck spans) and continuous decks (i.e. bearings mainly allowing free rotation between the pier and the deck).

It is also possible to identify the geographical area for which the bridge fragility functions have been derived, as shown in Figure 24. The apparent high proportion of European fragility curves should be moderated by the fact that most of these curves have been derived during the SYNER-G project and are extracted from a single reference (Tsionis and Fardis, 2014). On the contrary, fragility curves for bridges in the United States are found in a variety of references, thus covering a larger range of typologies and derivation methods.

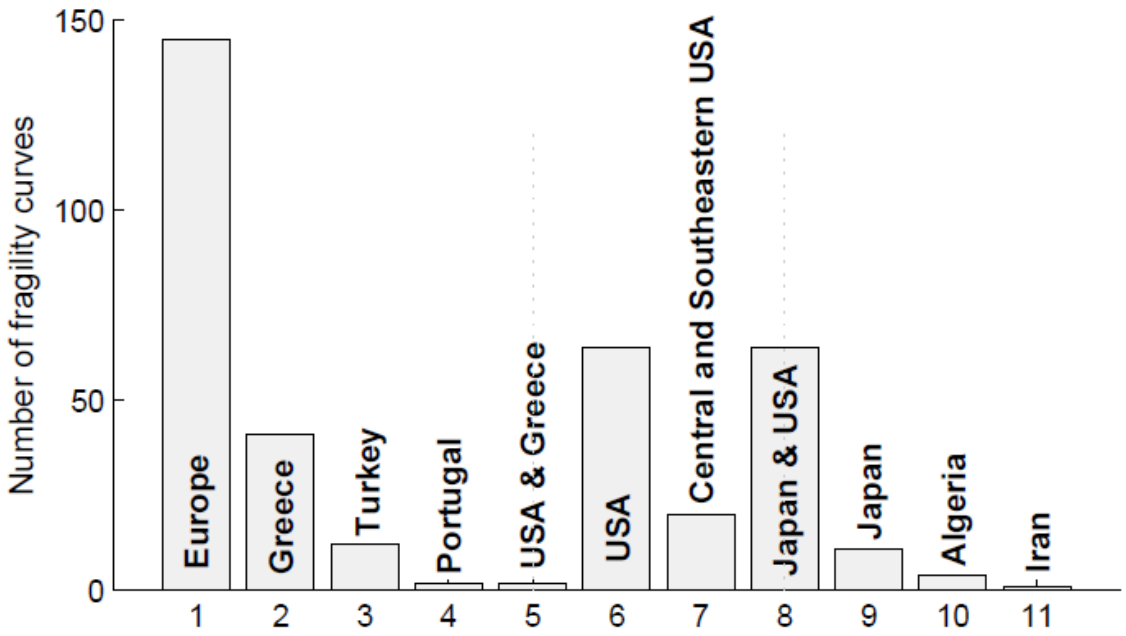

Figure 24: Geographical areas of applicability for the fragility curves contained in the SYNER-G database.

Tsionis and Fardis (2014) have also provided a comparative analysis of the respective merits of non-linear static and dynamic analyses, confirming the ability of non-linear dynamic analyses to account for the contribution of higher modes and for the ground-motion variability, while pushover-based fragility curves are usually derived with an arbitrary standard deviation. In general, fragility curves have been either defined for a single bridge or for a class of bridges. When generating fragility curves for a class of bridges, bridge taxonomies are created to define a variable space from which a set of mechanical or geometrical properties can be sampled (e.g. Padgett and DesRosches, 2007). In order to optimize the number of analyses on the different bridge models, parametrized fragility curves can then be derived, where the evolution of the fragility parameters as a function of the model variables is represented on a response surface (De Felice and Giannini, 2010; Park and Towashiraporn, 2014).

More recently, advanced fragility curves have been developed, as follows:

- Fragility curves have been derived for retrofitted bridges to quantify the effect of different retrofit measures on the bridge vulnerability (Padgett and DesRosches, 2009).
- The effect of the skew angle on the fragility curves has been studied by Avsar et al. (2011), where an increase in the mean of the fragility curve is observed for skew angles higher than 30.
- Spatial variability in the seismic loading for large span bridges may have a detrimental impact on the fragility curves, depending on the soil heterogeneity and the wave propagation velocity that can induce a loss of coherence in the input signal (Saxena et al., 2000; Lupoi et al., 2005).

- Temporal fragility curves can assess the vulnerability over the lifetime of the bridge, accounting for effects such as corrosion (Ghosh and Padgett, 2010), flood scour or cumulated seismic loadings (Franchin and Pinto, 2009).

While Tsionis and Fardis (2014) have proposed a method for fast fragility analysis of regular bridges with a reduced set of parameters such as the deck-pier connection type and the bridge geometry (e.g. pier height, span length), this approach follows the design procedures of Eurocode 2 (CEN, 2004a) and Eurocode 8 (CEN, 2004b), based on the level of seismic design. As a result, significant effort is still needed to assess the fragility of bridge with low design levels, prior to the application of Eurocodes.

4.3.2 Fragility functions for ground failure hazard

There is currently no fragility model available for bridge systems subjected to slope failure. The wide range of possible configurations regarding the bridge system and its soil environment makes it difficult to derive fragility functions for a given typology. In this case, the derivation of fragility functions should be case dependent, since a careful analysis of the bridge-soil configuration is usually required (e.g. soil conditions, near-surface geology, slope grade, position of foundations, etc.). Slope fragility curves may then be developed for a given case study, by using probabilistic slope stability analyses (Wu, 2013; Wu, 2014), where the factor of safety may be estimated with the limit equilibrium method (i.e. Bishop's simplified method), assuming a circular slip surface. The introduction of variability in the input parameters (i.e. epistemic uncertainties) can lead to the computation of a reliability index for the slope, thus leading to a fragility curve for slope failure.

The most common ground failure mode of bridges is the subsidence/settlement of the backfill soil, which may be quantified by performing a finite element analysis in order to estimate the permanent strain of the supporting soil when subjected to a ground motion time history at the base. Therefore an approach that is similar to the derivation of analytical fragility curves for embankments (Argyroudis and Kaynia, 2014; Argyroudis and Kaynia, 2015) may be used. Finally, fragility curves for the backfill of bridge abutments are proposed in Argyroudis and Kaynia (2014), with a bridge with a vertical retaining wall, for varying heights and EC8 soil types. The resulting fragility curves express the probability of exceeding four damage states as a function of PGA (i.e. earthquake-induced ground failure).

4.3.3 Fragility functions for flood hazard

Fragility curves for bridges with respect to flood hazard are less common than for seismic hazard, however a few references are presented in Table 11.

Reference	Method	Typology	Intensity Measure
Scour failure			
Alipour et al. (2013)	Analytical.	- Multi-span multi-column RC bridge	Scour depth
Tanasic et al. (2013)	Analytical.	- Multi-span continuous RC bridge	Soil cover height at the pier
Overtopping (deck unseating)			
Kameshwar and Padgett (2014)	Analytical. Logistic regression with non-linear terms.	- Multi-span simply supported concrete girder bridges (Eastern Southern U.S.)	Difference between bridge height and water height

Table 11: Available bridge fragility curves for flood hazard, in the case of scour or overtopping.

In the case of deck unseating due to water overtopping, the fragility model by Kameshwar and Padgett (2014) may be employed for a fluvial flood hazard. However, it should be noted that this model has been originally derived for multiple hazards, namely earthquakes and hurricanes. As a first approximation, fragility with respect to water height only may be obtained by setting the wave height and the earthquake intensity measure to zero.

The fragility curves proposed by Alipour et al. (2013) may not be seen as scour fragility curves per se, in the sense that they do not represent the direct bridge damage with respect to scour. Instead, scour depth is used as a modifying coefficient to adjust the parameters of the corresponding seismic fragility curve. Therefore this reference should be put to better use in the context of combined hazards (i.e. scour and earthquake).

Tanasic et al. (2013) have developed actual scour fragility curves that express the probability of bridge failure as a function of the height of ground that is still covering the pier foundations (i.e. the complement of the excavated scour depth). The bridge failure mode is explained by the degradation of the elastic and/or plastic soil parameters. This phenomenon can either induce:

- The sinking of the pier foundations, which in turn triggers a pier displacement, leading to kinematic mechanisms in the bridge.
- The degradation of the bearing capacity of the soil, until it is exceeded by the contact pressure load at the foundation.

No fragility curves for bridge failure due to debris accumulation (i.e. floating debris which are transported by the flood) are available. However, the detrimental effect of debris accumulation on the scour depth has been experimentally studied by Lagasse et al. (2010), for different shapes, sizes and porosity levels of debris masses. Regarding analytical models and scour equations (Richardson and Davis, 1995), the effect of debris accumulation may be approximated by an increased effective pier diameter, especially if the debris mass is located at the water surface on a single circular pier (Melville and Dongol, 1992). Other studies have also demonstrated that debris accumulation

increase flow velocity and bed shear, thus leading to aggravated general scour (Diehl, 1997; TAC, 2004).

4.4 From physical damage states to functional states

Once the physical damage states are defined and estimated through the application of fragility function curves, they need to be translated into functionality measures in order to properly estimate the effect of the damaged network elements on the global system performance, through the use of elaborate traffic models.

4.4.1 Correspondence between Component damage states and functionality loss

Functionality measures have to be useful for the subsequent network analysis, depending on the various global metrics that are studied, such as the amount of traffic, the additional delay, the travel distance between two locations or the possibility to conduct emergency operations (e.g. Modaressi et al., 2014). To this end, the following loss metrics are proposed to characterize the functional state of a given network element:

- **Functionality Loss (FL):** loss of functionality induced by the damage to the element. It can have various effects on the normal operation conditions: reduction of the speed limit, closure of a proportion of lanes, reduction of the vertical load capacity. Speed limits and number of lanes are key parameters to estimate the flow capacity of a road section, which is an essential component of network analysis models. Finally, the reduction in load capacity can provide indications on the type of traffic that will be allowed through the road section (e.g. personal cars, trucks, emergency vehicles, etc.).

- **Duration of intervention (Du):** the duration of the repair operations until the element is functional again.

- **Cost of intervention (Co):** the cost of the repair operations, generally expressed as a percentage of the replacement cost.

- **Functionality Loss during Intervention (FLI):** the additional functional loss that is induced by the repair operations.

These four loss metrics will serve different purposes, namely (i) quantification of the direct costs thanks to Co, (ii) quantification of indirect costs (i.e. consequences of traffic disruption) resulting from FL and Du, and (iii) elaboration of time-dependent restoration strategies resulting from FL, Du and FLI.

In order to efficiently quantify these loss metrics, it is necessary to consider the physical damage states at the component level, since it has been seen that each component type has very specific failure mechanisms when exposed to different hazard types. Therefore it is proposed to associate loss metrics with each of the failure modes summarized in Appendix A. To this end, a survey form has been sent to infrastructure managers and experts within the INFRARISK consortium, with the objective of quantifying the four loss metrics that correspond to each component failure mode. Three groups of experts have provided answers to the survey:

- **Group 1:** Five years of engineering experience on geotechnical works on transport networks, both design and contractual. Furthermore, relevant literature was consulted (Zezere et al., 2008; Klose, 2015; Transport Research Board guidelines, etc.).

- **Group 2:** Experts from various fields were solicited: geotechnical engineering, linear infrastructure, materials (pavements), structures (bridges), underground construction. They are working in technical departments providing support to construction sites worldwide, from Australia or Chile to Canada, the States or the UK. The range of experience of the different persons varies from a minimum of 10 years to probably 30 or more.

- **Group 3:** About 20 years of experience in inspection, assessment and maintenance of infrastructure elements. Replies were solely based on own experience and expert judgment, without the use of any 'documentation' or specific case studies assessed.

All groups of experts pointed out the difficulty in providing accurate answers for 'generic cases', since the loss metrics may vary greatly depending on the type of bridge (e.g. size, importance in the network, construction method, etc.). Another issue lies in the harmonization of the answers within each group, some proposed values varying greatly between the experts. Therefore all the answers are provided in the form of lower and upper bounds, in order to account for epistemic uncertainties. The results of the loss assessment survey are summarized in Appendix B.

The intervals of loss values proposed by each group of experts are then reconciled by building a probabilistic functionality model for each type of loss metric: an empirical cumulative distribution function can be assembled for each component damage state, as shown in Figure 25.

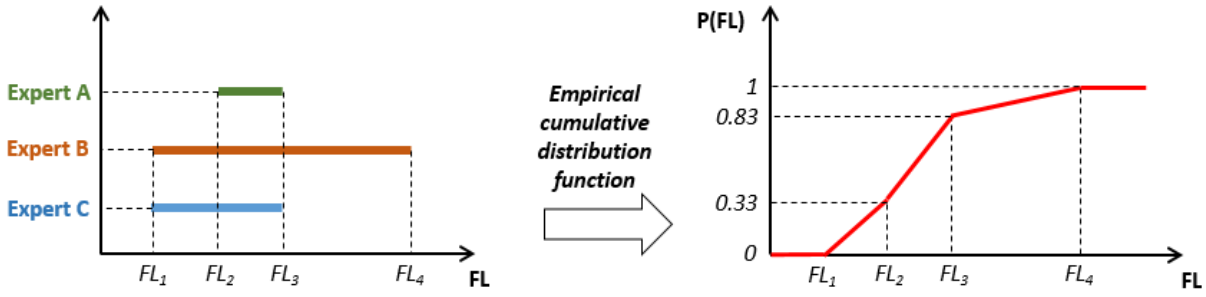

Figure 25: Construction of a probabilistic functionality model based on the expert-based survey, by assigning equal weight to all experts' answers.

This functionality model may then be used to sample the functional loss of a given infrastructure element based on the damage state of one of its components.

4.4.2 Functionality models for global damage states

The functionality models presented in the previous section enable the functional losses that are induced by a given failure mode to be estimated at the component level. However, such models require the specific development of component fragility functions, which will be the objective of section 4.6. Currently, global fragility functions are the most common model to quantify the vulnerability of a bridge system (e.g. Silva et al., 2014). Therefore, in order to be consistent and to

ensure the usefulness of these functionality models when existing fragility curves are used, it is proposed to develop probabilistic functionality models for system-level (or global) damage states.

As explained in section 4.2.1, most system-level damage scales for seismic risk are defined so that they are consistent across the various component damage states, e.g. a global damage state DS1 (i.e. slight or minor damage) is reached if one of the bridge components is in damage state DS1 (e.g. yielding of pier reinforcement, gap closure at bearings or abutments, etc.). The component failure modes in **Table 47** follow the same logic in the way the damage states are enumerated from D1 to D4. Therefore, for a given global damage state, all corresponding component-level loss metrics are assembled as shown in Figure 25. Finally, these assumptions enable functionality models to be developed for global damage states DS1 to DS4, for each of the loss metrics. The probabilistic functionality curves are presented in Figure 26 to Figure 31.

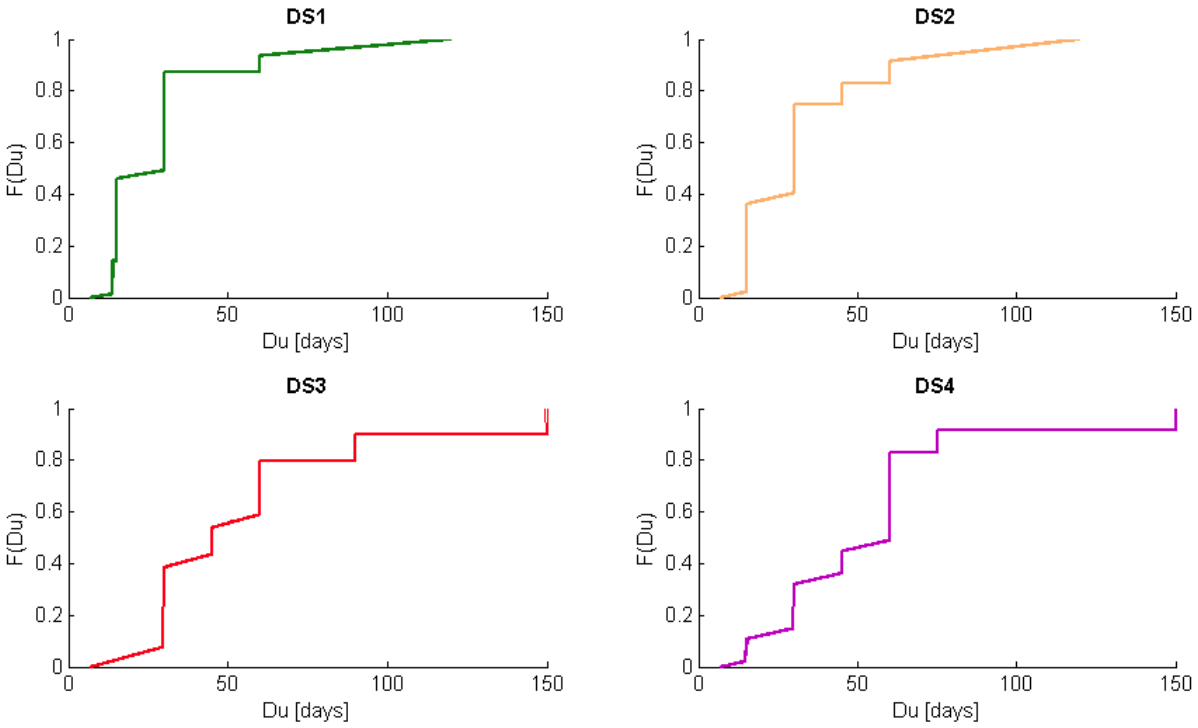

Figure 26: Duration of repair operations given global damage states DS1 to DS4.

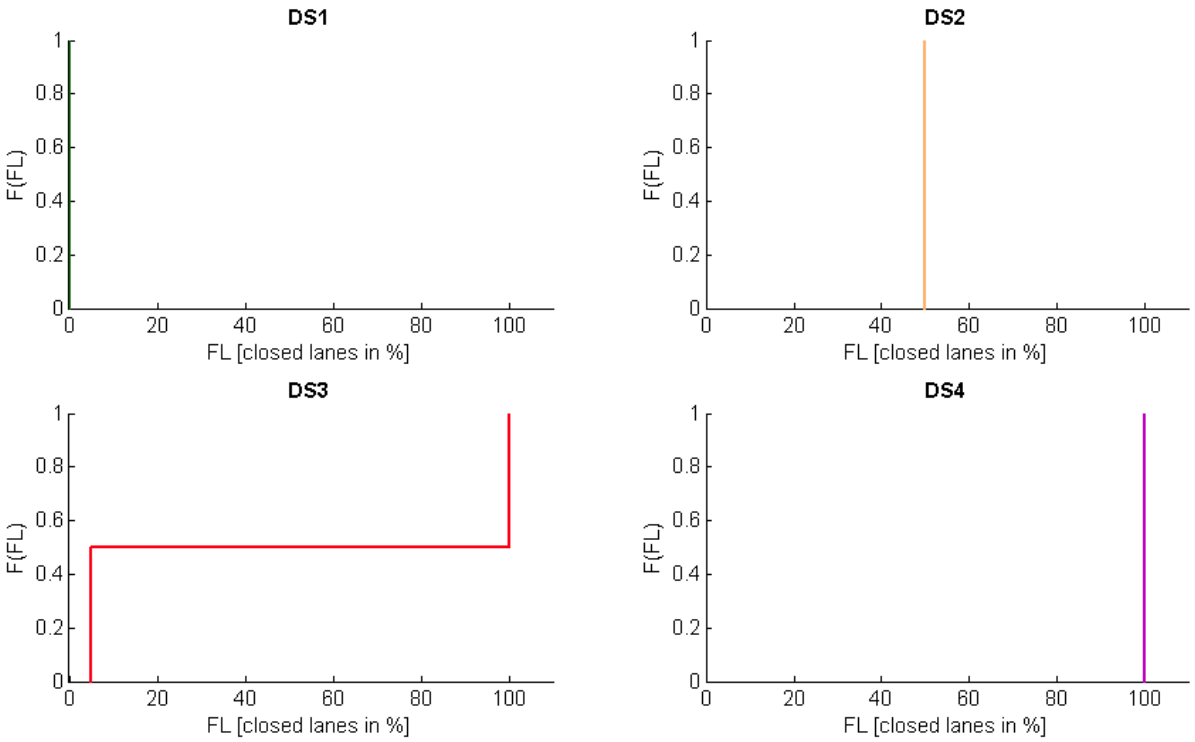

Figure 27: Functionality loss (expressed in proportion of closed lanes) given global damage states DS1 to DS4.

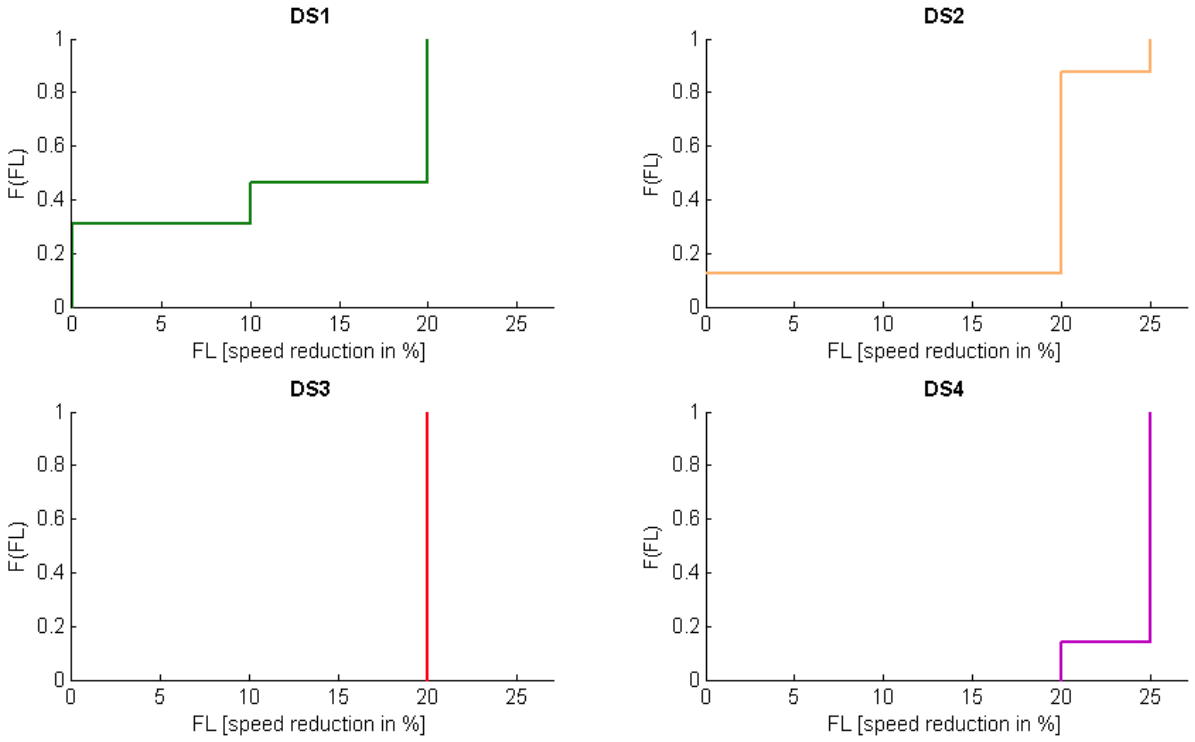

Figure 28: Functionality loss (expressed in speed reduction) given global damage states DS1 to DS4.

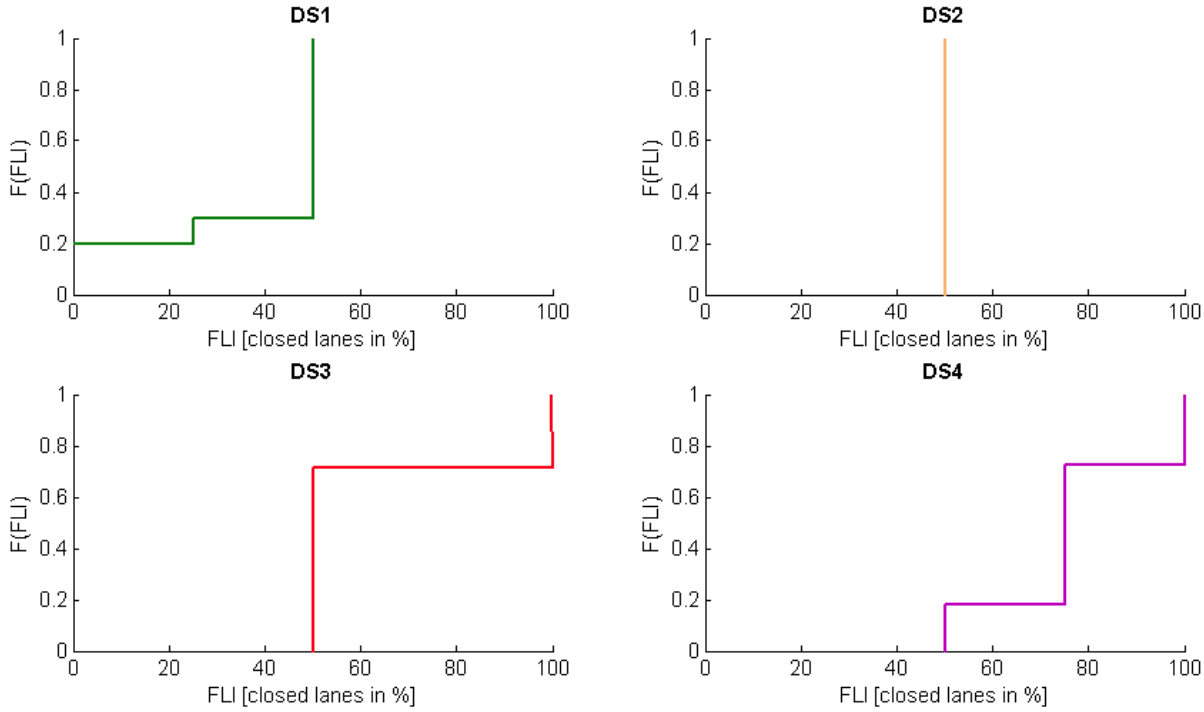

Figure 29: Functionality loss during intervention (expressed in proportion of closed lanes) given global damage states DS1 to DS4.

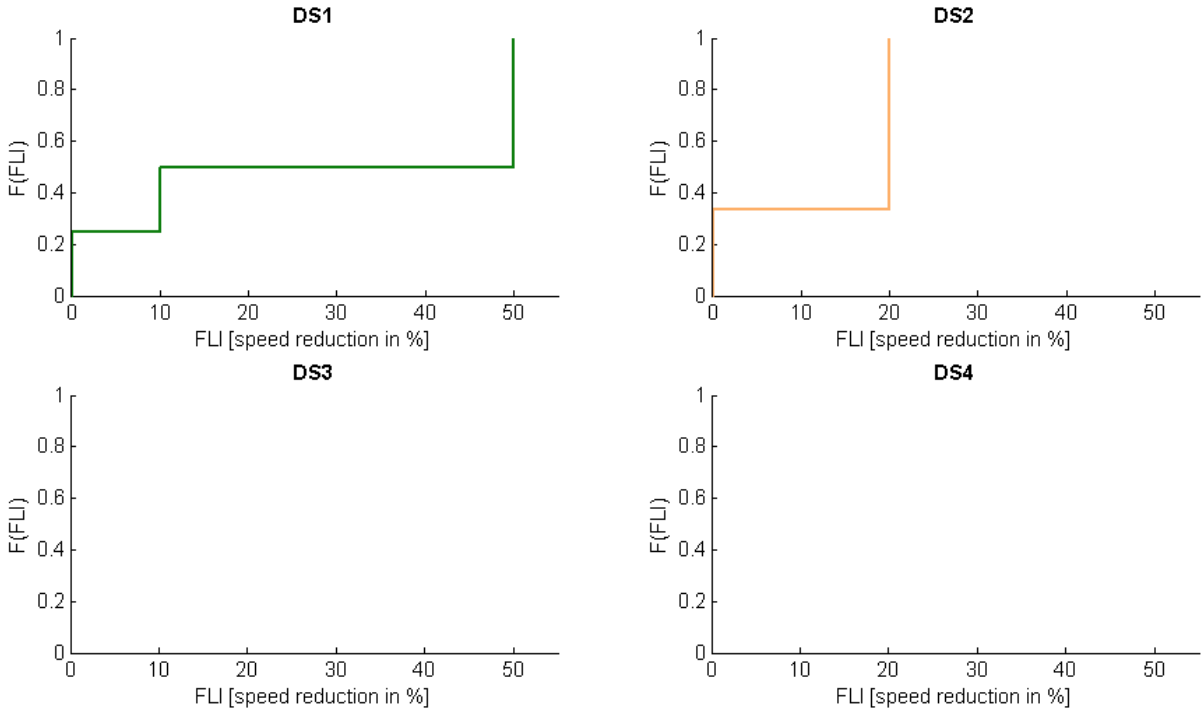

Figure 30: Functionality loss during intervention (expressed in speed reduction) given global damage states DS1 to DS4. No values are available for DS3 and DS4.

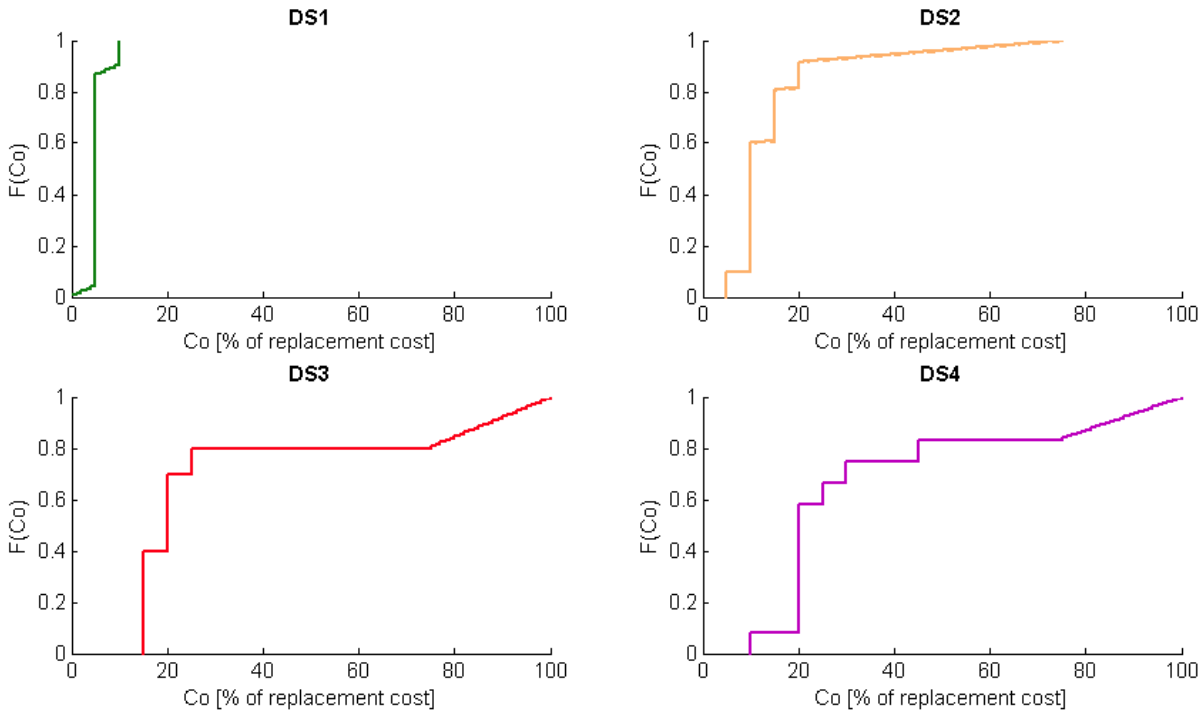

Figure 31: Cost of repair operations given global damage states DS1 to DS4.

Except in the case of the duration and cost metrics, most of the functionality models are very coarse and some of them are even not computable (i.e. FLI for DS3 and DS4). This is due to the lack of sufficiently constrained data that have been gathered from the expert-based survey. Therefore these curves should be seen as a first attempt at developing the concept of functionality curves, while additional data should be use to better constrain the proposed models.

While comparing the functionality curves across damage states, it can also be observed that there is no clear difference between some damage states: for instance, the downtime durations due to DS3 and DS4 are almost identical, or the functional loss in lane closure due to DS2 may be more severe than the one due to DS3. This perfectly exemplifies the limitations of the use of global damage states and global fragility functions: while damage states may be structurally consistent between components, their respective failure or damage mechanisms may induce a wide range of functional consequences that do not remain necessarily consistent at the system level.

The numerical values that are proposed in this section should be considered for illustrative purposes only, due to the scarcity of the collected data from the expert-based survey.

4.4.3 Calibration / Validation

In order to cope with the lack of expert-based data points, a literature review is conducted in order to extract functional loss values or downtime durations from past case-studies. In the case of bridges subjected to seismic risk, the following references provide information on the induced losses:

- **Werner et al. (2006):** traffic capacity (e.g. speed reduction), repair costs and duration of repairs are provided for three damage states of bridge approach fill (i.e. three levels of subsidence), as summarized in **Table 12**.

Damage state	Traffic capacity	Repair cost	Repair duration
DS1 – settlement ≤ 1 inch	100%	0%	-
DS2 – settlement ≤ 6 inch	0%	12%	1 day
DS3 – settlement > 6 inch	0%	55%	4 days

Table 12: Functionality and repair model for damage to bridge approach fill, from Werner et al. (2006).

- **SYNER-G work (Argyroudis and Kaynia, 2014) based on REDARS approach (Werner et al., 2006)**: based on four global damage states at the system level, the functionality loss in terms of lane closure is provided, as summarized in **Table 13**.

Bridge Damage state	DS1 – Minor	DS2 – Moderate	DS3 – Extensive	D4 – Complete
Functionality	open	partially open	closed	closed

Table 13: Functionality levels for bridge systems, from Argyroudis and Kaynia (2014).

- **HAZUS method (NIBS, 2004):** restoration curves for highway bridges are proposed in order to show the evolution of functionality with time. The INFRARISK approach does not make use of restoration curves, however theses curves can provide two useful data points, which are summarized in **Table 14**:
    - The remaining capacity immediately after the event gives the functionality loss;
    - The moment when the capacity is fully restored again gives the repair duration.

Bridge Damage state	DS1 – Minor	DS2 – Moderate	DS3 – Extensive	D4 – Complete
Functionality loss	25%	70%	95%	100%
Duration	1 day	7 days	130 days	370 days
Repair cost	1% - 3%	2% - 15%	10% - 40%	30% - 100%

Table 14: Functionality and repair model for highway bridges, adapted from HAZUS (NIBS, 2004).

These few data points from the literature references enable “literature-based” functionality models to be built, by using the same technique as in Figure 25. Finally, a direct comparison can be made between the INFRARISK functionality models and the literature references (see Figure 32 to Figure 35).

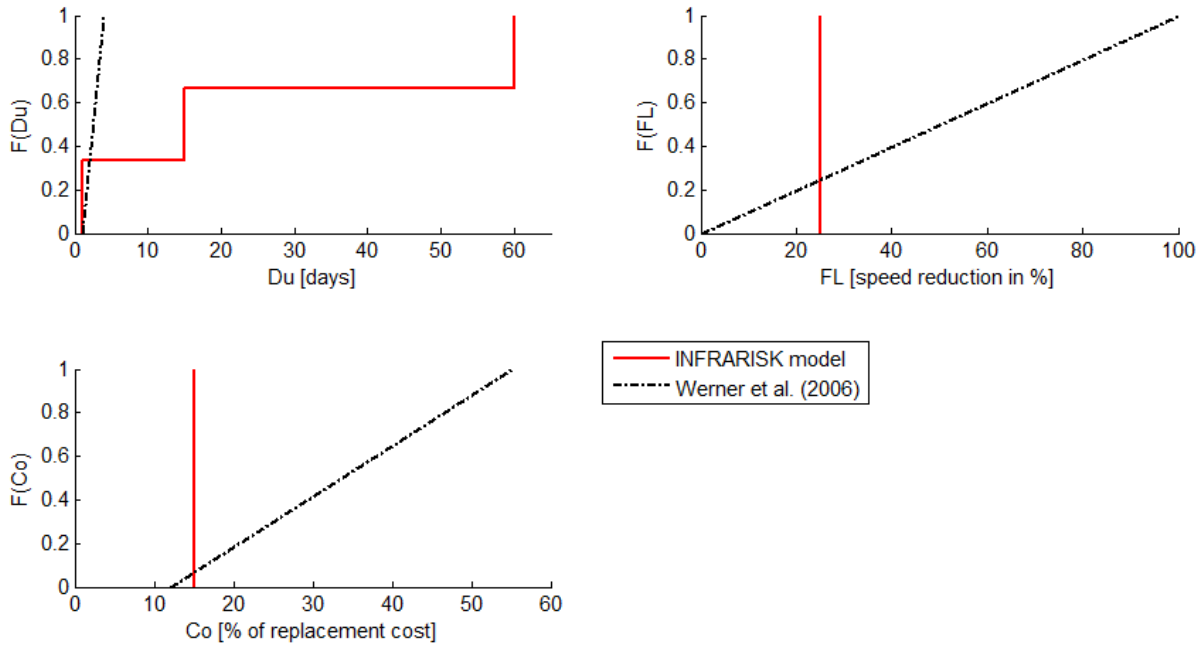

Figure 32: Comparison of the functionality models for subsidence to bridge approach fill (failure mode #16-D1)

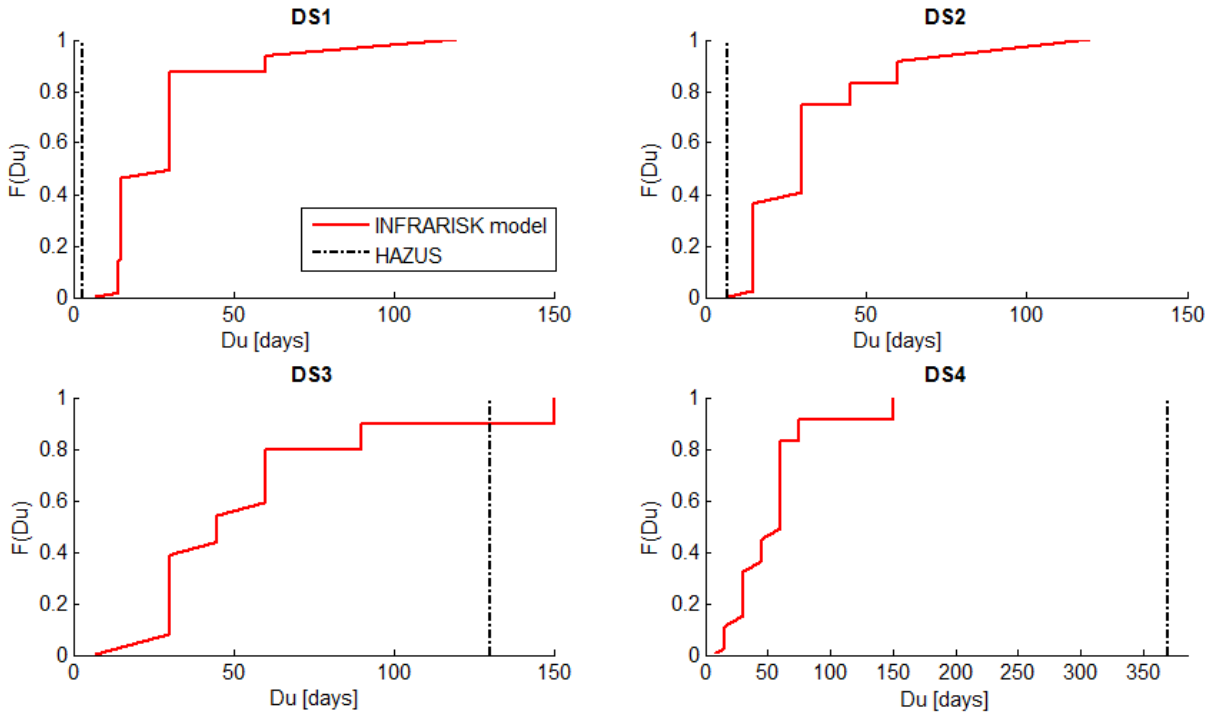

Figure 33: Comparison of the repair duration models for global damage states to bridges

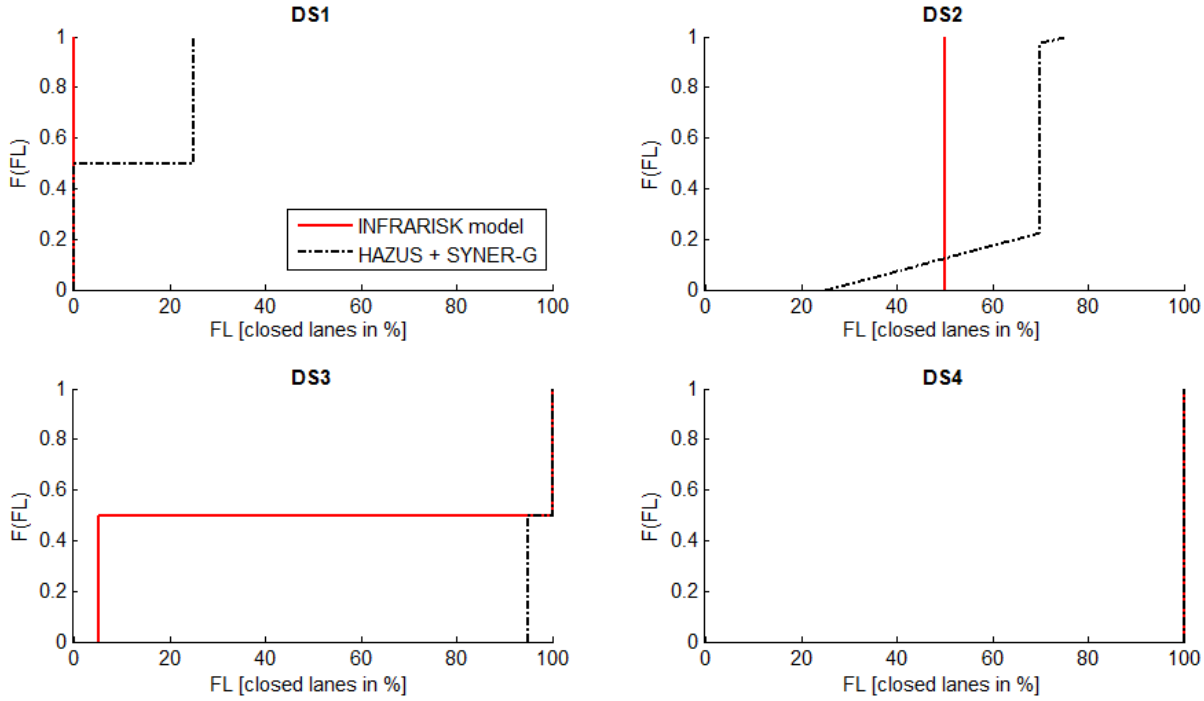

Figure 34: Comparison of the functional loss models for global damage states to bridges

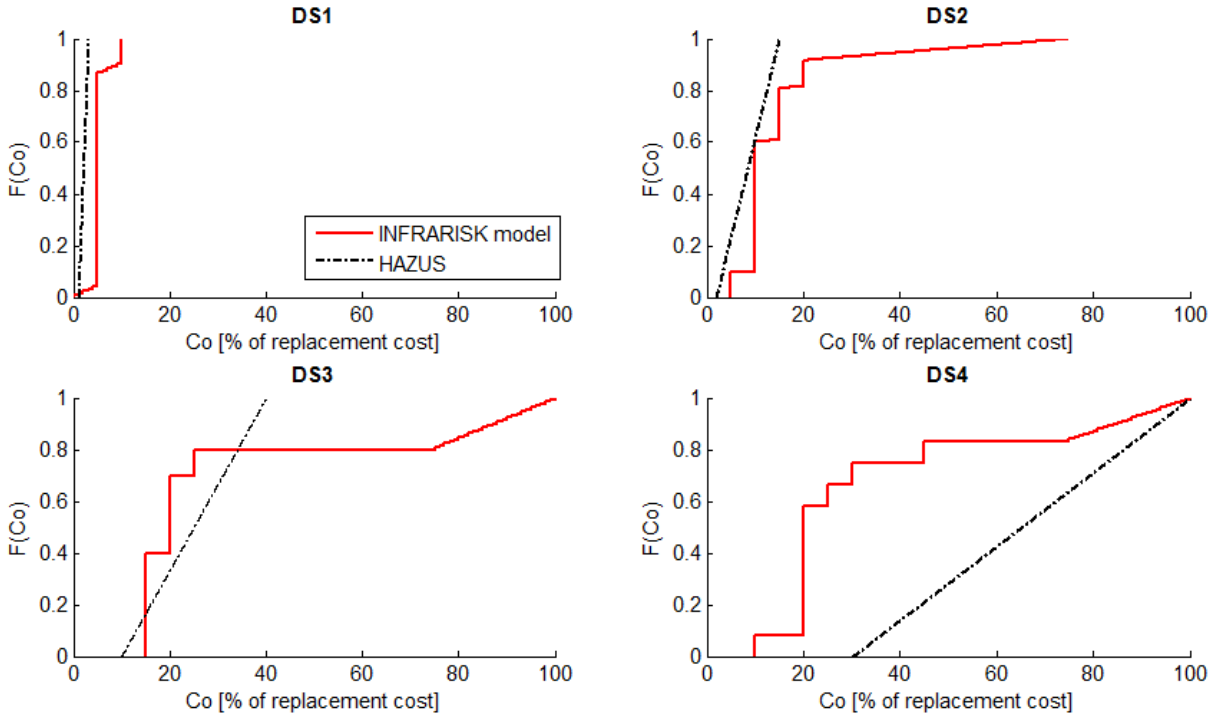

Figure 35: Comparison of the cost models for global damage states to bridges

The insufficient number of data points and the coarseness of some of the functional models (e.g. step functions) make it very difficult to draw definite conclusions on the validity of the proposed functional models. Still, most of the loss metrics are within the same range as the literature-based values, especially the cost model for global damage states (Figure 35). However, the repair duration model for global damage states (Figure 33) does not seem to be consistent with the values that have

been extracted from the HAZUS restoration curves: the downtime duration appears to be overestimated for low damage states (DS1 and DS2) and underestimated for heavier damage (DS3 and DS4). This is partly due to the fact that the proposed duration model does not evolve much from DS1 to DS4, the values being stuck around 20-50 days.

4.5 Global approach: selection from available fragility functions

In the case where large transportation networks are studied, the presence of numerous infrastructure elements does not realistically permit the analytical derivation of specific component fragility functions for each of them. Therefore a common approach is to select existing fragility curves for global damage states, based on common features or similar typologies. The following sections present some of the options that are explored in order to select existing functions and build composite fragility models.

4.5.1 Application of the SYNER-G database to a dataset of case-study bridges

As part of one of the INFRARISK case studies (Ni Choine et al., 2014), highways and secondary roads around the city of Bologna, Italy, have to be assessed with respect to seismic risk. A total of 340 bridges have been identified by the INFRARISK consortium. These bridges have been characterized by following the SYNER-G taxonomy (see section 4.1.1), even though the absence of a proper field inventory did not permit the full identification of all taxonomy parameters. As a result, most of the bridge descriptions are incomplete: they are described in **Table 54** in Appendix C.

The SYNER-G database of fragility functions for bridges (Silva et al., 2014) is described in section 4.3.1: it has been implemented in the Fragility Function Manager tool (http://www.vce.at/SYNER-G/files/downloads.html) in order to facilitate the reuse of these fragility curves in seismic risk studies. Since the SYNER-G database currently represents the most up-to-date collation of fragility curves for bridges and that the taxonomy used is consistent with the case-study data, it is proposed to make use of this dataset of 373 existing curves to develop corresponding fragility models for the case-study elements.

In order to facilitate the association between the case-study bridges and the existing curves, numerical parameters such as deck width, bridge length, pier height or span length are discretised into bins, which are summarized in **Table 15**. These bins have been defined so that each bin is populated with similar amounts of existing curves.

Bridge width (DC)		***Pier height (HP)***		***Span length (SC)***		***Bridge length***	
X	undefined	**X**	undefined	**X**	undefined	**X**	undefined
<20	< 20m	**<5**	< 5m	**<25**	< 25m	**<50**	< 50m
>20	≥ 20m	**<10**	[5;10[m	**<45**	[25;45[m	**<100**	[50;100[m
		>10	≥ 10m	**>45**	≥ 45m	**<200**	[100;200[m
						>200	≥ 200m

Table 15: Discrete bins used in the description of the bridges.

4.5.2 Option 1: pairing based on taxonomy parameters

It is proposed here to simply use the correspondence between the taxonomy parameters of the bridges and the SYNER-G database. If multiple candidates potentially match a given bridge description, then composite curves can be derived in order to account for epistemic uncertainties.

The first task is to associate each of the 340 case-study bridges with the various fragility references, based on the correspondence between the identified taxonomy parameters. The following rules are applied in the selection of the fragility models:

- For each bridge, all the fragility references that contain the same parameters (e.g. same material, same deck structural system, same level of seismic design, etc.) are selected. Therefore multiple fragility curves can be associated with a given typology.
- If a given bridge contains unspecified parameters (i.e. value '*X*' in **Table 54**), then the selection of the corresponding fragility reference(s) does not account for these parameters (i.e. only the specified parameters are used in the model matching).
- Conversely, fragility references with an unspecified parameter can be associated to various bridges that have specific values for this parameter.

Some examples of the application of these rules are shown in **Table 16**.

Parameters	***M1***	***M2***	***TD1***	***TD2***	***DC***	***DSS***	***PDC***	***TC1***	***TS1***	***TS2***	***HP***	***Sp***	***SC***	***Tca***	***BC***	***LS***	***Len.***
…																	
Bridge #1	**C**	**PC**	**X**	**X**	**<20**	**SSu**	**Is**	**McP**	**R**	**So**	**X**	**Ms**	**<45**	**Isl**	**R**	**NSD**	**<50**
Azevedo et al. (2010)	X	X	X	X	X	X	X	X	X	X	X	X	X	X	X	NSD	X
Mander (1999)	X	X	X	X	X	SSu	X	McP	X	X	X	X	X	X	X	NSD	X
…																	
Bridge #85	**C**	**RC**	**X**	**X**	**>20**	**X**	**X**	**X**	**X**	**X**	**X**	**Ssp**	**<25**	**M**	**R**	**SD**	**<50**
Azevedo et al. (2010)	X	X	X	X	X	X	X	X	X	X	X	X	X	X	X	SD	X
Basoz et al. (1999)	C	RC	X	X	X	SSu	X	X	X	X	X	X	X	X	X	SD	X
Basoz et al. (1999)	C	RC	X	X	X	Co	X	X	X	X	X	X	X	X	X	SD	X
Elnashai et al. (2004)	C	RC	X	X	X	X	X	X	X	X	X	X	X	X	X	X	X
Mander (1999)	X	X	Gb	B	X	X	X	ScP	X	X	X	X	X	X	X	SD	X
Mander (1999)	X	X	X	X	X	X	X	X	X	X	X	Ssp	X	X	X	SD	X
Mander (1999)	C	X	X	X	X	Co	X	X	X	X	X	X	X	X	X	SD	X
Mander (1999)	X	X	X	X	X	SSu	X	McP	X	X	X	X	X	X	X	SD	X
Shinozuka et al. (2000)	C	RC	X	X	X	SSu	X	X	R	So	X	X	X	X	X	X	X
Shinozuka et al. (2003)	C	RC	X	X	>20	X	X	X	X	X	X	X	X	X	X	X	X
Shinozuka et al. (2003)	C	RC	X	X	X	SSu	X	X	R	So	X	X	X	X	X	X	X
…																	

Table 16: Example of the selected fragility references for bridges #1 and #85.

In cases where multiple fragility references could be deemed appropriate to represent the fragility of a given bridge, the second step consists in deriving a composite fragility model.

According to Shinozuka et al. (2000), the existence of multiple fragility models for a given typology may be taken into account by building a combined fragility model: if a specific bridge typology is associated with *n* fragility models, it is assumed that the bridge population within the typology is equally distributed among *n* sub-types that correspond to each of the fragility models. In this context, Shinozuka et al. (2000) propose the following expression for the combined median *α* and standard deviation *β*:

$$\begin{cases} \alpha = \exp\left[\sum_{i=1}^{n} P_i \cdot \ln \alpha_i\right] \\ \beta^2 = \mathbf{P}^t \cdot \mathbf{Z} + \mathbf{A}^t \cdot \mathbf{Q} \cdot \mathbf{A} \end{cases} \quad \textbf{(11)}$$

Where:

- **P** is a column vector representing the proportion of each bridge sub-type in the sample (if equally distributed, $P_1 = P_i = 1/n$):

$$\mathbf{P} = \begin{bmatrix} P_1 \\ \dots \\ P_i \\ P_n \end{bmatrix} \quad \textbf{(12)}$$

- **Z** is a column vector representing the variance of each of the fragility models considered:

$$\mathbf{Z} = \begin{bmatrix} \beta_1^2 \\ \dots \\ \beta_i^2 \\ \beta_n^2 \end{bmatrix} \quad \textbf{(13)}$$

- **A** is a column vector representing the logarithm of the median of each of the fragility models considered:

$$\mathbf{A} = \begin{bmatrix} \ln \alpha_1 \\ \dots \\ \ln \alpha_i \\ \ln \alpha_n \end{bmatrix} \quad \textbf{(14)}$$

- **Q** is a matrix of the following form:

$$\mathbf{Q} = \begin{bmatrix} P_1 \cdot (1 - P_1) & \dots & -P_1 \cdot P_i & -P_1 \cdot P_n \\ \dots & \dots & \dots & \dots \\ \dots & \dots & \dots & \dots \\ -P_n \cdot P_1 & \dots & -P_n \cdot P_i & P_n \cdot (1 - P_n) \end{bmatrix} \quad \textbf{(15)}$$

This method appears to result in very flat averaged fragility curves (i.e. high standard deviation): this effect is not desirable since it tends to attenuate the differences between the different bridges, and most of the derived curves then provide very similar damage probabilities. Moreover, these combined fragility models do not make the distinction between the original standard deviation of the single fragility references and the standard deviation that results from the differences between the fragility curves.

An alternative to the aforementioned approach is to estimate a median fragility curve from the different fragility models, while considering confidence bounds in order to account for the model choice. Therefore the uncertainty can be broken down into two parts:

- The averaged dispersion β_R that is inherent to each individual fragility model: it usually expresses the earthquake variability (i.e. record-to-record variability), as well as the uncertainties in the modelling assumptions that are used to derive the individual fragility curves.
- The standard deviation β_U due to the choice of the fragility model. It is a way of expressing the 'width' of the family of fragility references.

The composite standard deviation can finally be expressed as a function of the two uncertainty sources:

$$\beta_C = \sqrt{\beta_R^2 + \beta_U^2} \quad \textbf{(16)}$$

This approach has been first theorized by Kennedy et al. (1980) and Kaplan et al. (1994): it is the one that is used here, since it enables the epistemic uncertainties that result from the choice of the fragility models to be clearly identified. Median fragility curves along with their 16%-84% confidence bounds are plotted in Figure 36 for a few bridge examples. Bridge #1 is a non-seismically designed structure with only two corresponding references (see **Table 16**), which explains the high fragility and the narrow confidence interval. Conversely, the seismically designed bridge #85 presents a lower fragility, but with much higher epistemic uncertainties due to the many literature references that may apply to this specific bridge.

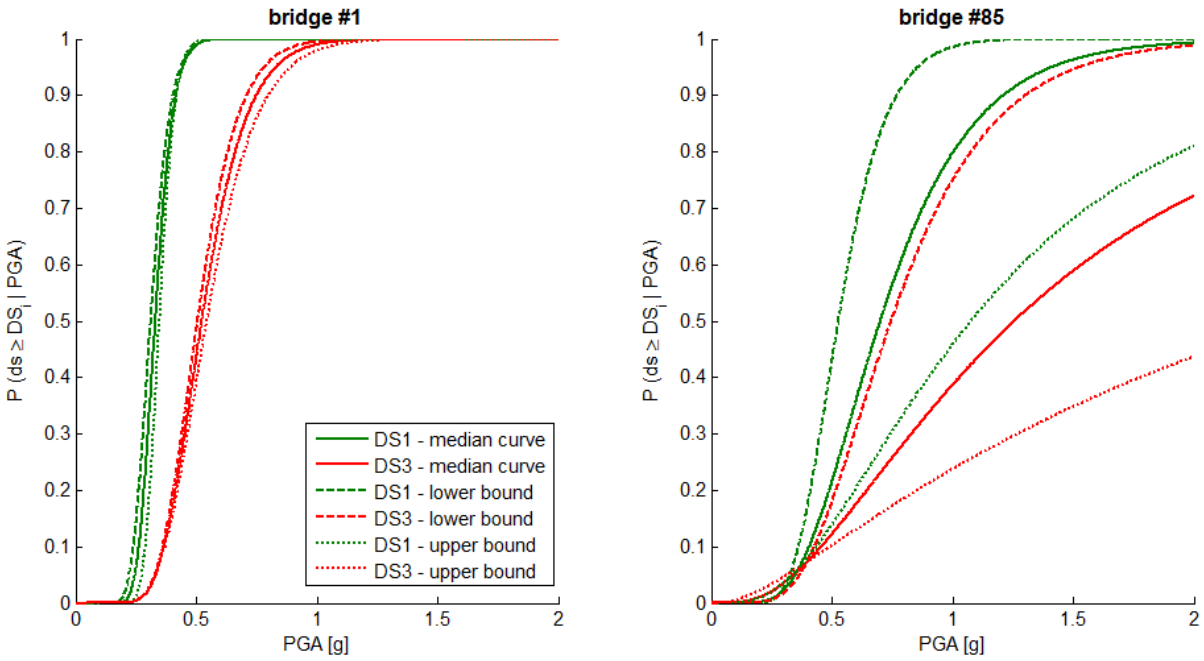

Figure 36: Composite fragility curves with their 16%-94% confidence bounds, for brides #1 and #85 and damage states DS1 and DS3

This method has the advantage of being rather straightforward, since it can be automated into a pairing algorithm in order to treat a large amount of bridge objects in a given risk study. However, it could be argued that all taxonomy parameters are given the same weighting, as if they had the same influence on the bridge fragility, which is not realistic. Moreover, a lot of the composite fragility curves are very similar to each other: this is not optimal as it leads to a multiplication of the fragility models, which may not bear a lot of physical meaning, especially for bridges that are almost identical.

4.5.3 Option 2: hierarchical clustering

For the reasons outlined in the previous section, a second option is explored here, with the objective of reducing the number of fragility models, while accounting for the taxonomy parameters that are the most meaningful. To this end, a multi-step scheme is devised, which involves the use of analysis of variance and hierarchical clustering (see Figure 37).

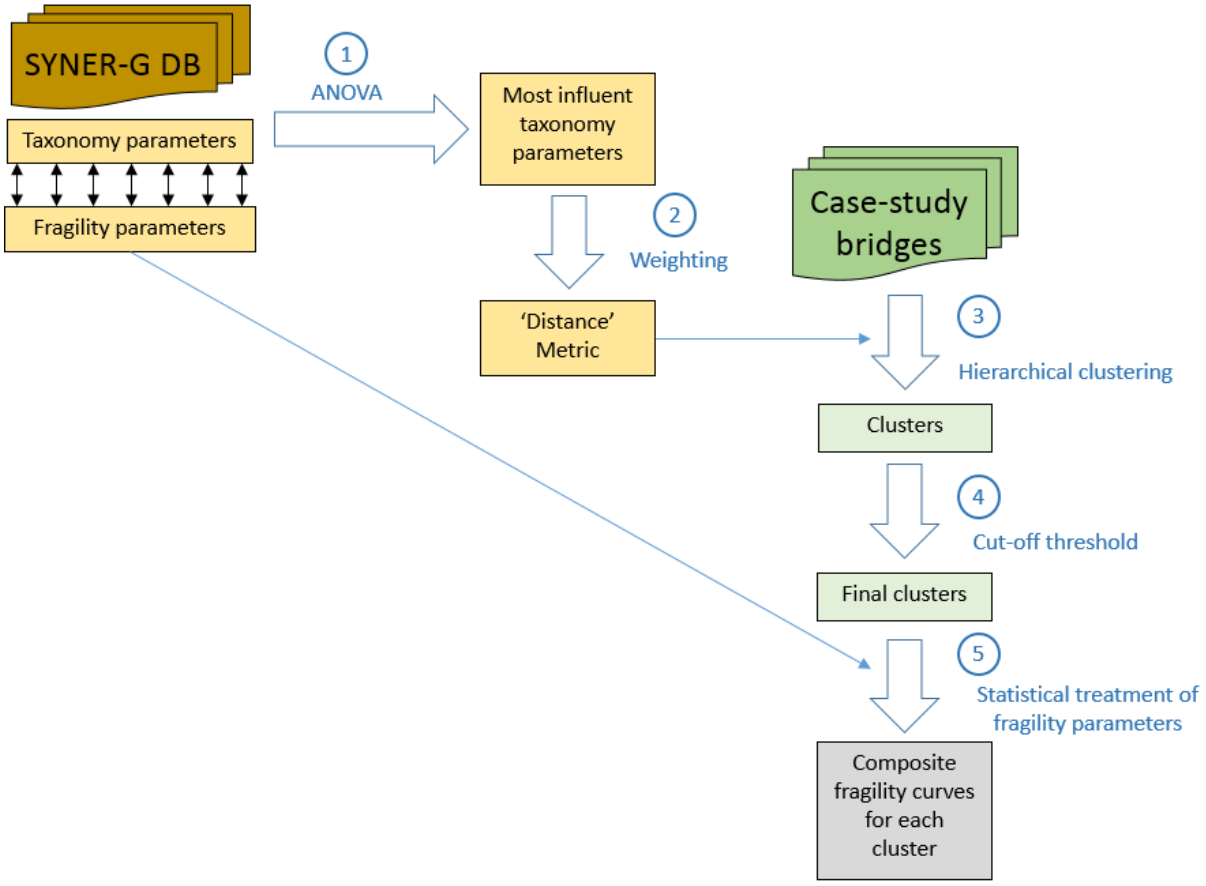

Figure 37: General workflow of the clustering approach (Option 2)

The different steps of the proposed method are outlined below:

1. Analysis of variance (ANOVA): The significance of each taxonomy parameter is assessed through an *n*-way ANOVA where the fragility parameters of the SYNER-G references (i.e. mean α) are used as the observations. This allows the parameters that have the most influence on the fragility curves to be determined. Several common assumptions of the ANOVA are not verified in the present case, such as the independence of the taxonomy parameters between each other or the homoscedasticity of these parameters (i.e. some of them do not cover all their possible values while other are more evenly distributed). Therefore the objective is not to quantify the effect of each parameter but more to qualitatively rank the parameters in different groups. Moreover, this task is complicated by the fact that the ANOVA results may vary depending on the damage state that corresponds to the fragility parameters. Finally, four groups of parameters have been selected, ranked from the most to the least significant: (i) Sp, LS; (ii) MM1, DC, TC1; (iii) Length, SC, TCa; (iv) MM2, DSS, PDC, TS1, TS2, BC.

2. Parameter weighting: In order to perform the hierarchical clustering on the bridges, a metric has to be built in order to quantify the 'distance' from one bridge configuration to another. The proposed metric is based on the differences between the parameters' values, while weights are assigned to the groups of parameters that have been previously identified with the ANOVA. Therefore the distance D_{ij} between bridge configurations *i* and *j* can be expressed as:

$$D_{ij} = w_1 \cdot \sum_{k=1}^{n1}\left(1-\delta_{ij}^{k}\right) + w_2 \cdot \sum_{k=1}^{n2}\left(1-\delta_{ij}^{k}\right) + w_3 \cdot \sum_{k=1}^{n3}\left(1-\delta_{ij}^{k}\right) + w_4 \cdot \sum_{k=1}^{n4}\left(1-\delta_{ij}^{k}\right) \quad \textbf{(17)}$$

Where $w_1 \ldots w_4$ represent the respective weights of the 4 groups of parameters, and $n_1 \ldots n_4$ are the number of parameters within each group. Kronecker's delta δ_{ij}^{k} is equal to 1 if the k-th parameter is the same between bridge i and j, and 0 if not. The main difficulty lies in the estimation of optimal weights for this metric: a trial-and-error search for the weights that will generate the optimal cluster distribution (i.e. reduced number of clusters for high homogeneity within each cluster and high heterogeneity between clusters) is necessary. Out of 20 tested weight combinations (see Figure 38), the following configuration is finally adopted: w_1 = 1; w_2 = 0.5; w_3 = w_4 = 0.25. Still, it has been observed that the evolution of the clusters is rather stable over the weight combinations.

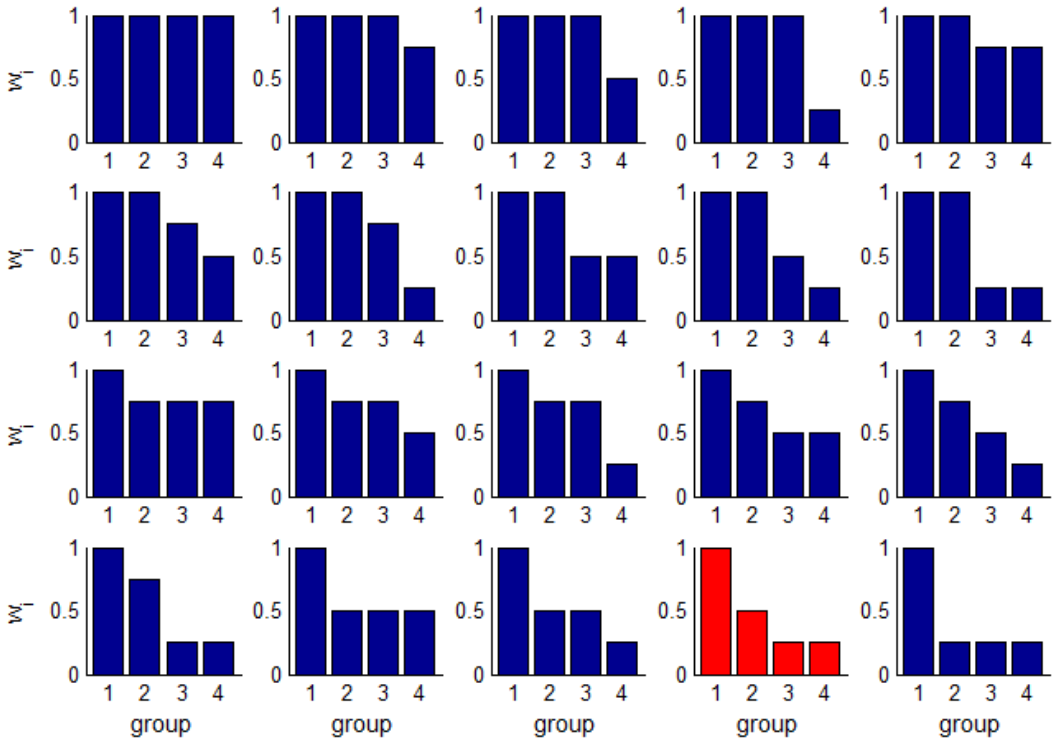

Figure 38: Weight combinations that have been tested. The red one is the combination that has been selected.

3. Hierarchical clustering: Once the metric has been defined, the taxonomy parameters of the 340 case-study bridges are extracted in order to build the linkage matrix between all bridge configurations. The dendrogram of the clusters (see Figure 39) can then be built using single-linkage clustering, with Euclidian distance. Each bridge configuration is located at one of the end branches of the tree: there are 117 branches because, out of the 340 bridges, 117 unique configurations have been found.

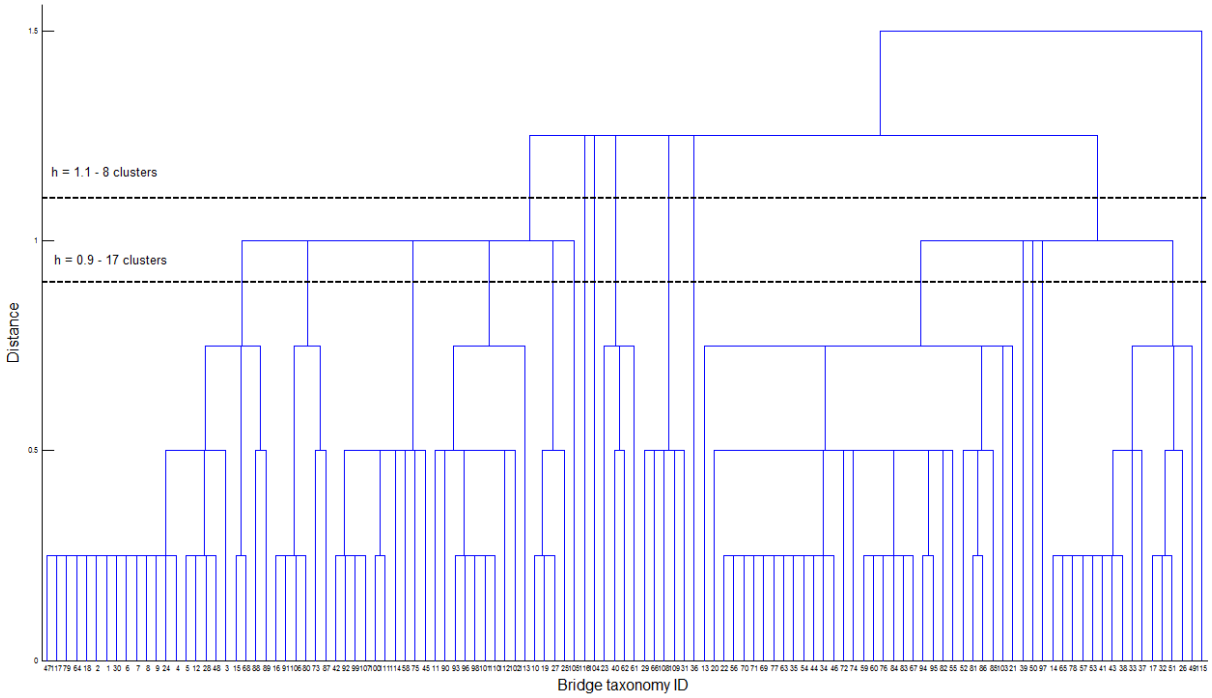

Figure 39: Dendrogram showing the hierarchical clusters of bridge configurations. The two horizontal lines represent hypothetical cut-off distances, generating either 8 or 17 clusters.

4. Cut-off threshold: The number of final clusters of bridge configurations is determined by the value of the cut-off threshold, as shown in Figure 39. Therefore another decision has to be made on the optimal cut-off distance to apply. As for the search for the optimal weight combination, the best cut-off distance should be a compromise between a reduced number of clusters, narrow confidence bounds around the fragility curves (i.e. homogeneous clusters) and very different fragility curves between clusters (i.e. specificity of each cluster). It is then proposed to follow the evolution of these criteria for different cut-off distances, with the objective of finding the optimal trade-off. To this end, two quantitative measures are introduced:

- The homogeneity within a cluster is measured by computing A_c, the area between the upper and lower confidence bounds of the fragility curves.
- The difference between two clusters is measured by computing d_{KS}, the Kolmogorov-Smirnov distance between the fragility curves from the two clusters. The Kolmogorov-Smirnov distance between two cumulative distribution functions is the maximum absolute distance that is measured between the functions over their support. It has been used in previous studies to check the goodness-of-fit between two fragility curves (Gehl et al., 2015).

In Figure 40, the evolution of the A_c and d_{KS} quantities (average, minimum and maximum across all clusters) is plotted with respect to the number of clusters. Globally, an increase of the number of clusters (i.e. a decrease of the cut-off threshold) leads to:

- A decrease of the confidence bounds area A_c (i.e. better homogeneity within each cluster). Still, the maximum A_c keeps increasing: this effect must be due to the fact

that a minority of clusters become too large, and all the bridge configurations they contain lead to high epistemic uncertainties.

- A decrease of the differences between clusters, materialized by d_{KS}: with too many clusters, some of them end up containing bridge configurations that are very similar, therefore leading to almost identical fragility curves (i.e. the minimum of d_{KS} converges towards 0). However, the maximum of d_{KS} seems to increase until it reaches a plateau: a minority of clusters are very different from the others and their specificity is not really altered by the evolution of the cut-off distance, expected for high cut-off values where these clusters begin to merge with more generic clusters.

The analysis of results in the selection of 17 clusters (i.e. cut-off distance of 0.9): this value is a trade-off between a reduced number of clusters, a low A_c, and a reasonably high d_{KS}. The content of each cluster is detailed in **Table 55** in Appendix D: it is interesting to note that the selected clusters have led to a clear separation between the levels of seismic design, while multi-span bridges and single-span bridges also end up in different clusters.

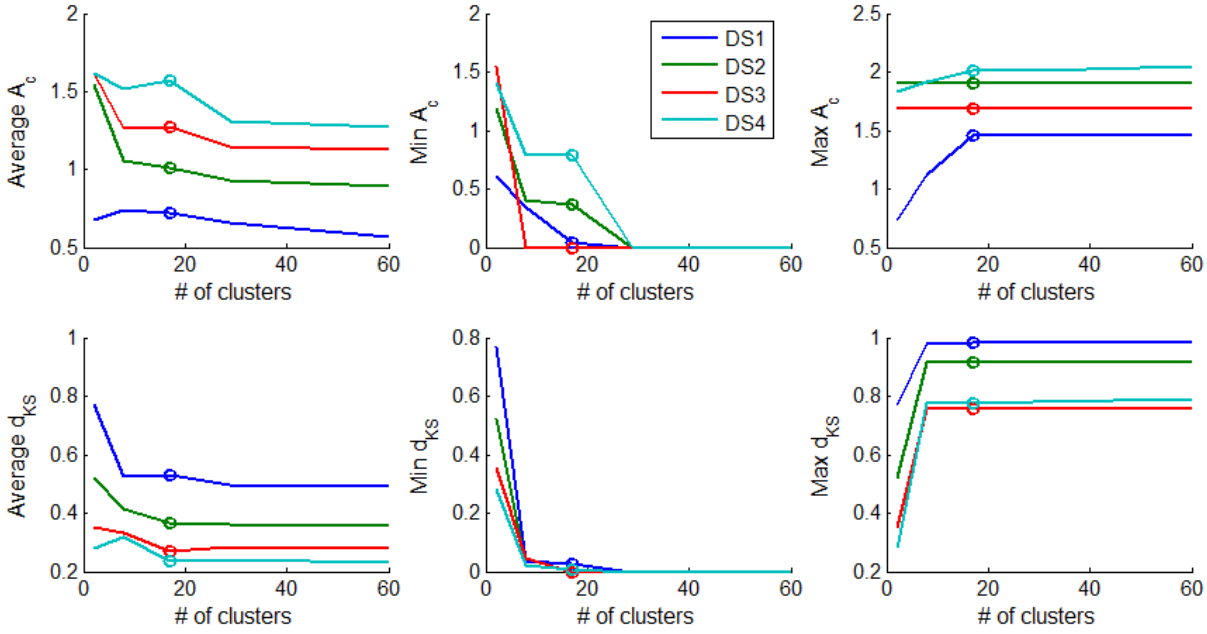

Figure 40: Evolution of A_c and d_{KS} with respect to the number of clusters, for all four damage states

5. Statistical treatment: Once the number of clusters has been set, the SYNER-G fragility references that correspond to the bridge configurations within each cluster are assembled by following the rules detailed in previous section (Option 1). Since it is expected that each cluster will contain more fragility references (i.e. each cluster should contain at least one bridge configuration), it is proposed to observe the distribution of the fragility parameters from the SYNER-G database in a scatter plot (see Figure 41). The potential correlation between the mean α and the standard deviation β of the fragility curves can then be observed, and a bivariate normal distribution can be fitted if enough data points are present. This statistical treatment allows to directly obtain the median fragility curves with their 16%-84% confidence bounds for each cluster:

$$\begin{cases} \log\alpha_{c,med} = \mathrm{E}[\log\alpha_i] \\ \log\alpha_{c,LB} = \mathrm{E}[\log\alpha_i] - \sigma[\log\alpha_i] \\ \log\alpha_{c,UB} = \mathrm{E}[\log\alpha_i] + \sigma[\log\alpha_i] \end{cases} \quad \begin{cases} \log\beta_{c,med} = \mathrm{E}[\log\beta_i] \\ \log\beta_{c,LB} = \mathrm{E}[\log\beta_i] - \rho\cdot\sigma[\log\beta_i] \\ \log\beta_{c,UB} = \mathrm{E}[\log\beta_i] + \rho\cdot\sigma[\log\beta_i] \end{cases} \quad (18)$$

Where α_i and β_i are the fragility parameters of the SYNER-G references that correspond to each cluster, and ρ is the correlation factor between log α_i and log β_i.

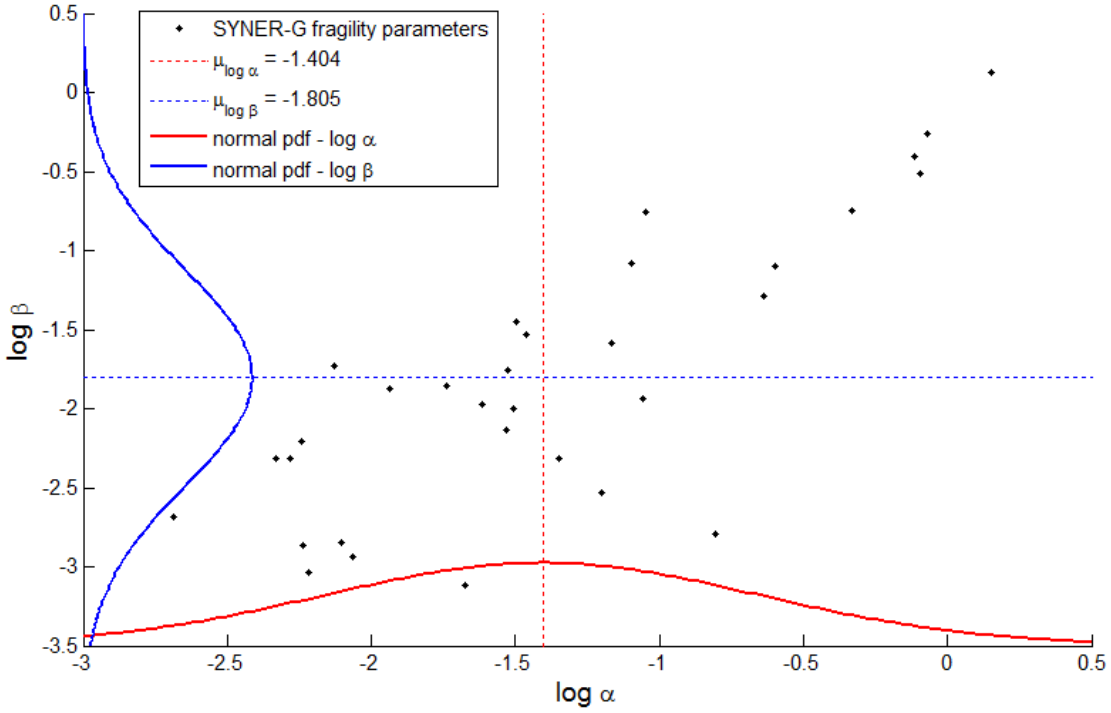

Figure 41: Distribution of the SYNER-G fragility parameters for cluster #3 and damage state DS1

An example of the composite fragility functions for the 17 clusters is presented in Figure 42, while all the fragility parameters are detailed in **Table 56** in Appendix D. Due to the lack of a sufficient amount data points in some clusters, it may happen that the confidence bounds are not well defined, potentially leading to an overlapping between lower and upper bounds. In this case, it is recommended to the limit the values of the lower/upper bound to the median curve in order to remain consistent (e.g. see example of cluster #7 in Figure 42).

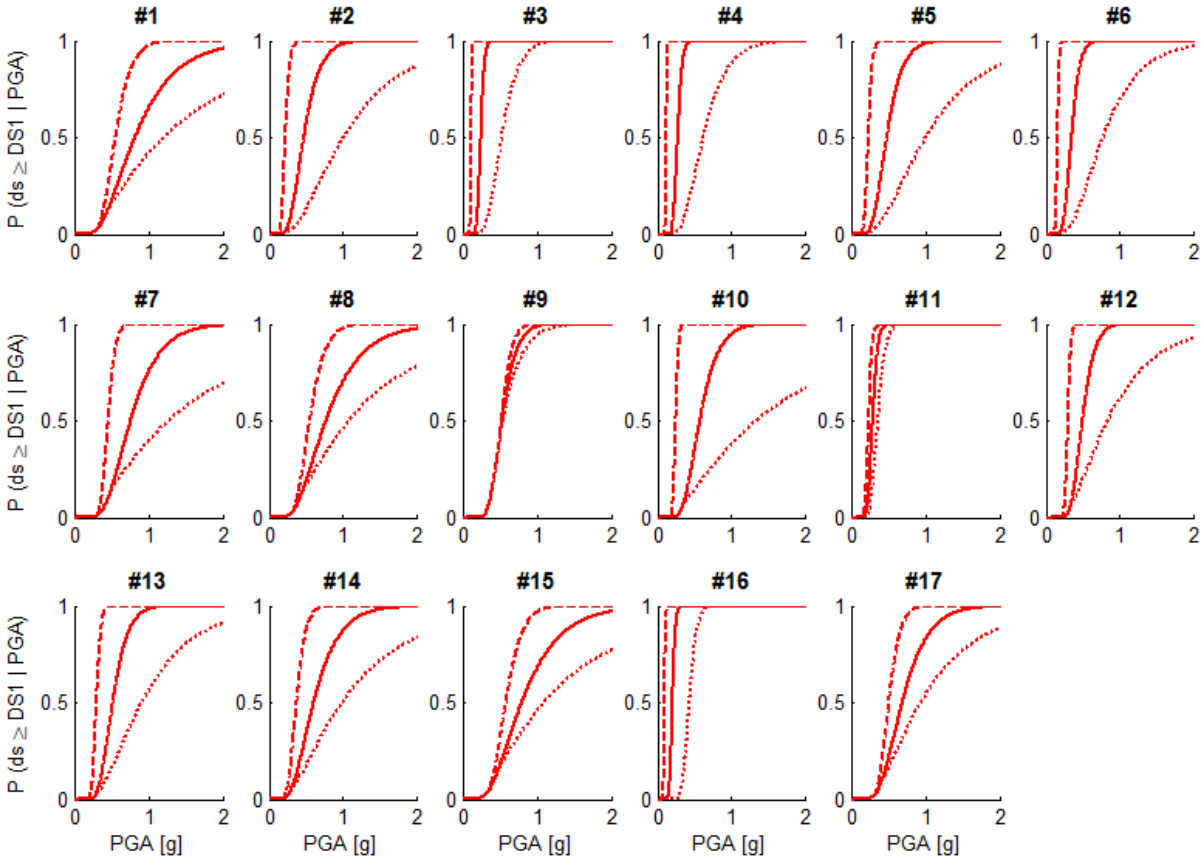

Figure 42: Fragility curves for DS1 for all 17 clusters. The solid line represents the median curve, the dashed line the lower bound, and the dotted line the upper bound.

Finally, the proposed approach permits the selection of adequate existing fragility functions for any bridge that can be described by a set of taxonomy parameters. The estimation of confidence bounds enables the epistemic uncertainties that are induced by the choice of the fragility model and by the lack of accurate knowledge on the bridge characteristics to be visualised. However, these confidence bounds should be interpreted with caution: their 'width' is heavily influenced by the number of fragility references that correspond to each cluster. For instance, it may happen that a poorly characterized bridge configuration is associated with very few fragility references because of the lack of corresponding models in the literature: consequently, the confidence interval will appear to be narrow, even though it should be much larger than a well-constrained bridge configuration.

4.6 Towards harmonized multi-risk fragility functions

This section is devoted to the application of the BN approach to a bridge system that is subjected to multiple loadings (i.e. earthquakes, ground failures and floods). The proposed example has been presented in Gehl and D'Ayala (2015a,b). The objective is to demonstrate that the proposed INFRARISK approach, i.e. identification of the failure modes for all components and harmonization across all hazard types through functional consequences, may be used to derive 'hazard-independent' fragility functions for infrastructure elements. While the derived fragility functions will still be expressed with respect to the hazard intensity levels, 'hazard independence' is justified by the fact that the same fragility models may be applied whatever the hazard type and that a common global damage scale (i.e. in terms of functional consequences) can be defined.

4.6.1 Bridge model and failure mechanisms

The model of a virtual yet realistic bridge is developed, assuming as reference for structural and geometrical properties the archetype bridge already studied by Nielson (2005): it is a multi-span simply-supported concrete (MSSSC) bridge composed of two seat-type abutments and two piers with three cylindrical reinforced concrete columns. Deck displacement is restrained by elastomeric bearings (i.e. alternation of expansion and fixed devices) in the longitudinal direction. Several additional features have also been integrated to the original model (Nielson, 2005), in order to account for the effect of multiple hazards (see Figure 43):

- Shear keys have been added at the pier caps in order to model the constraints and determine the bridge response in the transversal direction.
- At each bridge extremity, an embankment approach is added in order to simulate the transition between the plain roadway segment and the bridge and to evaluate the effect of ground failure.
- Foundation elements have been added at the pier footings in order to properly model the effects of scour.

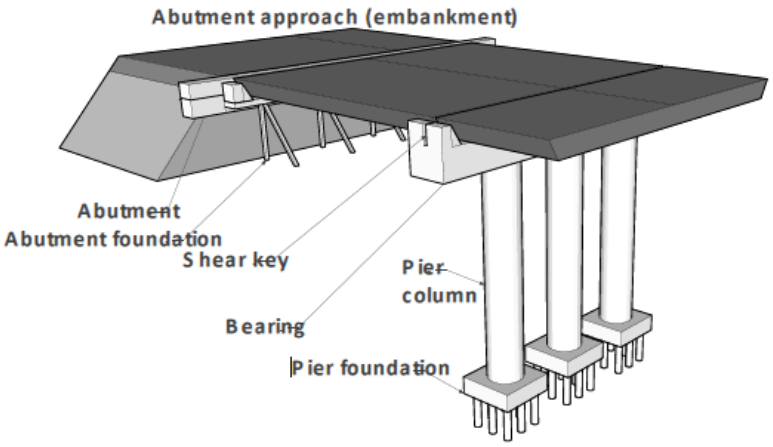

Figure 43: Half-sketch of the studied bridge system and its components

The considered bridge model is subjected to multiple loading mechanisms due to earthquake (EQ), ground failure (GF) and flood (FL) events. These three hazard events have been identified by Deng et al. (2015) as the main natural causes of bridge collapses in the United States in the 1990s. They have been chosen because they may affect a wide range of bridge components (see **Table 17**) through various failure mechanisms:

- Earthquakes affect most of the structural components of the bridge: abutments, piers, bearings, shear keys. Deck unseating may occur if large enough deformations are recorded for either bearings or shear keys in the longitudinal and transversal directions, respectively.
- Fluvial floods are the source of hydraulic forces that may damage shear keys or even dislodge deck spans in extreme cases (Padgett et al., 2008), while flood-induced scour may excavate pier foundations.

- Ground failures are likely to affect the approach embankment, as the difference in foundation depth and soil between the embankment and the bridge usually leads to vertical settlement (Puppala et al., 2009). Deep-seated circular landslides may lead to the failure of abutment foundations.

Component	EQ	FL	GF
Pier foundation		X	
Pier	X		
Bearing	X		
Deck		X	
Abutment foundation			X
Abutment	X		
Embankment			X
Shear key	X	X	

Table 17: Bridge components and corresponding hazard types to which they are susceptible.

Using the event taxonomy proposed by Lee and Sternberg (2008), the three hazard types considered here offer the opportunity to analyze *combined* events, i.e. a single event triggering multiple loading mechanisms such as an EQ event triggering a GF event, as well as *subsequent* events, i.e. unrelated single events triggered by different sources and possibly separated in time, such as a FL event followed by an EQ event. Therefore a flexible fragility model needs to be developed, where different hazard loading configurations can be taken into account, specifically:

- fragility to a single FL event;
- cumulated fragility to combined EQ and GF events;
- cumulated fragility to subsequent FL and EQ events (plus triggered GF event).

In this multi-hazard context, the modularity of the BN approach can prove very useful to combine the hazard-specific damage probabilities for each component, so that system-level fragility functions can be derived.

4.6.2 Derivation of component fragility curves

The modelling assumptions and the derivation of the fragility curves for each component damage state have been previously discussed in Gehl and D'Ayala (2015a). The following sub-sections detail the derivation process that has been adopted for each component and each hazard type.

a. Earthquake

To determine its seismic fragility curves, the MSSSC bridge has been modelled with the OpenSees platform (McKenna et al., 2000), using the same dimensions and constitutive models that are provided in Nielson (2005).

Additional pier foundations are also explicitly modelled. Pier foundations are assumed to be anchored down to a depth of 8 m: the group of pile foundations, as described by Nielson (2005), is approximated by an equivalent elastic beam, which is connected to the ground through a set of Winkler *p-y* springs in order to model the soil resistance (see Figure 44).

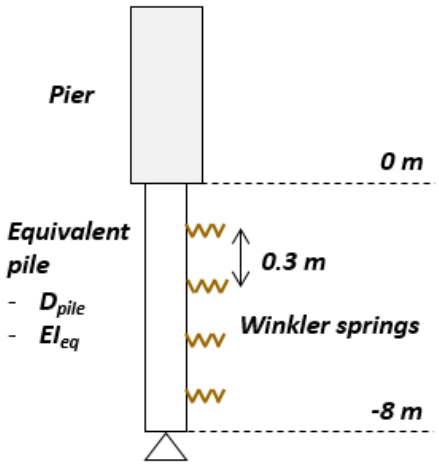

Figure 44: Schematic view of the equivalent pile foundations and the Winkler springs

A Winkler spring is located every 0.3 m between the altitudes 0 m and -8 m, in order to model the lateral resistance of the soil, as suggested by Prasad and Banerjee (2013). Each spring is associated with a *p*-*y* curve expressing the soil resistance *p* at a depth *h* as a function of pile deflection *y*:

$$p(y) = A \cdot p_u \cdot \tanh\left(\frac{k \cdot h}{A \cdot p_u} \cdot y\right) \quad \textbf{(19)}$$

where *A* is a modification factor to account for cyclic and static loading (*A* = 0.9), *k* is the initial modulus of subgrade reaction (*k* = 10,000 kPa), obtained from API (2000). The ultimate soil resistance p_u depends on the depth *h*:

$$p_u = \min\begin{cases}\left(C_1 \cdot h + C_2 \cdot D_{pile}\right) \cdot \gamma . h & \text{shallow foundation s} \\ C_3 \cdot D_{pile} \cdot \gamma . h & \text{deep foundation s}\end{cases} \quad \textbf{(20)}$$

where C_1, C_2 and C_3 are coefficients that can be determined using the API (2000) guidelines (C_1 = 1.9; C_2 = 2.65; C_3 = 28), *γ* is the volumetric mass of the soil, and D_{pile} is the equivalent diameter of the pile foundations.

Starting from a group of piles, an equivalent single pile has to be defined, as shown in Figure 44. The equivalent bending stiffness EI_{eq} for rocking motion can be computed according to Yin and Kanagai (2001), which enables the calculation of the equivalent diameter D_{pile} = 1.1 m. Finally, the *p*-*y* curves for the studied bridge model are computed for a few depths (see Figure 45).

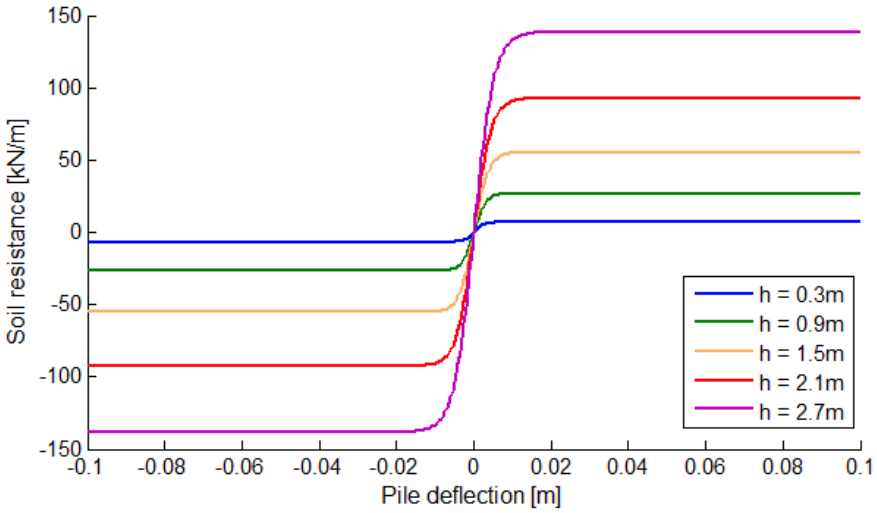

Figure 45: Force-deflection relations (*p-y* curves) for the soil surrounding the pile foundations, for different depths *h*

Additional shear keys are also added in order to account for the possibility of transversal movement of the deck spans. They are modelled according to a sliding friction shear mechanism: first, the deck slides on the pier cap according to a friction Coulomb law until the shear key is reached (i.e. gap closure). The capacity of the shear key is subsequently engaged until it ruptures through a shear mechanism. Once the shear key has failed, it is assumed that the deck keeps on moving freely until unseating. The assumed constitutive law for the shear keys is represented in Figure 46.

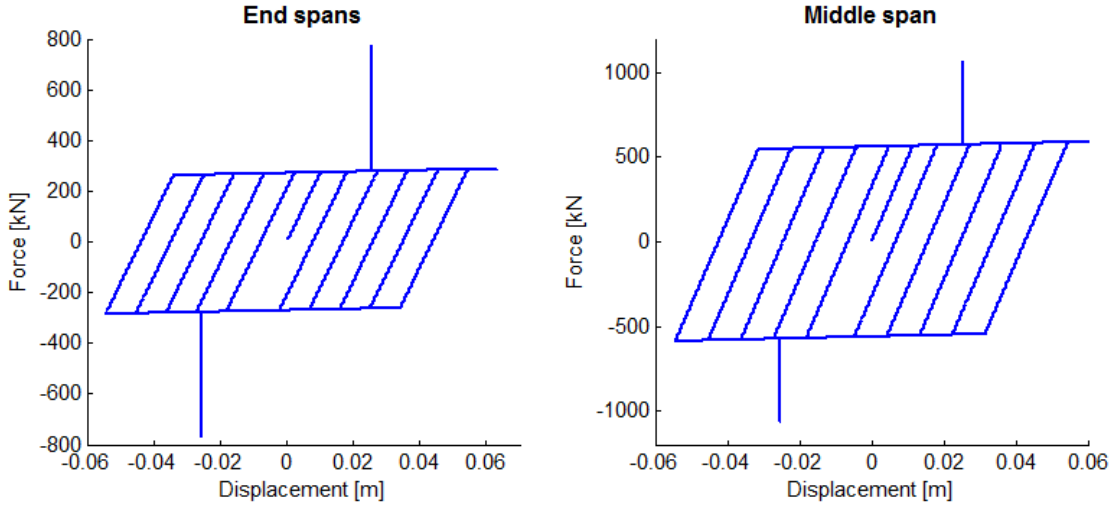

Figure 46: Force-displacement relationships for shear keys located at end and middle spans. The weight of the deck spans has a significant role on the friction behaviour.

For the purpose of deriving the fragility curves, non-linear dynamic analyses on the bridge models are carried out with 288 synthetic records for an appropriate range of magnitude and epicentral distance, based on the seismotectonic context of the area where the bridge has been modelled (i.e. Central Southern United States, see Nielson, 2005). The synthetic signals used here have been generated using a stochastic procedure developed by Pousse et al. (2006) and they are successively applied to the bridge system along the longitudinal and transversal directions. In the longitudinal direction, ten components are considered (i.e. piers P1 and P2, abutments A1 and A2, fixed and

expansion bearings B1 to B6), as well as in the transversal direction, except that the bearings are then replaced by the shear keys (i.e. Sh1 to Sh6), as shown in Figure 47.

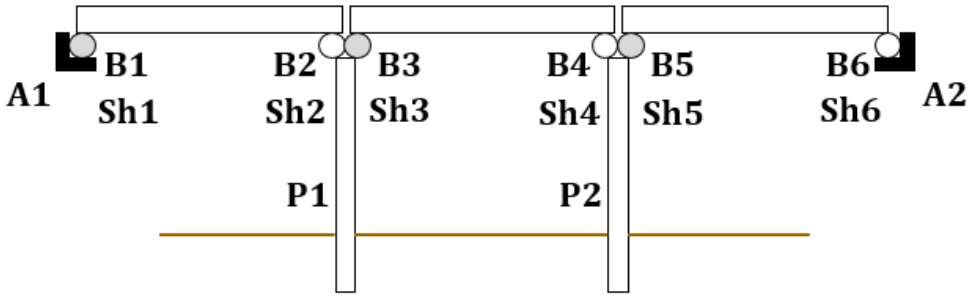

Figure 47: Bridge components in the seismic analysis. Grey circles represent fixed bearings, while empty ones are expansion bearings.

Fragility curves for each component and for each loading direction (i.e. longitudinal and transversal) are then derived, using the following damage states (see **Table 18**):

- Piers: yielding (D1) and ultimate deformation (D2) of the columns.
- Abutments: yielding of the abutment piles in tension (D1), i.e. active behaviour.
- Bearings: restraint failure (D1) and deck unseating (D2).
- Shear keys: shear key failure (D1) and deck unseating (D2).

Components	EDP	Longitudinal direction		Transversal direction	
		D1	D2	D1	D2
Piers	Curvature	1.29 $\Phi_{y,lon}$	5.24 $\Phi_{y,lon}$	1.29 $\Phi_{y,trans}$	5.24 $\Phi_{y,trans}$
Abutments	Displacement	0.0192 m	-	0.0192 m	-
Fixed bearings	Displacement	0.0125 m	0.1866 m	-	-
Expansion bearings	Displacement	0.0345 m	0.1866 m	-	-
Shear keys	Displacement	-	-	0.0255 m	0.1866 m

Table 18: Limit states for the component damage states (2005). Φ_y is the yield curvature corresponding to the yielding of the first steel reinforcement in the pier sections. The values for piers are based on Nielson (2005). For the other components, the values are based on the constitute laws (yield points or unseating limits).

The GLM regression (see section 2.2) is used to derive the seismic fragility curves, based on the components' responses from the 288 records, as shown in Figure 48. The fragility parameters for all components in both directions are summarized in **Table 19**.

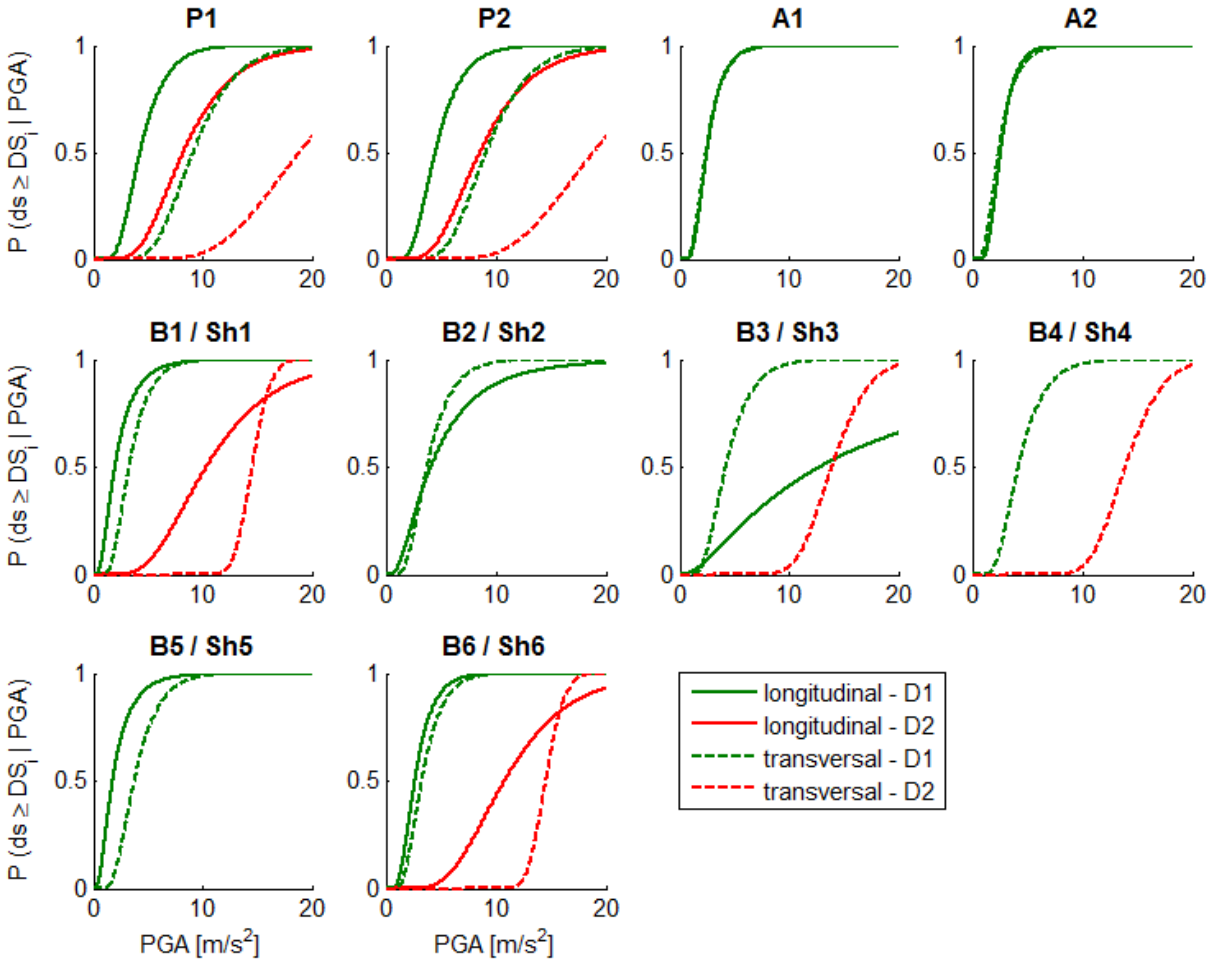

Figure 48: Fragility curves for the bridge components in both loading directions

Components	Longitudinal direction				Transversal direction				
	D1		D2		D1		D2		
	α [m/s^2]	β	α [m/s^2]	β	α [m/s^2]	β	α [m/s^2]	β	
P1	4.295	0.420	8.214	0.427	9.124	0.331	18.841	0.330	
P2	4.514	0.415	8.531	0.430	9.124	0.331	18.841	0.330	
A1	2.500	0.446	-	-	2.422	0.482	-	-	
A2	2.596	0.391	-	-	2.422	0.482	-	-	
B1 / Sh1	1.994	0.647	10.299	0.465	3.287	0.436	14.558	0.091	
B2 / Sh2	4.083	0.746	-	-	3.767	0.450	-	-	
B3 / Sh3	12.795	1.105	-	-	4.219	0.428	13.938	0.187	
B4 / Sh4	-	-	-	-	4.219	0.428	13.938	0.187	
B5 / Sh5	1.776	0.688	-	-	3.767	0.450	-	-	
B6 / Sh6	2.660	0.471	10.752	0.419	3.287	0.436	14.558	0.091	

Table 19: Fragility parameters (mean α and standard deviation β) for the bridge components in both loading directions. Some parameters are not defined since the damage state was not reached during the dynamic analyses.

b. Fluvial flood

It is assumed that the flood will affect mainly the interaction between the deck and the piers, by resulting in lateral pressure on the side of the deck. For simplicity, two subsequent damage states can be considered: the failure of the shear keys (D1) and the unseating of the deck (D2). The aim is to obtain a fragility curve describing the probability of reaching these damage states with respect to a flood IM, which can be represented by water height or velocity or flow discharge). Although there is anecdotal evidence on the vulnerability of bridges due to hurricanes and storm surges (Kameshwar and Padgett, 2014; Padgett et al., 2008), there is a dearth of data in literature to allow a robust quantification of the impact of fluvial floods on bridge superstructures. Pending the empirical or analytical development of suitable fragility models, in the present application it is proposed to use the fragility curve from Kameshwar and Padgett (2014) for bridge failure due to storm surge: a logit function has been used to represent deck unseating as a function of surge, bridge height and wave height (i.e. Eq. 16 in Kameshwar and Padgett, 2014) and it is proposed here to set the coefficient related to wave height equal to 0, in order to represent the fluvial flood as a very rough approximation. To determine the damage to shear keys (D1), a conservative assumption could consider failure as soon as the flow height reaches the top of the pier cap.

Although the aforementioned fragility models are expressed as a function of water height, it is proposed to convert this intensity measure into flow discharge *Q* in order to be consistent with the scour fragility curves (see next section). The fragility curves and parameters for these two damage states are presented in Figure 49 and in **Table 20**, respectively.

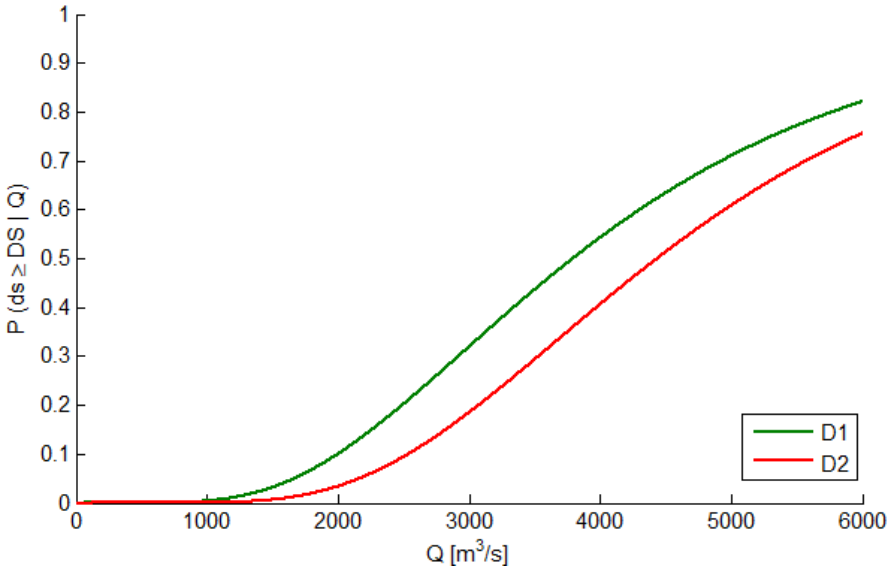

Figure 49: Fragility curves for the shear keys and deck spans exposed to fluvial flood

Damage states		α [m^3/s]	β
D1	Shear key failure	3789.9	0.500
D2	Deck unseating	4433.1	0.436

Table 20: Fragility parameters (mean α and standard deviation β) for the shear keys and deck spans exposed to fluvial flood.

It should be noted that the fragility curves proposed here are case-specific, since the expression of the flow discharge *Q* is directly based on the flow velocity and the width and depth of the river section. More generic fragility models should consist in a series of curves taking also into account parameters like that the dimensions of the river section.

c. Flood-induced scour

Another effect of fluvial flood is induced scour: in the present study, only local scour at piers is considered, since the general scour level (i.e. river bed degradation) is usually less significant than local scour (Barbetta et al., 2015). Also, contraction scour may be neglected if we assume that there is not sudden change in the river bed cross-section. Empirical equations from HEC-18 (Richardson and Davis, 1995) are used to estimate the local scour depth y_s:

$$y_s = 2 \cdot K_1 \cdot K_2 \cdot K_3 \cdot K_4 \cdot y \cdot \left(\frac{D}{y} \right)^{0.65} \cdot F^{0.43} \quad \textbf{(21)}$$

Where *y* represents the flow height, *D* is the pier width, *F* is the Froude number and the K_i parameters are corrective coefficients (see **Table 21**). The Froude number is expressed as:

$$F = \frac{v}{g \cdot y} \quad \textbf{(22)}$$

Since the Froude number is a function of both flow height and flow velocity, a way to keep the scour depth dependent on a single scalar IM is to combine these quantities into a new variable, such as the flow discharge *Q*. Assuming a rectangular river section, *Q* can be expressed as a function of velocity *v* and height *y* (Alipour et al., 2013), with river bed width *b*:

$$Q = b \cdot y \cdot v = \frac{b \cdot y}{n} \cdot \left(\frac{b \cdot y}{b + 2y} \right)^{2/3} \cdot S_0^{1/2} \quad \textbf{(23)}$$

Where Manning's roughness coefficient *n* and slope grade S_0 are also specified in **Table 21**.

Variable	Description	Distribution	Value
K_1	Factor for pier nose shape	-	1
K_2	Factor for flow angle of attack	uniform	[1;1.5]
K_3	Factor for bed condition	normal	μ = 1.1; σ = 0.055
K_4	Factor for bed material size	-	1
N	Manning's roughness coefficient	lognormal	μ = 0.025; σ = 0.275
S_0	Slope grade	lognormal	μ = 0.02; σ = 0.5

Table 21: Parameters used in the scour equations. Some of the probability distributions are taken from Alipour and Shafei (2012).

The input parameters in **Table 21** are then sampled through a Monte Carlo scheme in order to generate 10,000 couples of values [Q ; y_s], for different flow heights y. It is then possible to derive `scour fragility curves' that express the probability of reaching a given scour depth with respect to flow discharge *Q*.

Three damage states have been defined, based on the effect the scour level has on the pier initial stiffness and the response of the bridge system under seismic loading:

- For $y_s \geq 1$ m (D1): the first noticeable changes in the bridge's dynamic properties begin to appear;
- For $y_s \geq 3.6$ m (D2): significant changes in the bridge response can be observed;
- For $y_s \geq 5.1$ m (D3): the scour depth reaches almost the foundation length and it is assumed that the pier is not stable enough to support the bridge, as the moment capacity of the foundation is lost.

The fragility curves and parameters for these three damage states are presented in Figure 50 and in **Table 22**, respectively.

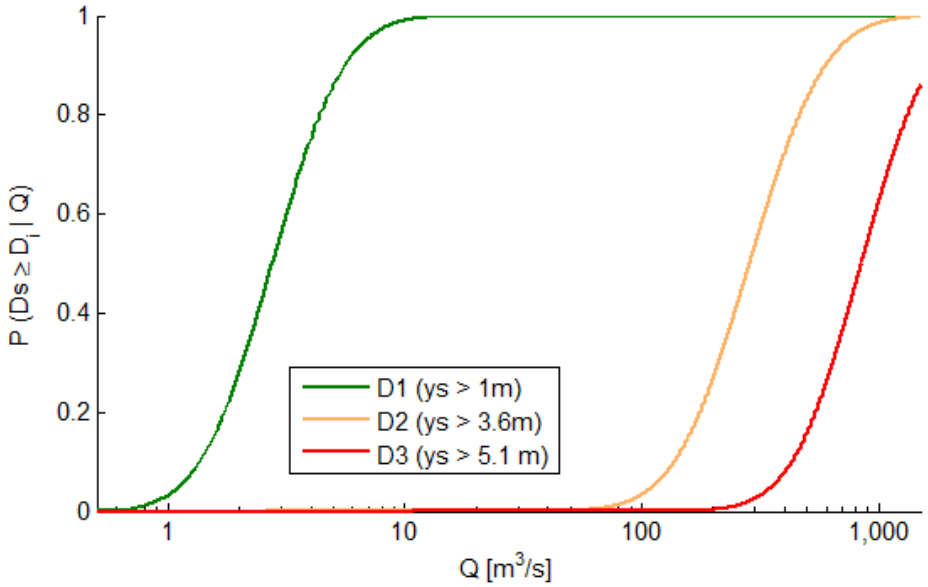

Figure 50: Fragility curves for pier foundations exposed to local scour

Damage states		α [m^3/s]	β
D1	$y_s \geq 1$ m	2.7	0.551
D2	$y_s \geq 3.6$ m	285.8	0.574
D3	$y_s \geq 5.1$ m	847.6	0.531

Table 22: Fragility parameters (mean α and standard deviation β) for the shear keys and deck spans exposed to fluvial flood.

Similarly to the case of fluvial floods in the previous subsection, the fragility curves for scour have been derived for a specific bridge, with given dimensions of river section and a given foundation length. For instance, the limit states for scour depend directly on the type of foundations thas is considered (i.e. deep or shallow), while the expression of the flow discharge Q as a function of flow height is only valid for this specific river section. Generic fragility curves for a set of bridges would require additional parameters representing various configurations of foundations and river sections.

d. Ground failure

The first components that are likely to be damaged by GF events are the approach embankments, which ensure the link between the plain road segment and the bridge causeway. Fragility curves derived by Kaynia et al. (2011) are used to assess the failure probability of embankments in the case of lateral spreading of the supporting soil. Two damage states are considered, namely slight damage corresponding to a permanent ground displacement of 30 mm (D1) and moderate damage corresponding to a permanent ground displacement of 150 mm (D2).

Slope failure may also affect abutments, however the depth of the foundations of well-designed bridge abutments usually prevents superficial landslides from having an effect on the abutment itself. Still, in the case of deep-seated circular landslides that generate ground displacements below the depth of the abutment footing, it is possible to witness significant differential displacements that may lead to bridge collapse. Hence circular slope failure is proposed as the relevant failure mechanism for abutment foundations, characterized by a single damage state D1. To this end, the factor of safety *FS* of potential sliding surfaces can be estimated with the limit equilibrium method (i.e. Bishop's simplified method). The surface is subdivided into a number *n* of vertical slices and the factor of safety *FS* is then expressed as the ratio of resisting versus destabilizing moments of all the slices (see Figure 51):

$$FS = \frac{\sum_{i=1}^{n} \frac{1}{F_\alpha} \cdot \left[c_i \cdot b_i + \tan \phi_i \cdot \left(W_i - u_i \cdot b_i \right) \right]}{\sum_{i=1}^{n} W_i \cdot \sin \theta_i + K_h \cdot W_i \cdot \frac{L_i}{R}} \quad \textbf{(24)}$$

Where K_h is the horizontal seismic coefficient expressed as a function of PGA (Noda et al., 1975):

$$K_h = \frac{1}{3} \cdot \left(\frac{\mathrm{PGA}}{g} \right)^{1/3} \quad \textbf{(25)}$$

The factor F_α is expressed as:

$$F_\alpha = \cos \theta_i + \frac{\tan \phi_i \cdot \sin \theta_i}{FS} \quad \textbf{(26)}$$

Since the factor *FS* is present in both sides of the equations, a small iteration process is required in order to converge to the final *FS* value after a few steps.

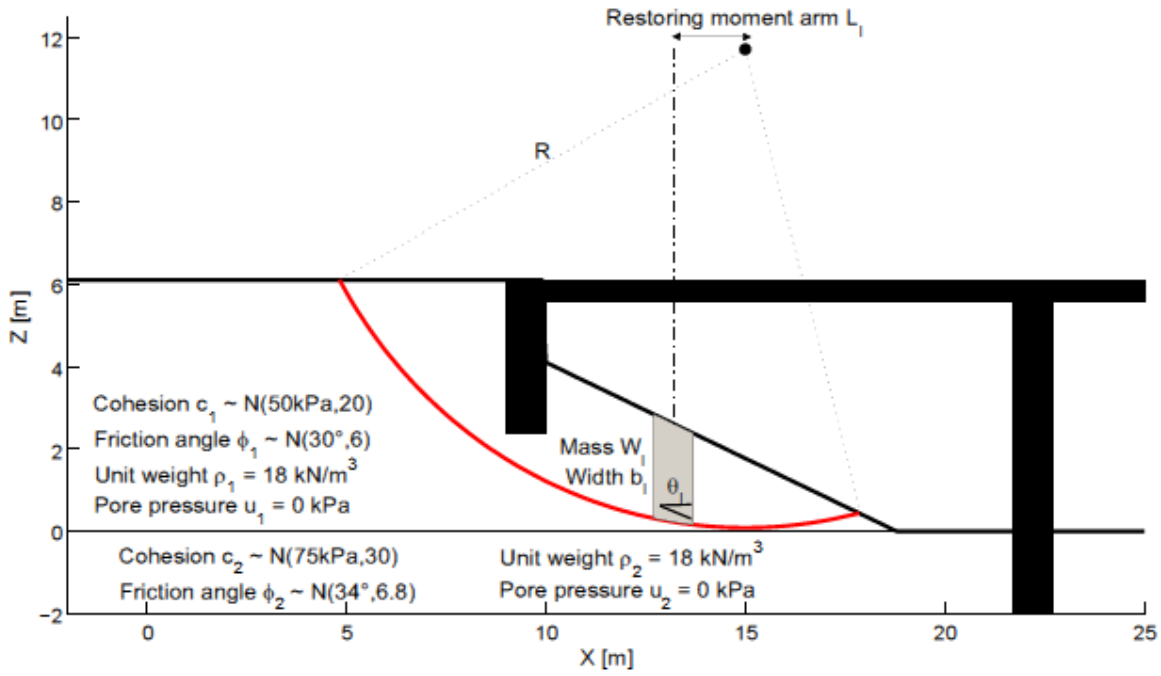

Figure 51: Slice equilibrium method for the estimation of the factor of safety for circular slope failure. The black shape is a simplified view of the studied bridge and its foundations.

Fragility functions for slope instability (D1) are then derived following the method proposed by Wu (2015): for each increasing value of PGA, the reliability index of log *FS* > 0 is estimated using a Mean-Value First-Order Second Moment (MFOSM) method:

$$\beta_{FS} = \frac{\log FS\left(\mu_{X_i}\right)}{\sqrt{\sum_{i=1}^{n}\left(\frac{\partial \log FS}{\partial X_i}\right)^2 \cdot \sigma^2[X_i] + 2\sum_{i,j=1}^{n}\left(\frac{\partial \log FS}{\partial X_i}\right)\cdot\left(\frac{\partial \log FS}{\partial X_j}\right)\cdot\rho\cdot\sigma[X_i]\cdot\sigma[X_j]}} \quad (27)$$

The input random variables X_i are the cohesion and friction angle of each soil layer, while a correlation factor of ρ = -0.4 is assumed between them (Wu, 2013). The search algorithm for the probabilistic critical surfaces proposed by Hassan and Wolff (1999) is used in order to ensure that the minimum reliability index is found for each combination of the soil parameters and each proposed surface, based on the distribution of the factor of safety with respect to the value 1. An additional constraint is introduced by the location of the abutments foundations, since the critical surface is unlikely to generate any bridge failures if it intersects with the bridge foundations: therefore the critical surfaces that are found with the limit equilibrium method have to be deep enough, so that the ground displacement is unhindered by the abutments foundations, as it is shown in Figure 6. Finally, the reliability index is converted into the probability of failure P_f and the points [PGA ; P_f] are fitted into a fragility curve with a lognormal cumulative distribution function.

The fragility curves and parameters for the component damage states due to ground failure are presented in Figure 52 and in **Table 23**, respectively.

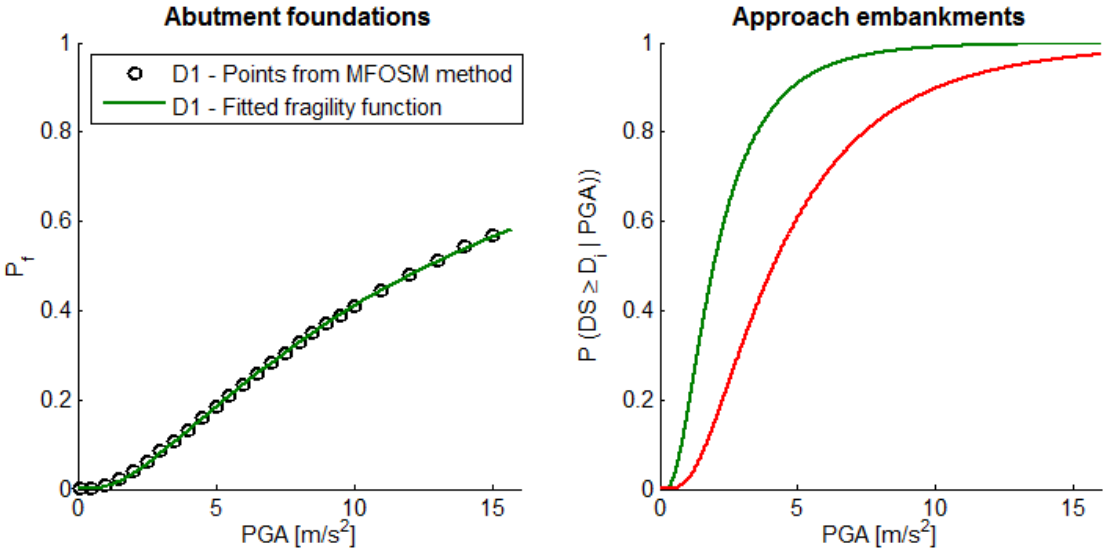

Figure 52: Fragility curves for components exposed to ground failure

Component	Damage states		α [m/s^2]	β
Approach embankments	**D1**	Subsidence ≥ 0.03 m	1.962	0.700
	D2	Subsidence ≥ 0.15 m	4.120	0.700
Abutment foundations	**D1**	Slope failure	12.617	1.032

Table 23: Fragility parameters (mean α and standard deviation β) for components exposed to ground failure.

e. Multi-hazard fragility functions

To determine the cascading effects of fluvial flood or scour on earthquake response, different bridge models must be developed, either by removing some Winkler springs (i.e. to model scour damage) or by removing the shear keys (i.e. to model damage due to fluvial flood). This step is essential to account for cumulated damage and multi-risk interactions at the vulnerability level, thus leading to a set of damage-dependent component fragility functions. Assuming a FL event followed by a subsequent EQ event, a total of six bridge configurations have to be considered, as shown in Table 24. The thresholds for the three scour damage states described in the previous subsection have been estimated by performing a sensitivity analysis on the seismic fragility of the bridge components, based on the number of Winkler springs that are removed. Scour depths for which a significant variation in the seismic fragility parameters is observed are then considered as the scour limit states. Finally, the seismic fragility curves are derived for each scour damage state by sampling the scour depth that is comprised between two consecutive scour thresholds.

Bridge configuration	Scour damage	Fluvial flood damage
1	D0	D0
2	D0	D1*
3	D1	D0
4	D1	D1*
5	D2	D0
6	D2	D1*

Table 24: Different bridge models considered to account for cumulated damage effects for FL and EQ events. The * symbol represents models that are only changing in the transversal direction**.** Scour damage D3 is not included since it has assumed that such level of scour would lead to the failure of the whole bridge system.

The seismic fragility parameters for flood-damaged bridge components are summarized in **Table 25** and **Table 26**, while the evolution of the mean α between the different configurations is represented in Figure 53).

Components	Scour damage D1				Scour damage D2			
	D1		D2		D1		D2	
	α [m/s^2]	β	α [m/s^2]	β	α [m/s^2]	β	α [m/s^2]	β
P1	5.279	0.471	9.878	0.445	17.245	0.539	17.837	0.558
P2	5.336	0.479	10.001	0.438	17.245	0.539	17.837	0.558
A1	2.527	0.456	-	-	2.498	0.475	-	-
A2	2.517	0.426	-	-	2.498	0.475	-	-
B1	1.933	0.615	9.409	0.461	2.042	0.660	6.917	0.564
B2	3.628	0.737	-	-	2.892	0.618	17.997	1.021
B3	14.164	1.020	-	-	-	-	-	-
B4	-	-	-	-	-	-	-	-
B5	1.634	0.677	-	-	1.400	0.702	-	-
B6	2.639	0.504	9.982	0.416	2.597	0.519	6.468	0.543

Table 25: Seismic fragility parameters (mean α and standard deviation β) for components in the longitudinal direction, for different damage configurations.

Components	Scour damage D1				Scour damage D2			
	D1		D2		D1		D2	
	α [m/s^2]	β	α [m/s^2]	β	α [m/s^2]	β	α [m/s^2]	β
Fluvial flood damage D0								
P1	14.458	0.319	18.591	0.267	14.896	0.251	14.896	0.251
P2	14.458	0.319	18.591	0.267	14.896	0.251	14.896	0.251
A1	2.389	0.488	-	-	2.385	0.495	-	-
A2	2.389	0.488	-	-	2.385	0.495	-	-
Sh1	2.561	0.521	13.559	0.301	2.80	0.525	11.475	0.415
Sh2	3.036	0.445	18.919	0.286	2.663	0.437	14..46	0.183
Sh3	10.260	0.740	15.375	0.193	14.199	0.101	-	-
Sh4	10.260	0.740	15.375	0.193	14.199	0.101	-	-
Sh5	3.036	0.445	18.919	0.286	2.663	0.437	14..46	0.183
Sh6	2.561	0.521	13.559	0.301	2.80	0.525	11.475	0.415
Fluvial flood damage D1								
P1	13.655	0.320	16.602	0.225	14.189	0.260	14.189	0.260
P2	13.655	0.320	16.602	0.225	14.189	0.260	14.189	0.260
A1	2.334	0.464	-	-	2.362	0.483	-	-
A2	2.334	0.464	-	-	2.362	0.483	-	-
Sh1	-	-	10.875	0.548	-	-	7.940	0.561
Sh2	-	-	14.764	0.128	-	-	-	-
Sh3	-	-	15.739	0.335	-	-	-	-
Sh4	-	-	15.739	0.335	-	-	-	-
Sh5	-	-	14.764	0.128	-	-	-	-
Sh6	-	-	10.875	0.548	-	-	7.940	0.561

Table 26: Seismic fragility parameters (mean α and standard deviation β) for components in the transversal direction, for different damage configurations.

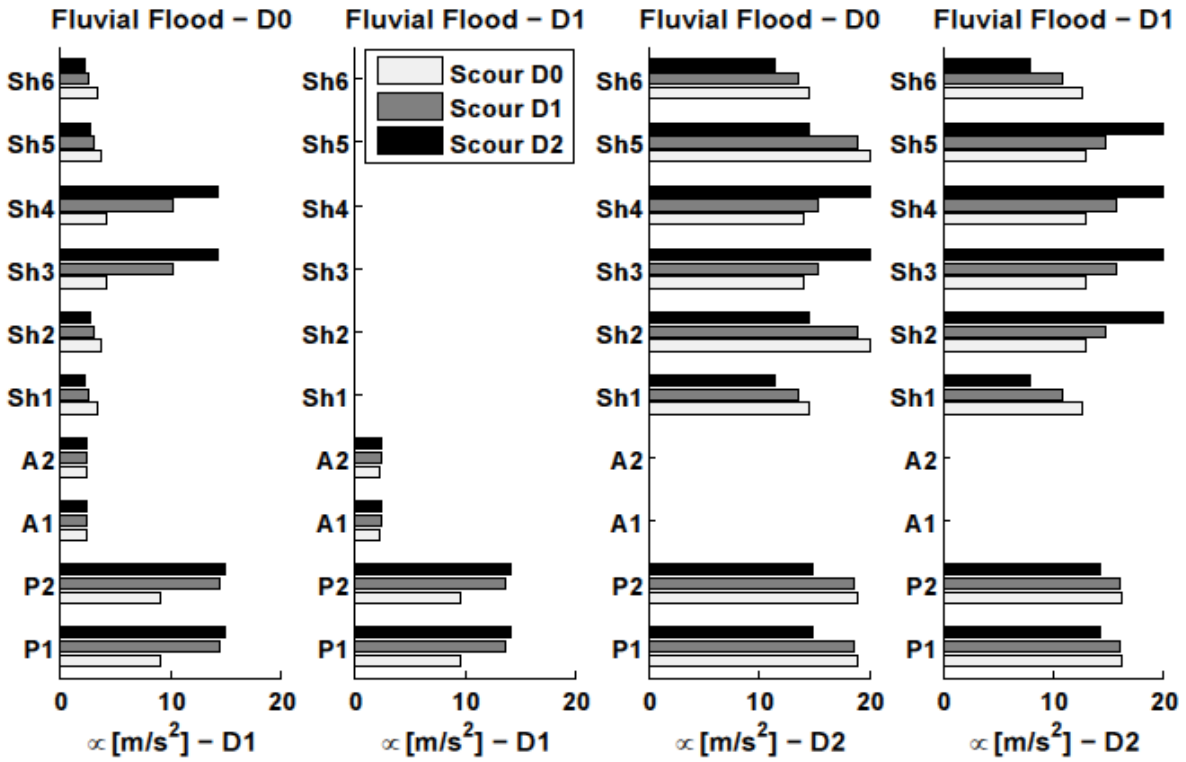

Figure 53: Evolution of the mean seismic fragility parameter α for both EQ damage states D1 and D2 and all components in the transversal direction, depending on the initial state of the bridge in terms of scour and fluvial flood damage

The resulting fragility parameters in Figure 53 show that scour globally tends to raise the seismic vulnerability of shear keys, except for the ones that are in the middle of the bridge (i.e. Sh3 and Sh4). Regarding piers, the removal of Winkler springs relaxes the connection at the pier base, which has the effect of lowering bending moments and decreasing the failure probability for higher scour levels. Finally, the response of abutments seems to remain stable across the different scour depths. Similar observations have been made when fragility curves are computed for the components in the longitudinal direction. When shear keys are removed (i.e. fluvial flood D1), the seismic fragility slightly increases for lower damage states, while this effect becomes more significant for further damage states (i.e. the absence of restraints favours the occurrence of deck unseating).

It should be noted that a perfectly symmetric shape of the bridge and the river bed is assumed, so that the probabilities of reaching the different scour levels are equal at each pier location. Also, in order to limit the number of bridge configurations, it is assumed that the scour events have a joint occurrence across the different piers: this assumption tends to be conservative, since a bridge for which all pier foundations are subjected to scour will experience a more altered seismic response than a bridge for which only a portion of the piers are affected. The study of all possible configurations should still deserve dedicated effort in order to refine the global failure probabilities.

4.6.3 Definition of system failure modes

According to the above discussions (see section 4.4), it is proposed to define a set of functionality loss levels and to associate them with specific system damage events, in order to identify the various damage configurations that may lead to similar consequences in terms of bridge closing time or repair operations.

These metrics represent the ultimate objective of the proposed BN approach, since they allow the evaluation of the bridge performance in terms of functionality, regardless of the component damage event or hazard event that led to it: therefore this framework is able to harmonize a system-level fragility function across multiple hazard types. Instead of speaking in terms of 'system damage states'', which implies a clear hierarchy in the severity of the damage states, it is more appropriate to refer to 'system failure modes', which allows for consideration of either intersecting or disjoint sample spaces (e.g. see Figure 54). In particular, this approach decouples the direct correlation between the severity of a hazard event and the magnitude of the consequences, which is implicit in the damage state definition. Investigating different failure modes which may or may-not occur concurrently with different probability levels, allows the direct effect on functionality of low probability events, with modest independent intensity, but high consequences to be investigated. Therefore, based on simple considerations on the severity of each component damage state and on the corresponding functionality loss levels they might induce, a rationale is proposed here in order to identify homogeneous system failure modes:

- Failure mode F1 corresponds to slight damage only to approach embankments (D1), as such damage would not have a significant impact on the bridge functionality, even though repair operations would be eventually necessary. This failure mode may correspond to a functionality loss level FL1, implying slight repairs but no closing time;

- Failure mode F2 corresponds to minor structural damage to bridge components (i.e. piers, abutments, bearings and shear keys in damage state D1 due to earthquake, approach embankments in damage state D2 due to ground failure, damaged shear keys D1 due to fluvial flood). This failure mode may correspond to a functionality loss level FL2, implying moderate repairs with a short closing time;

- Failure mode F3 corresponds to a deck unseating event that induces long term closure of the bridge, even though temporary deck spans could be installed if the substructure components have not collapsed (i.e. deck unseating D2 due to fluvial flood, bearings and shear keys in damage state D2 due to earthquake). This failure mode may correspond to a functionality loss level FL3, implying extensive repairs with a prolonged closing time.

- Failure mode F4 corresponds to substructure components that have collapsed, thus inducing the total failure of the bridge system (i.e. piers and abutments in damage state D2 due to earthquake, scour damage state D3 at pier foundations, slope failure D1 beneath abutment foundations). This failure mode may correspond to a functionality loss level FL4, implying irreparable damage (e.g. full collapse of the bridge system).

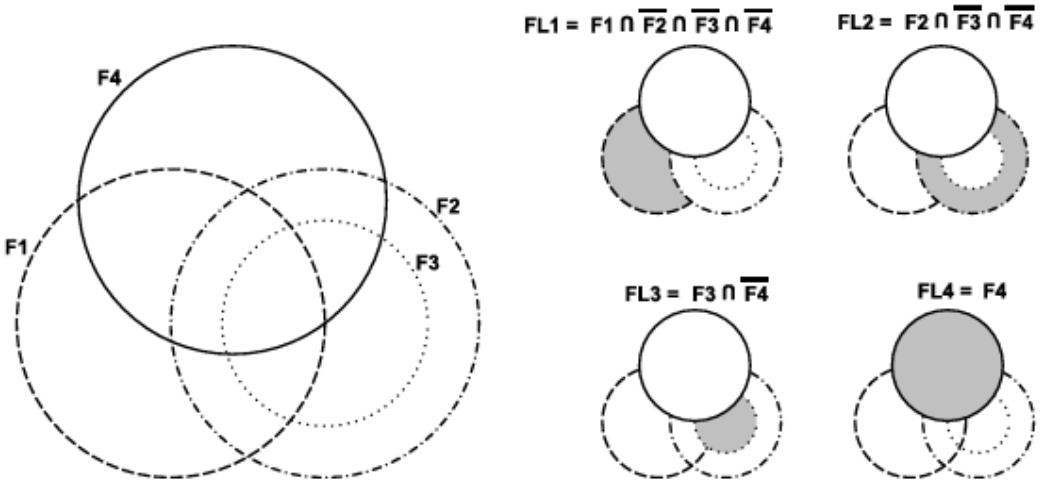

Figure 54: Venn diagrams representing the four failure modes and how they are assembled in order to specify the four functionality levels (grey area). F3 appears to be nested inside F2 because a quick analysis of the component failures leading to these failure modes reveals that the occurrence of F3 necessarily implies the occurrence of F2.

These failure modes are summarized in **Table 27**, where all the in-series component damage events are detailed for each mode. They are also represented as Venn diagrams in Figure 54 in order to demonstrate that they do not follow a clear hierarchy unlike regular damage states. Corresponding functionality loss levels, on the other hand, show a gradation in the repair costs and closing time: therefore it can be argued that, when two failure modes have a joint occurrence, the most severe functionality loss level is assumed (see right of Figure 54).

Failure mode	FL	EQ	GF
F1	-	-	Em(D1)
F2	-	P_x(D1), P_y(D1), A_x(D1), B(D1), Sh(D1)	Em(D2)
F3	De(D2)	B(D2), Sh(D2)	-
F4	P_f(D3)	P_x(D2), P_y(D2)	A_f(D1)

Table 27: Component damage states from the different hazard events leading to the four failure modes. For simplification purposes, only the component classes are displayed, and not the specific instances (e.g. only the component class bearing B is mentioned, to which six components belong in the actual model, while the number of them actually failing is not explicitly referred to). The x and y letters represent the component responses in the longitudinal and transversal directions, respectively. De represents the deck, Em the approach embankment, P_f the pier foundation and A_f the abutment foundations.

Finally, it should be noted that the proposed failure modes and functionality loss levels are mostly based on few literature references detailing usual causes of bridge failures (Doll and Sieber, 2011; Lebbe et al., 2014; Deng et al., 2015) or post-disaster accounts (Elnashai et al., 2010). Thanks to the expert-based survey aiming at quantifying functional consequences from component damage states (see section 4.4), this qualitative rationale may be refined in order to obtain an estimate of the expected functionality losses, downtime durations or repair costs. As a result, estimated bounds for functional consequence metrics are proposed in **Table 47**.

Failure mode	Duration	Functional Loss	Functional Loss during Intervention	Cost
F1	-	-	-	-
F2	1-90 days	0%-25% (speed)	0%-10% (speed)	0%-20%
F3	60-120 days	100% closed lanes	75% closed lanes	20%
F4	90-150 days	100% closed lanes	100% closed lanes	20%-100%

Table 28: Estimation of approximate loss metrics for the four failure modes identified, according to the INFRARISK expert-based survey.

Regarding failure mode 1 (i.e. slight subsidence of abutment approach), it is difficult to quantify the functional losses due to the very low damage extent: a 100% remaining functionality with very fast repair operations (e.g. less than a day) might be assumed.

4.6.4 Bayesian inference for the joint derivation of system fragility functions

Once the component fragility curves and the system failure modes have been fully described, it is possible to build the corresponding BN by using the various algorithms described in section 2.3.2. A simplified graph of the BN is shown in Figure 55, where components are represented by their class, as explained in **Table 27**: the actual BN that has been solved with the Bayes Net toolbox contains each of the components of the bridge model and results in 64 nodes and 140 edges.

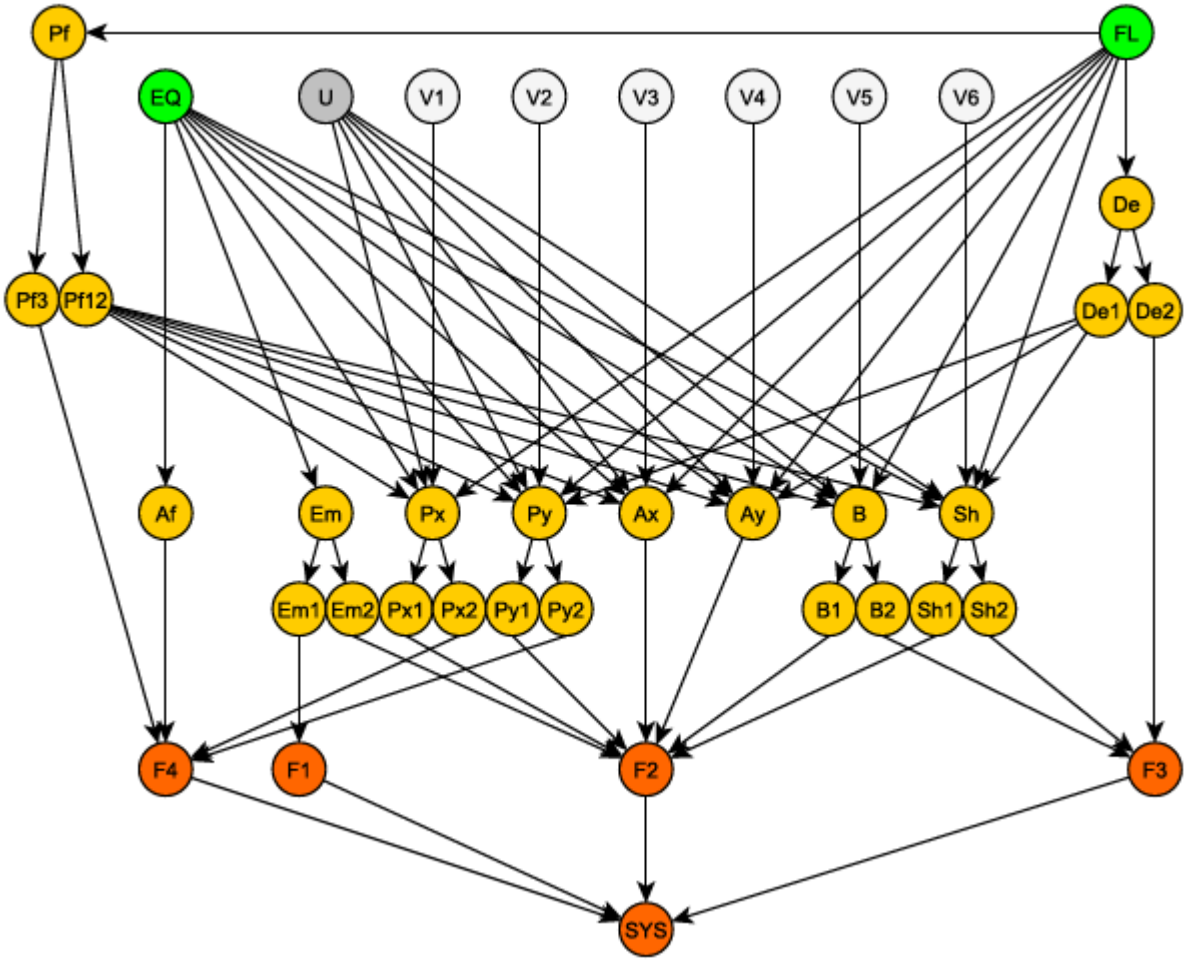

Figure 55: Global Bayesian Network for the bridge system exposed to seismic and flood loadings

Numerical seismic analyses of the bridge system (i.e. non-linear time history analyses) enable a straightforward correlation matrix of the component responses to be obtained, however this is not the case for floods and ground failures. It can however be assumed that flood- and earthquake-related failures are statistically independent, therefore a correlation factor of 0 is used between the damage events that are induced by different hazard types. Therefore the correlation matrix is only built for earthquake-related events and it is assembled from 20 elements (i.e. 10 bridge components in each direction, longitudinal and transversal). One limitation of the BN construction in Figure 66 is that the correlation coefficients r_i do not evolve with the different bridge configurations representing initial flood damage, since it may be expected that changes in the dynamic properties of the bridge system will alter the component responses and therefore the correlation matrix. However it has been observed that the changes are not significant for the present case-study: in cases for which the evolution of the correlation matrix would be too important to be neglected, additional BN nodes could still be added in order to represent the possible values of r_i.

In order to better explain the BN structure in Figure 55, the series of events leading to the `deck unseating' failure mode F3 can be summarized as follows (see Figure 56):

- Deck unseating **F3** occurs if one of the bearings (or shear keys) exceeds a given deformation level (damage state D2) in the longitudinal (or transversal) direction (i.e. component events **B2** or **Sh2**), or if the deck (i.e. component event **De2**) is directly upset by the fluvial flood (i.e. hazard event **FL**);
- Bearing (or shear key) deformation is triggered by seismic loading (i.e. hazard event **EQ**) and may be modified by the state of the pier foundations (i.e. component event **P_f12**);
- Piers foundations (i.e. component event **P_f**) are altered by scour due to fluvial flood);
- The seismic response of shear keys in the transversal direction is also influenced by the damage to shear keys (i.e. component event **De1**) due to fluvial flood.

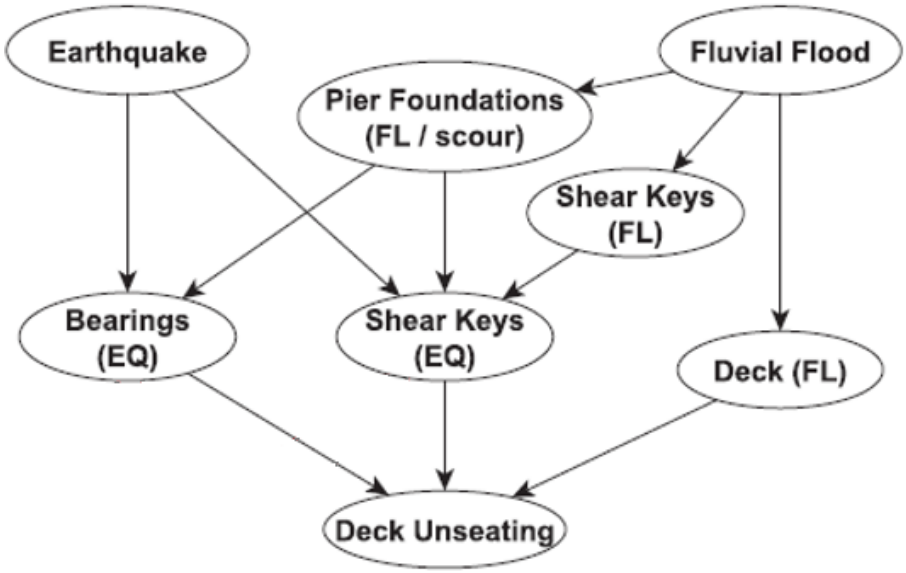

Figure 56: Simplified Bayesian Network summarizing the chain of events potentially leading to deck unseating

For each selected combination of values [PGA ; Q], the BN algorithm performs an inference in order to estimate the probability of occurrence of each of the failure modes. As a result, it is possible to express a system fragility function with respect to both seismic and flood intensity measures (see Figure 57). The output of the BN inference can be represented as fragility surfaces that express the failure probabilities with respect to two statistically independent intensity measures. If either an FL event or an EQ (triggering a GF) event has to be considered separately, the corresponding probabilities of functional damage can be evaluated just by reading the function values along the corresponding horizontal axis.

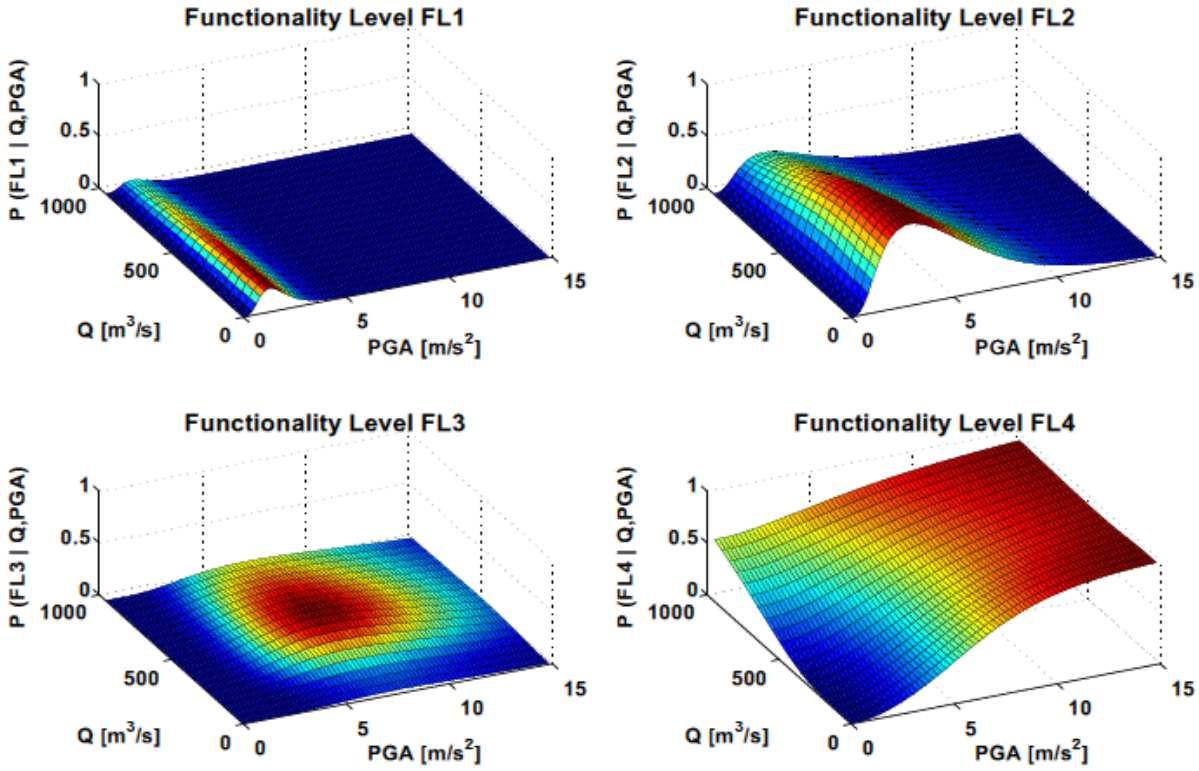

Figure 57: Multi-hazard fragility functions for the four functionality levels, expressed as a function of Q (flow discharge) and PGA (peak ground acceleration)

It can be seen that the effect of fluvial flood is mainly significant for heavier damage states, such as full collapse (i.e. FL4): this observation is in line with the fact that pier foundation scour or shear key removal have the greatest influence on the seismic response of bridge components for damage state D2 (see subsection 4.7.2.e). The [PGA ; Q] space where deck unseating (i.e. FL3) is the most likely to occur corresponds to very specific values of the intensity measures: this is another interesting feature of the proposed BN approach, since it enables low probability failure modes that may only occur under narrow ranges of combination of uncorrelated hazard events' intensities to be captured. Although the joint probability is low, the range of intensity of both hazards is relatively modest and hence their probability of occurrence commensurable to the life span of the structure and comparable in intensity to their reference design value: hence the functionality losses can be severe as they are unexpected.

5.0 FRAGILITY FUNCTIONS FOR TUNNELS

This section reviews the available fragility models that can be used for the different hazard types considered.

5.1 General description of tunnel elements

The following paragraphs describe the main components that usually comprise a tunnel system.

5.1.1 Typological classification

The NCHRP report on safety of transportation tunnels (NCHRP, 2006) provides a comprehensive summary of the main features and typologies associated with tunnels. One common way to classify tunnels is through their construction method (NCHRP, 2006):

- Immersed tube tunnels:
    - Employed to traverse a water body;
    - Precast sections are placed in a pre-excavated trench and connected;
    - Typical materials include steel and concrete immersed tunnels section;
    - After placement, tunnel is covered with soil;
- Cut-and-cover tunnels:
    - In urban areas;
    - Excavated from the surface, then constructed in place and backfill placed to bury structure;
    - For subway line structures, subway stations, and subsurface highway structures;
    - Typically concrete case-in place or precast sections;
    - Steel framing and concrete fill;
- Bored or mined tunnels:
    - In urban or remote locations in land, on mountains, or through water bodies;
    - Bored using a variety of techniques;
    - Supported by initial and final support systems;
    - Soft ground or rock tunneling;
    - Structure may have various liner systems, including rock reinforcement, shotcrete, steel ribs and lattice girders, precast concrete segment, cast-in-place concrete, and fabricated steel lining;
- Air-rights structure tunnels:
    - In urban areas;
    - Created when a structure is built over a roadway or trainway using the roadway's or trainway's air rights;
    - The limits that an air-rights structure imposes on the emergency accessibility and function of the roadway or trainway that is located beneath the structure should be assessed.

Usually bored or mined tunnels have a circular or horseshoe section, while it is rectangular for cut-and-cover tunnels. Critical elements of a tunnel include the lining, which serves to ensure the integrity of the tunnel section with respect to the surrounding soil or water pressure, and the tunnel portal, which is exposed to slope failures or rock falls that threaten to block the tunnel entrance. For road tunnels that are longer than a few hundred meters, forced air ventilation systems are usually

necessary (see Figure 58). For shorter railway tunnels, the train's piston action can be sufficient to ensure a proper ventilation of the tunnel.

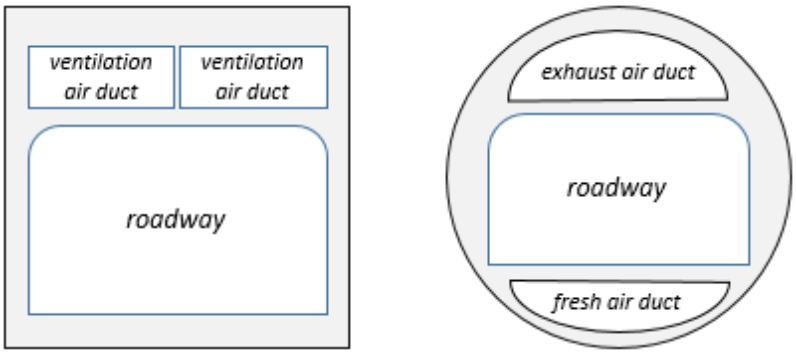

Figure 58: Schematic view of the layout of a cut-and-cover tunnel (left) and of a bored tunnel (b), adapted from NCHRP (2006)

A taxonomy of tunnel typologies has also been proposed Argyroudis and Kaynia (2014). It is based on characteristics such as:

- **Construction method:** Bored (B), Cut & Cover (C), Immersed (I)
- **Shape:** Circular (C), Rectangular (R), Horseshoe (H)
- **Depth:** Surface (Su), Shallow (Sh), Deep (D)
- **Geological conditions:** Rock (EC8 soil class A), Alluvial (EC8 soil classes B and higher)
- **Supporting system:** Concrete (C), Masonry (M), Steel (S), etc.

5.1.2 Tunnel components

Tunnel systems are usually decomposed into three main of components (NCHRP, 2006), which are briefly detailed below.

a. Tunnel liner

The tunnel liner consists of the structural system that prevents the surrounding soil pressure from crushing the tunnel cavity. It gives its shape to the tunnel section. Based on the type of soil and construction technique, various types of tunnel liners can be found (NCHRP, 2006):

- **Rock reinforcement:** steel bolts or dowels drilled into the surrounding rock in order to consolidate the strength of the rock mass;
- **Shotcrete:** layer of concrete projected over the surface in order to ensure the cohesion of the rock mass;
- **Steel ribs and lagging:** regularly-spaced ribs around the tunnel section;
- **Precast concrete segment lining:** bolted or unbolted concrete segments around the section;
- **Cast-in-place concrete lining:** usually used as a second inner lining;

- **Fabricated steel or cast iron lining:** designed to prevent leakage or withstand exterior water pressure.

The type of lining solution is heavily influenced by the geotechnical conditions, as summarized in Table 29.

Lining system	Strong rock	Medium rock	Soft rock	Soil
Rock bolts	**X**			
Rock bolts with wire mesh	**X**	**X**		
Rock bolts with shotcrete		**X**		
Steel ribs and lattice girder		**X**	**X**	**X**
Cast-in-place concrete			**X**	**X**
Concrete segments			**X**	**X**

Table 29: Type of lining and support systems depending on soil conditions (adapted from NCHRP, 2006).

b. Tunnel portal

The tunnel portal represents the entry of the tunnel as well as the surrounding area: it is highly exposed to ground failure events due to the presence of high-grade slopes in the vicinity, with the potential for slope failure or rock falls.

c. Support systems

Support systems represent all the essential utility systems that are required for the tunnel to operate under normal conditions of safety: air ventilation system, lighting and signalling system, emergency areas, auxiliary evacuation tunnel, etc.

5.2 Failure modes

The various tunnel components have a very specific susceptibility to the different hazard types, as demonstrated in the following paragraphs.

5.2.1 Possible failure modes and corresponding limit states for seismic hazard

This section reviews some of the recent studies that describe damage states and limit values for various tunnel components exposed to seismic hazard.

a. HAZUS technical manual for earthquakes (NIBS, 2004)

In the HAZUS (NIBS, 2004) framework, the following damage states are identified for tunnels:

- **DS2 (Slight/minor damage):** Minor cracking of the tunnel liner (damage requires no more than cosmetic repair) and some rock falling, or slight settlement of the ground at a tunnel portal.
- **DS3 (Moderate damage):** Moderate cracking of the tunnel liner and rock falling.
- **DS4 (Extensive damage):** Major ground settlement at a tunnel portal and extensive cracking of the tunnel liner.

- **DS5 (Complete damage):** Major cracking of the tunnel liner, which may include possible collapse.

The HAZUS damage scale contains five damage states, with DS1 representing the Intact/No damage State.

b. SYNER-G project (Argyroudis & Kaynia, 2014)

The FP7 SYNER-G project (2009-2013) proposes a review of existing fragility curves for road network elements. Based on a critical appraisal of available studies, damage states and corresponding functionality levels for tunnels have been defined (see Table 30).

Damage description		Serviceability
DS1	Minor cracking and spalling and other minor distress to tunnel liners	Open to traffic, close or partially closed during inspection , cleaning and possible repair works
DS2	Ranges from major cracking and spalling to rock falls	Closed during repair works for 2-3 days
DS3	Collapse of liner or surrounding soils to the extent that the tunnel is blocked either immediately or within a few days after the main shock	Closed for a long period of time

Table 30: Description of damage states for tunnels (Argyroudis & Kaynia, 2014).

The SYNER-G review of existing damage models also includes the work by Werner et al. (2006) in the REDARS methodology, where a damage scale is defined for tunnels:

- **Slight damage:** Minor cracking of tunnel liner (requiring only cosmetic repair). Some rock falling or slight ground settlement at tunnel portal.
- **Moderate damage:** Moderate structural cracking of tunnel liner and/or moderate rock falling.
- **Major damage:** Major structural cracking of tunnel liner and/or major settlement at tunnel portal.

Finally, the study by Huang et al. (1999) and Wang et al. (2001) is also mentioned, where a global tunnel damage classification is proposed. It is comprised of the various irregularities that can be observed in a tunnel after an earthquake:

- **No damage:** No damage detectable by visual inspection.
- **Slight damage:** Light damage detected on visual inspection, no effect on traffic (width of crack < 3mm, length of crack < 5 m).
- **Moderate damage:** Spalling / cracking of linings (width of crack > 3mm, length of crack > 5 m), exposed reinforcement, displacement of segmental joints, leaking of water, some disruption to traffic.
- **Severe damage:** Slope failure at openings, collapse of main tunnel structure, up-heave or differential movement of road and road shoulder, flooding, damaged ventilation and lighting system in long tunnels, total disruption to traffic.

c. Summary of possible failure modes

The selected literature references provide a variety of failures modes for the different types of tunnel elements and their components (see Figure 59).

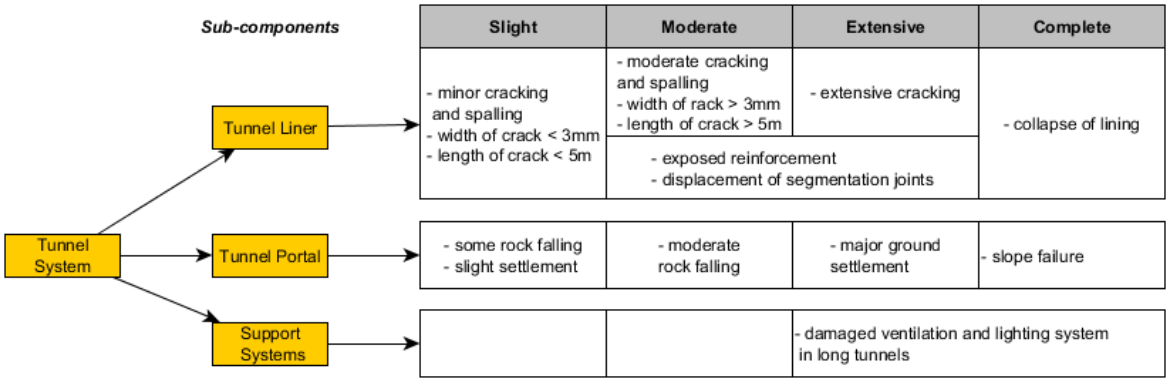

Figure 59: Summary of possible failure modes for tunnels.

5.2.2 Possible failure modes and corresponding limit states for ground failure hazard

The effect of ground failure hazard is somewhat redundant with the damage scales that have been proposed for the seismic hazard, since failures such as ground settlement or liner cracking can also be induced by landslides. Moreover, whatever happens at the tunnel portal (e.g. rock falls, settlement) can be treated as damages to roadway elements, such as embankments or roads along slopes (see next section). The selected failure modes are summarised in **Table 48** (Appendix A).

5.2.3 Possible failure modes and corresponding limit states for flood hazard

Since immersed tunnels are not considered in the present study, flood hazard does not represent a significant threat to the types of tunnels considered here.

5.3 Available fragility functions

This section describes the bridge fragility functions that can be selected from past studies.

5.3.1 Fragility functions for seismic hazard

A review of existing fragility curves for tunnels (Argyroudis and Kaynia, 2014) has been compiled in the frame of the FP7 SYNER-G project: it contains a limited amount of fragility models from a handful literature references (see **Table 31**).

Reference	Method	Typology	Intensity Measure
ALA (2001)	Empirical data using 217 damage cases.	- Rock (Bored) or Alluvial - Good or Poor to average quality	PGA
Argyroudis (2010)	Analytical.	- Circular (Bored) or Rectangular (Cut & Cover) - B, C or D soil classes (EC8)	PGA
Argyroudis and Pitilakis (2007)	Analytical.	- Circular (Bored) - B, C or D soil classes (EC8)	PGD
Corigliano (2007)	Empirical data using 120 damage cases.	- Deep tunnels (highway, railway, etc.)	PGV
HAZUS (NIBS, 2004)	Engineering judgment and empirical data.	- Bored or Cut & Cover	PGA and PGD (ground failure)
Salmon et al. (2003)	Analytical (specific to BART tunnels in the San Francisco Bay Area)	- Bored or Cut & Cover	PGA and PGD (fault offset)

Table 31: Seismic fragility curves for tunnels, taken from the SYNER-G review (Argyroudis and Kaynia, 2014).

Out of the available fragility curves, only the ones that are defined with respect to actual ground shaking are used in the present context (i.e. ALA, 2001; Argyroudis, 2010; Corigliano, 2007; NIBS, 2004). The fragility curves that are expressed as a function of PGD (permanent ground displacement) could be used for the earthquake-triggered ground failure hazard (see next section). Finally, the fragility curves from Salmon et al. (2003) are based on a very specific case-study (urban tunnels for subway system) and their transposition to other types of tunnels is not recommended.

5.3.2 Fragility functions for ground failure hazard

In the case of earthquake-triggered ground failures, fragility functions by HAZUS (NIBS, 2004) and Argyroudis and Pitilakis (2007) could be used in order to express tunnel damage as a function of permanent ground deformation (see Table 31).

5.3.3 Fragility functions for flood hazard

As discussed above, accounting for the fragility of tunnels with respect to flood hazard is out of the scope of the present context.

5.4 From physical damage states to functional states

Using the damage states of tunnel components (see Figure 53) such as the liner and the portal, global damage states for the tunnel system can be aggregated. Using the expert-based survey conducted within INFRARISK, functionality models can then be built for each of the four damage states, as represented in Figure 60 to Figure 62. The lack of reliable data for direct costs prevented the derivation of a cost model for tunnels. The scarcity of tunnel

damage events due to seismic or ground failure events, which are even less documented than for bridges, does not permit a comparison with literature references.

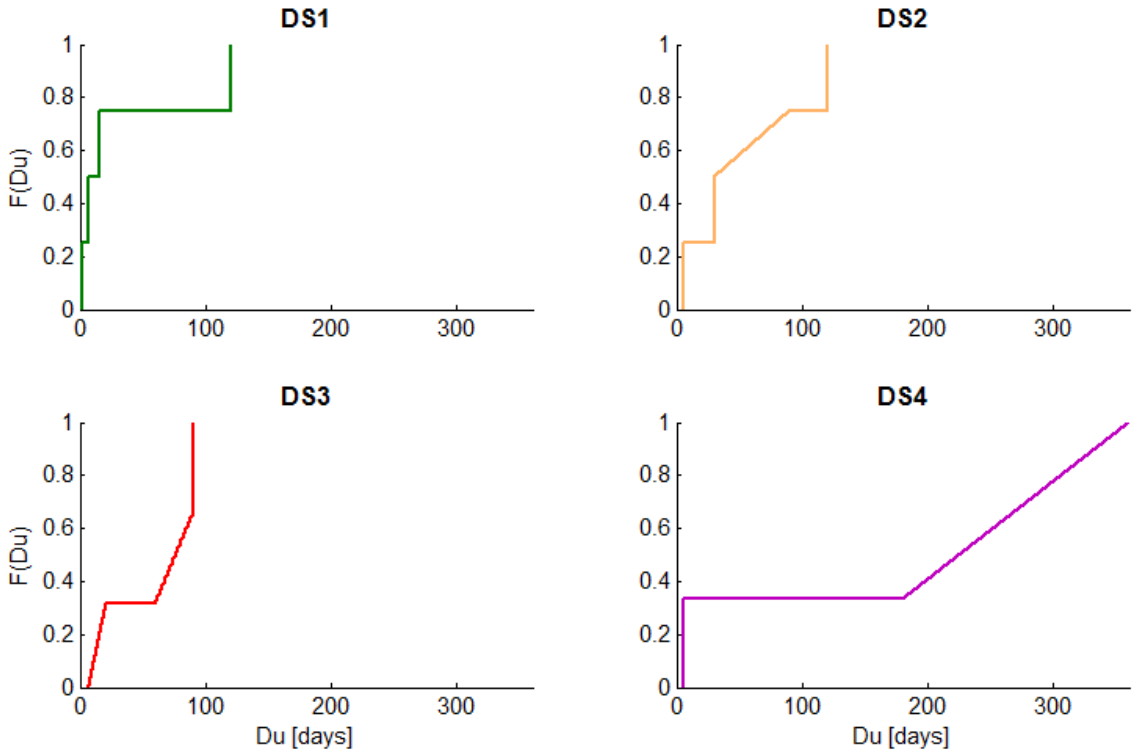

Figure 60: Duration of repair operations given global damage states DS1 to DS4

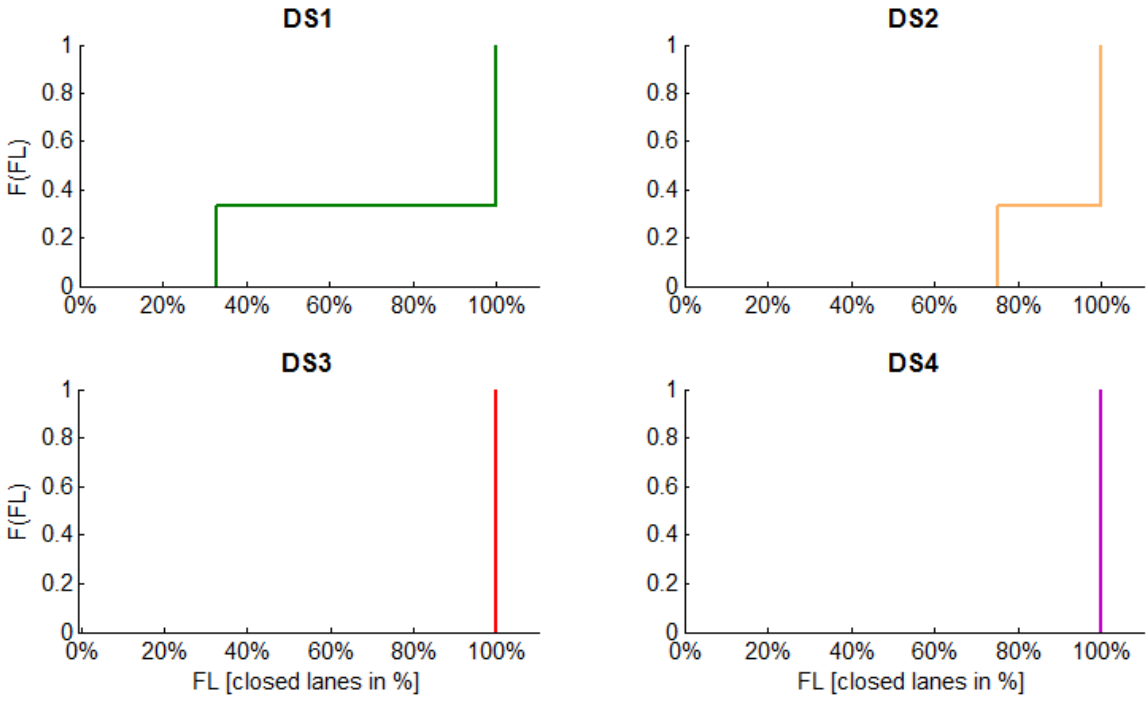

Figure 61: Functionality loss (expressed in proportion of closed lanes) given global damage states DS1 to DS4

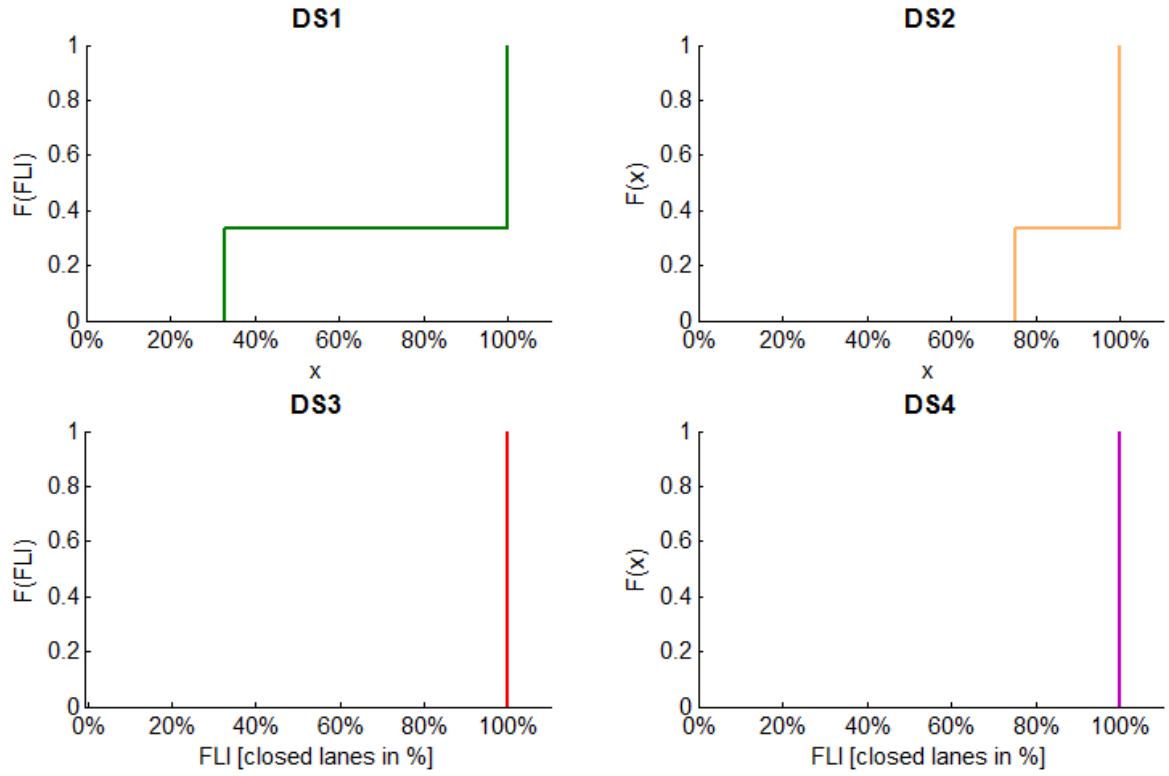

Figure 62: Functionality loss during intervention (expressed in proportion of closed lanes) given global damage states DS1 to DS4

The numerical values that are proposed in this section should be considered for illustrative purposes only, due to the scarcity of the collected data from the expert-based survey.

5.5 Global approach: selection from available fragility functions

The derivation of analytical fragility curves for tunnels exposed to seismic hazard requires specific developments that may not be realistic at the scale of a large infrastructure networks. Therefore a common approach is to select existing fragility curves for global damage states, based on common features or similar typologies. The following sections present the strategy in order to select existing functions and build composite fragility models, as it has been previously done for bridges (see section 4.5).

5.5.1 Application of the SYNER-G database to a dataset of case-study bridges

As part of one of the INFRARISK case-studies (Ni Choine et al., 2014), highways and secondary roads around the city of Bologna, Italy, have to be assessed with respect to seismic risk. A total of 30 tunnels have been identified by the INFRARISK consortium. These tunnels have been characterized by following the taxonomy proposed in section 5.1.1, as summarized in **Table 32**.

ID	*Construction Method*	*Shape*	*Depth*	*Geological Conditions*	*Supporting System*
1	Cut & Cover	Horseshoe	Deep	Alluvial	Concrete
2	Cut & Cover	Horseshoe	Deep	Alluvial	Concrete
3	Cut & Cover	Horseshoe	Shallow	Alluvial	Concrete
4	Cut & Cover	Horseshoe	Shallow	Alluvial	Concrete
5	Bored	Circular	Deep	Alluvial	Concrete
6	Cut & Cover	Horseshoe	Shallow	Alluvial	Concrete
7	Cut & Cover	Horseshoe	Shallow	Alluvial	Concrete
8	Cut & Cover	Horseshoe	Shallow	Alluvial	Concrete
9	Cut & Cover	Horseshoe	Shallow	Alluvial	Concrete
10	Cut & Cover	Rectangular	Shallow	Alluvial	Concrete
11	Cut & Cover	Rectangular	Shallow	Alluvial	Concrete
12	Bored	Circular	Deep	Rock	Concrete
13	Bored	Circular	Deep	Rock	Concrete
14	Bored	Circular	Deep	Alluvial	Concrete
15	Bored	Circular	Deep	Alluvial	Concrete
16	Bored	Circular	Deep	Alluvial	Concrete
17	Bored	Circular	Deep	Alluvial	Concrete
18	Bored	Circular	Deep	Alluvial	Concrete
19	Cut & Cover	Rectangular	Shallow	Alluvial	Concrete
20	Cut & Cover	Rectangular	Shallow	Alluvial	Concrete
21	Cut & Cover	Rectangular	Shallow	Alluvial	Concrete
22	Cut & Cover	Rectangular	Shallow	Alluvial	Concrete
23	Cut & Cover	Rectangular	Shallow	Alluvial	Concrete
24	Cut & Cover	Rectangular	Shallow	Alluvial	Concrete
25	Cut & Cover	Horseshoe	Shallow	Alluvial	Concrete
26	Cut & Cover	Rectangular	Shallow	Alluvial	Concrete
27	Cut & Cover	Rectangular	Shallow	Alluvial	Concrete
28	Bored	Circular	Deep	Alluvial	Concrete
29	Cut & Cover	Rectangular	Shallow	Alluvial	Concrete
30	Cut & Cover	Rectangular	Shallow	Alluvial	Concrete

Table 32: Characteristics of the case-study bridges according to the proposed taxonomy.

The table of existing fragility functions for tunnels (Table 31) is used in order to build composite models for the case-study tunnels. The fragility curves derived by Salmon et al. (2003) are not included here, because they are the result of a specific study (BART tunnels in the San Francisco Bay Area) which is not applicable to the INFRARISK context. The fragility curves from Argyroudis and Pitilakis (2007) are also not considered for the seismic risk analysis, since they are expressed as a function of permanent ground deformation.

5.5.2 Pairing based on taxonomy parameters

It is proposed here to simply use the correspondence between the taxonomy parameters of the tunnels and the references from Table 31. The same approach as detailed in section 4.5.2 in the case of bridges is used.

From **Table 32**, five unique configurations of tunnels have been identified and associated with a few reference fragility curves, as shown in **Table 33**. For each of these configurations, composite fragility models are then derived with a median curve and 16%-84% confidence bounds. The fragility curves and fragility parameters are presented in Figure 63 and **Table 34**, respectively. The fragility curves for DS4 cannot be computed, due to the absence of reference curves that would be able to predict tunnel collapse due to seismic hazard.

ID	*Construction Method*	*Shape*	*Depth*	*Geological Conditions*	*Supporting System*
#1	**Cut & Cover**	**Rectangular**	**Deep**	**Alluvial**	**Concrete**
NIBS (2004)	Cut & Cover	X	X	X	X
ALA (200)1	Cut & Cover	X	X	Alluvial	X
ALA (2001)	Cut & Cover	X	X	Alluvial	X
Corigliano (2007)	X	X	Deep	X	X
#2	**Cut & Cover**	**Horseshoe**	**Shallow**	**Alluvial**	**Concrete**
NIBS (2004)	Cut & Cover	X	X	X	X
ALA (200)1	Cut & Cover	X	X	Alluvial	X
ALA (2001)	Cut & Cover	X	X	Alluvial	X
#3	**Cut & Cover**	**Horseshoe**	**Deep**	**Alluvial**	**Concrete**
NIBS (2004)	Cut & Cover	X	X	X	X
ALA (200)1	Cut & Cover	X	X	Alluvial	X
ALA (2001)	Cut & Cover	X	X	Alluvial	X
Corigliano (2007)	X	X	Deep	X	X
#4	**Bored**	**Circular**	**Deep**	**Rock**	**Concrete**
NIBS (2004)	Bored	X	X	X	X
ALA (200)1	X	X	X	Rock	X
ALA (2001)	X	X	X	Rock	X
Corigliano (2007)	X	X	Deep	X	X
#5	**Bored**	**Circular**	**Deep**	**Alluvial**	**Concrete**
NIBS (2004)	Bored	X	X	X	X
Corigliano (2007)	X	X	Deep	X	X
Argyroudis (2010)	Bored	X	X	Alluvial	X

Table 33: Details of the 5 unique tunnel configurations and associated reference curves. The '*X*' index refers to undefined values.

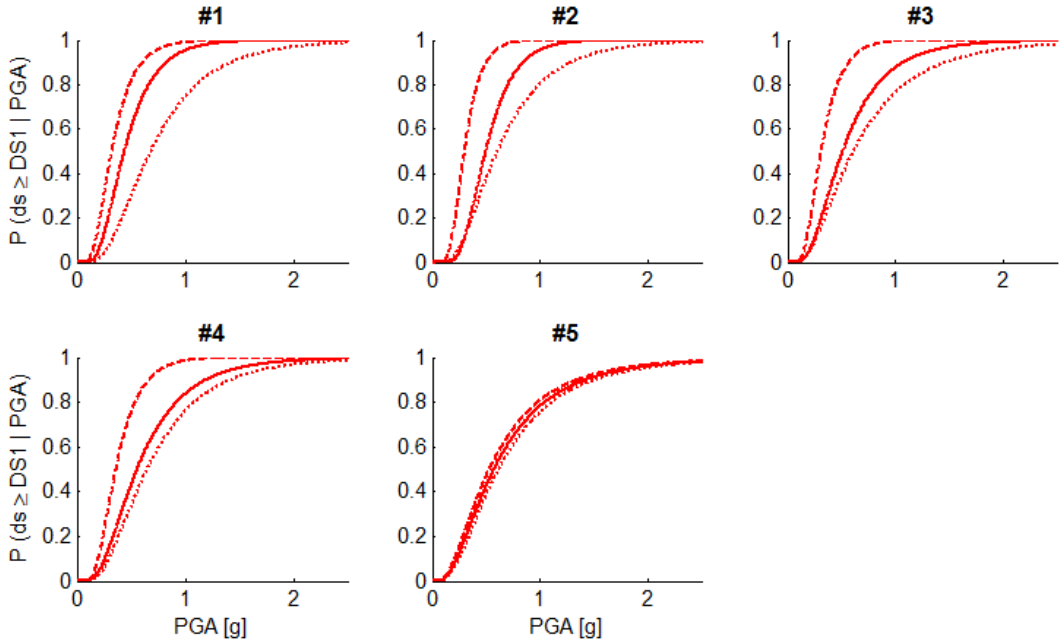

Figure 63: Fragility curves for DS1 for the 5 tunnel configurations. The solid line represents the median curve, the dashed line the lower bound, and the dotted line the upper bound.

DS1	Median		Lower Bound		Upper Bound	
	α [g]	β	α [g]	β	α [g]	β
clus1	0.439	0.491	0.324	0.483	0.680	0.577
clus2	0.498	0.410	0.300	0.400	0.604	0.590
clus3	0.510	0.580	0.314	0.457	0.610	0.685
clus4	0.555	0.597	0.361	0.471	0.646	0.615
clus5	0.572	0.714	0.530	0.729	0.613	0.706
DS2	Median		Lower Bound		Upper Bound	
	α [g]	β	α [g]	β	α [g]	β
clus1	0.749	0.543	0.541	0.480	1.041	0.609
clus2	0.693	0.419	0.450	0.400	0.810	0.580
clus3	0.731	0.439	0.475	0.435	0.891	0.438
clus4	0.796	0.428	0.572	0.432	0.897	0.433
clus5	0.840	0.443	0.768	0.461	0.909	0.439
DS3	Median		Lower Bound		Upper Bound	
	α [g]	β	α [g]	β	α [g]	β
clus1	1.065	0.550	0.963	0.509	1.624	0.572
clus2	0.950	0.500	0.950	0.500	0.950	0.500
clus3	0.950	0.500	0.950	0.500	0.950	0.500
clus4	1.100	0.500	1.100	0.500	1.100	0.500
clus5	Inf	1.000	Inf	1.000	Inf	1.000

Table 34: Fragility parameters for each of the 5 tunnels configurations, for the median curve and the 16%-84% confidence bounds.

6.0 FRAGILITY FUNCTIONS FOR ROAD SEGMENTS

This section reviews the available fragility models that can be used for the different hazard types considered.

6.1 General description of road segments

The following paragraphs describe the main components that usually comprise a road segment.

6.1.1 Typological classification

There are various possible typologies for roadway elements, however the taxonomy that has been defined in the SYNER-G project (Franchin et al., 2011) proposes to break down road segments in the following classes:

- Embankments (road on);
- Trenches (road in);
- Slopes (road along);
- Road segments;

Road pavements stand for the plain road surfaces that comprise the driving area, without any consideration of the surrounding geotechnical works. Specific features associated with the configuration of the road are represented in Figure 64.

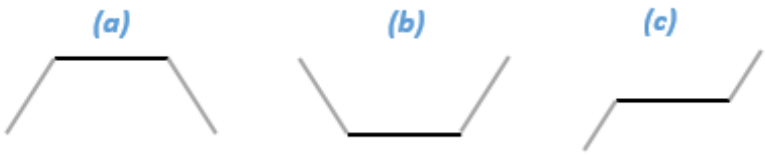

Figure 64: Schematic view of the layout of roads on embankments (a), in trenches (b) and along slopes (c).

The vulnerability and failures modes of the road sections are also influenced by the level of compaction of the subsurface soil, the slope angle or the soil class.

While many road classes can be defined based on the number of lanes, the traffic type, or their importance level (e.g. national, regional, local), the INFRARISK framework mainly concentrates on roads from the core TEN-T network (i.e. high speed roads or highways with multiple lanes).

6.1.2 Roadway components

Depending on their type and configuration (e.g. see Figure 64), road segments can usually be decomposed into the following components (see Figure 65):

- **Road surface/pavement:** it corresponds to the travelled way of the road element;

- **Shoulder:** it is located between the travelled way and the edge of the embankment, and it may be used as an emergency lane;
- **Ditch:** it is used for the drainage of water from the road surface;
- **Culvert:** it allows the flow of a small channel of water under the road, usually for drainage purposes;
- **Sub-base/base course:** these optional layers of engineered soil may be used as foundation for the road surface, when the soil bearing capacity is not sufficient;
- **Subgrade:** it constitutes the foundation of the road surface;
- **Filled slope (embankment) / Cut slope (back slope):** these side slopes may be engineered or natural, depending on the environmental constraints.

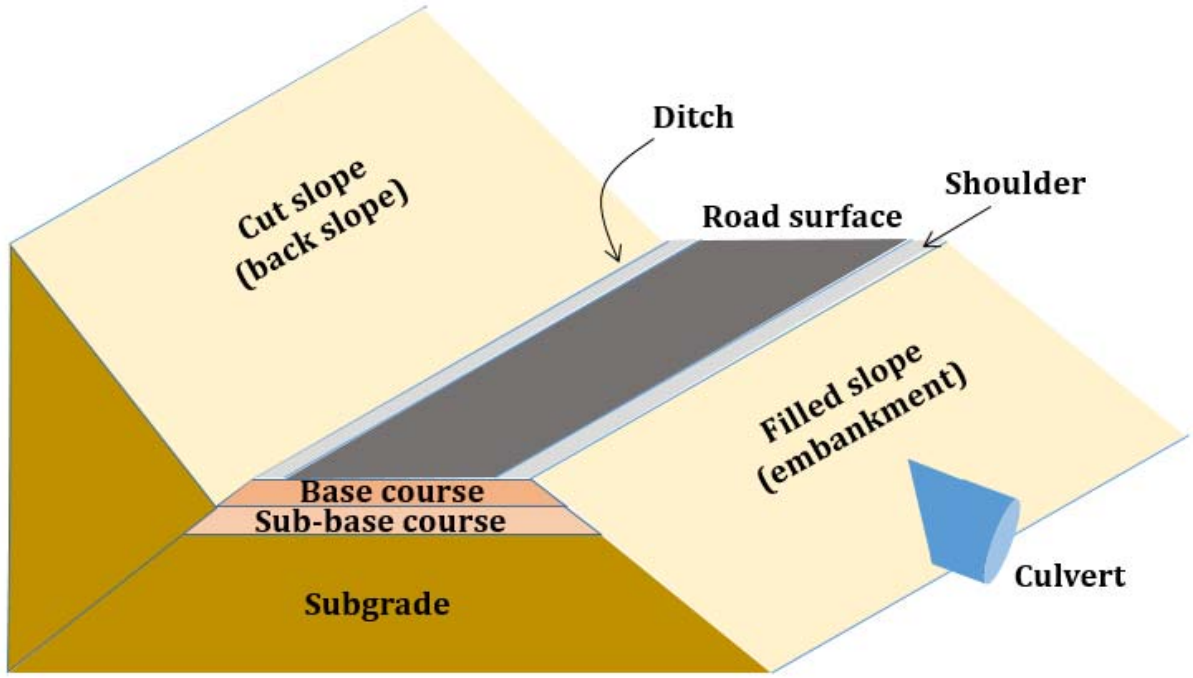

Figure 65: Schematic view of the usual component found along a roadway element

6.2 Failure modes

The various road segment components have a very specific susceptibility to the different hazard types, as demonstrated in the following paragraphs. The selected failure modes are summarised in **Table 49** (Appendix A).

6.2.1 Possible failure modes and corresponding limit states for seismic hazard

Since road pavements are not directly vulnerable to the earthquakes, in the strict sense of transient wave propagation, the damage mechanisms with respect to earthquake-induced phenomena such as fault rupture, liquefaction or lateral spreading are detailed in the next section, on ground failure hazards.

6.2.2 Possible failure modes and corresponding limit states for ground failure hazard

This section reviews some of the recent studies that describe damage states and limit values for various tunnel components exposed to ground failure hazard.

a. HAZUS technical manual for earthquakes (NIBS, 2004)

In the HAZUS framework (FEMA, 2003), the following damage states are identified for road pavements:

- **DS2 (Slight/minor damage):** Slight settlement (few inches) or offset of the ground.
- **DS3 (Moderate damage):** Moderate settlement (several inches) or offset of the ground.
- **DS4 (Extensive damage):** Major settlement of the ground (few feet).
- **DS5 (Complete damage):** Major settlement of the ground (i.e. same as DS4).

The HAZUS damage scale contains five damage states, with DS1 representing the Intact/No damage State.

b. HAZUS technical manual for earthquakes (NIBS, 2004)

The FP7 SYNER-G project (2009-2013) proposes a review of existing fragility curves for road network elements. Based on a critical appraisal of available studies, damage states and corresponding functionality levels for roadways are proposed.

For *embankments*, lateral spreading is the main cause of damage, which induces the sliding of the embankment slope and the opening of cracks on the pavement. A study by JRA (2007) classifies the severity of damage with three stages:

- **Minor damage:** Surface slide of embankment at the top of slope only, minor cracks on the surface of the road.
- **Medium damage:** Deep slide of embankment or slump involving traffic lines, medium cracks on the surface of the road and/or settlement of embankment.
- **Serious damage:** Serious slump of embankment, serious slide of embankment.

For *embankments* and *roads along slopes*, Maruyama et al. (2010) define the following damage states:

- **Minor damage:** Deformation of side slope.
- **Moderate damage:** Partial collapse of side slope.
- **Major damage:** Total collapse of side slope.

Finally, for *plain road pavements*, several studies propose damage states that are based on the extent of the induced displacement on the road surface. First, Maruyama et al. (2010) define displacement thresholds for both gaps and cracks in the roadway:

- **Gap / Vertical offset in roadway:**
    - **Very Minor damage:** less than 1cm.
    - **Minor damage:** traffic lane: 1 – 3 cm / shoulder: 1 – 20 cm.
    - **Moderate damage:** traffic lane: more than 3 cm / shoulder: more than 20 cm.
- **Crack in roadway:**
    - **Very minor damage:** less than 3 cm.
    - **Minor damage:** 3 – 5 cm.
    - **Moderate damage:** more than 5 cm.

The Risk-UE approach defines also damage states by using thresholds of settlement/offset of the ground (Argyroudis et al., 2003). The proposed damage scale appears to be very similar to the one used in the HAZUS framework (FEMA, 2003), except for the units used (from ft to cm):

- **Minor damage:** slight settlement or offset of the ground (< 30 cm).
- **Moderate damage:** moderate settlement or offset of the ground (30 to 60 cm).
- **Extensive damage:** major settlement or offset of the ground (> 60 cm).

Another study by Werner et al. (2006) introduces five damage states based on the permanent ground displacement (PGD in inches):

- **No damage:** PGD < 1 in, no repairs needed.
- **Slight damage:** PDG between 1 and 3 in, slight cracking/movement, no interruption of traffic.
- **Moderate damage:** PGD between 3 and 6 in, localized moderate cracking/movement, reduced structural integrity of surface.
- **Extensive damage:** PGD between 6 and 12 in, failure of pavement structure requiring replacement, movement but no failure of subsurface soils.
- **Irreparable damage:** PGD > 12 in, failure of pavement structure and subsurface soils.

Finally, based on the previous literature references, another damage scale for roadway elements has been presented in the SYNER-G project (Argyroudis and Kaynia, 2014):

- **No damage:** PGD < 3 cm.
- **Minor damage:** PDG between 3 and 15 cm.
- **Moderate damage:** PGD between 15 and 30 cm.
- **Extensive damage:** PGD between 30 and 60 cm.
- **Complete damage:** PGD between 60 and 150 cm.

c. SAFELAND project (Pitilakis et al., 2011)

The SAFELAND project on landslide risk in Europe proposes various fragility functions for road infrastructures subjected to rockfalls or debris flows (i.e. fast moving landslides). The damage scale associated with debris flows is the following, for high speed roads:

- **Limited damage:** encroachment limited to verge/hardstrip.
- **Serious damage:** blockage of hardstrip and one running lane.
- **Destroyed:** complete blockage of carriageway and/or repairable damage to surfacing.

Concerning the effect of rockfalls, no specific damage states are detailed for road pavements, however the report identifies the failure of rockfall protection galleries (see Figure 66) as the main failure mechanism: it can be expressed as a function of the rock's mass and impact velocity.

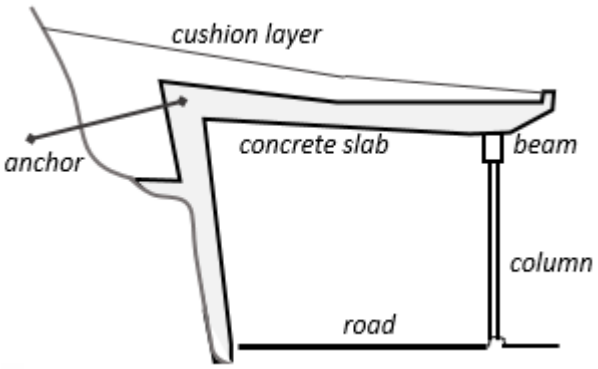

Figure 66: Schematic view of the layout of a rock protection gallery, adapted from Pitilakis et al. (2011)

d. Summary of possible failure modes

A variety of failure modes for the different types of roadway elements is outlined in Figure 67 based on Pitilakis et al., 2011). For most of the considered failure modes, no quantitative damage indices have been identified, yet the description of the severity of each physical impact allows some progressive damage states to be defined. Regarding failures modes related to cracks or an offset/settlement of the road surface, several studies propose thresholds of permanent ground displacement, but the limit values do not seem to be consistent between the different references.

It is important to note that Figure 67 focuses only on the consequences of ground failure on the infrastructure. The respective causes of the ground failures/displacements (e.g. earthquake- or rainfall-induced landslides, liquefaction, lateral spreading, or fault-rupture) are not an essential information in this context.

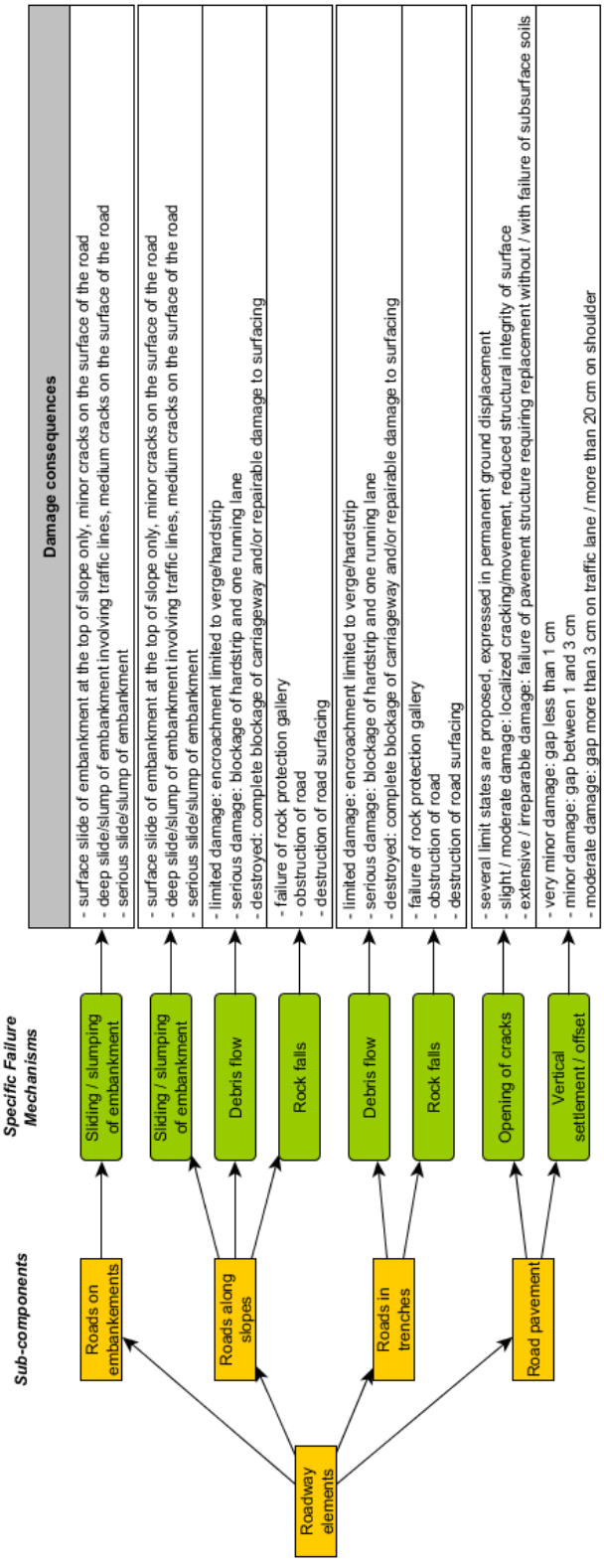

Figure 67: Summary of possible failure modes for common roadway elements.

6.2.3 Possible failure modes and corresponding limit states for flood hazard

This section reviews some of the recent studies that describe damage states and limit values for various roadway components exposed to flood hazard.

a. HAZUS technical manual for floods (NIBS, 2005)

In the HAZUS framework (NIBS, 2005), failure modes of plain road pavements are not detailed. However, a section is devoted to the limit values of inundation height for the damage of vehicles, as summarized in Table 35.

Flood level (m)	Car	Light truck	Heavy truck	Damage Ratio
Below carpet	< 0.46 m	< 0.82 m	< 1.52 m	15 %
Between carpet and dashboard	0.46 – 0.73 m	0.82 – 1.13 m	1.52 – 2.29 m	60 %
Above dashboard	> 0.73 m	> 1.13 m	> 2.29 m	100 %

Table 35: Limit inundation heights with respect to vehicle damage, from HAZUS (NIBS, 2005).

b. American Lifeline Alliance report (ALA, 2005)

The American Lifeline Alliance report (ALA, 2005) on local road systems is based on the analysis of several case-studies. This led to the identification of some of the most common failures modes for roadways:

- Deposition of sediments on roadbeds.
- Saturation and collapse of inundated roadbeds.
- Loss of paved surfaces through flotation or delamination.
- Washout of unpaved roadbeds.

Beside direct damage to road pavement, floods may also impact drainage elements through the following mechanisms:

- Damage to or loss of underdrain and cross-drainage pipes.
- Blockage of drainage ditches and underdrains by debris, exacerbating erosion and scour.
- Undermining of shoulders when ditch capacity is exceeded.

c. Summary of possible failure modes

No precise information in terms of limit values or progressive damage states could be found in the selected literature reference, however it is still possible to extract some general considerations on the physical impact of various loading mechanisms (see Figure 68). One of the criteria that could be used to assess the damage severity is the nature of potential repairs:

- Traffic is just interrupted / disrupted without any physical damage.
- Physical damage of the paved surface.
- Physical damage of the roadbed, which would require a geotechnical intervention to perform adequate repairs.

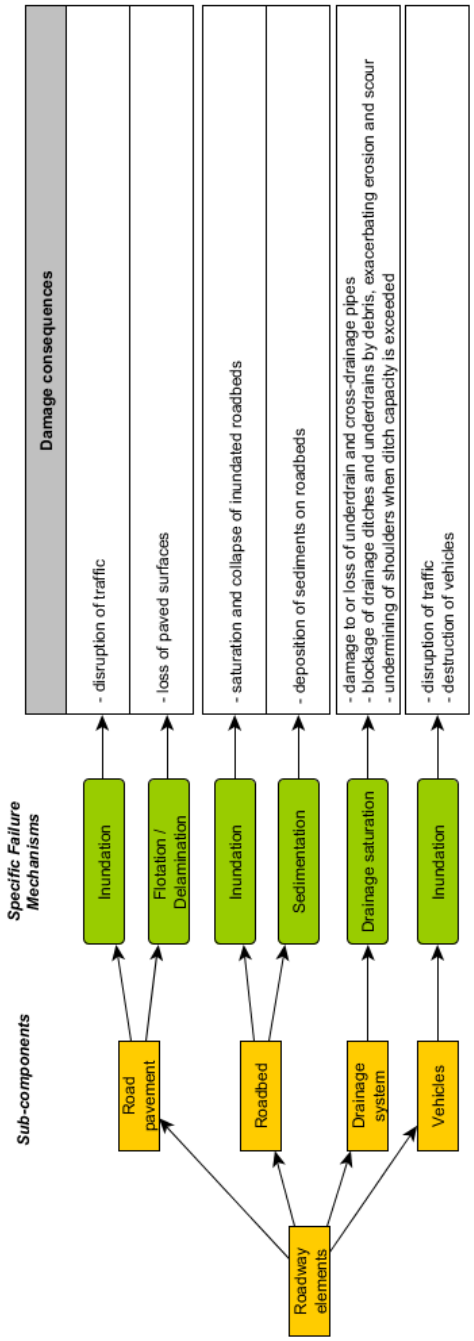

Figure 68: Summary of possible failure modes for common roadway elements.

6.3 Available fragility functions

This section describes the bridge fragility functions that can be selected from past studies.

6.3.1 Fragility functions for seismic hazard

The fragility curves for road damage due to earthquake-induced permanent deformation are presented in the next subsection (i.e. fragility functions for ground failure hazard).

6.3.2 Fragility functions for ground failure hazard

The various fragility curves reviewed by Argyroudis and Kaynia (2014) within the SYNER-G project are detailed in **Table 36**, as well as additional references.

Reference	Method	Typology	Intensity Measure
Embankment			
Lagaros et al. (2009)	Analytical.	- Trapezoid embankment	PGA
Maruyama et al. (2008,2010)	Empirical data from Japanese earthquakes.	- Japanese expressway embankments (height 5-10m)	PGV
SYNER-G (Argyroudis and Kaynia, 2014)	Analytical.	- Embankment height - EC8 soil classes	PGA
Argyroudis and Kaynia (2015)	Analytical.	- Embankment height - EC8 soil classes - Highway / railway	PGA
Sasaki et al. (2000)	Empirical	- Japanese embankments	PGA
Slope			
ATC-13 (1985)	Expert judgement.	- 6 different slope classes defined by yield acceleration k_y	Modified Mercalli Intensity (MMI)
SYNER-G (Argyroudis and Kaynia, 2014)	Analytical.	- different slope classes defined by yield acceleration k_y	PGA
SAFELAND (Pitilakis et al., 2011); Winter et al. (2014)	Expert judgement, for obstruction of roads by debris flow.	- local or high-speed roads	Volume of landslide
SAFELAND (Pitilakis et al., 2011)	Analytical, for destruction of road protection gallery due to rock fall	- rockfall protection gallery with concrete slab	Rock impact velocity and rock mass
Trench			
SYNER-G (Argyroudis and Kaynia, 2014)	Analytical	- EC8 soil classes	PGA
Road pavement			
HAZUS (NIBS, 2004)	Empirical data.	- major/highway roads (four or more lanes) or urban roads (two lanes)	PGD (ground failure)

Table 36: Seismic fragility curves for road segments, partly taken from the SYNER-G review (Argyroudis and Kaynia, 2014).

6.3.3 Fragility functions for flood hazard

There are currently no suitable fragility curves available for road elements due to flood hazards. Most of the past studies which deal with the flood risk assessment of transportation networks make use of simple assumptions regarding the functionality of roads with respect to water elevation (e.g. use of deterministic threshold, intersection of the road network with the flood layer, etc.) (Dawson et al., 2011; Kermanshah et al., 2014; Gleyze and Rousseaux, 2003).

Regarding the fragility of vehicles with respect to inundation, an experimental study by Teo et al. (2012) has identified the threshold values of water height and flow velocity that would lead to the

instability of three different brands of cars (see Figure 69). The data points obtained enable the stability area in the [water height; flow velocity] space to be mapped, which may be used to derive a fragility function. However, in the present context, knowledge on the vehicle instability due to hydraulic loads is not essential, since the flooded vehicles are not able to operate well before the instability threshold is reached (for instance, it is considered that the vehicles remain stable even for a water height of 3 m and a flow velocity of 2 m/s): it is expected that the road will have to be closed for much less severe flood conditions. Nonetheless, the results by Teo et al. (2012) may be used to estimate the likelihood of the total destruction of vehicles or the generation of potentially dangerous missiles (i.e. vehicles moving with the water flow).

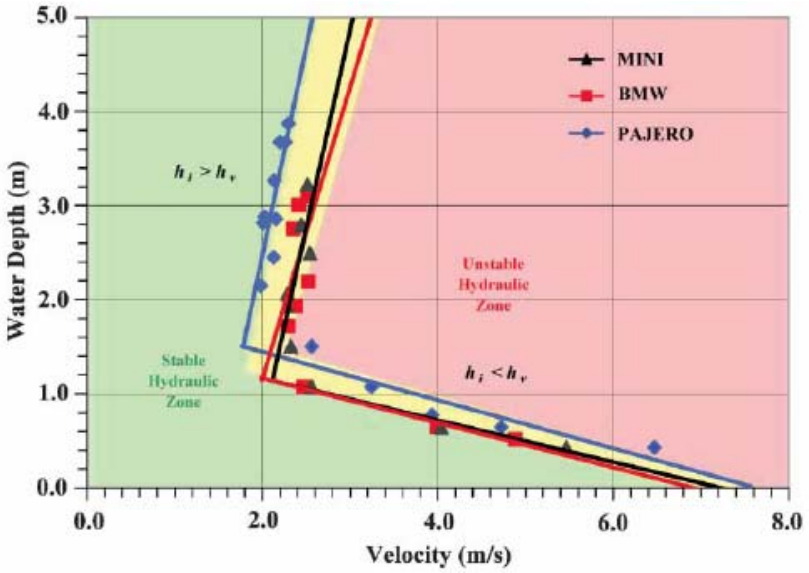

Figure 69: Vehicle stability thresholds for three brands of cars, taken from Teo et al. (2012)

However, fragility functions for flood protection structures should be accounted for, since they may potentially alter the exposure of the critical infrastructure (e.g. failure of a flood defence changing the pathway of the hazard, as shown in Figure 70).

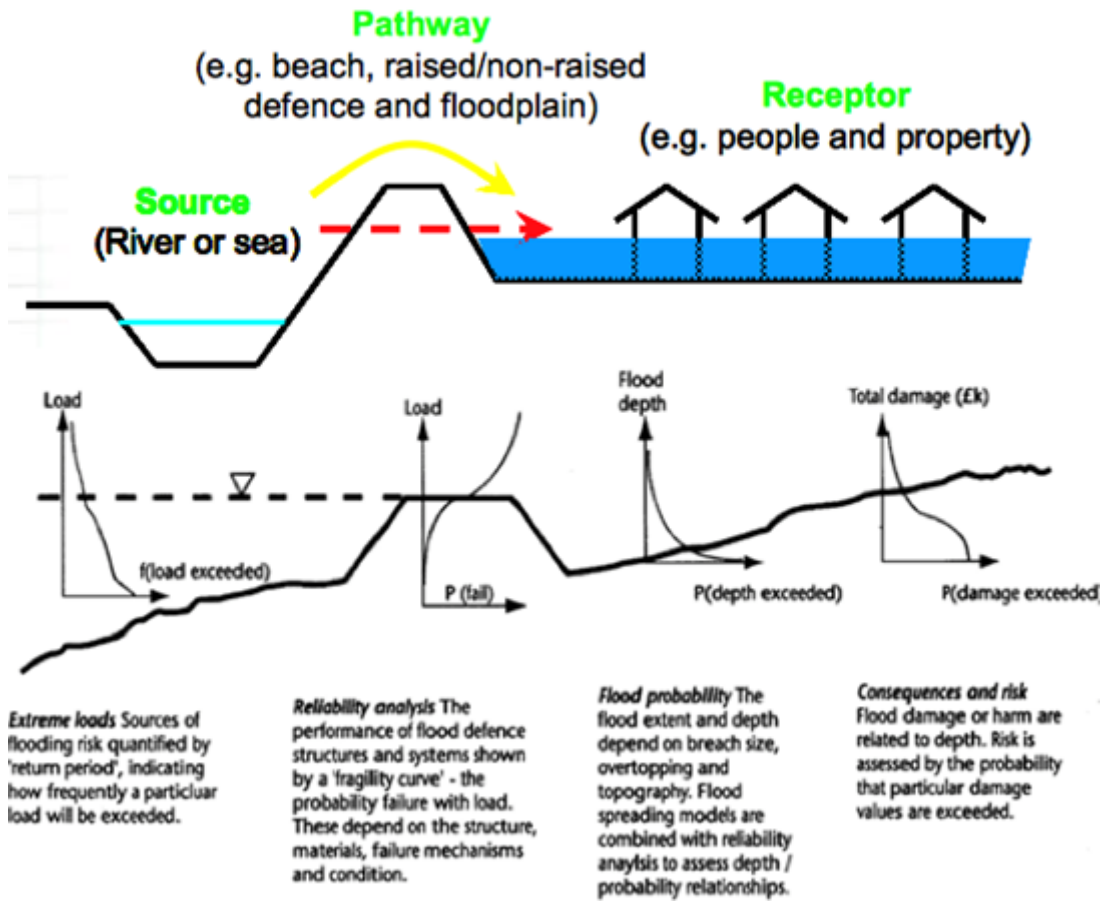

Figure 70: Fragility curves in flood system analysis (Simm et al., 2008)

Fragility functions for flood hazard typically represent the probability of damage/failure of structure relative to the hydraulic loading (water level, velocity or duration).

Four approaches to derive the fragility curves could be highlighted:

- Empirical (based on real data);
- Expert judgment (via what-if questions);
- Analytical or numerical (using models);
- Hybrid approach (combination of previous approaches).

The first approach uses the data from observations collected from sites affected by floods to fit the curve. This curve can be applied only to the assessment of the locations and structures in the same conditions. This is the main limitation of this approach.

Merz et al. (2004) describe the what-if analysis in the form of questions: "*Which damage would you expect if the water depth is 1m above the building floor?*" This approach has no limitation on data, but it can be influenced by experience of experts and it has no possibility to validate the results (Jeong and Elnashai, 2007).

Analytical or numerical approaches based on the application of models of structures or components of structures to withstand the loadings during the flood. The analytical approach has assumptions and simplifications (such as typically lognormal distributional form of the fragility curve, independence of the random variables, etc.) which makes the numerical methods more attractive

for research. However, there is a large number of factors which influence the accuracy and reliability of the calculations using the both methods. The main factors are presented in **Table 37**.

Factors	Description
Intensity Measure	Hazard parameters and their spatial resolution. IM estimation method (e.g. hydraulic model or recorded).
Damage Characterization	Damage scale; consideration of non-structural damage. Number of damage states (DS).
Class definition and sample size	Sample size (size of dataset and completeness). Single or multiple building classes.
Data quality/quantity	Post-flood survey method. Coverage, response and measurement errors in surveys. Quantity of data (e.g. number of buildings or loss observations). Number of flood events, range of IM and DS covered by data.
Derivation method	Data manipulation or combination. Statistical modelling. Treatment of uncertainty (sources of uncertainty, quantification).

Table 37: Factors affecting the reliability of fragility curves (Pregnolato et al., 2015).

The hybrid approach suggests combining two or more approaches described above to overcome the mentioned limitations (Jeong and Elnashai 2007). Schultz et al. (2010) summarized the advantages and disadvantages of all approaches, **Table 38**.

Approach	Advantages	Disadvantages
Judgmental	Not limited by data or models. Fast and cheap method if consequences of potential inaccuracy are small. Useful check on other fragility estimates.	Difficult to validate or verify. Subject to biases of experts. Not auditable. Cannot be improved over time.
Empirical	Data may come from either controlled or natural experiments. Useful and flexible if data are available. Does not assume a correlation structure or a lognormal form for the fragility curve.	Data can be scarce and source-specific. Experiments can be expensive. Difficult to validate independently of the dataset. Difficult to extrapolate fragility curves to other structures.
Analytical	Based on physical models that can be validated and verified, enhancing transparency. Easier to extrapolate results to new situations. Facilitates a distinction between aleatory and epistemic uncertainty.	May be based on simplifications and assumptions. Requires the availability of data and models. More time consuming to implement. Requires a higher level of training.
Hybrid	Limitations of any particular approach can be overcome with a complementary approach. Modelling results and observations can be combined to improve the "robustness" of fragility estimates using Bayesian Updating.	Limitations are the same as the individual approaches.

Table 38: Advantages and disadvantages of approaches to developing fragility curves (Schultz et al., 2010).

The analytical approach together with the empirical approach are the most popular methods to derive the fragility curve of the flood hazard. Their combinations also attract more and more researchers (Schultz et al., 2010).

The review of literature on targeted fragility functions has shown that most of the papers are devoted to the development of such curves for flood protection infrastructures (levees, dams, etc.) and buildings (residential and non-residential). Some examples are presented in **Table 39**.

Authors	*Approach*	*Type of analysis*	*Structure*	*Flood Intensity*	*Country*
Apel et al. (2004)	Analytical	Monte Carlo simulation	Earthen Levees	Overtopping height, overflowing time)	Germany
Zhai et al. (2005)	Empirical	Regression	House (wooden, non-wooden)	Water depth	Japan
Van der Meer et. al. (2009)	Analytical	-	Sea dike	Water level	The Netherlands
Bachmann et. al.(2009)	Analytical	Monte Carlo simulation	Artificial high ground, Dike, Flood wall, Water gate, etc.	Water level	Hypothetical
Schwarz and Maiwald (2009; 2012)	Empirical	Regression	Concrete, masonry	Water Depth, Specific energy height	Germany, Chile
Vorogushyn et al. (2009)	Analytical	Monte-Carlo simulation	Earthen levees	Overtopping height, overtopping duration, water height, impoundment duration	Germany
Gouldby et al. (2008)	Analytical	First-order reliability method	Various flood protection structures: Levees, floodwalls, etc.	Water level, crest level	United Kingdom
De Risi et. al. (2013)	Analytical	-	Houses	Water level	Tanzania
Simm et al. (2008)	Hybrid	-	Various forms of flood protection structures		United Kingdom

Table 39: Review of available fragility functions for flood protection infrastructures and buildings exposed to flood.

Examples of fragility curve calculation for technical flood protection structures could be found in the paper by Bachmann et al. (2009). They applied the probabilistic analyses via Monte-Carlo simulation to develop the curves for such type of structures as natural or artificial high grounds, dikes, flood walls etc. for different failure mechanisms. For a high ground the mechanism is overflow by water levels exceeding the ground level. An example of fragility function is presented in Figure 71 (Bachman et al., 2009).

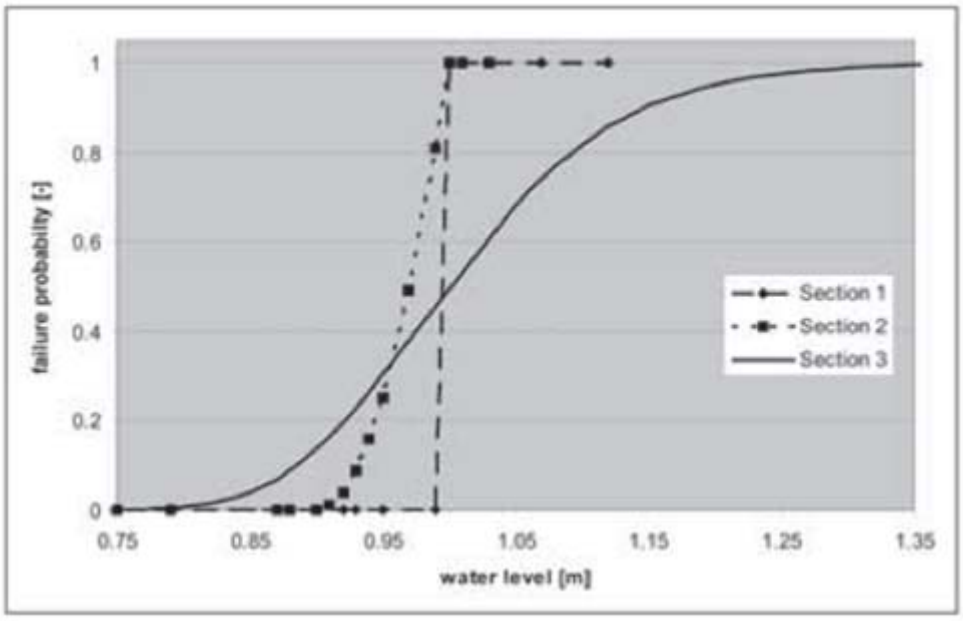

Figure 71: Examples of fragility curves for three different sections of the type *high ground*, from Bachmann et al. (2009)

Simm et al. (2008) developed a set of fragility curves for 15 levee types of Thames Barrier for 5 different condition grades. They used a "Reliability Tool" which consisted of Limit state equations for 72 failure modes, flexible fault trees and Monte-Carlo simulation for probabilistic failure analysis. Examples of fragility curves for embankments can be found in Figure 72.

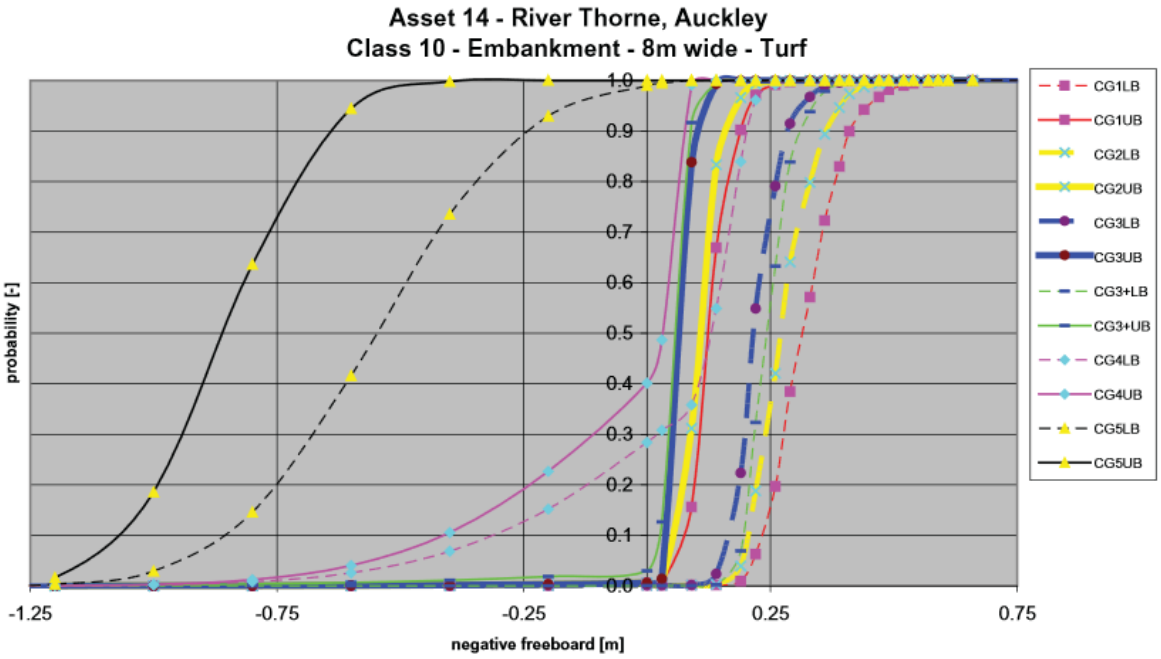

Figure 72: Examples of fragility curves for some embankments, from Simm et al. (2008)

6.4 Derivation of fragility functions for landslide hazard

For roads, earthquake-triggered landslides are a hazard. For example, the Wenchuan Earthquake in 2008 (8.0 magnitude) triggered over 50,000 landslides in an area of about 440,000km^2, causing extensive damage to roads. This included damage to approximately 24% of road section along a major highway due to earthquake-triggered landslides (Huang and Li, 2012). More recently, the 2015 Gorkhan, Nepal earthquake sequence triggered thousands of landslides, causing significant road damage (see Figure 73).

Figure 73: Earthquake-triggered landslide causing damage to a road section in Nepal (http://www.gettyimages.co.uk/detail/news-photo/road-damaged-in-landslide-triggered-after-a-fresh-news-photo/473145152)

A landslide is defined as a movement of a mass of soil (earth or debris) or rock down a slope (Couture, 2011), as outlined in Deliverable D3.1 (D'Ayala et al., 2014). Landslide hazard is defined as the probability of occurrence of a landslide of a given magnitude, in a pre-defined period of time, and in a given area (Varnes et al., 1984).

In the context of the INFRARISK project, landslides are treated as induced hazards that can be triggered by rainfall or earthquakes. Therefore, fragility curves are described for both earthquake-triggered landslides and rainfall-triggered landslides herein. The type of landslides considered within the INFRARISK framework consists of shallow planar slope failures.

6.4.1 Earthquake-triggered landslide hazard

Fragility curves to assess the effects of earthquakes on slope stability are in common use. Fotopoulou and Pitilakis (2013a,b) developed a methodology to assess the susceptibly of Reinforced Concrete (RC) objects located at the crest of a slope, to damage caused by earthquake triggered landslides. Intensity measures adopted include the seismic characteristics (PGA and PGV) and the permanent ground displacement (PGD). The strains developed in the RC objects were used to derive damage states. A similar approach that considered the impact of rock falls on reinforced concrete objects was developed by Mavrouli and Corominas (2010). In this case the kinetic energy of a

displaced rock block was used as the intensity measure. However, while these fragility curves are nominally developed for landslides, they actually address the vulnerability of adjacent building objects, rather than that of the slope itself.

The FP7 SYNER-G project developed fragility curves to assess the effects of earthquake loading on cuttings and embankment assets located on transport infrastructure networks. A model relating PGA (used as intensity measure) to PGD (used to define damage states) proposed by Bray and Travasarou (2007) was adopted. The capacity was assessed on the basis of Newmark's (1965) sliding block model. In constructing these fragility curves, a methodology for obtaining cumulative distribution functions based on the HAZUS guidelines (NIBS, 2004) was adopted. The probability P_f of reaching or exceeding a given damage state (DS_i) was derived using the mean value and standard deviation for each damage state:

$$P_f\left(ds \geq DS_i\right) = \Phi\left[\frac{1}{\sigma} \cdot \ln\frac{IM}{\overline{IM}}\right] \quad \textbf{(28)}$$

Where Φ is the standard cumulative probability function, σ is total lognormal standard deviation covering all sources of uncertainty, *IM* is value of intensity measure, and $\overline{IM}$ is the median value of intensity measure required to cause damage state DS_i. Whilst this two-parameter probabilistic approach is commonly used in developing fragility curves, Tsompanakis et al. (2010) presented a Monte Carlo Simulation (MCS) based method for developing fragility curves for embankments subjected to seismic loading.

Landslide hazards may be determined according to statistical methods (Van Den Eeckaut and Hervas, 2012) or geotechnical approaches (Rathje and Saygili, 2008). Within the framework of the INFRARISK project, earthquake-triggered landslides are evaluated according to a geotechnical approach using a rigid sliding block model (Newmark, 1965; Saygili and Rathje, 2009), as described in Deliverable D3.1 (D'Ayala et al., 2014). The vulnerability of the slope to an earthquake-triggered landslide is evaluated according to the yield acceleration (k_y) of the sliding block, which represents the horizontal acceleration that results in a factor of safety equal to 1.0 for the slope, at which sliding of the block initiates.

To quantify the risk of physical damage to roads due to earthquake-triggered landslides, fragility curves were developed by HAZUS based on empirical data and expert judgement (NIBS, 2004). The curves are defined in terms of Permanent Ground Displacement (PGD) and road classification (e.g. major or urban roads) (Figure 74). Urban roads refer to roads with two traffic lanes, whilst major roads refer to roads with four or more traffic lanes. The median (α) and dispersion (β) values for the existing HAZUS fragility curves are provided in **Table 40**. These curves enable the evaluation of the probability of attaining different levels of damage, depending on the level of seismic action experienced at the site of interest. A description of the various damage categories is provided in **Table 41**.

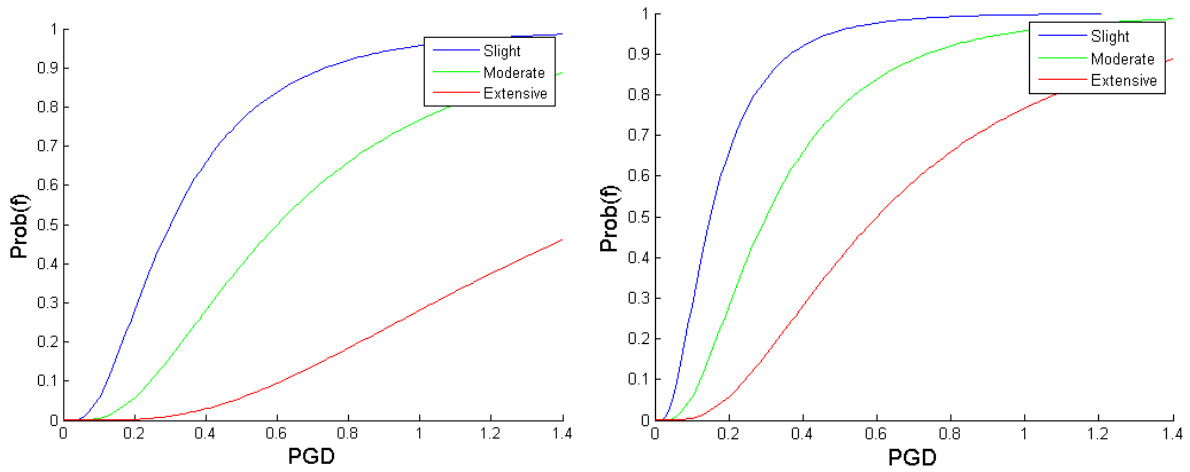

(a) Highways (Major) Roads (b)Urban Roads

Figure 74: Existing HAZUS fragility curves for roads due to earthquake-triggered landslides (NIBS, 2004)

	Permanent Ground Deformation		
Components	Damage states	α (m)	β
Major Road	Slight/Minor	0.30	0.7
	Moderate	0.60	0.7
	Extensive/Complete	1.50	0.7
Urban Road	Slight/Minor	0.15	0.7
	Moderate	0.30	0.7
	Extensive/Complete	0.60	0.7

Table 40: Median and dispersion values for HAZUS fragility curves (NIBS, 2004).

Damage State	Description
Slight	Slight settlement (few inches) or offset of the ground.
Moderate	Moderate settlement (several inches) of offset of the ground.
Extensive/Complete	Major settlement of the ground (few feet).

Table 41: Description of damage categories for roadways (NIBS, 2004).

Since the local topography and soil conditions are not accounted for using the HAZUS fragility curves, the SAFELAND project (http://www.safeland-fp7.eu/) further developed fragility curves for roads due to earthquake-triggered landslides considering local slope characteristics (e.g. yield acceleration values) and as a function of PGA (Pitilakis et al., 2011). To do so, a model proposed by Bray and Travasarou (2007) was employed, which relates the seismic PGD to the PGA of the ground motion for the rigid sliding block model (e.g. the initial fundamental period of the sliding mass is equal to 0s). This is the approach adopted within INFRARISK.

The relationship between PGA and PGD proposed by Bray and Travasarou (2007) is outlined below, where k_y is the landslide yield acceleration, M is the earthquake moment magnitude and ε is a normally distributed random variable with zero mean and a standard deviation σ = 0.66:

$$\ln PGD = -0.22 - 2.83 \cdot \ln k_y - 0.333 \cdot (\ln k_y)^2 + 0.566 \cdot \ln k_y \cdot \ln PGA + 3.04 \cdot \ln PGA - 0.244 \cdot (\ln PGA)^2 + 0.278 \cdot (M - 7) \pm \varepsilon \quad (29)$$

Once the relationship between PGA and PGD has been established for a given value of k_y, M and ε, fragility curves can be derived for a range of PGA values, as outlined in Figure 75 and Figure 76, for major and urban roads respectively. In this case, an earthquake moment magnitude equal to 7.0 was assumed. A summary of the median and dispersion fragility curve values is provided in **Table 42**.

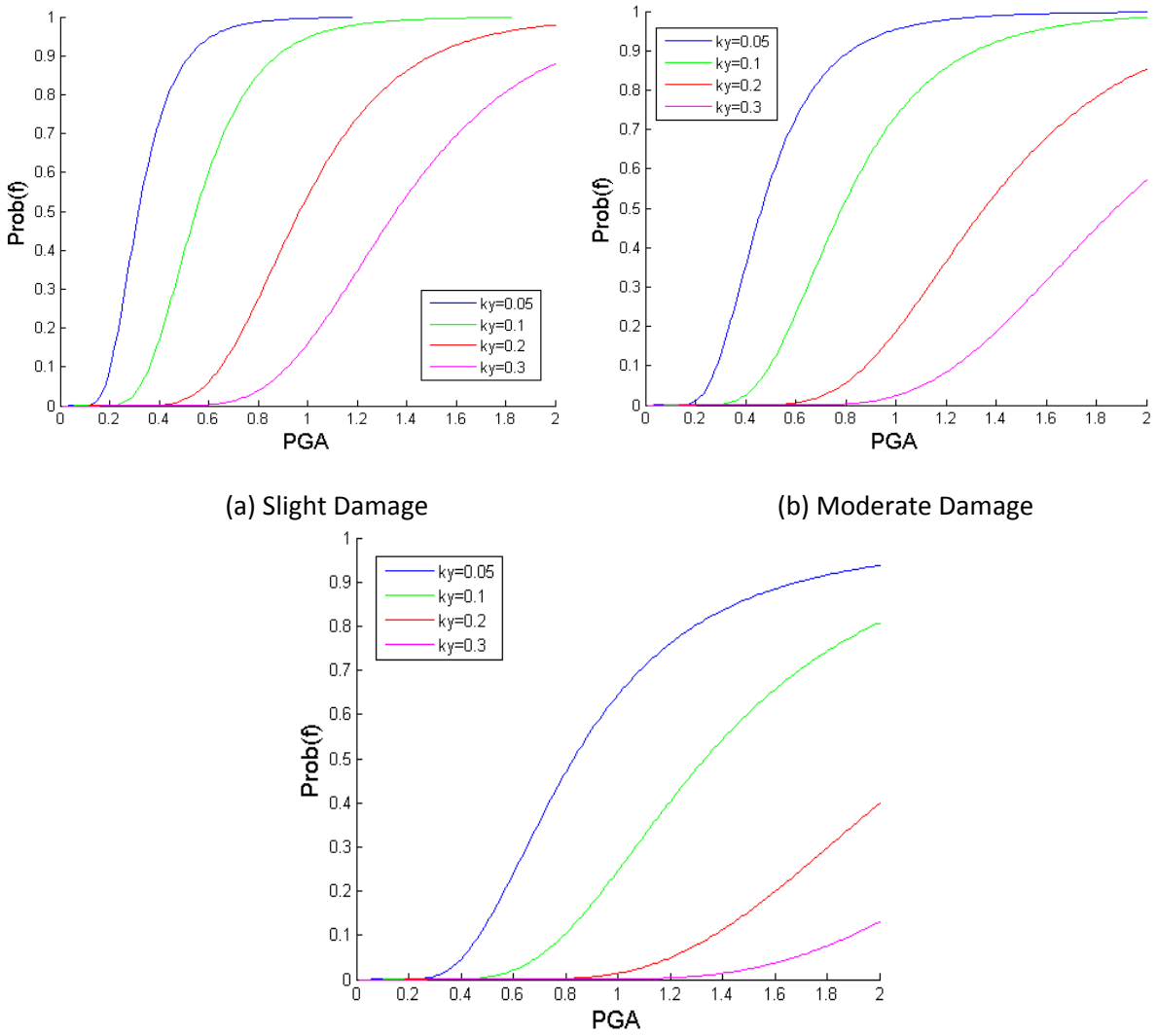

(a) Slight Damage

(b) Moderate Damage

(c) Extensive/Complete Damage

Figure 75: Fragility curves derived using Bray and Travasarou (2007) model for various damage states according to value of k_y for major roads due to earthquake-triggered landslides

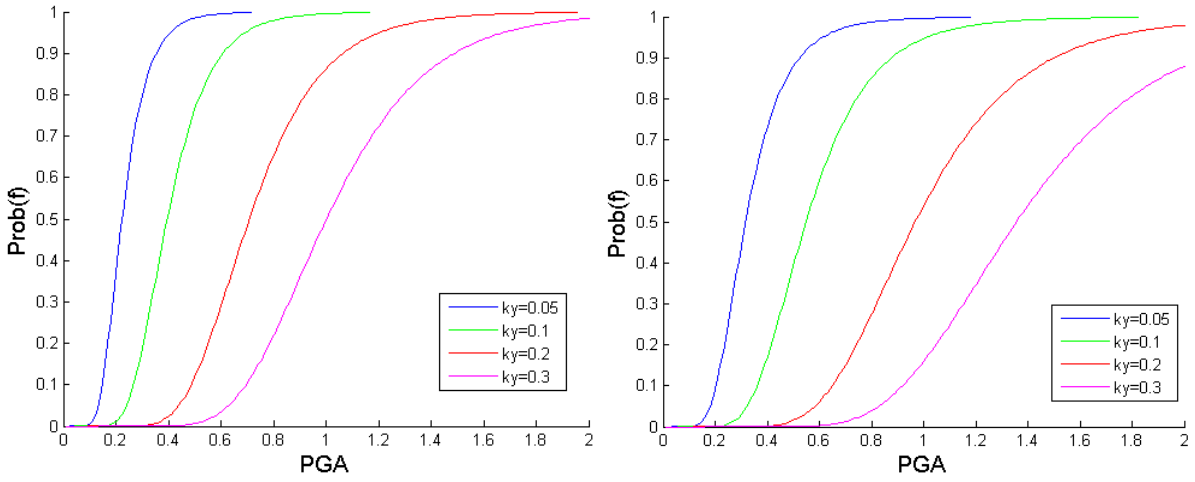

(a) Slight Damage (b) Moderate Damage

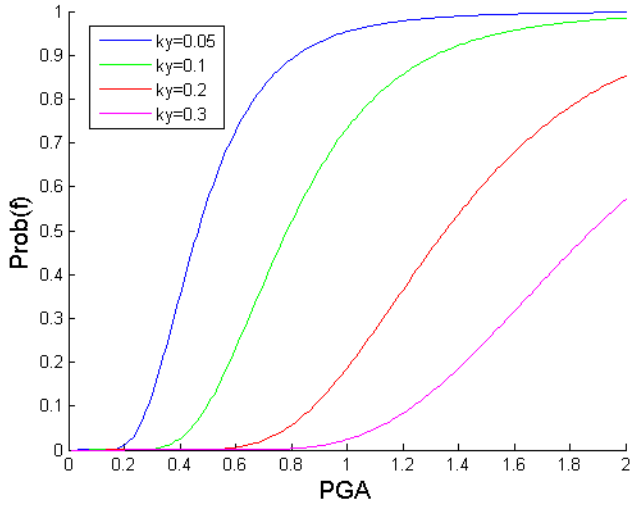

(c) Extensive/Complete Damage

Figure 76: Fragility curves derived using Bray and Travasarou (2007) model for various damage states according to value of k_y for urban roads due to earthquake-triggered landslides

		Permanent Ground Deformation							
		k_y = 0.05		k_y = 0.1		k_y = 0.2		k_y = 0.3	
Components	Damage states	θ (g)	β	θ (g)	B	θ (g)	β	θ (g)	β
Major Road	Slight/Minor	0.32	0.40	0.55	0.40	0.97	0.35	1.36	0.30
	Moderate	0.47	0.40	0.78	0.40	1.36	0.35	1.88	0.30
	Extensive/Complete	0.83	0.40	1.34	0.40	2.22	0.35	2.90	0.30
Urban Road	Slight/Minor	0.22	0.40	0.40	0.35	0.71	0.35	1.00	0.30
	Moderate	0.32	0.40	0.55	0.35	0.97	0.35	1.36	0.30
	Extensive/Complete	0.47	0.40	0.78	0.35	1.36	0.35	1.88	0.30

Table 42: Median and dispersion values for fragility curves derived using Bray and Travasarou (2007) model, as proposed by Pitilakis et al. (2011).

For earthquake-triggered landslide hazards, the spatial scale of the analysis is local, e.g. the road network is analysed at regular sections to assign fragility curves. Spatial information is therefore

required for the network being analysed, which is commonly analysed using a geographical information system (GIS) (Azevedo et al., 2004). Firstly, to evaluate the landslide susceptibility due to earthquakes, information regarding the local topography and geological conditions is required. In relation to the topography, a digital terrain model of the region being examined may be obtained (i.e. http://www.eea.europa.eu/data-and-maps/data/eu-dem#tab-metadata). This provides a global digital coverage of the topography in terms of elevation height, for which the terrain slope may be subsequently calculated in a GIS. Spatial information regarding geological conditions may be obtained from soil maps (i.e. http://eusoils.jrc.ec.europa.eu/ESDB_Archive/ESDB/index.htm) and rasterised in GIS at a grid spacing that corresponds to the resolution of the terrain slope values (Jibson et al., 2000). A similar approach may be adopted for the saturation ratio of failure surface (*m*), which requires knowledge of hydro-geological information (Saygili, 2008). Once the landslide susceptibility map has been established, the road network can be analysed at regular intervals to assign fragility curves for road sections due to earthquake-triggered landslides.

6.4.2 Rainfall-triggered landslide hazard

The development of fragility curves for rainfall-induced landslides, which are a very common failure mechanism across the globe, has received relatively little consideration. Smith & Winter (2013) presented empirical fragility curves for roads subjected to debris flows. The intensity measure used in this study was the volume of material blocking the road, originating from a road cutting or an adjacent natural slope. Damage states were described qualitatively as a portion of the road covered by the debris and classified as 'limited damage', 'serious damage' and 'destroyed'. Probabilities of these damage states occurring for each of the debris volumes considered were set following expert opinions collected through questionnaires. Whilst debris volumes were not related to any triggering rainfall event, this study introduced the concept of damage states defined by a measure of the network performance (the number of lanes not covered by debris and therefore open for traffic).

Wu (2014) presented a methodology for deriving fragility curves for slopes subjected to simultaneous earthquake and rainfall loading. Three failure mechanisms were considered; shallow translational failure, deep seated rotational failure, and rock wedge failure. For shallow translational type failures, Wu used a simplified geotechnical model with a shallow soil layer overlaying impermeable bedrock, with the failure plane located at the soil-rock interface. The groundwater table was assumed to rise from the interface up to the slope surface following a rainfall event. While this scenario can be observed on natural hillside soil slopes with shallow bedrock (the case considered in Wu's paper), it is unlike the failure mechanism observed in most natural slopes which involves a downward propagating wetting front. Two sets of fragility curves were developed, one with intensity measures consisting of seismic characteristics (PGA) and another with intensity measures consisting of the water table depth. Seismic loading was considered as the trigger in both sets, with groundwater table only affecting the results. The groundwater depth was not related to any external precipitation. Moreover, no damage states were defined, with the result that the methodology is not connected with a wider risk assessment analysis. However, this work confirmed the utilization of the MCS based approach in developing landslide fragility curves.

Reviews of the literature shows that while fragility curves have been developed for certain infrastructure elements like bridges there is a much smaller range of solutions for earthwork assets. Furthermore, virtually all of the fragility curves dedicated to landslides on cuttings and

embankments were developed for events triggered by earthquakes. In comparison very little work has been performed on fragility curves related to rainfall triggered landslides. Risk analyses for large transport networks require simultaneous performance results for all types of infrastructure elements and hazards expected in order to correctly assess the losses and post-event network behaviour. Exclusion of rainfall triggered failures on earthworks clearly overestimates the network resilience. This study aims to bridge this gap by developing a methodology for constructing fragility curves for shallow rainfall induced landslides on transport infrastructure earthworks.

A procedure has been developed within the INFRARISK project to calculate the probability of slope (cutting or embankment) reaching some pre-defined damage state triggered rainfall loading. The physical manifestation of the damage in the analytical slope stability formulation allows for only two outcomes: failure or no failure. This prevents the use of a parameter with a continuous range (e.g. displacement), as is the case for earthquake triggered landslides, to form the damage thresholds. However, the impact of the specific failure damage on the network performance following the attainment of a given serviceability state can provide a very good estimate of physical vulnerability. The following chapter describes a methodology on how rainfall loading (as an intensity measure) can be used to assess landslide failure, which is then translated into a meaningful damage index, finally resulting in the formation of the fragility curve.

A typology needs to be developed in order to classify the entirety of the earthworks present across transport network into a limited number of standardised types for which the fragility curves can be generated. The typology, or a classification system, should make asset inventory inputs compatible with the fragility curves requirements (Pitilakis et al., 2014). The typology proposed is shown in **Table 43**, with four categories: network type (rail or road) and level (highway, local road, urban road), slope type (cutting or embankment), slope geometry (in particular slope angle) and material type (each with a set of corresponding geotechnical soil parameters).

Category	***Classification***
Network type and level	Rail, Road; Local road, national road, motorway, etc.
Object type	Embankments; Cuttings
Geometry – slope angle	Defined range
Soil material	Soil groups typical for the observed network

Table 43: Proposed engineered earthwork typology.

The methodology for deriving the fragility curves is based on unsaturated soil mechanics theory and research conducted on the effects of rainfall infiltration into slopes on stability analyses (Fredlund, 1978; Cho and Lee, 2002; Ng and Shi, 1998). The failure mechanism developed as a result of rainfall infiltration is described in INFRARISK Deliverable 3.1 (D'Ayala et al., 2014).

A common description of rainfall event uses a combination of two factors: rainfall intensity *I* [mm/h] and duration *D* [h]. The intensity measure is herein quantified with one of the factors (intensity) being constant and another (duration) having a range of values. A family of fragility curves can be developed to cover various rainfall intensities. To showcase fragility curves in this study, a rainfall event with the intensity of 5 mm/h and sliding duration of 0-24 hr has been used.

Translational slope stability formulation describe only landslide initiation (i.e. when disturbing forces exceed resistance) and not run-out, meaning that criteria connected to soil displacement, commonly

used in fragility curves developed for earthquake triggered landslides, are not suitable for use as damage indices. The physical manifestation of slope response in the case of translational slope stability formulation is a discrete one: a slope either experiences failure (a slip occurs) or it does not. Subsequent landslide characteristics like the length of run-out are not considered. That means damage states thresholds cannot be selected as values from a continuous slope response function i.e. displacement. Instead, the effect of a failure as a single outcome on serviceability level of the asset has to be observed here.

The physical manifestation of damage is often connected to the serviceability (functionality) level of the element (Pitilakis, 2011). It is clear that the size of the landslide plays a major role in the resultant damage. For embankments, damage can range from surficial slope erosion to the significant loss of embankment body and damage to sleepers and tracks (or a road surface) at the crest. The size of a landslide can thus cause different types of serviceability loss, depending also on the relative position of rail tracks to the slope crest. Similar reasoning can be applied to cuttings, where the size of the landslide determines the reach of the debris: smaller landslides may only reach the intercepting drain while larger ones can spread the material across rail tracks (or road surface) located beneath the cutting. Both direct cost (debris removal, remediation works) and indirect cost (length of line closure) depend on this feature. A simple measure of shallow landslide size can be based on the depth of the failure plane. The landslide depth is there treated as a parameter whose threshold values can delineate different damage states.

Table 44 gives an overview of the three damage states considered (Low, Medium and High), together with a qualitative description of the resultant damage. As the landslide depth increases we move from a low to a high damage state (DS). The threshold values (between 0.6 m and 1.8m) adopted are based on clearances (distances from the edge of the outer track to the crest of the slope) determined from a statistical analysis of values measured on the Irish rail network. This absolute value of the threshold values defining damage states can be adjusted to suit specific network requirements.

Damage State	***Landslide depth***	***Damage description***	***Direct (cost) and indirect (network functionality) losses***
Low	H_1 (0.6 m*)	Minor slip, eroded surface, not affecting track elements	Short closure for inspection, no/minor intervention required
Medium	H_2 (1.2 m*)	Significant embankment material loss, not affecting track elements	Remediation measures required on embankment body, closure time during remediation
High	H_3 (1.8 m*)	Deeper slide, significant embankment material loss affecting track elements	Extensive remediation measures required on embankment body and track infrastructure, closure time during remediation

* values determined for the Irish rail network case study

Table 44: Damage States definition.

Rainfall infiltration causes a reduction in near surface suction and consequent loss of shear strength for soil. Since the resistance of a slope to the development of shallow slip surfaces is heavily dependent on near-surface suction, prolonged or high intensity rainfall can trigger failure. In this

work infiltration was modelled using the finite element software package Geostudio SEEP/W that solves Richards' equation (1931) for 2D seepage problems:

$$\frac{\partial}{\partial x}\left(k_x \cdot \frac{\partial H}{\partial x}\right)+\frac{\partial}{\partial y}\left(k_y \cdot \frac{\partial H}{\partial y}\right)+Q=\frac{\partial \theta}{\partial t} \quad (30)$$

Where H is the total head, k_x is the hydraulic conductivity in x-direction, k_y is the hydraulic conductivity in y-direction, Q is the applied boundary flux, ϑ is the volumetric water content and t is time.

A Matlab code was developed to perform batch calculations of stability using transient matrix suction values imported from SEEP/W for a range of discrete time steps. A Monte Carlo (MC) probabilistic analysis was carried out to model the variability of soil parameters (used in the stability analysis). The mean values of the parameters are shown in **Table 45**, whilst coefficients of variation (COV) for parameters were adopted from recommendations given by Babu and Murthy (2005). The probabilities of failure calculated are plotted against the respective time step, thus forming a fragility curve (see Figure 77).

Material	***Effective cohesion c'***	***Friction angle φ'***	***Unit weight γ***	***φ^b ****	***In-situ saturated permeability***	***Soil classification***
Glacial till	1.0 kN/m^2	37°	19 kN/m^3	30°	1.5x10^{-6} m/day	Sandy clay, sandy silt

*angle indicating the rate of increase in shear strength relative to the matric suction

Table 45: Geotechnical parameters of glacial till.

Figure 77 presents a typical family of fragility curves for a glacial till embankment with slope angle of 42.5°. The probability of exceeding a defined damage state as a function of rainfall duration is shown for low, medium and high damage states.

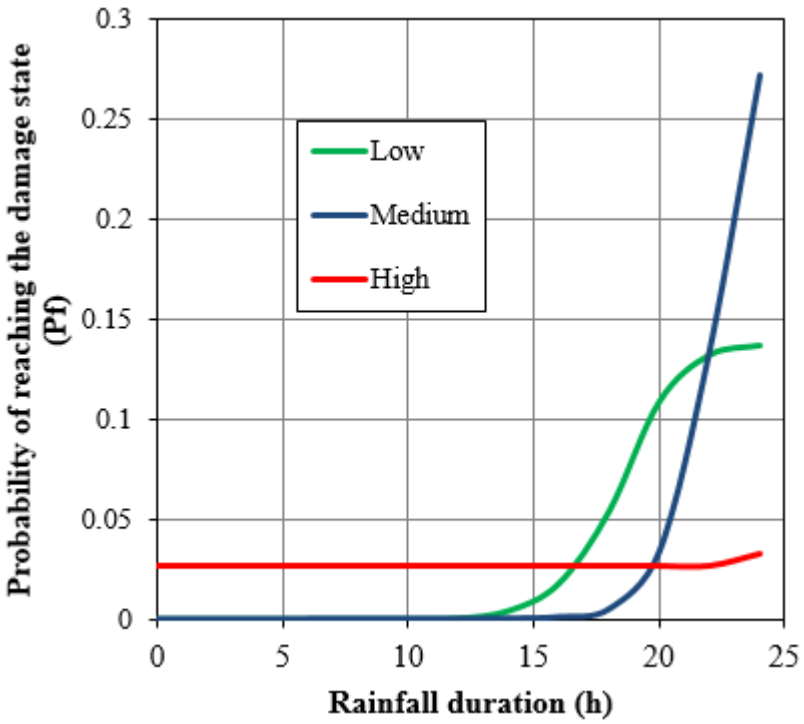

Figure 77: The fragility curves for low, medium and high damage states

The atypical shape of the fragility curves is a consequence of infiltration and slope stability models used to construct the curves. For example considering the curve for the low damage state, the P_f value approaches a plateau of around 0.14 after rainfall duration of 24 hours. This is because the duration is long enough for the wetting front depth to fully develop and by definition the suction has reduced to the residual values over this entire depth (0.6 m). Further infiltration cannot cause further reductions in suction (rather the wetting front depth increases beyond 0.6m). The probability of 0.14 is therefore the maximum probability of failure for this damage state and once this is reached, the Pf of failure for the medium damage state exceeds that for the low damage state. These curves have been verified against the failure database provided by the Irish Rail and they exhibit a good match to the observations in field. Additional details on the model development can be found in Martinovic et al. (2015).

6.5 From physical damage states to functional states

The expert-based survey that has been conducted within the INFRARISK project is used to estimate approximate functionality models for road segments. Based on the summary of the component failure modes (see **Table 49**), a probabilistic model is assembled for the repair duration and the percentage of closed lanes: it is based on the survey answers that are summarized in This appendix details the results of the expert-based survey: as stated before, the following numerical values should be considered for illustrative purposes only, due to the scarcity of collected data.

and **Table 51**.

Since Figure 67 provides a ranking of the damage severity of the various failure modes, this damage scale from DS1 and DS3 could be used in order to evaluate functionality levels that correspond to these global damage states (as it has been done for bridges and tunnels). However an additional

distinction is introduced between damaging mechanisms that occur below or above the road surface, since it is expected that these two main damage types might generate different types of repair operations and functional losses:

- **Above the road surface:** they correspond to damage mechanisms such as debris flows, rock falls or sedimentation of material from inundation (i.e. obstruction/failure from moving elements);
- **Below the road surface:** they correspond to damage mechanisms such as the formation of cracks, vertical settlements or the sliding/slumping of embankments (i.e. ground failure occurring beneath the road surface).

The functional loss and repair duration models for the damage states corresponding to these two main failure modes are then estimated and displayed in Figure 78 to Figure 81.

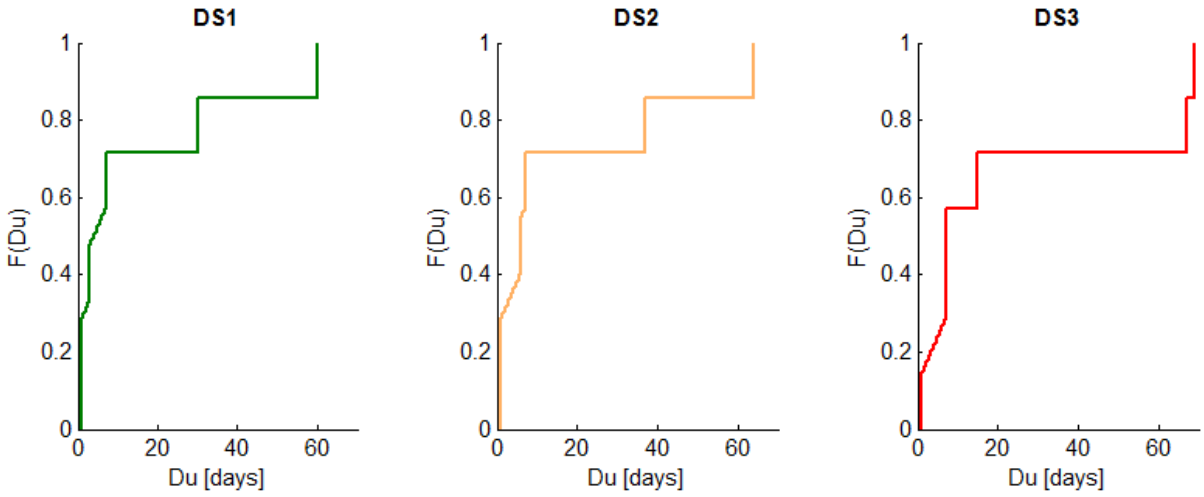

Figure 78: Duration of repair operations given global damage states DS1 to DS3, when considering obstruction/failure from moving elements

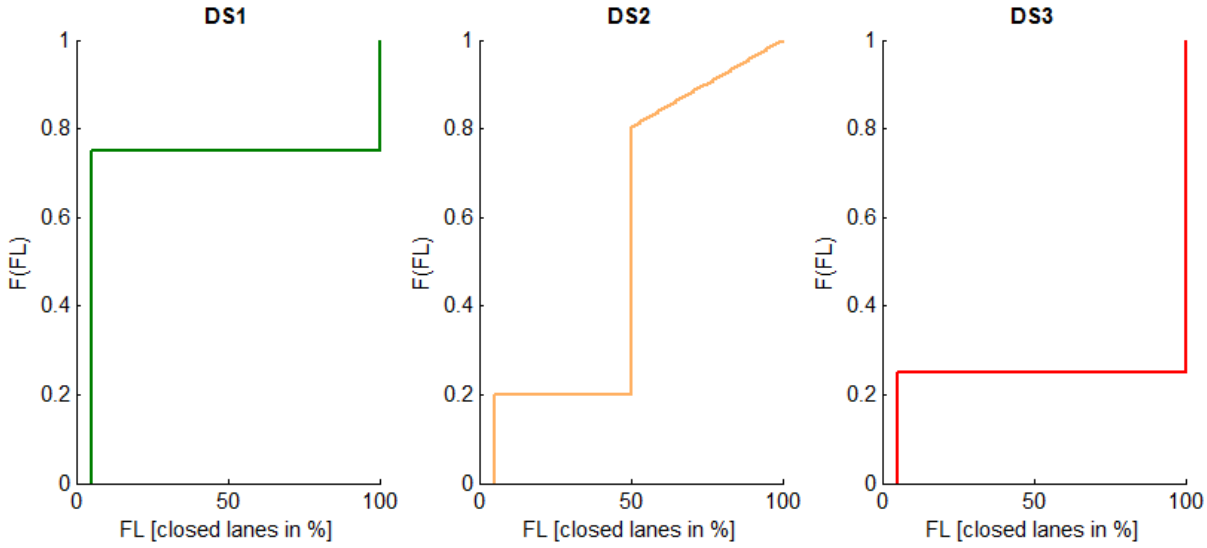

Figure 79: Functionality loss (expressed in proportion of closed lanes) given global damage states DS1 to DS3, when considering obstruction/failure from moving elements

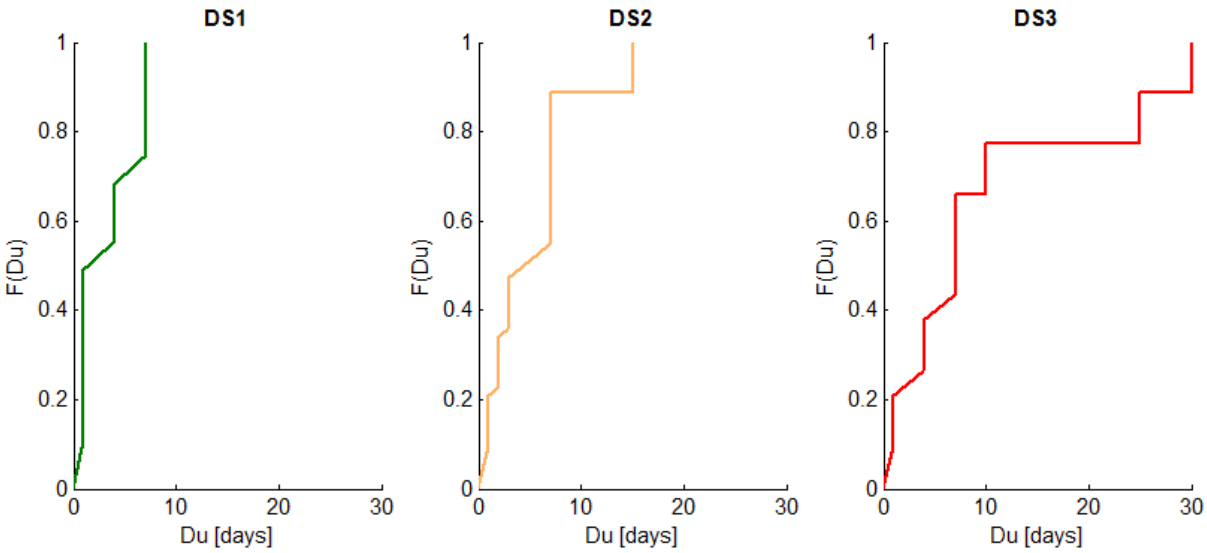

Figure 80: Duration of repair operations given global damage states DS1 to DS3, when considering ground failure occurring beneath the road surface

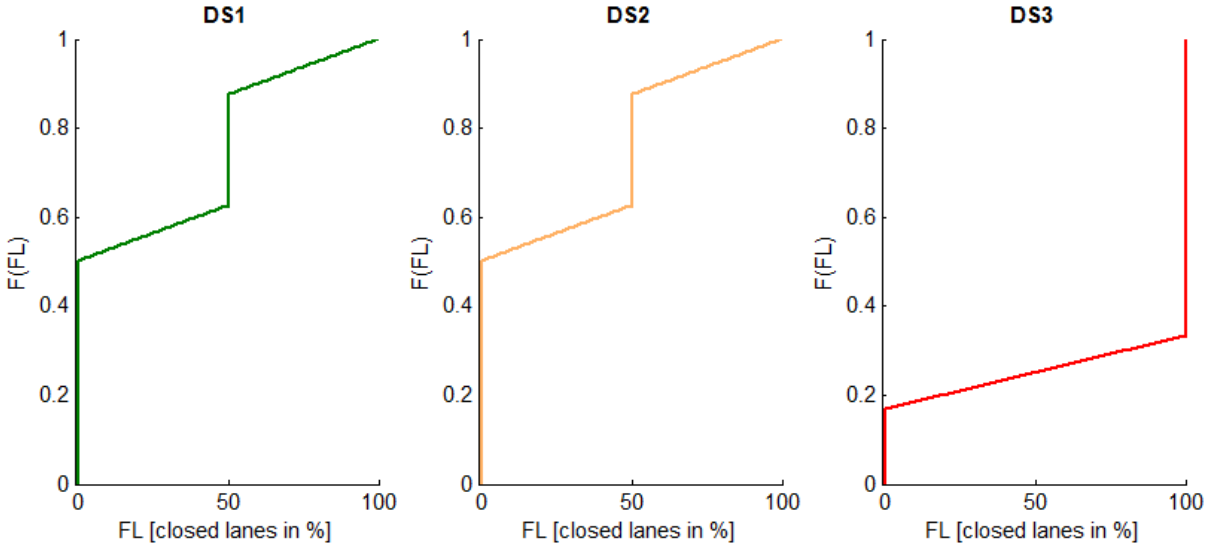

Figure 81: Functionality loss (expressed in proportion of closed lanes) given global damage states DS1 to DS3, when considering ground failure occurring beneath the road surface

The functionality models presented here may lead to the following observations:

- The hierarchy between the damage state severity and the extent of functional losses and repair durations is consistent, even though there is no significant difference between DS1 and DS2 for some models (e.g. see Figure 78 or Figure 81);
- The functional losses due to “below the surface” damages are slightly higher than for “above the surface” ones: this observation is consistent with the fact that one may expect more severe consequences when the ground fails directly beneath the road (i.e. necessity to reconsolidate the foundation layers and to rebuild the road surface in some cases) as opposed to debris or rocks covering the road surface (i.e. a cleanup of the road surface is sufficient in most cases). However it could be noted that the differences between the two loss models are not obvious.

- Concerning repair durations, it is observed that the “above the surface” damages have more severe consequences than “below the surface” ones, which is the contrary of what was expected. Here, a limit of the functionality models is highlighted, since the inclusion of the rock fall events implies the destruction of the rock protection gallery as one of the damage states: such an event would naturally lead to long and costly repair operations, however one may argue that such a component does not necessarily exist along all road segments.

The numerical values that are proposed in this section should be considered for illustrative purposes only, due to the scarcity of the collected data from the expert-based survey.

7.0 FRAGILITY FUNCTIONS MATRIX

The aforementioned developments and models are summarized in the fragility functions matrix (see **Table 46**), where the most common failure modes and corresponding fragility curves are detailed. For each type of infrastructure element, some system failure modes are proposed, and the corresponding damage mechanisms at the component level are then identified for each hazard type.

	Earthquake	**Ground failure**	**Flood**	**Scour**
Bridges				
System Failure mode 1 – Slight damage to bridge approach only				
EDP		Permanent vertical displacement (subsidence) of approach embankment		
Physical damage states		Slight damage (displacement > 30mm)		
Recommended method in INFRARISK		Use of literature references (analytical approaches)		
Fragility functions		SYNER-G based curves, from Kaynia et al. (2012)		
Functional damage states	Slight repairs and no closing time			
System Failure mode 2 – Minor structural damage				
EDP	- Curvature of piers - Displacement of bearings - Displacement of shear keys - Displacement of abutments	Permanent vertical displacement (subsidence) of approach embankment	Displacement of shear keys	Scour depth
Physical damage states	- Yielding of piers - Failure of the restraining device (bearings and shear keys) - Yielding of abutment piles in tension (active behaviour)	Moderate damage (displacement > 150mm)	Failure of the restraining device of shear keys	Reduction in lateral resistance of piers (2 discrete damage states are considered)
Recommended method in INFRARISK	Non-linear time-history analyses	Use of literature references (analytical approaches)	Use of literature references (empirical approaches)	Scour equations (empirical methods) + static pushover analysis of piers

Fragility functions	Fragility curves developed in Section 4.6.2	SYNER-G based curves, from Kaynia et al. (2012)	Empirical curves from Kameshwar and Padgett (2014)	Fragility curves developed in Section
Functional damage states	Moderate repairs with a short closing time			
System Failure mode 3 – Deck unseating				
EDP	- Displacement of bearings - Displacement of shear keys		Displacement of shear keys	Scour depth
Physical damage states	Displacement corresponding to deck unseating (bearings and shear keys)		Displacement corresponding to deck unseating	Reduction in lateral resistance of piers (2 discrete damage states are considered)
Recommended method in INFRARISK	Non-linear time-history analyses		Not currently available	Scour equations (empirical methods) + static pushover analysis of piers
Fragility functions	Fragility curves developed in Section 4.6.2		Assumption based on deck height and water depth	Fragility curves developed in Section
Functional damage states	Extensive repairs with a prolonged closing time			
System Failure mode 4 – Collapse of substructure components				
EDP	Curvature of piers			Scour depth
Physical damage states	Collapse of piers			Total loss of lateral resistance of piers
Recommended method in INFRARISK	Non-linear time-history analyses			Scour equations (empirical methods) + static pushover analysis of piers
Fragility functions	Fragility curves developed in Section 4.6.2			Fragility curves developed in Section
Functional damage states	Irreparable damage (i.e. full collapse of the bridge system)			
Tunnels				
Failure mode 1 – Slight damage				
EDP	Size of cracks in the tunnel liner	- Amount of rock fall at portal - Permanent ground displacement at portal		

Physical damage states	- Minor cracking and spalling - Width of crack < 3mm - Length of crack < 5m	- Some rock falling - Slight settlement		
Recommended method in INFRARISK	Use of literature references (analytical or empirical approaches)	Not currently available		
Fragility functions	Fragility functions selected in Section 5.5	Not currently available		
Functional damage states	33% to 100% lane closure – repair duration around ~10-20 days (according to proposed functionality model)			
Failure mode 2 – Moderate damage				
EDP	Size of cracks in the tunnel liner	Amount of rock fall at portal		
Physical damage states	- Moderate cracking and spalling - Width of crack > 3mm - Length of crack > 5m	Moderate rock falling		
Recommended method in INFRARISK	Use of literature references (analytical or empirical approaches)	Not currently available		
Fragility functions	Fragility functions selected in Section 5.5	Not currently available		
Functional damage states	75% to 100% lane closure – repair duration around ~10-50 days (according to proposed functionality model)			
Failure mode 3 – Extensive damage				
EDP	Size of cracks in the tunnel liner	Permanent ground displacement at portal		
Physical damage states	Extensive cracking	Major ground settlement		
Recommended method in INFRARISK	Use of literature references (analytical or empirical approaches)	Analytical approach (both earthquake- and rainfall-triggered landslides)		
Fragility functions	Fragility functions selected in Section 5.5	Fragility curves developed in Section 6.4		
Functional damage states	100% lane closure – repair duration around ~20-100 days (according to proposed functionality model)			
Failure mode 4 – Complete damage				
EDP	Size of cracks in the tunnel liner	Permanent ground displacement at portal		

Physical damage states	Collapse of lining	Slope failure		
Recommended method in INFRARISK	Use of literature references (analytical approaches)	Analytical approach (both earthquake- and rainfall-triggered landslides)		
Fragility functions	Fragility functions selected in Section 5.5	Fragility curves developed in Section 6.4		
Functional damage states	100% lane closure – repair duration longer than ~200 days (according to proposed functionality model)			
Road segments				
Failure mode 1 – Failure of the soil supporting the road pavement				
EDP	- Amount of cracks on the road pavement - Amount of vertical settlement	- Amount of cracks on the road pavement - Extent of slide/slump of the embankment	- Saturation and collapse of inundated roadbeds - Blockage of drainage ditches and underdrains by debris, exacerbating erosion and scour - Undermining of shoulders when ditch capacity is exceeded	
Physical damage states	- Very minor damage: gap less than 1 cm - Minor damage: gap between 1 and 3 cm - Moderate damage: gap more than 3 cm on traffic lane / more than 20 cm on shoulder	- D1: surface slide of embankment at the top of slope only, minor cracks on the surface of the road - D2: deep slide/slump of embankment involving traffic lines, medium cracks on the surface of the road - D3: serious slide/slump of embankment	Based on the subsidence level, remaining bearing capacity of the soil	
Recommended method in INFRARISK	Use of literature references (analytical approaches)	Use of literature references (analytical approaches)	Not currently available	
Fragility functions	- SYNER-G based curves, from Kaynia et al. (2012) - Fragility curves developed in Section 6.4	- SYNER-G based curves, from Kaynia et al. (2012) - Fragility curves developed in Section 6.4	Not currently available	

Functional damage states	Lane closure from 0% to 100%, depending on the severity of the damage – repair duration around ~1-30 days (according to proposed functionality model)			
Failure mode 2 – Failure/obstruction of road pavement due to moving elements				
EDP		- Volume of debris flow - Amount of rock fall	Volume of accumulated material (sedimentation)	
Physical damage states		Debris flow: - Limited damage: encroachment limited to verge/hardstrip - Serious damage: blockage of hardstrip and one running lane - Destroyed: complete blockage of carriageway and/or repairable damage to surfacing Rock fall: - D1: Failure of rock protection gallery - D2: Obstruction of road - D3: Destruction of road surfacing	Based on the height/volume of material, with or without damage on the road pavement	
Recommended method in INFRARISK		Analytical approach (both earthquake- and rainfall-triggered landslides)	Not currently available	
Fragility functions		- SAFELAND-based curves (Pitilakis et al., 2011); - curves from Winter et al. (2014)	Not currently available	
Functional damage states	Lane closure from 0% to 100%, depending on the severity of the damage – repair duration around ~1-60 days (according to proposed functionality model)			
Failure mode 3 – Inundation of road segments				
EDP			Water height	
Physical damage states			Discrete damage states based on water height, may be related to the height of the wheel drive of cars/trucks	
Recommended method in INFRARISK			Not currently available / Use of few literature references	

Fragility functions			One example from Teo et al. (2012)	
Functional damage states	Disruption of traffic, destruction of vehicles – Duration of closure depending on the time the water takes to recede			

Table 46: Fragility Functions Matrix

8.0 CONCLUSION

The deliverable has specified a Fragility Functions Matrix which defines adequate fragility models for each infrastructure element type and hazard type considered in the INFRARISK project. Following the harmonization of the hazard models in INFRARISK deliverable D3.1 (D'Ayala et al., 2014), this deliverable has proposed a framework to harmonize the fragility models between hazard types, which consists of the following steps:

1. Identify all possible failure modes for the infrastructure element (e.g. bridge), which are specific to each component type (e.g. bearings, piers, etc.) and to each loading mechanism (e.g. ground shaking, water pressure, etc.).

2. Select from existing or analytically derive fragility curves for each of the component failure modes identified.

3. Estimate the losses (i.e. functional losses before and during intervention, repair costs, duration of repair operations) corresponding to each component failure mode based on expert-based judgment.

4. Introduce system failure modes (i.e. assembly of specific component failure modes) that may correspond to homogeneous loss levels.

5. Aggregate the component-level fragility functions to quantify the probability of reaching one of the system failure modes. This process may use Bayesian Networks and permits the generations of a hazard-independent fragility model: the term "hazard-independent" does not mean that the derived fragility functions are not dependent on the hazard intensity, but they that the same fragility model may be used whatever the hazard type considered, with a harmonized damage scale (i.e. use of functionality levels instead of physical damage states).

This framework has been applied to a bridge system that is susceptible to be exposed to earthquakes, ground failures and floods: the procedure resulted in four harmonized functionality levels which probability of occurrence depends on the seismic intensity level (i.e. peak ground acceleration *PGA*) and the flow intensity level (i.e. flow discharge *Q*).

Steps 1 to 3 of the proposed approach have also been applied to the case of tunnels or road segments, but the proper definition of system failure modes and the Bayesian approach have not been carried out for these elements, even though the necessary framework is available. For these elements, the high uncertainties around the estimation of functional consequences and the lack of accurate fragility models for some components would not result in a meaningful Bayesian analysis.

Regarding the development of hazard-specific component fragility functions, most models for seismic risk are available in the literature (e.g. SYNER-G work on fragility functions for infrastructure elements) or can be analytically derived through state-of-the-art practices, especially for bridges (e.g. use of finite element codes and non-linear time-history analyses). In the case of ground failures, several fragility curves may be selected from the literature (especially for embankments) while some simplified analysis models are available for specific cases (e.g. application of infinite slope model or circular failure analysis for landslides): in the multi-risk context of the INFRARISK project, fragility

curves for both earthquake- and rainfall-induced landslides have also been derived. Finally, failure modes related to flood hazard cannot often be associated with fragility functions, due the lack of research or available models in this area: empirical equations predicting scour depth might still be jointly used with finite element models in order to evaluate the potential damage to the bridge system that is induced by the flood level. However, there is lack a of fragility models that could quantify the effects of submersion or hydraulic pressure on the infrastructure elements.

In the case where the component-level approach cannot be applied (e.g. lack of census data, large extent of the network preventing the application of refined models), typical fragility functions for global damage states may also be used (i.e. direct derivation of global fragility curves for pre-defined physical damage states): this approach requires less modelling efforts but it remains specific to each hazard type, and the definition of the global damage states is not necessarily consistent with the induced losses. Probabilistic functionality models have then been derived for these global damage states by aggregating all the functional consequences that are implied by the definition of these damage states, in order to facilitate the application of the global fragility models.

Finally, the results of this deliverable can be assembled with the hazard models from INFRARISK deliverable D3.1 in order to conduct corresponding risk analyses, both in the case of single hazards or interacting hazards (i.e. INFRARISK deliverable D3.3). The fragility and functionality models that have been described here can also be directly integrated into the case-study tasks (Work Package 8) or implemented into the INFRARISK Decision Support Tool (IDST developed in Work Package 7).

9.0 REFERENCES

ALA (2005). Flood-Resistant Local Road Systems: A report Based on Case Studies, American Lifelines Alliance.

Alipour, A., and Shafei, B. (2012). Performance assessment of highway bridges under earthquake and scour effects, Proceedings of the Fifteenth World Conference on Earthquake Engineering, Lisbon, Portugal.

Alipour, A., Shafei, B., and Shinozuka, M. (2013). Reliability-Based Calibration of Load and Resistance Factors for Design of RC Bridges under Multiple Extreme Events: Scour and Earthquake, *Journal of Bridge Engineering* 18:362-371.

Apel, H., Thieken, A.H., Merz, B., and Bloschl, G. (2004). Flood risk assessment and associated uncertainty, *Natural Hazards and Earth System Science* 4: 295-308.

API (2000). Recommended practice for planning, designing and constructing fixed offshore platforms, API Recommended Practice 2A-WSD (RP 2A), American Petroleum Institute, Washington, D.C.

Argyroudis, S. (2010). Contribution to Seismic Vulnerability and Risk of Transportation Networks in Urban Environment, PhD Thesis (in Greek), Dept. of Civil Engineering, Aristotle University of Thessaloniki, Greece.

Argyroudis, S., and Kaynia, A.M. (2015). Analytical seismic fragility functions for highway and railway embankments and cuts, *Earthquake Engineering and Structural Dynamics*, In press.

Argyroudis, S., and Kaynia, A.M. (2014). Fragility Functions of Highway and Railway Infrastructure, In: SYNER-G: Typology Definition and Fragility Functions for Physical Elements at Seismic Risk, K. Pitilakis K., H. Crowley, A.M. Kaynia (Eds), Springer Netherlands, ISBN 978-94-007-7871-9, p299-326.

Argyroudis, S., Monge, O., Finazzi, D., and Pessina, V. (2003). Vulnerability assessment of lifelines and essential facilities (WP06): Methodological Handbook – Appendix 1: Roadway Transportation System, Risk-UE Final Report, Report n◦GTR-RSK0101-152av7.

Avsar, O., Yakut, A., and Caner, A. (2011). Analytical fragility curves for ordinary highway bridges in Turkey, *Earthquake Spectra* 27(4):971-996.

Azevedo, J. et al. (2004). Seismic impact on lifelines in the Great Lisbon Area, Proceedings of the 13th World Conference on Earthquake Engineering, Vancouver, Canada.

Azevedo, J., Guerreiro, L., Bento, R., Lopes, M., and Proenca, J. (2010). Seismic vulnerability of lifelines in the greater Lisbon area, *Bulletin of Earthquake Engineering* 8(1):157–180.

Bachmann, D., Huber, N.P., and Schüttrumpf, H. (2009). Fragility curve calculation for technical flood protection measures by the Monte Carlo analysis, Proceedings of the European conference on flood risk management research into practice (Floodrisk 2008), Oxford, UK.

Baker, J.W. (2015). Efficient analytical fragility function fitting using dynamic structural analysis, *Earthquake Spectra* 31(1):579-599.

Baker, J.W. (2007). Probabilistic structural response assessment using vector-valued intensity measures, *Earthquake Engineering and Structural Dynamics* 36(13):1861-1883.

Banerjee, S., and Shinozuka, M. (2008). Mechanistic quantification of RC bridge damage states under earthquake through fragility analysis, *Probabilistic Engineering Mechanics* 23(1):12-22.

Barbetta, S., Camici, S., and Moramarco, T. (2015). Reappraisal of bridge piers scour vulnerability: a case study in the Upper Tiber River basin (central Italy), *Journal of Flood Risk Management*, In press.

Bartlett, S.F. (2014). Liquefaction-Induced Ground Failures and Bridge Damage in Southern Alaska Along the Alaskan Railroad and Highway during the 1964 Alaskan Earthquake, Proceedings of the 10th National Conference on Earthquake Engineering, Earthquake Engineering Research Institute, Anchorage, AK.

Basoz, N., and Kiremidjian, A.S. (1996). Risk assessment for highway transportation systems, Technical Report NCEER-118, John A. Blume Earthquake Engineering Center.

Basoz, N., Kiremidjian, A.S., King, S.A., and Law, K.H. (1999). Statistical analysis of bridge damage data from 1994 Northridge, CA earthquake, *Earthquake Spectra* 15(1):25-54.

Benn, J. (2012). Railway Bridge Failure during Flood in the UK and Ireland: Learning from the Past, Institution of Civil Engineers.

Bensi, M.T., Der Kiureghian A., and Straub, D. (2013). Efficient Bayesian network modeling of systems, Reliability Engineering and System Safety 112:200-213.

Bensi, M.T., Der Kiureghian, A., and Straub, D. (2011). A Bayesian Network methodology for infrastructure seismic risk assessment and decision support, Technical Report 2011/02, Pacific Earthquake Engineering Research Center, Berkeley, California.

Bird, J.F., and Bommer, J.J. (2004). Evaluating earthquake losses due to ground failure and identifying their relative contribution, Proceedings of the 13th World Conference on Earthquake Engineering, Vancouver, Canada.

Bousias, E., Palios, X., Fardis, M., Strepelias, I., and Alexakis, C. (2007), Experimental and analytical investigation of seismic isolation with and without additional damping, ASProGe Project, Deliverable 4.2 (in Greek).

Bradley, B.A. (2010). Epistemic uncertainties in component fragility functions, *Earthquake Spectra* 26(1):41-62.

Bray, J.D., and Travasarou, F. (2007). Simplified procedure for estimating earthquake-induced deciatoric slope displacements, *Journal of Geotechnical and Geoenvironmental Engineering* 133(4):381-392.

Byers, W.G. (2004). Railroad lifeline damage in earthquakes, Proceedings of the 13th World Conference on Earthquake Engineering, Vancouver, Canada.

Caltrans (1993). Bridge Design Specifications, California Department of Transportation.

Calvi, G.M., Pinho, R., Magenes, G., Bommer, J.J., and Crowley, H. (2006). Development of seismic vulnerability assessment methodologies over the past 30 years, *Journal of Earthquake Technology* 43(3):75-104.

Cardone, D. (2014). Displacement limits and performance displacement profiles in support of direct displacement-based seismic assessment of bridges, *Earthquake Engineering and Structural Dynamics* 43(8):1239-1263.

Cardone, D., Perrone, G., and Sofis, S. (2011). A performance-based adaptive methodology for the seismic evaluation of multi-span simply supported deck bridges, *Bulletin of Earthquake Engineering* 9:1463-1498.

CEN (2004a). EN 1992-1-1 Eurocode 2: design of concrete structures – Part 1-1: General rules and rules for buildings, European Committee for Standardization, Brussels.

CEN (2004b). EN 1998-1 Eurocode 8: design of structures for earthquake resistance – Part 1: General rules, seismic actions and rules for buildings, European Committee for Standardization, Brussels.

CEN (2005). Eurocode: Basis of structural design – Annex A2: Application for bridges (Normative), European Committee for Standardization.

Cho, S.E., and Lee, S.R. (2002). Evaluation of surficial stability for homogeneous slopes considering rainfall characteristics, *Journal of Geotechnical and Geoenvironmental Engineering* 128(9):756-763.

Choi, E., DesRoches, R., and Nielson, B. (2004). Seismic fragility of typical bridges in moderate seismic zones, *Engineering Structures* 26:187-199.

Cornell, C.A., Jalayer, F., Hamburger, R.O. and Foutch, D.A. (2002). Probabilistic basis for 2000 SAC Federal Emergency Management Agency steel moment frame guidelines, *Journal of Structural Engineering* 128(4): 526-533.

Crowley, H., Colombi, M., Silva, S., Monteiro, R., Ozcebe, S., Fardis, M., Tsionis, G., and Askouni, P. (2011). Fragility functions for roadway bridges. SYNER-G Report D3.6, www.syner-g.eu.

Couture, 2. (2011). Landslide Terminology - National Technical Guidelines and Best Practices on Landslides, Geological Survey of Canada.

D'Ayala, D. (2005). Force and Displacement Based Vulnerability Assessment for Traditional Buildings, *Bulletin of Earthquake Engineering* 3:235–265.

D'Ayala, D., and Gehl, P. (2015). Uncertainty Quantification, INFRARISK Deliverable D3.3.

D'Ayala, D., Meslem, A., Vamvatsikos, D., Porter, K., Rossetto, T., Crowley, H., and Silva, V. (2014). Guidelines for analytical vulnerability assessment of low-mid-rise buildings - Methodology, Technical report, Vulnerability Global Component Project, Global Earthquake Model.

Dawson, R.J., Peppe, R., and Wang, M. (2011). An agent-based model for risk-based flood incident management. *Natural Hazards* 59(1), 167-189.

De Risi, R., Jalayer, F., De Paola, F., Iervolino, I., Giugni, M., Topa, M., Mbuya, E., Kyessi, A., Manfredi, G., and Gasparini, P. (2013). Flood risk assessment for informal settlements, *Natural Hazards* 69(1):1003-1032.

Deierlein, G.G., Krawinkler, H., and Cornell, C.A. (2003). A framework for performance-based earthquake engineering, Proceedings of the 7th Pacific Conference on Earthquake Engineering, Christchurch, New Zealand.

Deng, L., Wang, W., and Yu, Y. (2015). State-of-the-art review on the causes and mechanisms of bridge collapse, *ASCE Journal of Performance of Constructed Facilities* 0401500.

Der Kiureghian, A., and Song, J. (2008). Multi-scale reliability analysis and updating of complex systems by use of linear programming, *Reliability Engineering & System Safety* 93: 288-297.

Der Kiureghian, A., Haukaas, T., Hahnel, A., Franchin, P., Song, J., Pakzad, S., and Sudret, B. (1999). FERUM, Available from: http://www.ce.berkeley.edu/FERUM.

Dickenson, S.E., McCullough, N.J., Barkau, M.G., and Wavra, B.J. (2002). Assessment and mitigation of liquefaction hazards to bridge approach embankments in Oregon, Technical Report SPR 361, Federal Highway Administration, Washington, D.C.

Diehl, T.H. (1997). Potential Drift Accumulation at Bridges, FHWA RD-97-28, Turner-Fairbank Highway Research Center, Federal Highway Administration Research and Development, U.S. Department of Transportation, McLean, Virginia.

Doll, C., and Sieber, N. (2011). Transport sector vulnerability: Vulnerability assessment for road transport, Deliverable 2, WEATHER Project.

Dunnett, C.W., and Sobel, M. (1955). Approximations to the probability integral and certain percentage points of a multivariate analogue of Student's t-distribution, *Biometrica* 42(1-2):258-260.

Elnashai, A.S., Gencturk, B., Kwon, O.S., Al-Qadi, I.L., Hashash, Y., Roesler, J.R., Kim, S.J., Jeong S.H., Dukes, J., and Valdivia, A. (2010). The Maule (Chile) earthquake of February 27, 2010: Consequence assessment and case studies, Technical Report MAE/10-04, Mid-America Earthquake Center.

Elnashai, A.S., Borzi, B., Vlachos, S. (2004). Deformation-based vulnerability functions for RC bridges, *Structural Engineering* 17(2):215-244.

Fotopoulou, S.D., and Pitilakis, K.D. (2013a). Fragility curves for reinforced concrete buildings to seismically triggered slow-moving slides, *Soil Dynamics and Earthquake Engineering* 48:143-161.

Fotopoulou, S.D., and Pitilakis, K.D. (2013b). Vulnerability assessment of reinforced concrete buildings subjected to seismically triggered slow-moving earth slides, *Landslides* 10(5):563-582.

Franchin, P., Cavalieri, F., Pinto, P.E., Lupoi, A., Vanzi, I., Gehl, P., Khazai, B., Weatherhill, G., Esposito, S., and Kakderi, K. (2011). General methodology for systemic vulnerability assessment, SYNER-G Report D2.1, www.syner-g.eu.

Fredlund, D. G., Morgenstern, N.R., and Widger, R.A. (1978). The shear strength of unsaturated soils, *Canadian Geotechnical Journal* 15(3):313-321.

Gehl, P., and D'Ayala, D. (2015a). Integrated multi-hazard framework for the fragility analysis of roadway bridges, Proceedings of the 12th International Conference on Applied Statistics and Probability in Civil Engineering, Vancouver, Canada.

Gehl, P., and D'Ayala, D (2015b). Development of Bayesian Networks for the multi-risk fragility assessment of bridge systems, *Structural Safety*, Under review.

Gehl, P., Douglas, J., and Seyedi, D.M. (2015). Influence of the number of dynamic analyses on the accuracy of structural response estimates, *Earthquake Spectra* 31(1):97-113.

Gehl, P., Seyedi, D.M., and Douglas, J. (2013). Vector-valued fragility functions for seismic risk evaluation, *Bulletin of Earthquake Engineering* 11(2):365-384.

Ghosh, J., and Padgett, J.E. (2010). Aging considerations in the development of time-dependent seismic fragility curves, *ASCE Journal of Structural Engineering* 136(12):1497–1511.

Gleyze, J.F., and Rousseaux, F. (2003). Impact of relief accuracy on flood simulations and road network vulnerability analysis, Proceeding of ECQTG, Lucca, Italy.

Grunthal, G. (1998). European Macroseismic Scale, Technical report, European Seismological Commission, Sub-commission on Engineering Seismology, Working Group on Macroseismic scales, Luxembourg.

Hassan, A.M., and Wolff, T.F. (1999). Search algorithm for minimum reliability index of earth slopes, *Journal of Geotechnical and Geoenvironmental Engineering* 125:301-308.

Huang, R.Q., and Li, W.L. (2012). Co-Seismic Fault Effects of Landslides Triggered by Wechuan Ms 8.0 Earthquake, China, In: New Frontiers in Engineering Geology and the Environment, Proceedings of the International Symposium on Coastal Engineering Geology, Shanghai.

Ioannou, I., Rossetto, T., and Grant, D.N. (2012). Use of regression analysis for the construction of empirical fragility curves, Fifteenth World Conference on Earthquake Engineering, Lisbon, Portugal.

Japan Road Association (2007), Guideline for restoration work of road after earthquakes (in Japanese).

Jaiswal, K., Perkins, D., Aspinal, W.P., and Kiremidjian, A.S. (2013). Estimating structural collapse fragility of generic building typologies using expert judgement, Proceedings of 11th International Conference on Structural Safety & Reliability, New York, USA.

Jaiswal, K., Wald, D., and D'Ayala, D. (2011). Developing empirical collapse fragility functions for global building types, *Earthquake Spectra* 27(3):775-795.

Jeong, S.H., and Elnashai, A.S. (2007). Probabilistic fragility analysis parameterized by fundamental response quantities, *Engineering Structures* 29(6):1238-1251.

Jibson, R.W., Harp, E.L., and Michael, J.A. (2000). A method for producing digital probabilistic seismic landslide hazard maps, *Engineering Geology* 58:271-289.

Kameshwar, S., and Padgett, J.E. (2014). Multi-hazard risk assessment of highway bridges subjected to earthquake and hurricane hazards, *Engineering Structures* 78:154-166.

Kang, W.H., Song, J., and Gardoni, P. (2008). Matrix-based system reliability method and applications to bridge networks, *Reliability Engineering & System Safety* 93: 1584-1593.

Kaplan, S., Bier, V.M., and Bley, D.C. (1994). A note on families of fragility curves—is the composite curve equivalent to the mean curve?, *Reliability Engineering & System Safety* 43(3):257-261.

Kappos, A., Panagopoulos, G., Panagiotopoulos, C., and Penelis, G. (2006). A hybrid method for the vulnerability assessment of RC and URM buildings, *Bulletin of Earthquake Engineering* 4(4):391-413.

Kaynia, A.M., Mayoral, J.M., Johansson, J., Argyroudis, S., Pitilakis, K., and Anastasiadis, A. (2011). Fragility functions for roadway system elements, SYNER-G Report D3.7, www.syner-g.eu.

Kennedy, R.P., Cornell, C.A., Campbell, R.D., Kaplan, S., and Perla, H.F. (1980). Probabilistic seismic safety study of an existing nuclear power plant, *Nuclear Engineering and Design* 59:315-338.

Kermanshah, A., Karduni, A., Peiravian, F., and Derrible, S. (2014). Impact analysis of extreme events on flows in spatial networks, *2014 IEEE International Conference on Big Data* , p29-34).

Kim, S.H., and Shinozuka, M. (2004). Development of fragility curves of bridges retrofitted by column jacketing, *Probab. Eng. Mech.* 19(1–2):105–112.

Klose, M. (2015). Landslide Databases as Tools for Integrated Assessment of Landslide Risk, Springer Theses.

Krawinkler, H. (1999). Challenges and progress in performance-based earthquake engineering, International Seminar on Seismic Engineering for Tomorrow, In Honor of Professor Hiroshi Akiyama, Tokyo, Japan.

Lagasse, P.F., Clopper, P.E., Zevenbergen, L.W., Spitz, W.J., and Girard, L.G. (2010). Effects of Debris on Bridge Pier Scour, NCHRP Report 653, Transportation Research Board of the National Academies, Washington, D.C., 2010.

Lebbe, M.F.K., Lokuge, W., Setunge, S., and Zhang, K. (2014). Failure mechanisms of bridge infrastructure in an extreme flood event, Proceedings of the First International Conference on Infrastructure Failures and Consequences, Melbourne, Australia.

Lee, G.C., and Sternberg, E. (2008). A new system for preventing bridge collapses, *Issues in Science and Technology* 24 (3).

Lehman, D., Moehle, J., Mahin, S., Calderone, A., and Henry, L. (2004). Experimental evaluation of the seismic performance of reinforced concrete bridge columns, *ASCE Journal of Structural Engineering* 130(6):869-879.

Li, J., Spencer, B.F., and Elnashai, A.S. (2012). Bayesian updating of fragility functions using hybrid simulation, *ASCE Journal of Structural Engineering* 139(7):1160–1171.

Lin, C. (2012). Evaluation of lateral behavior of pile-supported bridges under scour conditions, PhD Thesis, University of Kansas, U.S.

Mackie, K., and Stojadinovic, B. (2006). Post-earthquake functionality of highway overpass bridges, *Earthquake Engineering and Structural Dynamics* 35(1):77-93.

Mander, J.B. (1999). Fragility curve development for assessing the seismic vulnerability of highway bridges, University at Buffalo, State University of New York.

Martinovic, K., Reale, C., and Gavin, K. (2015). A methodology for developing fragility curves for shallow rainfall-induced landslides on transport infrastructure, *International Journal of Landslides*, Under Review.

Maruyama, Y., Yamazaki, F., Mizuno, K., Tsuchiya, Y., and Yogai, H. (2010). Fragility curves for expressway embankments based on damage datasets after recent earthquakes in Japan, *Soil Dynamics and Earthquake Engineering* 30:1158-1167.

Mavrouli, O., and Corominas, J. (2010). Rockfall vulnerability assessment for reinforced concrete buildings, *Natural Hazards and Earth System Science* 10(10):2055-2066.

McKenna, F., Fenves, G.L., and Scott, M.H. (2000). Open system for earthquake engineering simulation, Pacific Earthquake Engineering Research Center, University of California, Berkeley, California.

Melville, B.W., and Dongol, D.M. (1992). Bridge Pier Scour with Debris Accumulation, *Journal of Hydraulic Engineering* 118 (9):1306–1310.

Michel, C., Gueguen, P., El Arem, S., Mazars, J., and Kotronis, P. (2010). Full scale dynamic response of a RC building under weak seismic motions using earthquake loadings, ambient vibrations and modelling, *Earthquake Engineering and Structural Dynamics* 39(4):419-441.

Modaressi, H., Desramaut, N., and Gehl, P. (2014). Specification of the vulnerability of physical systems, In: SYNER-G: Systemic Seismic Vulnerability and Risk Assessment of Complex Urban, Utility, Lifeline Systems and Critical Facilities – Methodology and Applications, K. Pitilakis, P. Franchin, B. Khazai, H. Wenzel (Eds), Springer, p131-184.

Monti, G., and Nisticò, N. (2002). Simple Probability-Based Assessment of Bridges under Scenario Earthquakes, *Journal of Bridge Engineering*.

Moschonas, I.F., Kappos, A.J., Panetsos, P., Papadopoulos, V., Makarios, T., and Thanopoulos, P. (2009). Seismic fragility curves for Greek bridges: methodology and case studies, *Bulletin of Earthquake Engineering* 7(2):439-468.

Murphy, K. (2007). Bayes Net Toolbox, Available from: https://github.com/bayesnet/bnt.

National Cooperative Highway Research Program (2006). Makings Transportation Tunnels Safe and Secure, NCHRP Report 525, Vol. 12.

Negulescu, C., and Gehl, P. (2013). Mechanical Methods: Fragility Curves and Pushover Analysis, In: Seismic Vulnerability of Structures, P. Gueguen (Ed.), John Wiley & Sons, p63-110.

Newmark, N.M. (1965). Effects of earthquakes on dams and embankments, *Geotechnique* 15:139-160.

Ng, C.W.W., and Shi, Q. (1998). A numerical investigation of the stability of unsaturated soil slopes subjected to transient seepage, *Computers and Geotechnics* 22(1):1-28.

Ni Choine, M., Martinovic, K., and Gavin K. (2014). Critical infrastructure case-studies, INFRARISK Project Report D8.1.

NIBS (2005). HAZUS-MH MR1: Technical Manual, Vol. Flood Model, Federal Emergency Management Agency, Washington DC.

NIBS (2004). HAZUS-MH MR1: Technical Manual, Vol. Earthquake Model, Federal Emergency Management Agency, Washington DC.

Nielson, B.G. (2005). Analytical fragility curves for highway bridges in moderate seismic zones, Ph.D. Thesis, Georgia Institute of Technology, US.

Nielson, B.G., and DesRoches, R. (2007). Seismic Fragility Methodology for Highway Bridges Using a Component Level Approach, *Earthquake Engineering and Structural Dymamics*, 36:823–839.

Noda, S., Uwabe, T., and Chiba, T. (1975). Relation between seismic coefficient and ground acceleration for gravity quay wall, *Report of the Port and Harbour Research Institute* 14(4):67–111

Padgett, J.E., and DesRoches, R. (2009). Retrofitted bridge fragility analysis for typical classes of multispan bridges, *Earthquake Spectra* 25(1):117-141.

Padgett, J.E., DesRoches, R., Nielson, B.G., Yashinsky, M., Kwon, O.S., Burdette, N., and Tavera, E. (2008). Bridge damage and repair costs from hurricane Katrina, *Journal of Bridge Engineering* 13:6-14.

Pearson, D., Stein, S., and Jones, J.S. (2002). HYRISK Methodology and User Guide, FHWA Report No. FHWA-RD-02-XXX, Federal Highway Administration, Virginia.

Pitilakis, K., Crowley, H., and Kaynia, A. (2014). SYNER-G: typology definition and fragility functions for physical elements at seismic risk, Geotechnical, Geological and Earthquake Engineering, Springer Netherlands.

Pitilakis, K., Fotopoulou, S., Argyroudis, S., Pitilakis, D., Senetakis, K., Treulopoulos, K., Kakderi, K., and Riga, E. (2011). Physical vulnerability of elements at risk to landslides: Methodology for evaluation, fragility curves and damage states for buildings and lifelines, SAFELAND Report D2.5.

Pousse G., Bonilla, L.F., Cotton, F., and Margerin, L. (2006). Non-stationary stochastic simulation of strong ground motion time-histories including natural variability: Application to the K-net Japanese database, *Bulletin of the Seismological Society of America* 96 (6):2103-2117.

Porter, K., Kennedy, K., and Bachman, R. (2007). Creating fragility functions for performance-based earthquake engineering, *Earthquake Spectra* 23(2):471-489.

Prasad, G.G., and Banerjee, S. (2013). The impact of flood-induced scour on seismic fragility characteristics of bridges, *Journal of Earthquake Engineering* 17:803-828.

Pregnolato, M., Galasso, C., and Parisi, F. (2015). A Compendium of Existing Vulnerability and Fragility Relationships for Flood: Preliminary Results, Proceedings of the 12th International Conference on Applications of Statistics and Probability in Civil Engineering, ICASP12, Vancouver, Canada.

Puppala, A.J., Saride, S., Archeewa, E., Hoyos, L.R., and Nazarian, S. (2009). Recommendations for design, construction and maintenance of brdige approach slabs: synthesis report, Techinal Report FHWA/TX-09/0-6022-1, Texas Department of Transportation, Arlington, Texas.

Qi'ang, W., Ziyan, W., and Shukui, L. (2012). Seismic fragility analysis of highway bridges considering multi-dimensional performance limit state, *Earthquake Engineering and Engineering Vibration* 11(2):185–193.

Rathje, E.M., and Saygili, G. (2008). Probabilistic seismic hazard analysis for the sliding displacement of slopes: scalar and vector approaches, *Journal of Geotechnical and Geoenvironmental Engineering* 134:804-814.

Richards, L.A. (1931). Capillary conduction of liquids through porous mediums, *Journal of Applied Physics* 1(5):318-333.

Richardson, E.V., and Davis, S.R. (1995). Evaluating scour at bridges, Report No. FHWA-IP-90-017, Federal Highway Administration, Washington, D.C.

Rossetto, T., and Elnashai, A. (2003). Derivation of vulnerability functions for European-type RC structures based on observational data, *Engineering Structures* 25(10):1241-1263.

Rossetto, T., and Elnashai, A. (2005). A new analytical procedure for the derivation of displacement-based vulnerability curves for populations of RC structures, *Engineering Structures* 7(3): 397-409.

Rota, M., Penna, A., and Strobbia, C. (2006). Typological fragility curves from Italian earthquake damage data, First European Conference on Earthquake Engineering and Seismology, Geneva, Switzerland.

Sasaki, Y., Shimizu, Y., and Sunasaka, Y. (2000). Development of fragility curves of civil structures based on observed structural damages in past great earthquakes, Proceedings of Conference by Institute of Social Safety Science, p17–20 (in Japanese).

Saxena, V., Deodatis, G., Shinozuka M., and Feng, M.Q. (2000). Development of fragility curves for multi-span reinforced concrete bridges, International Conference on Monte Carlo Simulation.

Saygili, G. (2008). A Probabilistic Approach for Evaluating Earthquake-Induced Landslides, PhD Thesis, The University of Texas, Austin, TX.

Saygili, G., and Rathje, E.M. (2009). Probabilistcally based seismic landslide hazard maps: an application in Southern California, *Engineering Geology* 109(3-4):183-194.

Schultz, M., Gouldby, B., Simm, J., and Wibowo, J. (2010). Beyond the Factor of Safety: Developing Fragility Curves to Characterize System Reliability, US Army Corps of Engineering, Washington D.C.

Schwarz, J., and Maiwald, H. (2009). Damage and loss prediction model based on the vulnerability of building types, RIMAX Contributions at the 4th International Symposium on Flood Defence.

Schwarz, J., and Maiwald, H. (2012). Empirical vulnerability assessment and damage for description natural hazards following the principles of modern microseismic scales, Proceedings of the 15th World Conference on Earthquake Engineering, Lisbon, Portugal.

Shinozuka, M., Feng, M.Q., Kim, H.K., Uzawa, T., and Ueda, T. (2003). Statistical analysis of fragility curves, Technical Report MCEER-03-0002, State University of New York, Buffalo.

Shinozuka, M., Feng, M.Q., Lee, J., and Naganuma T. (2000). Statistical analysis of fragility curves, *ASCE Journal of Engineering Mechanics* 126(12):1224-1231.

Silva, V., Crowley, H., and Colombi, M. (2014). Fragility Function Manager Tool, In: SYNER-G: Typology Definition and Fragility Functions for Physical Elements at Seismic Risk, K. Pitilakis K., H. Crowley, A.M. Kaynia (Eds), Springer Netherlands, ISBN 978-94-007-7871-9, p385-402.

Simm, J., Gouldby, B., Sayers, P., Flikweert, J, Wersching, S., and Bramley, M. (2008). Representing fragility of flood and coastal defences: getting into the detail, Proceedings of the European conference on flood risk management research into practice (Floodrisk 2008), Oxford, UK.

Singhal, A., and Kiremidjian, A.S. (1998). Bayesian updating of fragilities with application to RC frames, *Journal of Structural Engineering* 124(8):922-929.

Sivakumar Babu, G.L., and Murthy, D.S. (2005). Reliability analysis of unsaturated soil slopes, *Journal of Geotechnical and Geoenvironmental Engineering* 131(11):1423-1428.

Smith, J., Winter, M., Fotopoulou, S., Pitilakis, K., Mavrouli, O.C., Corominas Dulcet, J., and Argyroudis, S. (2013). The physical vulnerability of roads to debris flows: an expert judgement approach, International Symposium on Landslides, "Landslides and Engineered Slopes", Banff, CRC Press, Taylor & Francies Group, p. 307-313.

Spence, R., Coburn, A.W., and Pomonis, A. (1993). Correlation of ground-motion with building damage: the definition of a new damage-based seismic Intensity scale, Tenth World Conference on Earthquake Engineering, Madrid, Spain.

Song, J., and Kang, W.H. (2007). Risk quantification of complex systems by matrix-based system reliability method, Special Workshop on Risk Acceptance and Risk Communication, Standford University, California.

Song, J., and Kang, W.H. (2009). System reliability and sensitivity under statistical dependence by matrix-based system reliability method, *Structural Safety* 31:148-156.

Stewart, J.P., Taciroglu, E., Wallace, J.W., Ahlberg, E.R., Lemnitzer, A., Rha, C., Tehrani, P.K., Keowen, S., Nigbor, R.L., and Salamanca, A. (2007). Full scale cyclic testing of foundation support systems for highway bridges. Part II: Abutment backwalls, Report No. UCLA-SGEL 2007/02, Structural and Geotechnical Engineering Laboratory, University of California, L.A.

SYNER-G (2009-2013). Systemic Seismic Vulnerability and Risk Analysis for Buildings, Lifeline Networks and Infrastructures Safety Gain, European Collaborative Research Project, www.syner-g.eu.

Tanasic, N., Ilic, V., and Hajdin, R. (2013). Vulnerability Assessment of Bridges Exposed to Scour, *Transportation Research Record: Journal of the Transportation Research Board* 2360:36-44.

Teo, F.Y., Xia, J., Falconer, R.A., and Lin, B. (2012). Experimental studies on the interaction between vehicles and floodplain flows, *International Journal of River Basin Management* 10(2):149-160.

Transportation Association of Canada (TAC) (2004). Guide to Bridge Hydraulics, Second Edition, Thomas Telford, London, 181 p.

Tsionis, G., and Fardis, M.N. (2014). Fragility Functions of Road and Roadway Bridges, In: SYNER-G: Typology Definition and Fragility Functions for Physical Elements at Seismic Risk, K. Pitilakis K., H. Crowley, A.M. Kaynia (Eds), Springer Netherlands, ISBN 978-94-007-7871-9, p259-298.

Tsompanakis, Y., Lagaros, N.D., Psarropoulos, P.N., and Georgopoulos, E.C. (2010). Probabilistic seismic slope stability assessment of geostructures, *Structure and Infrastructure Engineering* 6(1-2):179-191.

Vamvatsikos, D., and Cornell, C.A. (2002). Incremental dynamic analysis, *Earthquake Engineering and Structural Dynamics* 31(3):491-514.

Van Den Eeckhaut, M., and Hervas, J. (2012). State of the art of national landslide databases in Europe and their potential for assessing landslide susceptibility, hazard and risk, *Geomorphology* 139-140:545-558.

van der Meer, J.W., ter Horst, W.L.A., and van Velzen, E.H. (2009). Calculation of fragility curves for flood defence assets, Flood Risk Management: Research and Practice – Samuels et al. (eds), London, pp.567-573.

Varnes, D.J., andIAEG Commission on Landslides (1984). Landslide hazard zonation: a review of principles and practice, UNESCO, Paris.

Wen, Y.K., Ellingwood, B.R., Veneziano, D., and Bracci, J. (2003). Uncertainty modeling in earthquake engineering, Technical report, MAE Center Project FD-2 Report.

Werner, S.D., Taylor, C.E., Cho, S., Lavoie, J-P., Huyck, C., Eitzel, C., Chung, H., and Eguchi, R.T. (2006). REDARS 2: Methodology and Software for Seismic Risk Analysis of Highway Systems, Technical Report MCEER-06-SP08.

Winter, M.G., Smith, J.T., Fotopoulou, S., Pitilakis, K., Mavrouli, O., Corominas, J., and Argyroudis, S. (2014). An expert judgement approach to determining the physical vulnerability of roads to debris flow, *Bulletin of Engineering Geology and the Environment* 73(2):291-305.

Wu, X.Z. (2015). Development of fragility functions for slope instability analysis, *Landslides*, In press.

Wu, X.Z. (2013). Probabilistic slope stability analysis by a copula-based sampling method, *Computers and Geosciences* 17:739–755.

Yi J.H., Kim S.H., and Kushiyama, S. (2007). PDF interpolation technique, for seismic fragility analysis of bridges, *Engineering Structures* 29(7):1312-1322.

Yin, Y., and Konagai, K. (2001). A simplified method for expression of the dynamic stiffness of large-scaled grouped piles in sway and rocking motions, *JSCE Journal of Applied Mechanics* 4:415–422.

Zentner, I. (2007). Methodes probabilistes dans les analyses sismiques : Modelisation, propagation et hierarchisation des incertitudes, 7eme Colloque National AFPS, Paris, France (in French).

Zêzere, J.L., Trigo, R.,M., Fragoso, M., Oliveira, S.C., and Garcia, R.A.C. (2008). Rainfall-triggered landslides in the Lisbon region over 2006 relationships with the north Atlantic Oscillation, *Natural Hazards and Earth System Science* 8(3):483–499.

Zhai, G., Fukuzono, T., and Ikeda, S. (2005). Modeling Flood damage: Case of Tokai Flood 2000, *J. Am. Water Resour. Assoc.* 41(1):77-92.

Zhang, J., Huo, Y., Brandenberg, S.J., and Kashighandi, P. (2008). Effects of structural characterizations on fragility functions of bridges subject to seismic shaking and lateral spreading, *Earthquake Engineering and Engineering Vibration* 7(4):369–382.

APPENDIX A: COMPONENT FAILURE MODES FOR ROAD NETWORK ELEMENTS

ID	Component	Sub-type	Failure mode	D1	D2	D3	D4
1	**Pier**	**-**	**Bending**	- minor cracking and spalling - yielding	- cracking and spalling (still structurally sound)	- column degrading without collapse (structurally unsafe)	- column collapsing - reinforcement buckling
2	**Pier**	**-**	**Shear**			- brittle shear failure	
3	**Pier**	**-**	**Tilting**				- tilting of substructure due to foundation failure
4	**Abutment**	**-**	**Piles (active)**	- minor cracking and spalling	- first yielding point	- ultimate deformation - vertical offset	
5	**Abutment**	**-**	**Backfill (passive)**	- displacement = gap (joint closure)	- passive resistance of backfill soil is reached		- ultimate displacement of the abutment / backfill system
6	**Shear keys**	**-**	**Transverse loading**	- displacement = gap (joint closure) - minor cracks	- extensive cracking and spalling	- failure (sliding shear or strut-and-tie mechanism)	
7	**Bearing**	**Fixed**	**-**		- shear strength reached (collapse of the device or of the anchor bolt)		- displacement corresponding to deck unseating
8	**Bearing**	**Steel pendulum**	**-**	- displacement capacity of the bearing under non-seismic conditions	- displacement corresponding to vertical instability		- displacement corresponding to deck unseating
9	**Bearing**	**Sliding / roller**	**-**	- displacement capacity of the bearing under non-seismic conditions			- displacement corresponding to deck unseating
10	**Bearing**	**Bolted neoprene**	**-**	- 150% of the shear strain amplitude of rubber	- 200% of the shear strain amplitude of rubber	- 300% of the shear strain amplitude of rubber	- displacement corresponding to deck unseating
11	**Bearing**	**Unbolted neoprene**	**Friction / slipping**	- friction resistance is reached		- displacement corresponding to pad dimensions	- displacement corresponding to deck unseating
12	**Bearing**	**Unbolted neoprene**	**Rollover**	- 1/3 of displacement corresponding to pad dimensions	- 1/2 of displacement corresponding to pad dimensions	- displacement corresponding to pad dimensions	- displacement corresponding to deck unseating
13	**Bearing**	**Elastomeric w/ dowels**	**-**	- noticeable deformation	- deck may have to be realigned and possible dowel fracture	- necessary girder retention and deck realignment	- displacement corresponding to deck unseating
14	**Deck**	**-**	**-**	- minor cracking - deck curvature and curvature limits			- deck collapse
15	**Pier / Abutment foundations**	**-**	**Slope failure**	- if slope failure under footing, induced differential displacement that could lead to deck collapse (rare)			
16	**Abutment approach**	**-**	**Subsidence / Settlement**	- settlement of poorly compacted backfill soil on the abutment approach (common)			
17	**Pier foundations**	**-**	**Local scour**	- dimensionless depth ratio of scour: below footing / within footing dimensions / above footing - scour vulnerability grade from 0 to 9			
18	**Pier foundations**	**-**	**Downcutting of streambed**	- affect bridge abutments/piers and undercut culvert inlets and outlets			
19	**Abutment foundations**	**-**	**Local scour**	- dimensionless depth ratio of scour: below footing / within footing dimensions / above footing - scour vulnerability grade from 0 to 9			
20	**Abutment foundations**	**-**	**Downcutting of streambed**	- affect bridge abutments/piers and undercut culvert inlets and outlets			
21	**Deck**		**Overtopping**	- shifting of bridge decks due to pressure of rising floodwaters / hydraulic pressure			
22	**Waterway**	**-**	**Debris accumulation**	- reduction of the hydraulic capacity of crossings - backup of water and damage to adjacent properties			
23	**Waterway**	**-**	**Channel modification**	- shifting or migration of waterway channel alignment			

Table 47: Summary of the component failure modes identified for bridges

ID	Component	Sub-type	Failure mode	D1	D2	D3	D4
24	**Tunnel liner**	-	-	- minor cracking and spalling - width of crack < 3mm - length of crack < 5m	- moderate cracking and spalling - width of crack > 3mm - length of crack > 5m	- extensive cracking - exposed reinforcement - displacement of segmentation joints	- collapse of lining
25	**Tunnel portal**	-	-	- some rock falling - slight settlement	- moderate rock falling	- major ground settlement	- slope failure [depends heavily on size!]
26	**Support systems**	-	-			- damaged ventilation and lighting systems in long tunnels	

Table 48: Summary of the component failure modes identified for tunnels

ID	Component	Sub-type	Failure mode	D1	D2	D3
27	**Embankment**	-	**Sliding / slumping of embankment**	- surface slide of embankment at the top of slope only, minor cracks on the surface of the road	- deep slide/slump of embankment involving traffic lines, medium cracks on the surface of the road	- serious slide/slump of embankment
28	**Slope**	-	**Sliding / slumping of embankment**	- surface slide of embankment at the top of slope only, minor cracks on the surface of the road	- deep slide/slump of embankment involving traffic lines, medium cracks on the surface of the road	- serious slide/slump of embankment
29	**Slope**	-	**Debris flow**	- limited damage: encroachment limited to verge/hardstrip	- serious damage: blockage of hardstrip and one running lane	- destroyed: complete blockage of carriageway and/or repairable damage to surfacing
30	**Slope**	-	**Rock falls**	- failure of rock protection gallery	- obstruction of road	- destruction of road surfacing
31	**Trench**	-	**Debris flow**	- limited damage: encroachment limited to verge/hardstrip	- serious damage: blockage of hardstrip and one running lane	- destroyed: complete blockage of carriageway and/or repairable damage to surfacing
32	**Trench**	-	**Rock falls**	- failure of rock protection gallery	- obstruction of road	- destruction of road surfacing
33	**Road pavement**	-	**Opening of cracks**	- several limit states are proposed, expressed in permanent ground displacement	- slight / moderate damage: localized cracking/movement, reduced structural integrity of surface	- extensive / irreparable damage: failure of pavement structure requiring replacement without / with failure of subsurface soils
34	**Road pavement**	-	**Vertical settlement / offset**	- very minor damage: gap less than 1 cm	- minor damage: gap between 1 and 3 cm	- moderate damage: gap more than 3 cm on traffic lane / more than 20 cm on shoulder
35	**Road pavement**	-	**Inundation**	- disruption of traffic		
36	**Road pavement**	-	**Flotation / delamination**	- loss of paved surfaces		
37	**Roadbed**	-	**Inundation**	- saturation and collapse of inundated roadbeds		
38	**Roadbed**	-	**Sedimentation**	- deposition of sediments on roadbeds		
39	**Drainage system**	-	**Drainage saturation**	- damage to or loss of underdrain and cross-drainage pipes - blockage of drainage ditches and underdrains by debris, exacerbating erosion and scour - undermining of shoulders when ditch capacity is exceeded		
40	**Vehicles**	-	**Inundation**	- disruption of traffic - destruction of vehicles		

Table 49: Summary of the component failure modes identified for road segments

APPENDIX B: EXPERT-BASED COMPONENT FUNCTIONALITY LOSSES

This appendix details the results of the expert-based survey: as stated before, the following numerical values should be considered for illustrative purposes only, due to the scarcity of collected data.

ID	Du-	Du+	ID	Du-	Du+	ID	Du-	Du+
1-D1	7	30	**16-D1**	15	15	**29-D3**	15	15
	14	14		1	1		1	7
1-D2	7	30		60	60		7	7
	30	30	**17-D1**	7	60	**30-D1**	60	60
1-D3	30	60		30	30		7	7
	60	60	**18-D1**	7	60		30	30
1-D4	7	30		30	30	**30-D2**	4	4
	150	150	**19-D1**	7	60		7	7
2-D3	7	30		30	30		7	7
	60	60	**20-D1**	7	60	**30-D3**	5	5
3-D4	30	60		30	30		7	7
	75	75	**21-D1**	120	120		30	30
4-D1	14	14		60	60	**31-D1**	3	3
4-D2	30	30	**22-D1**	7	7		1	7
4-D3	150	150		15	15		1	1
5-D1	60	60	**23-D1**	7	7	**31-D2**	6	6
	30	30		30	30		1	7
5-D2	60	120	**24-D1**	7	7		1	1
	45	45	**24-D2**	30	30	**31-D3**	15	15
5-D4	60	60	**24-D3**	60	90		7	7
6-D1	60	120	**24-D4**	180	360	**32-D1**	60	60
	30	30	**25-D1**	120	120		7	7
6-D2	60	60		15	15		30	30
6-D3	90	90		2	2	**32-D2**	4	4
7-D2	15	15	**25-D2**	120	120		7	7
7-D4	30	30		30	90		7	7
8-D1	15	15		6	6	**32-D3**	5	5
8-D2	30	30	**25-D3**	90	90		7	7
8-D4	30	30	**25-D4**	180	360		30	30
9-D1	30	30		6	6	**33-D1**	1	7
	15	15	**26-D3**	7	21		1	1
9-D4	45	45	**27-D1**	4	4	**33-D2**	3	3
10-D1	30	30		7	7		1	7
	15	15		1	1		1	1
10-D2	15	15	**27-D2**	15	15	**33-D3**	10	10
10-D3	30	30		7	7		1	7
10-D4	60	60		7	7		1	1

11-D1	30	30	**27-D3**	25	25	**34-D1**	1	1
	15	15		7	7		7	7
11-D2	30	30		30	30		0	1
11-D3	60	60	**28-D1**	4	4	**34-D2**	2	2
12-D1	30	30		7	7		7	7
	15	15		1	1		0	1
12-D2	15	15	**28-D2**	15	15	**34-D3**	4	4
12-D3	30	30		7	7		7	7
12-D4	60	60		7	7		0	1
13-D1	15	15	**28-D3**	25	25	**35-D1**	30	120
13-D2	30	30		7	7	**36-D1**	30	120
13-D3	45	45		7	7	**37-D1**	30	120
13-D4	60	60	**29-D1**	3	3		2	10
14-D1	7	7		1	7	**38-D1**	1	1
14-D4	30	30		1	1	**39-D1**	1	7
15-D1	30	90	**29-D2**	6	6		1	10
	60	60		1	7	**40-D1**	1	15
				1	1			

Table 50: Duration of repair operations (lower and upper bounds in days) for each of the component failure modes identified. Multiple lines for a given damage states indicate multiple propositions from the different groups of experts.

ID	FL_ind	FL_val-	FL_val+	ID	FL_ind	FL_val-	FL_val+	ID	FL_ind	FL_val-	FL_val+
1-D1	speed	0%	0%	**16-D1**	speed	25%	25%	**29-D3**	closed	5%	5%
	speed	10%	10%		emerg	-	-		closed	100%	100%
1-D2	speed	0%	0%	**17-D1**	load	20%	20%		closed	100%	100%
	speed	20%	20%		load	0%	100%	**30-D1**	closed	5%	5%
1-D3	load	40%	40%	**18-D1**	closed	50%	50%		speed	50%	50%
	load	100%	100%		load	0%	100%		closed	100%	100%
1-D4	closed	100%	100%	**19-D1**	load	20%	20%	**30-D2**	speed	50%	50%
	load	100%	100%		load	0%	100%		closed	50%	50%
2-D3	load	40%	40%	**20-D1**	closed	50%	50%		closed	50%	100%
	load	100%	100%		load	0%	100%	**30-D3**	speed	50%	50%
3-D4	closed	100%	100%	**21-D1**	load	25%	25%		closed	100%	100%
	load	100%	100%		closed	100%	100%		emerg	-	-
4-D1	speed	0%	0%	**22-D1**	speed	0%	0%	**31-D1**	closed	5%	5%
	speed	10%	10%	**23-D1**	speed	0%	0%		speed	30%	30%
4-D2	speed	20%	20%		speed	20%	20%	**31-D2**	closed	5%	5%
4-D3	closed	100%	100%	**24-D1**	closed	100%	100%		closed	50%	50%
5-D1	speed	0%	0%	**24-D2**	closed	100%	100%		closed	50%	50%
	speed	20%	20%	**24-D3**	closed	100%	100%	**31-D3**	closed	100%	100%
5-D2	speed	20%	20%	**24-D4**	closed	100%	100%		closed	100%	100%
	closed	50%	50%	**25-D1**	closed	33%	33%	**32-D1**	closed	5%	5%

5-D4	closed	100%	100%		closed	100%	100%		speed	50%	50%
6-D1	speed	0%	0%	**25-D2**	closed	75%	75%		closed	100%	100%
	speed	20%	20%		closed	100%	100%	**32-D2**	speed	50%	50%
6-D2	load	25%	25%	**25-D3**	closed	100%	100%		closed	50%	50%
6-D3	load	40%	40%	**25-D4**	closed	100%	100%		closed	50%	100%
7-D2	speed	25%	25%	**26-D3**	speed	100%	100%	**32-D3**	speed	50%	50%
7-D4	speed	25%	25%	**27-D1**	closed	5%	5%		closed	100%	100%
8-D1	closed	0%	0%		closed	50%	50%		emerg	-	-
8-D2	closed	50%	50%		closed	0%	100%	**33-D1**	closed	0%	0%
8-D4	speed	25%	25%	**27-D2**	closed	50%	50%		speed	20%	40%
9-D1	speed	20%	20%		closed	0%	100%	**33-D2**	closed	0%	0%
9-D4	speed	25%	25%		emerg	-	-		speed	20%	40%
10-D1	speed	20%	20%	**27-D3**	closed	100%	100%		load	50%	50%
10-D2	speed	20%	20%		closed	0%	100%	**33-D3**	speed	20%	40%
10-D3	speed	20%	20%		closed	100%	100%		closed	100%	100%
10-D4	speed	25%	25%	**28-D1**	closed	5%	5%		closed	100%	100%
11-D1	speed	20%	20%		closed	50%	50%	**34-D1**	closed	0%	0%
11-D2	speed	20%	20%		closed	0%	100%		load	10%	10%
11-D3	speed	25%	25%	**28-D2**	closed	50%	50%		speed	0%	40%
12-D1	speed	20%	20%		closed	0%	100%	**34-D2**	closed	0%	0%
12-D2	speed	20%	20%		emerg	-	-		speed	0%	40%
12-D3	speed	20%	20%	**28-D3**	closed	0%	100%	**34-D3**	closed	0%	0%
12-D4	speed	25%	25%		closed	100%	100%		speed	0%	40%
13-D1	speed	20%	20%	**29-D1**	closed	5%	5%		load	70%	70%
13-D2	speed	20%	20%		closed	5%	5%	**35-D1**	emerg	-	-
13-D3	speed	20%	20%		speed	30%	30%	**36-D1**	emerg	-	-
13-D4	speed	25%	25%	**29-D2**	closed	5%	5%	**37-D1**	closed	50%	100%
14-D1	speed	-	-		closed	50%	50%		emerg	-	-
14-D4	closed	100%	100%		closed	50%	50%	**38-D1**	speed	20%	20%
15-D1	closed	0%	100%					**39-D1**	speed	50%	50%
	closed	100%	100%						closed	0%	50%
								40-D1	speed	50%	50%

Table 51: Reduction of functionality in % (lower and upper bounds, either for proportion of closed lanes, speed reduction or vertical load capacity reduction) for each of the component failure modes identified. Multiple lines for a given damage states indicate multiple propositions from the different groups of experts. The '*emerg*' index means that the infrastructure element is open for emergency vehicles only.

ID	FLI_ind	FLI_val-	FLI_val+	ID	FLI_ind	FLI_val-	FLI_val+	ID	FLI_ind	FLI_val-	FLI_val+
1-D1	speed	0%	0%	**13-D4**	closed	75%	75%	**29-D1**	closed	33%	33%
	speed	10%	10%	**14-D1**	closed	-	-		closed	5%	5%
1-D2	speed	0%	0%	**14-D4**	closed	100%	100%	**29-D2**	speed	30%	30%
	speed	20%	20%	**15-D1**	closed	100%	100%		closed	50%	50%

1-D3	load	100%	100%		closed	25%	25%	**29-D3**	emerg	-	-
	load	40%	40%		emerg	-	-		closed	100%	100%
1-D4	closed	100%	100%	**16-D1**	emerg	-	-	**30-D1**	closed	100%	100%
	load	100%	100%		closed	50%	50%		speed	50%	50%
2-D3	closed	100%	100%	**17-D1**	closed	0%	100%		closed	5%	5%
	load	40%	40%		load	20%	20%	**30-D2**	emerg	-	-
3-D4	closed	50%	50%	**18-D1**	closed	0%	100%		speed	50%	50%
	closed	100%	100%		closed	50%	50%		closed	50%	50%
4-D1	speed	0%	0%	**19-D1**	closed	0%	100%	**30-D3**	emerg	-	-
	speed	10%	10%		load	20%	20%		speed	50%	50%
4-D2	speed	20%	20%	**20-D1**	closed	0%	100%		closed	100%	100%
4-D3	closed	100%	100%		closed	50%	50%	**31-D1**	closed	33%	33%
5-D1	closed	25%	25%	**21-D1**	closed	100%	100%		closed	5%	5%
	closed	50%	50%		speed	50%	50%	**31-D2**	speed	30%	30%
5-D2	closed	50%	50%	**22-D1**	speed	50%	50%		closed	50%	50%
	closed	50%	50%		speed	20%	20%	**31-D3**	emerg	-	-
5-D4	closed	100%	100%	**23-D1**	speed	0%	0%		closed	100%	100%
6-D1	closed	0%	0%		speed	20%	20%	**32-D1**	closed	100%	100%
	closed	50%	50%	**24-D1**	closed	100%	100%		speed	50%	50%
6-D2	closed	50%	50%	**24-D2**	closed	100%	100%		closed	5%	5%
6-D3	closed	50%	50%	**24-D3**	closed	100%	100%	**32-D2**	emerg	-	-
7-D2	closed	50%	50%	**24-D4**	closed	100%	100%		speed	50%	50%
7-D4	closed	75%	75%	**25-D1**	closed	100%	100%		closed	50%	50%
8-D1	closed	0%	0%		closed	33%	33%	**32-D3**	emerg	-	-
8-D2	closed	50%	50%	**25-D2**	closed	100%	100%		speed	50%	50%
8-D4	closed	75%	75%		closed	75%	75%		closed	100%	100%
9-D1	speed	50%	50%	**25-D3**	closed	100%	100%	**33-D1**	closed	50%	50%
	closed	50%	50%	**25-D4**	emerg	-	-	**33-D2**	closed	50%	50%
9-D4	closed	75%	75%	**26-D3**	closed	100%	100%		closed	50%	50%
10-D1	speed	50%	50%	**27-D1**	closed	50%	50%	**33-D3**	closed	100%	100%
	closed	50%	50%		closed	25%	25%		closed	50%	50%
10-D2	closed	50%	50%		closed	5%	5%	**34-D1**	closed	33%	33%
10-D3	closed	50%	50%	**27-D2**	emerg	-	-		closed	0%	50%
10-D4	closed	75%	75%		closed	25%	25%	**34-D2**	closed	33%	33%
11-D1	speed	50%	50%		closed	50%	50%		closed	0%	50%
	closed	50%	50%	**27-D3**	closed	100%	100%	**34-D3**	closed	50%	50%
11-D2	closed	50%	50%		closed	25%	25%		closed	0%	50%
11-D3	closed	75%	75%		closed	100%	100%	**35-D1**	closed	50%	50%
12-D1	speed	50%	50%	**28-D1**	closed	50%	50%	**36-D1**	closed	50%	50%
	closed	50%	50%		closed	25%	25%	**37-D1**	closed	50%	50%
12-D2	closed	50%	50%		closed	5%	5%		closed	50%	100%
12-D3	closed	50%	50%	**28-D2**	emerg	-	-	**38-D1**	closed	25%	25%
12-D4	closed	75%	75%		closed	25%	25%	**39-D1**	closed	25%	25%
13-D1	closed	50%	50%		closed	50%	50%		closed	0%	50%

13-D2	closed	50%	50%	**28-D3**	closed	100%	100%	**40-D1**	speed	50%	50%
13-D3	closed	50%	50%		closed	25%	25%				
					closed	100%	100%				

Table 52: Reduction of functionality during repair operations in % (lower and upper bounds, either for proportion of closed lanes, speed reduction or vertical load capacity reduction) for each of the component failure modes identified. Multiple lines for a given damage states indicate multiple propositions from the different groups of experts. The '*emerg*' index means that the infrastructure element is open for emergency vehicles only.

ID	Co_ind	Co-	Co+	ID	Co_ind	Co-	Co+	ID	Co_ind	Co-	Co+
1-D1	qual	low	low	**16-D1**	abs	10k€	50k€	**29-D3**	abs	50k€	200k€
	percent	5%	5%		abs	10k€	10k€		abs	1.5k€	1.5k€
1-D2	qual	low	medium		percent	15%	15%		qual	medium	medium
	percent	10%	10%	**17-D1**	abs	10k€	100k€	**30-D1**	abs	500k€	
1-D3	qual	high	high		percent	15%	15%		abs	5k€	20k€
	percent	20%	20%	**18-D1**	abs	10k€	100k€		qual	medium	medium
1-D4	qual	high	high		percent	10%	10%	**30-D2**	abs	15k€	150k€
	percent	45%	45%	**19-D1**	abs	10k€	100k€		abs	5k€	20k€
2-D3	qual	high	high		percent	15%	15%		qual	medium	medium
	percent	20%	20%	**20-D1**	abs	10k€	100k€	**30-D3**	abs	20k€	50k€
3-D4	qual	high	high		percent	10%	10%		abs	5k€	20k€
	percent	25%	25%	**21-D1**	abs	100k€	500k€		qual	high	high
4-D1	percent	5%	5%		percent	20%	20%	**31-D1**	abs	5k€	20k€
4-D2	percent	10%	10%	**22-D1**	abs	10k€	10k€		abs	1.5k€	1.5k€
4-D3	percent	25%	25%		percent	5%	5%		qual	very low	very low
5-D1	abs	100k€	100k€	**23-D1**	abs	1k€	1k€	**31-D2**	abs	20k€	50k€
	percent	10%	10%		percent	10%	10%		abs	1.5k€	1.5k€
5-D2	abs	100k€		**24-D1**	abs		100k€		qual	low	low
	percent	20%	20%	**24-D2**	abs	500k€	500k€	**31-D3**	abs	50k€	200k€
5-D4	percent	30%	30%	**24-D3**	abs	1000k€	1000k€		qual	medium	medium
6-D1	abs	10k€	10k€	**24-D4**	abs	3000k€	5000k€	**32-D1**	abs	500k€	
	percent	5%	5%	**25-D1**	abs	150k€	150k€		abs	5k€	20k€
6-D2	percent	10%	10%		abs	100k€	100k€		qual	medium	medium
6-D3	percent	20%	20%		abs	10k€	10k€	**32-D2**	abs	15k€	150k€
7-D2	percent	5%	5%	**25-D2**	abs	150k€	150k€		abs	5k€	20k€
7-D4	percent	20%	20%		abs	1000k€	1000k€		qual	medium	medium
8-D1	percent	5%	5%		abs	20k€	50k€	**32-D3**	abs	20k€	50k€
8-D2	percent	15%	15%	**25-D3**	abs	3000k€	3000k€		abs	5k€	20k€
8-D4	percent	20%	20%	**25-D4**	abs	5000k€	10000k€		qual	high	high
9-D1	abs	100k€	100k€		abs	50k€	250k€	**33-D1**	abs	5k€	50k€
	percent	5%	5%	**26-D3**	abs	500k€	500k€		qual	low	medium
9-D4	percent	20%	20%	**27-D1**	abs	10k€	20k€	**33-D2**	abs	10k€	20k€
10-D1	abs	100k€	100k€		abs	10k€	50k€		abs	5k€	50k€

	percent	5%	5%		qual	very low	very low		qual	low	medium
10-D2	percent	10%	10%	**27-D2**	abs	50k€	100k€	**33-D3**	abs	25k€	75k€
10-D3	percent	15%	15%		abs	10k€	50k€		abs	5k€	50k€
10-D4	percent	20%	20%		qual	medium	medium		qual	low	medium
11-D1	abs	100k€	100k€	**27-D3**	abs	100k€	350k€	**34-D1**	abs	10k€	10k€
	percent	5%	5%		abs	10k€	50k€		abs	20k€	20k€
11-D2	percent	15%	15%		qual	high	high		qual	very low	low
11-D3	percent	20%	20%	**28-D1**	abs	10k€	20k€	**34-D2**	abs	10k€	30k€
12-D1	abs	100k€	100k€		abs	10k€	50k€		abs	20k€	20k€
	percent	5%	5%		qual	very low	very low		qual	very low	low
12-D2	percent	10%	10%	**28-D2**	abs	50k€	100k€	**34-D3**	abs	30k€	50k€
12-D3	percent	15%	15%		abs	10k€	50k€		abs	20k€	20k€
12-D4	percent	20%	20%		qual	medium	medium		qual	very low	low
13-D1	percent	5%	5%	**28-D3**	abs	100k€	350k€	**35-D1**	abs	20k€	100k€
13-D2	percent	15%	15%		abs	10k€	50k€	**36-D1**	abs	20k€	100k€
13-D3	percent	15%	15%		qual	medium	medium	**37-D1**	abs	20k€	100k€
13-D4	percent	20%	20%	**29-D1**	abs	5k€	20k€		abs	4.6k€	8.6k€
14-D1	abs		100k€		abs	1.5k€	1.5k€	**38-D1**	abs	0.5k€	0.5k€
14-D4	abs	1000k€	1000k€		qual	very low	very low	**39-D1**	abs	0.5k€	5k€
15-D1	abs	50k€	500k€	**29-D2**	abs	20k€	50k€		abs	10k€	15k€
	percent	15%	15%		abs	1.5k€	1.5k€	**40-D1**	abs	1.5k€	1.5k€
					qual	low	low				

Table 53: Cost of repair operations (lower and upper bounds) for each of the component failure modes identified. Multiple lines for a given damage states indicate multiple propositions from the different groups of experts. The '*qual*' index refers to qualitative estimations, '*abs*' to absolute costs in euros per km, and '*percent*' to percentages of the replacement cost.

APPENDIX C: DESCRIPTION OF THE CASE STUDY BRIDGES

ID	*MM1*	*MM2*	*TD1*	*TD2*	*DC*	*DSS*	*PDC*	*TC1*	*TS1*	*TS2*	*HP*	*Sp*	*SC*	*Tca*	*BC*	*LS*	*Length*
1	C	PC	X	X	<20	SSu	Is	McP	R	So	X	Ms	<45	Isl	R	NSD	<50
2	C	PC	X	X	<20	SSu	Is	McP	R	So	X	Ms	<25	Isl	R	NSD	<100
3	C	PC	X	X	<20	SSu	Is	McP	R	So	X	Ms	<25	Isl	R	NSD	<100
4	C	PC	X	X	<20	SSu	Is	McP	Cy	So	X	Ms	<45	Isl	R	NSD	<100
5	C	PC	X	X	<20	SSu	Is	McP	R	So	X	Ms	<45	Isl	R	NSD	<50
6	C	PC	X	X	<20	SSu	Is	McP	R	So	X	Ms	<45	Isl	R	NSD	>200
7	C	PC	X	X	<20	SSu	Is	McP	R	So	X	Ms	<45	Isl	R	NSD	<50
8	C	PC	X	X	<20	SSu	Is	McP	R	So	X	Ms	<25	Isl	R	NSD	<50
9	C	PC	X	X	<20	SSu	Is	McP	Cy	So	X	Ms	<25	Isl	R	NSD	<50
10	C	PC	X	X	<20	SSu	Is	McP	R	So	X	Ms	<45	Isl	R	NSD	<100
11	C	PC	X	X	>20	SSu	Is	McP	R	So	X	Ms	<25	Isl	R	NSD	<100
12	C	PC	X	X	>20	SSu	Is	McP	Cy	So	X	Ms	<25	Isl	R	NSD	>200
13	C	PC	X	X	<20	SSu	Is	McP	Cy	So	X	Ms	<45	Isl	R	NSD	<100
14	C	PC	X	X	<20	SSu	Is	McP	Cy	So	X	Ms	<25	Isl	R	NSD	<100
15	C	PC	X	X	<20	SSu	Is	McP	Cy	So	X	Ms	<45	Isl	R	NSD	<100
16	C	PC	X	X	<20	SSu	Is	McP	Cy	So	X	Ms	<45	Isl	R	NSD	<100
17	C	PC	X	X	<20	SSu	Is	McP	Cy	So	X	Ms	<25	Isl	R	NSD	<100
18	C	PC	X	X	<20	SSu	Is	McP	R	Ho	X	Ms	<45	Isl	R	SD	<200
19	C	PC	X	X	<20	SSu	Is	McP	R	Ho	X	Ms	<45	Isl	R	SD	<200
20	C	PC	X	X	<20	SSu	Is	McP	R	Ho	X	Ms	<45	Isl	IR	SD	>200
21	C	PC	X	X	<20	SSu	Is	McP	R	Ho	X	Ms	<45	Isl	IR	SD	>200
22	C	PC	X	X	<20	SSu	Is	McP	R	Ho	X	Ms	<45	Isl	R	SD	>200
23	C	PC	X	X	<20	SSu	Is	McP	R	Ho	X	Ms	<45	Isl	R	SD	>200
24	C	PC	X	X	<20	SSu	Is	McP	Cy	So	X	Ms	<45	Isl	R	SD	<200
25	C	PC	X	X	<20	SSu	Is	McP	R	So	X	Ms	<45	Isl	R	SD	<50
26	C	PC	X	X	<20	SSu	Is	McP	R	So	X	Ms	<25	Isl	R	SD	<100
27	C	PC	X	X	<20	SSu	Is	McP	Cy	So	X	Ms	<45	Isl	R	SD	<200
28	C	PC	X	X	<20	SSu	Is	McP	R	So	X	Ms	<45	Isl	R	SD	<50
29	C	PC	X	X	>20	SSu	Is	McP	R	So	X	Ms	<45	Isl	R	SD	<50
30	C	PC	X	X	>20	SSu	Is	McP	Cy	So	X	Ms	<45	Isl	R	SD	<200
31	C	PC	X	X	>20	SSu	Is	McP	R	So	X	Ms	<45	Isl	R	SD	<50
32	C	PC	X	X	<20	SSu	Is	McP	R	So	X	Ms	<45	Isl	R	SD	<100
33	C	PC	X	X	<20	SSu	Is	McP	R	So	X	Ms	<45	Isl	R	SD	<50
34	C	PC	X	X	>20	SSu	Is	McP	R	So	X	Ms	<45	Isl	R	SD	<50
35	C	PC	X	X	>20	SSu	Is	McP	R	So	X	Ms	<45	Isl	R	SD	<50
36	C	PC	X	X	<20	SSu	Is	McP	Cy	So	X	Ms	<25	Isl	R	SD	<100
37	C	PC	X	X	<20	SSu	Is	McP	Cy	So	X	Ms	<45	Isl	R	SD	>200
38	C	PC	X	X	<20	SSu	Is	McP	Cy	So	X	Ms	<25	Isl	R	SD	<200
39	C	PC	X	X	<20	SSu	Is	McP	R	So	X	Ms	<45	Isl	R	SD	<50
40	C	PC	X	X	<20	SSu	Is	McP	R	So	X	Ms	<45	Isl	R	SD	<50
41	C	PC	X	X	<20	SSu	Is	McP	R	So	X	Ms	<45	Isl	R	SD	<50
42	C	PC	X	X	<20	SSu	Is	McP	R	So	X	Ms	<45	Isl	R	SD	<50
43	C	PC	X	X	<20	SSu	Is	McP	R	So	X	Ms	<45	Isl	R	SD	<50
44	C	PC	X	X	<20	SSu	Is	McP	R	So	X	Ms	<45	Isl	R	SD	<50
45	C	PC	X	X	<20	SSu	Is	McP	Cy	So	X	Ms	<45	Isl	R	SD	<100
46	C	PC	X	X	<20	SSu	Is	McP	Cy	So	X	Ms	<45	Isl	R	SD	<200
47	C	PC	X	X	<20	SSu	Is	McP	R	So	X	Ms	<45	Isl	R	SD	<100
48	C	PC	X	X	<20	SSu	Is	ScP	W	So	X	Ms	<25	Isl	R	NSD	<50
49	C	PC	X	X	<20	SSu	Is	ScP	W	So	X	Ms	<25	Isl	R	NSD	<100
50	C	PC	X	X	>20	SSu	Is	ScP	W	So	X	Ms	<25	Isl	R	NSD	<50
51	C	PC	X	X	<20	SSu	Is	ScP	W	So	X	Ms	<45	Isl	R	NSD	<100
52	C	PC	X	X	<20	SSu	Is	ScP	W	So	X	Ms	<45	Isl	R	NSD	<100
53	C	PC	X	X	<20	SSu	Is	ScP	Ob	So	X	Ms	<45	Isl	R	SD	<100
54	C	PC	X	X	<20	SSu	Is	ScP	Cy	So	X	Ms	<45	Isl	IR	SD	<200
55	C	PC	X	X	<20	SSu	Is	ScP	W	So	X	Ms	<45	Isl	R	SD	<100
56	C	PC	X	X	<20	SSu	Is	ScP	Ob	So	X	Ms	<45	Isl	R	SD	<200
57	C	PC	X	X	<20	SSu	Is	ScP	Cy	So	X	Ms	<45	Isl	R	SD	<200
58	C	PC	X	X	<20	Co	Is	McP	R	So	X	Ms	<25	Isl	R	SD	<100
59	C	PC	X	X	<20	Co	Is	McP	R	So	X	Ms	<25	Isl	R	SD	<200
60	C	PC	X	X	<20	Co	Is	ScP	W	So	X	Ms	<25	X	R	SD	<50
61	C	PC	X	X	<20	Co	Is	ScP	W	So	X	Ms	X	Isl	IR	SD	>200
62	C	PC	X	X	<20	Co	Is	ScP	W	So	X	Ms	X	Isl	IR	SD	>200
63	C	PC	X	X	>20	Co	Is	Scp	W	So	X	Ms	<25	Isl	R	SD	<50
64	C	PC	X	X	<20	Co	Is	ScP	W	So	X	Ms	<45	Isl	R	SD	<100
65	C	PC	X	X	>20	Co	Is	ScP	W	So	X	Ms	<45	Isl	R	SD	<100
66	C	RC	X	X	<20	X	X	X	X	X	X	Ssp	<25	Mo	R	NSD	<50
67	C	RC	X	X	<20	X	X	X	X	X	X	Ssp	<25	Mo	R	SD	<50
68	C	RC	X	X	<20	X	X	X	X	X	X	Ssp	<25	Mo	R	SD	<50
69	C	RC	X	X	<20	X	X	X	X	X	X	Ssp	<25	Mo	R	SD	<50
70	C	RC	X	X	<20	X	X	X	X	X	X	Ssp	<25	X	R	SD	<50
71	C	RC	X	X	<20	X	X	X	X	X	X	Ssp	<25	Mo	R	SD	<50
72	C	RC	X	X	<20	X	X	X	X	X	X	Ssp	<25	Mo	R	SD	<50

73	C	RC	X	X	>20	X	X	X	X	X	X	Ssp	<25	Mo	R	SD	<50
74	C	RC	X	X	<20	X	X	X	X	X	X	Ssp	<25	Mo	R	SD	<50
75	C	RC	X	X	>20	X	X	X	X	X	X	Ssp	<25	Mo	R	SD	<50
76	C	RC	X	X	>20	X	X	X	X	X	X	Ssp	<25	Mo	R	SD	<50
77	C	RC	X	X	<20	X	X	X	X	X	X	Ssp	<25	Mo	R	SD	<50
78	C	RC	X	X	<20	X	X	X	X	X	X	Ssp	<25	Mo	R	SD	<50
79	C	RC	X	X	<20	X	X	X	X	X	X	Ssp	<25	Mo	R	SD	<50
80	C	RC	X	X	<20	X	X	X	X	X	X	Ssp	<25	Mo	R	SD	<50
81	C	RC	X	X	<20	X	X	X	X	X	X	Ssp	<25	Mo	R	SD	<50
82	C	RC	X	X	>20	X	X	X	X	X	X	Ssp	<25	Mo	R	SD	<50
83	C	RC	X	X	<20	X	X	X	X	X	X	Ssp	<25	Mo	R	SD	<50
84	C	RC	X	X	>20	X	X	X	X	X	X	Ssp	<25	Mo	R	SD	<50
85	C	RC	X	X	>20	X	X	X	X	X	X	Ssp	<25	Mo	R	SD	<50
86	C	RC	X	X	<20	X	X	X	X	X	X	Ssp	<25	Mo	R	SD	<50
87	C	RC	X	X	<20	X	X	X	X	X	X	Ssp	<25	Isl	R	SD	<50
88	C	RC	X	X	<20	X	X	X	X	X	X	Ssp	<25	Mo	R	SD	<50
89	C	RC	X	X	<20	X	X	X	X	X	X	Ssp	<25	Mo	R	SD	<50
90	C	RC	X	X	<20	X	X	X	X	X	X	Ssp	<25	Mo	R	SD	<50
91	C	RC	X	X	<20	X	X	X	X	X	X	Ssp	<25	Mo	R	SD	<50
92	C	RC	X	X	<20	X	X	X	X	X	X	Ssp	<25	Mo	R	SD	<50
93	C	RC	X	X	<20	X	X	X	X	X	X	Ssp	<25	Mo	R	SD	<50
94	C	RC	X	X	<20	X	X	X	X	X	X	Ssp	<25	Mo	R	SD	<50
95	C	RC	X	X	<20	X	X	X	X	X	X	Ssp	<25	Mo	R	SD	<50
96	C	RC	X	X	<20	X	X	X	X	X	X	Ssp	<25	Mo	R	SD	<50
97	C	RC	X	X	<20	X	X	X	X	X	X	Ssp	<25	Mo	R	SD	<50
98	C	RC	X	X	<20	X	X	X	X	X	X	Ssp	<25	Mo	R	SD	<50
99	S	X	X	X	<20	SSu	Is	ScP	W	So	X	Ms	<45	Isl	R	NSD	<100
100	S	X	X	X	<20	SSu	Is	ScP	W	So	X	Ms	<45	Isl	R	NSD	<100
101	S	X	X	X	<20	SSu	Is	ScP	W	So	X	Ms	<45	Isl	R	NSD	<100
102	S	X	X	X	<20	SSu	Is	ScP	W	So	X	Ms	>45	Isl	R	SD	>200
103	S	X	X	X	<20	SSu	X	X	X	X	X	Ssp	>45	Isl	R	NSD	<100
104	S	X	X	X	<20	SSu	X	X	X	X	X	Ssp	>45	Isl	R	SD	<100
105	S	X	X	X	<20	Co	Is	ScP	W	So	X	Ms	>45	Isl	R	SD	<100
106	S	X	X	X	<20	Co	Is	ScP	W	So	X	Ms	>45	Isl	R	SD	<100
107	S	X	X	X	<20	Co	Is	ScP	W	So	X	Ms	<45	Isl	R	SD	<100
108	S	RC	X	X	<20	Co	Is	ScP	Ob	So	X	Ms	<45	Isl	R	SD	<100
109	S	RC	X	X	<20	Co	Is	ScP	Ob	So	X	Ms	<45	Isl	R	SD	<100
110	S	RC	X	X	<20	Co	Is	ScP	Ob	So	X	Ms	<45	Isl	R	SD	<100
111	S	RC	X	X	<20	Co	Is	ScP	Ob	So	X	Ms	<45	Isl	R	SD	<100
112	S	RC	X	X	<20	Co	Is	ScP	Ob	So	X	Ms	<45	Isl	R	SD	<100
113	S	RC	X	X	<20	Co	Is	ScP	Ob	So	X	Ms	<45	Isl	R	SD	<100
114	S	RC	X	X	<20	Co	Is	ScP	Ob	So	X	Ms	<45	Isl	R	SD	<100
115	X	X	X	X	<20	X	X	X	X	X	X	X	X	X	IR	X	>200
116	X	X	X	X	<20	X	X	X	X	X	X	X	X	X	IR	X	>200
117	X	X	X	X	<20	X	X	X	X	X	X	X	X	X	IR	X	<200
118	X	X	X	X	<20	X	X	X	X	X	X	X	X	X	IR	X	<200
119	X	X	X	X	<20	X	X	X	X	X	X	X	X	X	IR	X	>200
120	X	X	X	X	<20	X	X	X	X	X	X	X	X	X	IR	X	>200
121	X	X	X	X	<20	X	X	X	X	X	X	Ms	<45	X	R	X	<100
122	X	X	X	X	<20	X	X	X	X	X	X	Ms	<45	X	R	X	<100
123	X	X	X	X	X	X	X	X	X	X	X	Ms	X	X	R	X	X
124	X	X	X	X	X	X	X	X	X	X	X	X	X	X	R	X	X
125	X	X	X	X	X	X	X	X	X	X	X	X	X	X	R	X	X
126	X	X	X	X	X	X	X	X	X	X	X	X	X	X	R	X	X
127	X	X	X	X	X	X	X	X	X	X	X	Ms	X	X	R	X	X
128	X	X	X	X	X	X	X	X	X	X	X	X	X	X	R	X	X
129	X	X	X	X	X	X	X	X	X	X	X	X	X	X	R	X	X
130	X	X	X	X	<20	X	X	X	X	X	X	X	X	X	IR	X	<200
131	X	X	X	X	<20	X	X	X	X	X	X	X	X	X	IR	X	<200
132	X	X	X	X	<20	X	X	X	X	X	X	X	X	X	IR	X	<200
133	X	X	X	X	<20	X	X	X	X	X	X	X	X	X	IR	X	<200
134	X	X	X	X	X	X	X	X	X	X	X	X	X	X	R	X	X
135	X	X	X	X	X	X	X	X	X	X	X	X	X	X	R	X	X
136	X	X	X	X	X	X	X	X	X	X	X	X	X	X	R	X	X
137	X	X	X	X	X	X	X	X	X	X	X	X	X	X	R	X	X
138	X	X	X	X	<20	X	X	X	X	X	X	X	X	X	IR	X	>200
139	X	X	X	X	<20	X	X	X	X	X	X	X	X	X	IR	X	>200
140	X	X	X	X	X	X	X	X	X	X	X	X	X	X	R	X	X
141	X	X	X	X	X	X	X	X	X	X	X	X	X	X	R	X	X
142	X	X	X	X	<20	X	X	X	X	X	X	X	X	X	IR	X	>200
143	X	X	X	X	<20	X	X	X	X	X	X	X	X	X	IR	X	>200
144	X	X	X	X	X	X	X	X	X	X	X	Ms	X	X	R	X	X
145	X	X	X	X	X	X	X	X	X	X	X	X	X	X	R	X	X
146	X	X	X	X	X	X	X	X	X	X	X	X	X	X	R	X	X
147	X	X	X	X	<20	X	X	X	X	X	X	Ssp	X	X	R	X	<50
148	X	X	X	X	X	X	X	X	X	X	X	X	X	X	R	X	X
149	X	X	X	X	X	X	X	X	X	X	X	X	X	X	R	X	X

150	X	X	X	X	X	X	X	X	X	X	X	X	X	X	R	X	X
151	X	X	X	X	<20	X	X	X	X	X	X	X	X	X	IR	X	>200
152	X	X	X	X	<20	X	X	X	X	X	X	X	X	X	IR	X	>200
153	X	X	X	X	<20	X	Is	ScP	Ob	So	X	Ms	X	Isl	R	SD	<200
154	X	X	X	X	X	X	X	X	X	X	X	X	X	X	R	X	X
155	X	X	X	X	<20	X	X	X	X	X	X	X	X	X	R	X	<100
156	X	X	X	X	<20	X	X	X	X	X	X	X	X	X	R	X	<100
157	X	X	X	X	X	X	X	X	X	X	X	X	X	X	R	X	X
158	X	X	X	X	X	X	X	X	X	X	X	X	X	X	R	X	X
159	X	X	X	X	X	X	X	X	X	X	X	X	X	X	R	X	X
160	X	X	X	X	X	X	X	X	X	X	X	X	X	X	R	X	X
161	X	X	X	X	X	X	X	X	X	X	X	X	X	X	R	X	X
162	X	X	X	X	X	X	X	X	X	X	X	X	X	X	R	X	X
163	X	X	X	X	<20	X	X	X	X	X	X	X	X	X	IR	X	>200
164	X	X	X	X	<20	X	X	X	X	X	X	X	X	X	IR	X	>200
165	X	X	X	X	X	X	X	X	X	X	X	X	X	X	R	X	X
166	X	X	X	X	X	X	X	X	X	X	X	X	X	X	R	X	X
167	X	X	X	X	X	X	X	X	X	X	X	X	X	X	R	X	X
168	X	X	X	X	X	X	X	X	X	X	X	X	X	X	R	X	X
169	X	X	X	X	X	X	X	X	X	X	X	X	X	X	R	X	X
170	X	X	X	X	X	X	X	X	X	X	X	X	X	X	R	X	X
171	X	X	X	X	X	X	X	X	X	X	X	X	X	X	R	X	X
172	X	X	X	X	X	X	X	X	X	X	X	X	X	X	R	X	X
173	X	X	X	X	X	X	X	X	X	X	X	X	X	X	R	X	X
174	X	X	X	X	X	X	X	X	X	X	X	X	X	X	R	X	X
175	X	X	X	X	X	X	X	X	X	X	X	X	X	X	R	X	X
176	X	X	X	X	X	X	X	X	X	X	X	X	X	X	R	X	X
177	X	X	X	X	X	X	X	X	X	X	X	X	X	X	R	X	X
178	X	X	X	X	X	X	X	X	X	X	X	X	X	X	R	X	X
179	X	X	X	X	X	X	X	X	X	X	X	X	X	X	R	X	X
180	X	X	X	X	<20	X	X	X	X	X	X	Ms	<45	X	R	X	<100
181	X	X	X	X	X	X	X	X	X	X	X	X	X	X	R	X	X
182	X	X	X	X	X	X	X	X	X	X	X	X	X	X	R	X	X
183	X	X	X	X	X	X	X	X	X	X	X	X	X	X	R	X	X
184	X	X	X	X	<20	X	X	McP	Cy	So	X	X	X	X	R	X	X
185	X	X	X	X	X	X	X	X	X	X	X	X	X	X	R	X	X
186	X	X	X	X	X	X	X	X	X	X	X	X	X	X	R	X	X
187	X	X	X	X	X	X	X	X	X	X	X	X	X	X	R	X	X
188	X	X	X	X	X	X	X	X	X	X	X	X	X	X	R	X	X
189	X	X	X	X	X	X	X	X	X	X	X	X	X	X	R	X	X
190	X	X	X	X	X	X	X	X	X	X	X	X	X	X	R	X	X
191	X	X	X	X	X	X	X	X	X	X	X	X	X	X	R	X	X
192	X	X	X	X	X	X	X	X	X	X	X	X	X	X	R	X	X
193	X	X	X	X	<20	X	X	X	X	X	X	Ssp	<45	X	R	X	<50
194	X	X	X	X	X	X	X	X	X	X	X	Ms	X	X	R	X	X
195	X	X	X	X	X	X	X	X	X	X	X	X	X	X	R	X	X
196	X	X	X	X	<20	X	X	X	X	X	X	X	X	X	R	X	X
197	X	X	X	X	X	X	X	X	X	X	X	X	X	X	R	X	X
198	X	X	X	X	X	X	X	X	X	X	X	X	X	X	R	X	X
199	X	X	X	X	>20	X	X	X	X	X	X	X	X	X	R	X	<50
200	X	X	X	X	X	X	X	X	X	X	X	X	X	X	R	X	X
201	X	X	X	X	X	X	X	X	X	X	X	X	X	X	R	X	X
202	X	X	X	X	X	X	X	X	X	X	X	X	X	X	R	X	X
203	X	X	X	X	X	X	X	X	X	X	X	X	X	X	R	X	X
204	X	X	X	X	<20	X	X	X	X	X	X	X	X	X	R	X	X
205	X	X	X	X	X	X	X	X	X	X	X	X	X	X	R	X	X
206	X	X	X	X	X	X	X	X	X	X	X	Ms	X	X	R	X	X
207	X	X	X	X	X	X	X	X	X	X	X	X	X	X	R	X	X
208	X	X	X	X	X	X	X	X	X	X	X	X	X	X	R	X	X
209	X	X	X	X	X	X	X	X	X	X	X	X	X	X	R	X	X
210	X	X	X	X	X	X	X	X	X	X	X	X	X	X	R	X	X
211	X	X	X	X	X	X	X	X	X	X	X	X	X	X	R	X	X
212	X	X	X	X	X	X	X	X	X	X	X	Ms	<45	X	R	X	<200
213	X	X	X	X	>20	X	X	X	X	X	X	X	X	X	R	X	<50
214	X	X	X	X	X	X	X	X	X	X	X	Ms	X	X	R	X	>200
215	X	X	X	X	X	X	X	X	X	X	X	X	X	X	R	X	X
216	X	X	X	X	X	X	X	X	X	X	X	X	X	X	R	X	X
217	X	X	X	X	<20	X	X	X	X	X	X	Ms	X	X	R	X	>200
218	X	X	X	X	X	X	X	X	X	X	X	X	X	X	R	X	X
219	X	X	X	X	>20	X	X	X	X	X	X	X	X	X	R	X	<100
220	X	X	X	X	>20	X	X	X	X	X	X	X	X	X	IR	X	>200
221	X	X	X	X	X	X	X	X	X	X	X	X	<25	X	R	X	<50
222	X	X	X	X	X	X	X	X	X	X	X	X	<25	X	R	X	<50
223	X	X	X	X	>20	X	X	X	X	X	X	Ms	<45	X	R	X	<50
224	X	X	X	X	X	X	X	X	X	X	X	X	X	X	R	X	X
225	X	X	X	X	X	X	X	X	X	X	X	X	X	X	R	X	X
226	X	X	X	X	X	X	X	X	X	X	X	X	X	X	R	X	X

227	X	X	X	X	<20	X	X	X	X	X	X	Ms	X	X	R	X	X
228	X	X	X	X	X	X	X	X	X	X	X	X	X	X	R	X	X
229	X	X	X	X	X	X	X	X	X	X	X	X	X	X	R	X	X
230	X	X	X	X	X	X	X	X	X	X	X	X	X	X	R	X	X
231	X	X	X	X	X	X	X	X	X	X	X	X	X	X	R	X	X
232	X	X	X	X	X	X	X	X	X	X	X	X	X	X	R	X	X
233	X	X	X	X	<20	X	X	X	X	X	X	Ssp	<25	X	R	X	<50
234	X	X	X	X	<20	X	X	X	X	X	X	Ms	X	X	R	X	<50
235	X	X	X	X	<20	X	X	X	X	X	X	Ssp	X	X	R	X	X
236	X	X	X	X	X	X	X	X	X	X	X	X	X	X	R	X	X
237	X	X	X	X	<20	X	X	X	X	X	X	Ms	<25	X	R	X	<50
238	X	X	X	X	<20	X	X	X	X	X	X	X	X	X	R	X	>200
239	C	PC	X	X	<20	X	X	X	X	X	X	Ssp	<25	Isl	R	NSD	<50
240	C	PC	X	X	<20	X	X	X	X	X	X	Ssp	<25	Isl	R	NSD	<50
241	C	PC	X	X	<20	X	X	X	X	X	X	Ssp	<25	Isl	R	NSD	<50
242	C	PC	X	X	>20	X	X	X	X	X	X	Ssp	<25	Isl	R	NSD	<50
243	C	PC	X	X	>20	X	X	X	X	X	X	Ssp	<25	Isl	R	NSD	<50
244	C	PC	X	X	>20	X	X	X	X	X	X	Ssp	<25	Isl	R	NSD	<50
245	C	PC	X	X	>20	X	X	X	X	X	X	Ssp	<25	Isl	R	NSD	<50
246	C	PC	X	X	<20	X	X	X	X	X	X	Ssp	<25	Isl	R	NSD	<50
247	C	PC	X	X	<20	X	X	X	X	X	X	Ssp	<45	Mo	R	SD	<50
248	C	PC	X	X	<20	X	X	X	X	X	X	Ssp	<45	Isl	R	SD	<50
249	C	PC	X	X	<20	X	X	X	X	X	X	Ssp	<25	Isl	R	SD	<50
250	C	PC	X	X	<20	X	X	X	X	X	X	Ssp	<45	Isl	R	SD	<50
251	C	PC	X	X	<20	X	X	X	X	X	X	Ssp	<45	Isl	R	SD	<50
252	C	PC	X	X	<20	X	X	X	X	X	X	Ssp	<25	Isl	R	SD	<50
253	C	PC	X	X	<20	X	X	X	X	X	X	Ssp	<25	Isl	R	SD	<50
254	C	PC	X	X	<20	X	X	X	X	X	X	Ssp	<25	Isl	R	SD	<50
255	C	PC	X	X	<20	X	X	X	X	X	X	Ssp	<25	Isl	R	SD	<50
256	C	PC	X	X	<20	X	X	X	X	X	X	Ssp	<25	Isl	R	SD	<50
257	C	PC	X	X	<20	X	X	X	X	X	X	Ssp	<25	Isl	IR	SD	<50
258	C	PC	X	X	<20	X	X	X	X	X	X	Ssp	<25	Isl	R	SD	<50
259	C	PC	X	X	>20	X	X	X	X	X	X	Ssp	<25	Isl	R	SD	<50
260	C	PC	X	X	>20	X	X	X	X	X	X	Ssp	<45	Isl	R	SD	<50
261	C	PC	X	X	<20	X	X	X	X	X	X	Ssp	<25	Isl	R	SD	<50
262	C	PC	X	X	<20	X	X	X	X	X	X	Ssp	<25	Mo	R	SD	<50
263	C	PC	X	X	<20	X	X	X	X	X	X	Ssp	<45	Isl	R	SD	<50
264	C	PC	X	X	>20	X	X	X	X	X	X	Ssp	<25	Isl	R	SD	<50
265	C	PC	X	X	<20	X	X	X	X	X	X	Ssp	<45	Isl	R	SD	<50
266	C	PC	X	X	>20	X	X	X	X	X	X	Ssp	<25	Isl	R	SD	<50
267	C	PC	X	X	>20	X	X	X	X	X	X	Ssp	<25	Isl	R	SD	<50
268	C	PC	X	X	>20	X	X	X	X	X	X	Ssp	<25	Mo	R	SD	<50
269	C	PC	X	X	<20	X	X	X	X	X	X	Ssp	<25	Isl	R	SD	<50
270	C	PC	X	X	<20	X	X	X	X	X	X	Ssp	<25	Isl	R	SD	<50
271	C	PC	X	X	<20	X	X	X	X	X	X	Ssp	<25	Isl	R	SD	<50
272	C	PC	X	X	<20	X	X	X	X	X	X	Ssp	<25	Mo	R	SD	<50
273	C	PC	X	X	<20	X	X	X	X	X	X	Ssp	<25	Mo	R	SD	<50
274	C	PC	X	X	<20	X	X	X	X	X	X	Ssp	<25	Mo	R	SD	<50
275	C	PC	X	X	<20	X	X	X	X	X	X	Ssp	<45	X	R	SD	<50
276	C	PC	X	X	<20	X	X	X	X	X	X	Ssp	<25	Mo	R	SD	<50
277	C	PC	X	X	>20	X	X	X	X	X	X	Ssp	<45	Isl	R	SD	<50
278	C	PC	X	X	<20	X	X	X	X	X	X	Ssp	<25	Isl	R	SD	<50
279	C	PC	X	X	<20	X	X	X	X	X	X	Ssp	<25	Mo	R	SD	<50
280	C	PC	X	X	<20	X	X	X	X	X	X	Ssp	<25	Isl	R	SD	<50
281	C	PC	X	X	<20	X	X	X	X	X	X	Ssp	<25	Isl	R	SD	<50
282	C	PC	X	X	>20	X	X	X	X	X	X	Ssp	<25	Isl	R	SD	<50
283	C	PC	X	X	<20	X	X	X	X	X	X	Ssp	<25	Isl	R	SD	<50
284	C	PC	X	X	<20	X	X	X	X	X	X	Ssp	<25	Isl	R	SD	<50
285	C	PC	X	X	<20	X	X	X	X	X	X	Ssp	<25	Isl	R	SD	<50
286	C	PC	X	X	<20	X	X	X	X	X	X	Ssp	<25	Isl	R	SD	<50
287	C	PC	X	X	>20	X	X	X	X	X	X	Ssp	<25	Isl	R	SD	<50
288	C	PC	X	X	<20	X	X	X	X	X	X	Ssp	<25	Isl	R	SD	<50
289	C	PC	X	X	<20	X	X	X	X	X	X	Ssp	<25	Isl	R	SD	<50
290	C	PC	X	X	>20	X	X	X	X	X	X	Ssp	<25	Isl	R	SD	<50
291	C	PC	X	X	<20	X	X	X	X	X	X	Ssp	<25	F	R	SD	<50
292	C	PC	X	X	<20	X	X	X	X	X	X	Ssp	<25	Isl	R	SD	<50
293	C	PC	X	X	<20	X	X	X	X	X	X	Ssp	<25	Isl	R	SD	<50
294	C	PC	X	X	<20	X	X	X	X	X	X	Ssp	<25	Isl	R	SD	<50
295	C	PC	X	X	>20	X	X	X	X	X	X	Ssp	<25	Mo	R	SD	<50
296	C	PC	X	X	>20	X	X	X	X	X	X	Ssp	<25	Mo	R	SD	<50
297	C	PC	X	X	>20	X	X	X	X	X	X	Ssp	<25	Mo	R	SD	<50
298	C	PC	X	X	>20	X	X	X	X	X	X	Ssp	<25	Mo	R	SD	<50
299	C	PC	X	X	>20	X	X	X	X	X	X	Ssp	<25	Mo	R	SD	<50
300	C	PC	X	X	<20	X	X	X	X	X	X	Ssp	<25	Mo	R	SD	<50
301	C	PC	X	X	<20	X	X	X	X	X	X	Ssp	<25	Isl	R	SD	<50
302	C	PC	X	X	<20	X	X	X	X	X	X	Ssp	<25	Mo	R	SD	<50
303	C	PC	X	X	<20	X	X	X	X	X	X	Ssp	<25	Isl	R	SD	<50

304	C	PC	X	X	<20	X	X	X	X	X	X	Ssp	<25	Isl	R	SD	<50
305	C	PC	X	X	<20	X	X	X	X	X	X	Ssp	<25	Isl	R	SD	<50
306	C	PC	X	X	<20	X	X	X	X	X	X	Ssp	<25	Isl	R	SD	<50
307	C	PC	X	X	<20	X	X	X	X	X	X	Ssp	<25	Isl	R	SD	<50
308	C	PC	X	X	<20	X	X	X	X	X	X	Ssp	<45	Isl	R	SD	<50
309	C	RC	X	X	>20	X	X	X	X	X	X	Ssp	<25	Mo	R	SD	<50
310	C	PC	X	X	<20	X	X	McP	X	X	X	X	X	X	IR	X	>200
311	C	PC	X	X	<20	X	X	McP	X	X	X	X	X	X	IR	X	>200
312	C	PC	X	X	>20	Co	NIs	McP	R	So	X	Ms	<25	Mo	R	SD	<100
313	C	PC	X	X	X	X	X	X	X	X	X	X	X	X	R	X	X
314	C	PC	X	X	<20	X	Is	ScP	R	So	X	Ms	X	Isl	R	SD	<100
315	C	PC	X	X	<20	X	Is	ScP	Ob	So	X	Ms	X	Isl	R	SD	<100
316	C	RC	X	X	<20	Co	NIs	ScP	W	So	X	Ms	<25	Mo	R	SD	<50
317	C	RC	X	X	<20	X	X	X	X	X	X	Ms	<25	Mo	R	SD	X
318	C	X	X	X	X	X	X	X	X	X	X	Ms	X	X	R	X	X
319	C	X	X	X	<20	X	X	X	X	X	X	Ms	<25	X	R	SD	<100
320	C	X	X	X	<20	X	X	X	X	X	X	Ms	<45	X	R	SD	<200
321	C	X	X	X	<20	X	X	X	X	X	X	Ssp	<25	X	R	SD	<50
322	C	X	X	X	>20	X	X	X	X	X	X	Ssp	<25	Mo	R	SD	<50
323	C	X	X	X	<20	X	X	ScP	W	So	X	Ms	X	Mo	R	SD	X
324	S	RC	X	X	<20	X	X	X	X	X	X	Ssp	>45	Isl	R	SD	<100
325	S	X	X	X	<20	SSu	Is	McP	R	So	X	Ms	<45	Isl	R	SD	<200
326	S	X	X	X	<20	X	X	X	X	X	X	Ssp	<45	Isl	R	NSD	<50
327	S	X	X	X	<20	X	X	X	X	X	X	Ssp	<45	Isl	R	SD	<50
328	S	X	X	X	<20	X	X	X	X	X	X	Ssp	<25	Isl	R	SD	<50
329	M	X	X	X	<20	X	X	ScP	W	So	X	Ms	<25	Mo	R	NSD	<100
330	M	X	X	X	<20	X	X	ScP	W	So	X	Ms	<25	Mo	R	SD	<50
331	M	X	X	X	<20	X	X	ScP	W	So	X	Ms	<45	Mo	R	SD	>200
332	M	X	X	X	<20	X	X	ScP	W	So	X	Ms	<25	Mo	R	SD	<50
333	M	X	X	X	<20	X	X	ScP	W	So	X	Ms	<25	Mo	R	SD	<50
334	M	X	X	X	<20	X	X	X	X	X	X	Ssp	<25	Mo	R	SD	<50
335	M	X	X	X	X	X	X	ScP	W	So	X	Ssp	X	Mo	R	SD	X
336	M	X	X	X	<20	X	X	ScP	Ob	So	X	Ms	<25	Mo	R	SD	<100
337	M	X	X	X	<20	X	X	X	X	X	X	Ms	<45	Mo	R	SD	<200
338	M	X	X	X	<20	X	X	ScP	W	So	X	Ms	X	Mo	R	SD	X
339	C	PC	X	X	X	X	X	ScP	Cy	So	X	Ms	X	X	R	X	X
340	C	PC	X	X	<20	X	X	X	X	X	X	Ssp	<25	Mo	R	X	<50

Table 54: Characteristics of the case-study bridges according to the SYNER-G taxonomy (see section 4.1.1 for the meaning of the acronyms). '*X*' refers to unknown parameters.

APPENDIX D: FRAGILITY FUNCTIONS FOR THE CASE-STUDY BRIDGES

ID	*MM1*	*MM2*	*TD1*	*TD2*	*DC*	*DSS*	*PDC*	*TC1*	*TS1*	*TS2*	*HP*	*Sp*	*SC*	*Tca*	*BC*	*LS*	*Length*
clus1	**102 bridges**																
	S	RC	X	X	<20	X	X	X	X	X	X	Ssp	>45	Isl	R	SD	<100
	S	X	X	X	<20	X	X	X	X	X	X	Ssp	<25	Isl	R	SD	<50
	S	X	X	X	<20	SSu	X	X	X	X	X	Ssp	>45	Isl	R	SD	<100
	M	X	X	X	<20	X	X	X	X	X	X	Ssp	<25	M	R	SD	<50
	S	X	X	X	<20	X	X	X	X	X	X	Ssp	<45	Isl	R	SD	<50
	C	RC	X	X	<20	X	X	X	X	X	X	Ssp	<25	Isl	R	SD	<50
	C	PC	X	X	>20	X	X	X	X	X	X	Ssp	<45	Isl	R	SD	<50
	C	PC	X	X	<20	X	X	X	X	X	X	Ssp	<25	Isl	IR	SD	<50
	C	RC	X	X	>20	X	X	X	X	X	X	Ssp	<25	M	R	SD	<50
	C	RC	X	X	<20	X	X	X	X	X	X	Ssp	<25	X	R	SD	<50
	C	PC	X	X	>20	X	X	X	X	X	X	Ssp	<25	M	R	SD	<50
	C	X	X	X	<20	X	X	X	X	X	X	Ssp	<25	X	R	SD	<50
	C	PC	X	X	>20	X	X	X	X	X	X	Ssp	<25	Isl	R	SD	<50
	C	X	X	X	<20	X	X	X	X	X	X	Ssp	<25	M	R	SD	<50
	C	PC	X	X	<20	X	X	X	X	X	X	Ssp	<25	Isl	R	SD	<50
	C	PC	X	X	<20	X	X	X	X	X	X	Ssp	<25	F	R	SD	<50
	C	RC	X	X	<20	X	X	X	X	X	X	Ssp	<25	F	R	SD	<50
	C	RC	X	X	<20	X	X	X	X	X	X	Ssp	<25	M	R	SD	<50
	C	PC	X	X	<20	X	X	X	X	X	X	Ssp	<25	M	R	SD	<50
	C	PC	X	X	<20	X	X	X	X	X	X	Ssp	<45	M	R	SD	<50
	C	PC	X	X	<20	X	X	X	X	X	X	Ssp	<45	X	R	SD	<50
	C	PC	X	X	<20	X	X	X	X	X	X	Ssp	<45	Isl	R	SD	<50
	C	PC	X	X	<20	X	X	X	X	X	X	Ssp	X	Isl	R	SD	<50
clus2	**6 bridges**																
	X	X	X	X	<20	X	X	X	X	X	X	Ssp	<45	X	R	NSD	<50
	S	X	X	X	<20	X	X	X	X	X	X	Ssp	<45	Isl	R	NSD	<50
	X	X	X	X	<20	X	X	X	X	X	X	Ssp	<25	X	R	NSD	<50
	S	X	X	X	<20	SSu	X	X	X	X	X	Ssp	>45	Isl	R	NSD	<50
	X	X	X	X	<20	X	X	X	X	X	X	Ssp	X	X	R	NSD	<50
	X	X	X	X	<20	X	X	X	X	X	X	Ssp	X	X	R	NSD	X
clus3	**16 bridges**																
	X	X	X	X	>20	X	X	X	X	X	X	Ms	<25	X	R	NSD	<50
	X	X	X	X	X	X	X	X	X	X	X	Ms	<45	X	R	NSD	<200
	X	X	X	X	<20	X	X	X	X	X	X	Ms	<45	X	R	NSD	<100
	X	X	X	X	<20	X	X	X	X	X	X	Ms	<25	X	R	NSD	<50
	C	X	X	X	X	X	X	X	X	X	X	Ms	X	X	R	NSD	X
	X	X	X	X	<20	X	X	X	X	X	X	Ms	X	X	R	NSD	<50
	X	X	X	X	X	X	X	X	X	X	X	Ms	X	X	R	NSD	>200
	X	X	X	X	<20	X	X	X	X	X	X	Ms	X	X	R	NSD	>200
	X	X	X	X	X	X	X	X	X	X	X	Ms	X	X	R	NSD	X
	X	X	X	X	<20	X	X	X	X	X	X	Ms	X	X	R	NSD	X
clus4	**104 bridges**																
	C	PC	X	X	X	X	X	X	X	X	X	X	X	X	R	NSD	X
	X	X	X	X	X	X	X	X	X	X	X	X	<25	X	R	NSD	<50
	X	X	X	X	>20	X	X	X	X	X	X	X	X	X	R	NSD	<50
	X	X	X	X	>20	X	X	X	X	X	X	X	X	X	IR	NSD	>200
	X	X	X	X	X	X	X	X	X	X	X	X	X	X	R	NSD	X
	X	X	X	X	<20	X	X	X	X	X	X	X	X	X	R	NSD	<100
	X	X	X	X	<20	X	X	X	X	X	X	X	X	X	IR	NSD	<200
	X	X	X	X	<20	X	X	X	X	X	X	X	X	X	IR	NSD	>200
	X	X	X	X	<20	X	X	X	X	X	X	X	X	X	R	NSD	>200
	X	X	X	X	<20	X	X	X	X	X	X	X	X	X	R	NSD	X
clus5	**10 bridges**																
	C	PC	X	X	>20	X	X	X	X	X	X	Ssp	<25	Isl	R	NSD	<50
	C	RC	X	X	<20	X	X	X	X	X	X	Ssp	<25	M	R	NSD	<50
	C	PC	X	X	<20	X	X	X	X	X	X	Ssp	<25	Isl	R	NSD	<50
	C	PC	X	X	<20	X	X	X	X	X	X	Ssp	<25	M	R	NSD	<50
clus6	**1 bridge**																
	X	X	X	X	<20	X	X	McP	Cy	So	X	X	X	X	R	NSD	X
clus7	**1 bridge**																
	C	PC	X	X	>20	Co	NIs	McP	R	So	X	Ms	<25	M	R	SD	<100
clus8	**57 bridges**																
	C	RC	X	X	<20	Co	NIs	ScP	W	So	X	Ms	<25	M	R	SD	<50
	C	PC	X	X	<20	Co	Is	ScP	W	So	X	Ms	<25	X	R	SD	<50
	C	PC	X	X	<20	Co	Is	ScP	W	So	X	Ms	X	Isl	IR	SD	>200
	S	X	X	X	<20	SSu	Is	ScP	W	So	X	Ms	<45	Isl	R	SD	>200

	C	PC	X	X	>20	Co	Is	ScP	W	So	X	Ms	<25	Isl	R	SD	<50
	S	RC	X	X	<20	Co	Is	ScP	Ob	So	X	Ms	<45	Isl	R	SD	<100
	C	PC	X	X	>20	SSu	Is	McP	R	So	X	Ms	<45	Isl	R	SD	<50
	S	X	X	X	<20	Co	Is	ScP	W	So	X	Ms	<45	Isl	R	SD	<100
	C	PC	X	X	>20	Co	Is	ScP	W	So	X	Ms	<45	Isl	R	SD	<100
	S	X	X	X	<20	Co	Is	ScP	W	So	X	Ms	>45	Isl	R	SD	<100
	C	PC	X	X	<20	X	Is	ScP	Ob	So	X	Ms	X	Isl	R	SD	<100
	C	PC	X	X	<20	Co	Is	ScP	W	So	X	Ms	<45	Isl	R	SD	<100
	C	PC	X	X	<20	X	Is	ScP	R	So	X	Ms	X	Isl	R	SD	<100
	C	PC	X	X	>20	SSu	Is	McP	Cy	So	X	Ms	<45	Isl	R	SD	<200
	C	PC	X	X	<20	SSu	Is	ScP	W	So	X	Ms	<45	Isl	R	SD	<100
	C	PC	X	X	<20	SSu	Is	McP	R	Ho	X	Ms	<45	Isl	IR	SD	>200
	C	PC	X	X	<20	SSu	Is	ScP	Ob	So	X	Ms	<45	Isl	R	SD	<100
	C	PC	X	X	<20	SSu	Is	McP	R	So	X	Ms	<25	Isl	R	SD	<50
	C	PC	X	X	<20	SSu	Is	ScP	Cy	So	X	Ms	<45	Isl	IR	SD	<200
	C	PC	X	X	<20	SSu	Is	McP	Cy	So	X	Ms	<25	Isl	R	SD	<100
	C	PC	X	X	<20	SSu	Is	ScP	Cy	So	X	Ms	<45	Isl	R	SD	<200
	C	PC	X	X	<20	SSu	Is	McP	Cy	So	X	Ms	<25	Isl	R	SD	<200
	C	PC	X	X	<20	SSu	Is	ScP	Ob	So	X	Ms	<45	Isl	R	SD	<200
	C	PC	X	X	<20	SSu	Is	McP	R	So	X	Ms	<45	Isl	R	SD	<50
	C	PC	X	X	<20	Co	Is	McP	R	So	X	Ms	<25	Isl	R	SD	<100
	C	PC	X	X	<20	SSu	Is	McP	Cy	So	X	Ms	<45	Isl	R	SD	<200
	C	PC	X	X	<20	SSu	Is	McP	Cy	So	X	Ms	<45	Isl	R	SD	>200
	C	PC	X	X	<20	SSu	Is	McP	Cy	So	X	Ms	<45	Isl	R	SD	<100
	C	PC	X	X	<20	SSu	Is	McP	R	Ho	X	Ms	<45	Isl	R	SD	<200
	C	PC	X	X	<20	SSu	Is	McP	R	Ho	X	Ms	<45	Isl	R	SD	<100
	C	PC	X	X	<20	SSu	Is	McP	R	So	X	Ms	<25	Isl	R	SD	<100
	C	PC	X	X	<20	SSu	Is	McP	R	So	X	Ms	<45	Isl	R	SD	<100
clus9	**1 bridge**																
	S	X	X	X	<20	SSu	Is	McP	R	So	X	Ms	<45	Isl	R	SD	<200
clus10	**1 bridge**																
	X	X	X	X	<20	X	Is	ScP	Ob	So	X	Ms	X	Isl	R	SD	<200
clus11	**25 bridges**																
	S	X	X	X	<20	SSu	Is	ScP	W	So	X	Ms	<45	Isl	R	NSD	<100
	C	PC	X	X	>20	SSu	Is	ScP	W	So	X	Ms	<25	Isl	R	NSD	<50
	C	PC	X	X	>20	SSu	Is	McP	Cy	So	X	Ms	<25	Isl	R	NSD	>200
	C	PC	X	X	<20	SSu	Is	ScP	W	So	X	Ms	<45	Isl	R	NSD	<100
	C	PC	X	X	>20	SSu	Is	McP	R	So	X	Ms	<25	Isl	R	NSD	<100
	C	PC	X	X	<20	SSu	Is	ScP	W	So	X	Ms	<25	Isl	R	NSD	<50
	C	PC	X	X	<20	SSu	Is	McP	Cy	So	X	Ms	<25	Isl	R	NSD	<100
	C	PC	X	X	<20	SSu	Is	ScP	W	So	X	Ms	<25	Isl	R	NSD	<100
	C	PC	X	X	<20	SSu	Is	McP	Cy	So	X	Ms	<25	Isl	R	NSD	<50
	C	PC	X	X	<20	SSu	Is	McP	R	So	X	Ms	<25	Isl	R	NSD	<50
	C	PC	X	X	<20	SSu	Is	McP	R	So	X	Ms	<45	Isl	R	NSD	<50
	C	PC	X	X	<20	SSu	Is	McP	Cy	So	X	Ms	<45	Isl	R	NSD	<100
	C	PC	X	X	<20	SSu	Is	McP	R	So	X	Ms	<45	Isl	R	NSD	>200
	C	PC	X	X	<20	SSu	Is	McP	R	So	X	Ms	<25	Isl	R	NSD	<100
	C	PC	X	X	<20	SSu	Is	McP	R	So	X	Ms	<45	Isl	R	NSD	<100
clus12	**1 bridge**																
	C	PC	X	X	X	X	X	ScP	Cy	So	X	Ms	X	X	R	NSD	X
clus13	**2 bridges**																
	C	PC	X	X	<20	X	X	McP	X	X	X	X	X	X	IR	NSD	>200
clus14	**4 bridges**																
	C	RC	X	X	<20	X	X	X	X	X	X	Ms	<25	M	R	SD	X
	M	X	X	X	<20	X	X	X	X	X	X	Ms	<45	M	R	SD	<200
	C	X	X	X	<20	X	X	X	X	X	X	Ms	<25	X	R	SD	<100
	C	X	X	X	<20	X	X	X	X	X	X	Ms	<45	X	R	SD	<200
clus15	**7 bridges**																
	M	X	X	X	<20	X	X	ScP	Ob	So	X	Ms	<25	M	R	SD	<100
	M	X	X	X	<20	X	X	ScP	W	So	X	Ms	<25	M	R	SD	<50
	M	X	X	X	<20	X	X	ScP	W	So	X	Ms	<45	M	R	SD	>200
	C	X	X	X	<20	X	X	ScP	W	So	X	Ms	X	M	R	SD	X
	M	X	X	X	<20	X	X	ScP	W	So	X	Ms	X	M	R	SD	X
clus16	**1 bridge**																
	M	X	X	X	<20	X	X	ScP	W	So	X	Ms	<25	M	R	NSD	<100
clus17	**1 bridge**																
	M	X	X	X	X	X	X	ScP	W	So	X	Ssp	X	M	R	SD	X

Table 55: Bridge configurations corresponding to each of the 17 clusters selected.

DS1	Median		Lower Bound		Upper Bound	
	α [g]	β	α [g]	β	α [g]	β
clus1	0.817	0.516	0.558	0.298	1.196	0.894
clus2	0.473	0.360	0.223	0.209	1.006	0.619
clus3	0.246	0.165	0.115	0.083	0.527	0.324
clus4	0.275	0.181	0.121	0.083	0.625	0.395
clus5	0.484	0.337	0.234	0.186	0.999	0.608
clus6	0.349	0.253	0.158	0.127	0.773	0.502
clus7	0.760	0.398	0.458	0.173	1.264	0.915
clus8	0.773	0.484	0.554	0.292	1.078	0.801
clus9	0.535	0.280	0.529	0.200	0.541	0.392
clus10	0.576	0.339	0.248	0.123	1.338	0.936
clus11	0.293	0.185	0.238	0.156	0.360	0.221
clus12	0.499	0.261	0.299	0.113	0.835	0.605
clus13	0.522	0.306	0.301	0.158	0.904	0.594
clus14	0.607	0.438	0.374	0.263	0.986	0.731
clus15	0.796	0.491	0.583	0.291	1.086	0.828
clus16	0.203	0.160	0.096	0.138	0.433	0.186
clus17	0.690	0.390	0.511	0.237	0.932	0.643
DS2	Median		Lower Bound		Upper Bound	
	α [g]	β	α [g]	β	α [g]	β
clus1	1.067	0.642	0.636	0.327	1.792	1.259
clus2	0.670	0.500	0.312	0.268	1.438	0.934
clus3	0.499	0.303	0.280	0.182	0.890	0.503
clus4	0.563	0.351	0.295	0.178	1.076	0.691
clus5	0.615	0.418	0.323	0.246	1.170	0.711
clus6	0.524	0.364	0.238	0.178	1.154	0.744
clus7	0.841	0.441	0.584	0.222	1.212	0.877
clus8	0.954	0.573	0.702	0.321	1.295	1.024
clus9	0.769	0.403	0.606	0.230	0.976	0.706
clus10	0.888	0.479	0.620	0.254	1.274	0.903
clus11	0.498	0.310	0.380	0.177	0.653	0.543
clus12	0.640	0.335	0.368	0.139	1.112	0.806
clus13	0.656	0.385	0.397	0.205	1.082	0.721
clus14	0.781	0.471	0.512	0.286	1.193	0.777
clus15	0.969	0.551	0.695	0.303	1.351	1.001
clus16	0.273	0.221	0.143	0.165	0.524	0.295
clus17	1.335	0.755	0.564	0.263	3.162	2.163
DS3	Median		Lower Bound		Upper Bound	
	α [g]	β	α [g]	β	α [g]	β
clus1	1.408	0.774	0.811	0.366	2.442	1.638
clus2	1.093	0.689	0.609	0.298	1.961	1.593
clus3	0.738	0.469	0.414	0.205	1.314	1.072
clus4	0.836	0.547	0.437	0.224	1.601	1.340
clus5	0.932	0.543	0.541	0.250	1.606	1.181
clus6	0.830	0.476	0.404	0.190	1.703	1.189
clus7	1.017	0.533	0.754	0.286	1.372	0.994
clus8	1.281	0.733	0.849	0.372	1.933	1.444
clus9	1.017	0.533	0.754	0.286	1.372	0.994
clus10	1.324	0.695	0.869	0.367	2.019	1.316
clus11	0.686	0.418	0.429	0.201	1.097	0.871
clus12	0.809	0.424	0.433	0.164	1.509	1.093
clus13	0.829	0.482	0.487	0.251	1.411	0.926
clus14	1.013	0.538	0.608	0.307	1.686	0.943
clus15	1.333	0.680	0.850	0.343	2.091	1.351
clus16	0.520	0.217	0.520	0.217	0.520	0.217

clus17	1.646	0.930	0.770	0.353	3.521	2.451
DS4	**Median**		**Lower Bound**		**Upper Bound**	
	α [g]	**β**	**α [g]**	**β**	**α [g]**	**β**
clus1	1.882	0.990	0.947	0.475	3.742	2.063
clus2	1.159	0.847	0.437	0.340	3.074	2.109
clus3	0.950	0.613	0.414	0.270	2.177	1.392
clus4	1.092	0.698	0.499	0.309	2.392	1.578
clus5	1.061	0.696	0.429	0.285	2.627	1.698
clus6	1.150	0.868	0.438	0.344	3.020	2.190
clus7	1.344	0.704	1.005	0.381	1.799	1.303
clus8	1.887	1.209	0.973	0.478	3.660	3.054
clus9	1.416	0.742	0.983	0.373	2.038	1.475
clus10	1.690	0.879	0.787	0.375	3.629	2.063
clus11	1.110	0.660	0.579	0.274	2.131	1.591
clus12	1.111	0.582	0.634	0.240	1.947	1.410
clus13	1.165	0.684	0.711	0.364	1.907	1.285
clus14	1.351	0.668	0.617	0.297	2.962	1.500
clus15	2.145	1.117	1.001	0.479	4.593	2.605
clus16	0.434	0.337	0.202	0.301	0.935	0.377
clus17	2.015	1.139	1.003	0.464	4.049	2.796

Table 56: Fragility parameters for each of the 17 clusters selected, for the median curve and the 16%-84% confidence bounds.